The nature and origin of the REE mineralization in the Wicheeda Carbonatite, British Columbia, Canada

By

Joel Trofanenko

A thesis submitted to the Faculty of Graduate Studies and Research in partial fulfillment of the requirements for the degree of Master of Science

Department of Earth and Planetary Sciences
McGill University, Montreal, QC, Canada
December 2014

Abstract

In response to rising demand of the rare earth elements (REE), recent exploration of the British Columbia alkaline province has identified the Wicheeda Carbonatite, which contains an estimated 11.3 million tons of light REE-enriched ore grading 1.95 wt.% TREO, to be the highest-grade prospect known in British Columbia. However, research of the deposit is restricted to one paper describing mineralization in carbonatite dikes adjacent to the main plug. This study describes the nature and origin of REE-mineralization in the Wicheeda plug.

The carbonatite was emplaced in metasedimentary limestone and argillaceous limestone belonging to the Kechika Group, which has been altered to potassic fenite immediately adjacent to the carbonatite and to sodic fenite at greater distances from it. The carbonatite comprises a ferroan dolomite core, which passes outwards gradationally into calcite carbonatite. Three texturally distinct varieties of dolomite have been recognized. Dolomite 1 constitutes most of the carbonatite; Dolomite 2 replaced Dolomite 1 near veins and vugs; Dolomite 3 occurs as a fracture and vug-lining phase with the REE mineralization. Stable carbon and oxygen isotopic ratios indicate that the calcite carbonatite is of mantle origin, that Dolomite 1 is of primary igneous origin, that Dolomite 2 is largely primary igneous with minor hydrothermal signature contamination, and that Dolomite 3 is of hydrothermal origin. Rare-metal mineralization in the deposit is, with the exception of pyrochlore, which occurs in the calcite carbonatite, restricted to veins and vugs in the dolomite carbonatite. There it occurs as hydrothermal veins and in

vugs infilled by REE-fluorocarbonates, i.e., bastnäsite-(Ce), ancylite-(Ce), and monazite-(Ce) together with accessory pyrite, barite, molybdenite, and thorite.

A model is proposed in which calcite carbonatite was the earliest magmatic phase to crystallize. The calcite carbonatite magma saturated with niobium relatively early, precipitating pyrochlore. The magma later evolved to a dolomite carbonatite composition which, upon cooling exsolved an aqueous carbonic fluid, which altered the Kechika metasediments to potassic fenite and mixed with formational waters further from the carbonatite to produce sodic fenite. This fluid mobilized the REE as chloride complexes into vugs and fractures in the dolomite carbonatite. Upon progressive fluid-rock interaction, the REE precipitated largely in response to cooling and pH. Hydrothermal concentration led to remarkable grade consistency, with virtually all of the dolomite carbonatite containing >1 wt.% TREO, making the Wicheeda Carbonatite a very attractive exploration target.

Sommaire

En réponse à la demande industrielle croissante pour les éléments du groupe des terres rares (ETR), l'exploration de la province alcaline de Colombie Britannique a récemment permis d'identifier la carbonatite de Wicheeda (11.3 millions de tonnes de minerai enrichi en terres rares légères, affichant une teneur de 1.95 % TREO (l'oxide des terres rares total) comme l'un des prospects de terres rares les plus prometteurs. Les précédentes investigations menées sur ce gisement se limitent aux rapports des compagnies ayant exploré la zone pour ses ressources potentielles en terres rares. La présente étude décrit la minéralisation en éléments des terres rares de la carbonatite de Wicheeda, et combine l'étude de données pétrographiques et géochimiques dans le but de développer un modèle génétique pour ce gisement.

La carbonatite de Wicheeda s'est mise en place dans les formations de calcaires métasédimentaires et calcaires argileux du Groupe de Kechika, qui ont été altérées en fénite potassique au contact de la carbonatite et en fénite sodique de manière plus distale. La composition de la carbonatite montre une évolution graduelle depuis son cœur (dolomite ferrifère) vers sa périphérie (carbonatite calcitique). Trois variétés de dolomites ont été distinguées sur la base d'évidences texturales. La dolomite 1 est le composant principal de la carbonatite, la dolomite 2 remplace la dolomite 1 à proximité des veines et des pores. La dolomite 3 se met en place en fracture et en remplissage de la porosité, et accompagne la minéralisation en terres rares. Les ratios des isotopes stables du carbone et de l'oxygène indiquent que la carbonatite calcitique est d'origine mantellique et la dolomite 1 d'origine ignée. La dolomite 2 montre une signature ignée faiblement

modifiée par l'altération hydrothermale subséquente et la dolomite 3 est d'origine hydrothermale.

Un modèle est proposé dans lequel la carbonatite calcitique est la phase magmatique la plus précoce. Cette phase a atteint la saturation en niobium très tôt, entrainant la précipitation du pyrochlore. Le magma a évolué plus tardivement vers une composition de carbonatite dolomitique qui, lors de son refroidissement, a exsolvé un fluide aquo-carbonique altérant les métasédiments de Kechika en fénite potassique et se mélangeant avec les eaux formationelles, plus distales, pour produire les fénites sodiques.

Le fluide aquo-carbonique a mobilisé et transporté les ETR sous la forme de complexes chlorurés, au sein de la porosité et des fractures de la carbonatite dolomitique. A la suite des interactions fluide-roche prolongées, les ETR ont précipité du fait du refroidissement et de l'augmentation du pH ; la présence d'apatite a entrainé la formation de monazite-(Ce). La concentration hydrothermale a permis une répartition homogène des teneurs, avec la carbonatite dolomitique contenant dans son ensemble plus de 1 % TREO, faisant de Wicheeda un gisement très attrayant.

Contributions of Authors

This thesis has been written in manuscript format in accordance with the regulations put forth by the Faculty of Graduate Studies and Research at McGill University. It contains one manuscript submitted to Economic Geology. In addition, there are two supporting chapters and eleven appendices.

The manuscript (Chapter 2) is entitled "The nature and origin of the REE mineralization in the Wicheeda Carbonatite, British Columbia, Canada" and is co-authored by Joel Trofanenko, Anthony E. Williams-Jones, and George J. Simandl. It includes descriptions of the Wicheeda Carbonatites and fenites, and the associated rare metal mineralization, as well as an interpretation of their origins.

Joel Trofanenko mapped the available outcrops and collected diamond drill core data during the summer of 2013. Anthony Williams-Jones, Duncan Mackay, and George Simandl provided valuable advice and scientific discussion during field investigations and Williams-Jones during laboratory research at McGill University. Trofanenko conducted the sample preparation, petrographic examination, geochemical analyses and data interpretation with guidance and assistance of Williams-Jones. Trofanenko prepared the first draft of the thesis, which was subsequently revised based on comments by Williams-Jones. Williams-Jones helped edit the final version of the thesis.

Acknowledgments

I would like to express my sincerest thanks to my supervisor, Professor A.E. Williams-Jones, for his guidance, support, and continued enthusiasm over the course of the project. His role as a mentor encouraged, challenged, and inspired me during my time at McGill. I am indebted to him for his incredible depth of knowledge and support for the past two years. I could not have completed this thesis without him.

Table of Contents

List of Figures

List of Tables

List of Appendices

CHAPTER I: Introduction

General Statement

Introduction

The rare earth elements (REE) are in high demand for a variety of applications in a wide range of emerging technologies, notably batteries and super magnets for use in hybrid cars, phosphors for use in lasers, LED lighting and LED and LCD flat screen televisions, and additives to improve the efficiency of solar panels. Despite their name, many of the REE have higher crustal abundances than other commonly mined metals such as Sn or Mo (Hu and Gao, 2008), however, only a small number of deposits contain mineable REE concentrations.

Throughout the early 20th century, placer deposits in India and Brazil met the global demand for REE but by the middle of the century rapidly developing technologies increased the global demand for REE. The Steenkampskraal mine in South Africa was the dominant supplier of REE in the 1950s (Kremers, 1958), and in 1965 the carbonatite-hosted Mountain Pass deposit in California began full-scale extraction of REE, primarily the light REE (LREE) before closing in 2002 (Castor and Hedrick, 2006). Since the mid 1980s, China has been the largest supplier of REE mainly from vein-hosted bastnäsite-(Ce) and monazite-(Ce) in the massive Bayan Obo deposit (Chao et al., 1997). Estimated reserves at Bayan Obo exceed 80 million tons at a grade of 6 wt.% total rare earth oxides (TREO), making it the largest known rare earth deposit (Kynicky et al., 2012). There is additional Chinese production from the Maoniuping carbonatite deposit (1.5 million tons) and the heavy REE (HREE) ion-adsorption clay deposits of South

China (5-10 million tons) (Kynicky et al., 2012). These deposits currently account for 90% of the world's REE production and 36% of the identified reserves (USGS, 2014). China recently reduced exports of the REE by 40% (Hatch, 2012), leading to a sharp increase in the demand for these elements. In order to meet this demand, the Mountain Pass deposit re-opened in 2012, producing LREE-enriched ore. There has also been intensive exploration outside of China leading to the discovery of many new deposits. None of these, however, has yet gone into production. In Canada, the Nechalacho (NWT) and Strange Lake (Quebec) deposits are at advanced stages of development. Among the different types of REE deposits, carbonatites are often the most LREE-enriched and represent an important exploration target as a result.

Examples of Carbonatite-hosted deposits

The Mountain Pass sövite (calcite carbonatite) and beforsite (dolomite carbonatite) host the largest and highest grade deposit in North America and only known occurrence of LREE mineralization in a carbonatite that is solely magmatic in origin. The ore body is hosted in the Sulfide Queen Carbonatite and has current reserves of approximately 18.4 million tons grading 7.98 wt.% REO (mainly LREE) together with minor barium (Sims and Blackman, 2012). The REE are concentrated mainly in coarse-grained bastnäsite-(Ce) in the sövite and fine-grained bastnäsite-(Ce) and monazite-(Ce) in the beforsite (Castor, 2008).

The Bear Lodge (Wyoming) carbonatite-hosted REE deposit is another North American example. The REE mineralization at this deposit was the product of post-magmatic

hydrothermal processes of calcite carbonatite and carbonatite diatreme breccias (Moore et al., 2015). The deposit has estimated reserves of 52.1 million tons of ore with an average grade of 2.71 wt.% TREO (Moore et al., 2015; Noble et al., 2013). The REE mineralization is complex and consists of primary burbankite, which was altered by hydrothermal fluids to ancylite, barite, strontianite, and REE fluorocarbonates (Moore et al., 2015). Ancylite was later replaced by monazite-(Ce) (Moore et al., 2015).

A third North American example is the St. Honoré carbonatite REE prospect in Quebec. It measures approximately 8 km^2 in plan view and comprises calcite and dolomite emplaced in alkaline syenite (Fortin-Bélanger, 1977; Fournier, 1993). The latter carbonatite was altered to ankerite carbonatite by hydrothermal fluids, which brecciated the carbonatite and precipitated bastnäsite-(Ce), parisite-(Ce), synchysite-(Ce), and monazite-(Ce). The ankerite core of the carbonatite has an average grade of 1.64 wt.% TREO. As at Bear Lodge, the mineralization is interpreted to be a product of a post-magmatic hydrothermal fluid that precipitated the REE through a combination of decreasing temperature and increasing pH as a result of interaction of the ore fluid with the dolomite (Fournier, 1993; Grenier et al., 2013).

In India, the late Cretaceous to early Tertiary Amba Dongar Complex is another example of a carbonatite containing elevated REE concentrations that has been extensively altered by hydrothermal fluids. It is a carbonatite-nephelinite subvolcanic diatreme comprising a sövite ring dike that has an inner rim of carbonatite breccia surrounded by fenitized sandstone. The chronology of the Complex, including the REE mineralization, has been

summarized by Doroshkevich et al. (2009) and comprises the intrusion of nephelinites and phonolites followed by the emplacement of the carbonatites and metasomatic alteration (fenitization) of the host rocks. This post-magmatic hydrothermal activity led to REE enrichment and fluorite mineralization. During emplacement of the sövite, exsolving aqueous fluids fractured the carbonatite and precipitated florencite, barite, strontianite, quartz, and REE-fluorocarbonates in microveinlets and vugs.

The tectonic setting and origin of carbonatite magmas

Many of the recently discovered REE deposits are hosted by carbonatite intrusions. Carbonatites are so classified on the basis of their high modal abundance of primary carbonate minerals (>50%) and low silica (silica-undersaturated) content (<20%), and are subdivided into calcite- dolomite- or ankerite- carbonatites (Le Bas and Streckeisen, 1991). Their bulk lithochemistry is characterized by contain relatively little alkalis, elevated barium, and high halogen contents (mainly fluorine) and high field strength elements (HFSE) contents (Woolley and Kempe, 1989). Carbonatites commonly form in intra-continental, anorogenic extensional settings in which the thinning continental lithosphere favors decompressional melting of the mantle and emplacement of magma (Chakhmouradian and Zaitsev, 2012). The incompatible elements are initially concentrated in them due to the small degree of partial melting and the subsequent evolution of the carbonatite and/or related magmas (Hamilton et al., 1989; Meet et al., 1989; Chakhmouradian and Zaitsev, 2012). Abundant isotopic evidence suggests that the parental magmas are derived from lithospheric and asthenospheric mantle sources (Chakhmouradian and Zaitsev, 2012). The carbonatites are thought to form through 1) a

combination of batch melting and subsequent extreme fractional crystallization of a parental silicate melt (Garson, 1965; Lee and Wyllie, 1994; Slagel 1997; Mitchell, 2005), 2) liquid immiscibility (exsolution of the carbonatite melt from the silicate melt) (Freestone and Hamilton, 1980; Kjarsgaard and Hamilton, 1988; Lee and Wyllie, 1998), or 3) directly from partial melting of carbonated mantle peridotite (von Eckermann, 1948; Eggler, 1974; Eggler, 1978; Eggler, 1989; Sweeney, 1994; Gittins and Harmer, 1997). The first two hypotheses were prompted by the common field association of carbonatites with a wide range of silicate rocks including ijolite (nepheline+augite) at Alnö, Sweden (see Kresten, 1976; Kresten et al., 1977) and Fen, Norway (see Andersen, 1984), and nepheline syenites at Khibina in the Kola alkaline province of Russia (see Zaitsev, 1998; 2014). In these examples, the carbonatites cut the earlier (deeper) silicate portions of the plutonic complex. Experimental studies have supported these hypotheses by demonstrating that batch melting and extreme fractional crystallization can produce carbonatites (Lee and Wyllie, 1994 and the existence of a miscibility gap between carbonate and silicate liquids (Brooker, 1998; Kjaarsgard, 1998; Lee and Wyllie, 1998). On the basis of carbonatite chemistry, Harmer and Gittins (1998) suggested that source magmas for carbonatites and silicates are different and the only link between them is the conduit through which they ascend. Their hypothesis is supported by neodymium and strontium isotopic compositions of African carbonatite-containing alkaline igneous suites indicating considerable differences between the carbonatites and their alkaline silicate counterparts (Harmer and Gittins, 1998).

Magmatic Concentration of REE

Rare metal enrichment in carbonatites is attributed mainly to the unusual chemical nature of the REE. The REE typically occur in the 3+ valence state, with the exception of Ce and Eu, (which are sensitive to redox conditions and also occur in the 4+ and 2+ valence states, respectively), and have atomic radii that decrease from lanthanum (La) to lutetium (Lu). As a result, the LREE have a larger ionic radius than the HREE and are more incompatible. If carbonatites form directly from small degrees of partial melting, they will therefore be preferentially enriched in the LREE. Fluorine is enriched in carbonatites for the same reason and may also form complexes with the REE, which help facilitate their enrichment. The same reasoning applies if carbonatites form from extreme fractional crystallization of nepheline syenite magmas. In this case, the incompatible elements, i.e., the LREE, are concentrated in the extremely fractionated CO_2-rich residual magma. The partition coefficient of the LREE between carbonate and silicate melt is close to one but is much lower for the HREE (Veksler et al., 2012). Consequently, the liquid immiscibility hypothesis also predicts that the carbonatites will be preferentially enriched in the LREE.

Most research suggests that regardless of the manner in which they form, the REE enrichment of carbonatites is not solely due to magmatic processes but also results from post-magmatic hydrothermal processes (Morogan and Woolley, 1988; Zaitsev, 1998; Arzamastsev et al., 2001; Doroshkevich et al., 2009; Moore et al., 2015).

The Role of Hydrothermal Processes

Fenitization

During emplacement, carbonate and silicate magmas exsolve aqueous fluids that can potentially mobilize the REE and alter the adjacent host rocks (Currie and Ferguson, 1971; Kresten 1988; Gittins et al., 1990). The latter process is called fenitization and leads to the progressive metasomatic enrichment of alkalis and desilicification of the host rock, resulting in an increasingly alkali-rich rock. The resulting mineral assemblages are dependent on the composition of the host rocks and fenitizing fluids, as well as the temperature of the fluid (Le Bas, 1981; Woolley, 1982; Rubie and Gunter, 1983; Morogan, 1994). High temperature metasomatism in the deeper parts of an intrusion typically produces sodic mineral assemblages (McKie, 1966; Vartiainen and Woolley, 1976; Le Bas, 1977; Le Bas, 2008), whereas low temperature alteration produces potassic mineral assemblages (e.g., Vartiainen and Woolley, 1976; Viladkar, 1981; Viladkar, 1986). The variation in the fenitization could also be due to the different sources of the fluids; sodic fenites have been attributed to an ijolitic (e.g., nepheline+augite) magma and potassic fenites to carbonatitic magmas (Le Bas, 1977; Morogan, 1994; Le Bas, 2008).

Brøgger (1921) first described fenites at the Fen Complex (Norway). The Complex is hosted in Proterozoic gneissic granite, which was emplaced during the early Cambrian (Verschure and Maijer, 1984) and is related to the early stages of the Oslo Rift (Griffin and Taylor, 1975). The magmatic history of the Complex is as follows: 1) emplacement of melteigite-ijolite-urtite series rocks, alkali pyroxenites, and nepheline syenites; 2)

intrusion of coarse-grained calcite carbonatites (sövites) and silico-sövites; 3) intrusion of dolomite and ankerite carbonatite; and 4) intrusion of alkaline lamprophyres (Brøgger, 1921; Sæther, 1957; Barth and Ramberg, 1966; Andersen, 1984). Extensive fenitization by fluids exsolved from the ijolitic magma is interpreted to have led to the development of sodic and potassic fenites and altered the dolomite and ankerite carbonatite. During late alteration, the ankerite carbonatite was locally replaced by a hematite-calcite-dolomite assemblage (rødberg) though interaction with an oxidizing fluid at temperatures <300°C (Andersen 1984).

Similar fenitizing processes to those at Fen have been described at Alnö, Sweden, where pyroxenite was emplaced in Precambrian migmatitic gneisses, followed by melteigite-ijolite-urtite, nepheline syenite, and finally sövite (Kresten 1979). The gneisses are composed of quartz, plagioclase, biotite, and potassium feldspar, and were altered progressively to sodic and potassic fenite. The earliest (weakest) stages of alteration resulted in the removal of quartz and breakdown of biotite to potassium feldspar and amphibole at the edges of the intrusion. Later, the rock was more intensely altered to sodic fenite as is evidenced by the complete replacement of the protolith mineralogy by albite; the latter replaced plagioclase, amphibole (e.g., arfvedsonite), and pyroxene (e.g., aegirine-augite) (Morogan and Woolley, 1988). Morogan and Woolley (1988) proposed that the fenitization was caused by an oxidizing, high temperature (>500°C) fluid with high alkali, F, and P contents that exsolved from the carbonatite. The distribution of the fenites is interpreted to reflect a relationship in which the hottest fluids proximal to the intrusion caused albitization, and cooler fluids further from the intrusion generated a

potassic mineral assemblage (Lagache and Weisbrod, 1977; Morogan and Woolley, 1988).

As mentioned previously, the late Cretaceous to early Tertiary Amba Dongar carbonatite-alkaline Complex experienced extensive hydrothermal alteration. It is hosted in quartzite (96-98% quartz), which makes it an ideal example to study fenitizing processes in a simple protolith. As calcite carbonatite intruded the sandstone, it exsolved two aqueous orthomagmatic fluids (Williams-Jones and Palmer, 2002). The first (deeper) fluid had a significant carbonic component and exsolved when conditions evolved to lower temperature and pressure. By contrast, the second fluid exsolved at shallower depths leading to fracturing of the host sandstone, and alteration of the quartz to potassium feldspar (Viladkar, 1981; Viladkar, 1986; Roelofsen, 1997; Williams-Jones and Palmer, 2002; Doroshkevich et al., 2009).

Hydrothermal Concentration of REE

Examples of hydrothermal REE deposits

In order to constitute a rare-metal deposit, the REE and HFSE must be concentrated in carbonatites to a greater degree than can generally occur solely by magmatic processes (Chakhmouradian and Zaitsev, 2012). Hydrothermal processes like those reported for Bear Lodge and Amba Dongar (see above) led to extensive alteration of the host carbonatite and concentration of the REE. In the case of Bear Lodge, hydrothermal fluids characterized by high F^-, CO_2, and SO_4^{2-} contents led to the replacement of primary

burbankite by REE fluorocarbonate and REE hydrocarbonate minerals [e.g., bastnäsite-(Ce), and ancylite-(Ce), respectively], and monazite-(Ce) (Moore et al., 2015).

The giant Bayan Obo Fe-Nb-REE deposit is the archetypal example of economic rare metal mineralization in rocks that have undergone intense hydrothermal alteration. It formed from intense alteration of sedimentary dolomite leading to stratified ore bodies. An overlying shale unit acted as a cap-rock as hot (>400°C) acidic hydrothermal fluids dissolved the host dolomite, releasing CO_2 and neutralizing the acidity of the fluid, which drove precipitation of monazite-(Ce) and bastnäsite-(Ce) and to a much lesser extent parisite-(Ce), huanghoite-(Ce) and cebaite-(Ce) as it cooled (Drew et al., 1990; Smith and Henderson, 2000; Smith and Henderson, 2000; Wu, 2007).

Processes of hydrothermal REE enrichment

The chemical behavior of the REE leading to their concentration in hydrothermal systems is reliably predicted by Pearson's rules (Pearson, 1963). According to Pearson (1963), non-polarizable cations bond preferentially with non-polarizable anions. Because the REE have a common 3+ valence state and consequently small ionic radii, they are hard cations and should form stable aqueous complexes (in decreasing stability) with hard anions, e.g., monovalent anions in the order of $F^- > OH^- > NO_3^- > Cl^-$ (Pearson, 1963). In the case of the divalent anions, the order is $CO_3^{2-} > SO_4^{2-} > P_2O_5^{2-}$. Experimental studies (e.g., Migdisov and Williams-Jones, 2004; 2006; 2007; Migdisov et al., 2009; Migdisov et al., 2011; Williams-Jones et al., 2012) have demonstrated that the REE form stable complexes with F^- and Cl^-; however, REE-fluoride minerals have very low solubility

except under extremely acidic conditions, which precludes REE transport as fluoride complexes. Instead, the REE are most likely transported as REE-chloride complexes and F, which exists as HF at low pH conditions, acts as a depositional ligand (Williams-Jones et al., 2012). Similarly, the solubility of the REE-carbonates [e.g., ancylite-(Ce)] and REE-phosphates is also quite low suggesting that CO_3^{2-} and PO_4^{3-} may play an important role in the deposition of REE rather than their transport.

The deposition of REE from solution as bastnäsite-(Ce) ($REECO_3F$) can be described by the reaction:

$$REECl^{2+} + HF + HCO_3^- = REECO_3F + 2H^+ + Cl^-$$
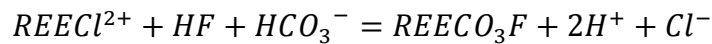
The deposition of bastnäsite-(Ce) is dependent on HCO_3^- and H^+ and thus any reaction that increases the activity of HCO_3^- and pH will favor its precipitation (Williams-Jones et al., 2012). As proposed for Bayan Obo (dolomite), the acidic REE-bearing hydrothermal fluids are partially neutralized by interaction with the host carbonate material through the reaction:

$$2H^+ + CaMg(CO_3)_2 = Ca^{2+} + Mg^{2+} + 2HCO_3^-$$
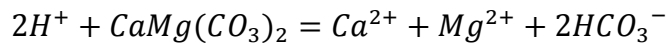
This leads to an increase in pH and HCO_3^- activity and drives the precipitation of bastnäsite-(Ce) (Williams-Jones et al., 2012). The remobilization and precipitation of the REE as ancylite-(Ce) and fluorocarbonates in the Bear Lodge calcite carbonatite can be modeled in an identical fashion.

This study

The purpose of the present study is to describe and understand the nature of rare earth element mineralization in the Wicheeda Carbonatite, British Columbia (Canada), a small intrusion consisting mainly of dolomite carbonatite that hosts significant REE (predominantly light REE) and Nb mineralization. It first garnered interest in the 1980s, but has been the subject of limited exploration until recently. The Wicheeda Complex is prominent on aeromagnetic maps as an ellipse that is part of a NW-trending magnetic anomaly approximately 5.5 km long and 2.5 km wide. The anomaly includes several small carbonatite plugs and dikes, and syenite dikes (e.g., Dalsin et al., 2015) in addition to the main intrusion that is the focus of this study. The carbonatites and accompanying syenites were emplaced within metasediments deposited along the ancestral margin of North America.

Previous Work

In 1961, the Geophysics Division of the Geological Survey of Canada conducted a 1:63,360 regional aeromagnetic survey across parts of British Columbia, including the Wicheeda Lake area, revealing northwest-trending linear magnetic anomalies, one of which is over the Wicheeda Carbonatite and nearby dikes. Regional mapping was conducted on the McLeod Lake (Armstrong et al., 1969) and Monkman Pass (Taylor and Stott, 1979) map sheets (Prince and George grids), both of which cover parts of the area that is the focus of the present study. The mapping revealed that the host rocks in the vicinity of the Wicheeda Carbonatite belong to the Kechika Group metasediments comprising thickly bedded, steeply dipping limestone, argillaceous limestone and weakly

13

foliated grey slates (Armstrong et al., 1969; Taylor and Stott, 1979). The strata generally strike 120-140° with steep dips to the NW and are in fault contact with unassigned limestone and siltstone east of the carbonatite. Adjacent to the carbonatite, they have been weakly mineralized.

Limited prospecting by Kol Lovang in the 1970s identified minor base metal showings and prompted him to stake the area. However, no follow up work was conducted and the claims were permitted to lapse. Teck Explorations Ltd. (Teck) later assayed Lovang's samples and obtained elevated niobium contents (Betmanis, 1987). This prompted the company to conduct a preliminary exploration program including geological and geophysical mapping, soil sampling, hand trenching, and stream sediment sampling. Teck staked several claims (PG 1, PG 2, Fata, Morgana, Prince, Lake, George, F, and D) and identified areas for further exploration. The Prince, George, and F grids were mapped at a line spacing of 150 m with soil samples collected every 50 m. The Lake and D grids were mapped at 250 m and 300 m line spacing, respectively. Total field magnetometer readings were taken at 25 m intervals on the Prince, George, and Lake grids. Test pits and seven trenches totaling 79.5 m in length were blasted on the Prince grid. X-ray fluorescence analyses of the soil samples indicated an average of 0.23% total rare earth elements (TREE) and up to 0.24% Nb, whereas the George grid samples contained an average of 7.98% TREE and 0.03% Nb.

Limited trenching and geological mapping by the British Columbia Geological Survey (Mäder and Greenwood, 1987) revealed the presence of carbonatite exposed irregularly

14

over an area with a diameter of ~250 m, containing 5 cm diameter rhombic ankerite phenocrysts, 2 cm diameter pyrite cubes together with accessory potassium feldspar, ilmenite, and a Ca-REE-fluorocarbonate mineral. Mäder and Greenwood (1987) described the argillaceous and calcareous metasedimentary rocks adjacent to the carbonatite as being "somewhat baked, but with no macroscopically visible contact metamorphic assemblages". There is no record of further exploration at Wicheeda Lake until 2008.

In 2008, Spectrum Mining Corp. began a diamond drilling exploration program on the Wicheeda Carbonatite (Lane, 2009). Four 40.7 mm diameter holes were drilled from one drill set-up in a fan-like pattern, with a total length of 866 m. The drill pad was located approximately 10 m west of the north end of Trench GT-2 (Betmanis, 1987). The drill holes intersected dolomite carbonatite, calcite carbonatite, carbonatite breccia, and fenites. Lane (2009) noted that the intrusion is dolomitic near the surface and becomes increasingly calcite-rich with depth. The width of the carbonatite was determined to be approximately 180 m and 110 m to the northwest and northeast, respectively. Drill core logging and geochemical analyses revealed that the carbonatite is most strongly REE-enriched near the surface, in the oxidized dolomite carbonatite, and is preferentially LREE-enriched with an La/Lu ratio up to 57,348. Anomalous values of Mo, Ba, Sr, Mn, As, P, Y, Th were noted. Petrographic analyses of the dolomite carbonatite identified accessory potassium feldspar and albite as well as traces of niobian rutile, biotite, pyrochlore, thorite, pyrite, galena, and molybdenite (Lane, 2009). The dominant REE mineral identified was monazite-(Ce). Subordinate proportions of Ca-REE-

fluorocarbonate interpreted to be parisite-(Ce), röntgenite-(Ce), or synchysite-(Ce) was also observed. Allanite and euxenite were identified in one sample.

In 2009, Spectrum Mining Corp. conducted additional drilling on the carbonatite including 14 56 mm diameter diamond drill holes from three drill pads (Site A, Site B, Site C) with a total length of 1835 m (Lane, 2010). Site A was located approximately 100 m northeast of the 2008 drill site, was collared at 1100 m above sea level (asl) and included six drill holes (WI09-05 to WI09-10), one of which was vertical and terminated at 1044 m asl. The other five holes had dips ranging from 50 to 55 degrees and ended at depths ranging from 991 to 981 m asl. The drill holes at Site A intersected REE-mineralized dolomite carbonatite and all, except WI09-10, terminated in fenite. Site B was 150 m northeast of the 2008 drill site and was collared at 1035 m asl. Four NW holes (WI09-11 to WI09-14) were drilled, including a vertical hole that reached a depth of 888 m asl. The three other holes had dips of 45, 55, and 60 degrees and were stopped at depths of 918, 914, and 963 m asl. Drill holes WI09-11 and WI09-12 ended in fenite. Drill hole WI09-14 intersected calcite carbonatite at all depths. Site C was located approximately 400 m northwest of the carbonatite and outside the study area. Three holes were drilled and all intersected coarse-grained calcite carbonatite but no significant REE mineralization (<1% TREO). Assays of the main carbonatite body drilled in 2008 and 2009 averaged TREO of 1.93 wt.%. Anthony Mariano estimated a resource of 11.3 million tons grading 1.16% Ce+La+Nd, mainly concentrated in coarse-grained bastnäsite-(Ce) and monazite-(Ce) (Lane, 2010).

In July 2010, Canadian International Minerals Inc. (CIN) conducted a 566.1 line-km helicopter-borne aeroTEM system electromagnetic, magnetic, and radiometric survey of the Wicheeda Carbonatite and former Prince grid claims (presently owned by Commerce Resources). Magnetic and radiometric anomalies were noted southeast of Wicheeda Lake, including a small (<150 nT) ellipsoidal anomaly at the Wicheeda Carbonatite and linear anomalies on the CIN properties southeast of the intrusion (Bruland, 2011). Diamond drilling on the CIN properties revealed a series of carbonatite dikes and veins, and mafic dikes (Bruland, 2011; Dalsin and Groat, 2011). The highest-grade REE intersection was encountered in a carbonatite dike averaging 4.68 wt.% TREO over 0.9 m.

The REE mineralogy, geochemistry and geochronology of the carbonatite dikes and veins on the properties southeast of the Wicheeda Carbonatite have been the subject of a detailed study by Dalsin et al. (2015). They interpreted the REE mineralization, which is hosted in calcite, ankerite and dolomite carbonatite, to be magmatic and the product of late-stage crystallization during rapid cooling. The major REE minerals identified are Ca-REE-fluorocarbonates, Ba-REE-fluorocarbonates, ancylite-(Ce), monazite-(Ce), allanite-(Ce), and euxenite-(Y). The Ca-REE-fluorocarbonate mineralization is described as comprising fine-grained subhedral crystals with syntaxial intergrowths of bastnäsite-(Ce) and parisite-(Ce). The Ba-REE-fluorocarbonates are described as "very fine-grained crystals of varying morphologies […] subject to rimming and infilling by fine-grained parisite-(Ce), synchysite-(Ce), and monazite-(Ce)" (Dalsin et al., 2015) and are interpreted to be magmatic. The synchysite-(Ce), which occurs as fine-grained masses

17

forming around the Ba-REE-fluorocarbonates and as fracture infill was also interpreted to be magmatic. Accessory apatite, ilmenite, thorite, fluorite, pyrochlore, and various sulfides were identified.

Objectives and Methodology

The objective of this thesis is to determine the nature and origin of REE, Nb, and Th mineralization in the Wicheeda Carbonatite and the adjacent Kechika Group metasedimentary rocks.

The research objectives were achieved through:

1. Field work at the Wicheeda Carbonatite, including mapping, outcrop description, drill core logging, and sampling of rocks for petrographic and geochemical analyses.

2. Preparing a detailed geological map of the deposit to determine its nature and that of the adjacent Kechika Group metasedimentary rocks, and their relationships to major structural features in the field area.

3. Optical petrographic examination of polished thin sections to identify the main rock-forming and ore minerals, evaluate their modal abundances, determine their textural relationships, and place them in an overall paragenetic sequence.

4. Compilation and analysis of bulk rock geochemical data acquired by Spectrum Mining Corp.

5. Energy dispersive scanning electron microscopy (SEM) and quantitative electron microprobe analyses to identify and determine the chemical composition of rock forming, ore, and alteration minerals.   These data confirmed the optical

identification of the minerals, assisted in evaluating textural relationships and helped determine the paragenetic sequence. SEM and microprobe analyses were conducted using a JEOL JXA-8900L electron microprobe equipped with five wavelength-dispersive X-ray spectrometers and a Si(Li) energy-dispersive X-ray detector at McGill University. Spot analyses using wavelength-dispersive spectrometry were conducted at a voltage of 15 kV and a 30 nA beam current together with a 10 μ m beam diameter for pyroxene and a 5 μ m beam diameter for apatite. A 20nA beam current and a 5 μm beam diameter was used for amphibole and mica, and a 10 μm beam size was used for feldspar. Dolomite was analyzed using a 20 nA beam current and a 20 μm beam diameter. The REE minerals were analyzed using a 20 nA beam current and a 10 μm beam diameter.

6. Stable isotope analyses of carbon and oxygen to determine the ratios of these elements in calcite carbonatite and dolomite carbonatite. Measurement of ^{13}C and ^{18}O isotopes were conducted using a Nu Instruments large-radius mass spectrometer at McGill University. All samples were ground using a drill press. Carbon dioxide was released from reaction with phosphoric acid and transferred cryogenically to a dual micro inlet followed by isotopic measurement. The δ ^{13}C data was standardized to Vienna Pee Dee Belemnite (V-PDB) and the δ ^{18}O data to Vienna Standard Mean Ocean Water (V-SMOW).

7. Modeling of the calcite and dolomite carbonatite isotope data using the multicomponent Rayleigh isotopic fractionation model of Ray and Ramesh (2000) to estimate the initial δ ^{13}C and δ ^{18}O isotopic compositions of the carbonatites,

and determine whether the carbon isotopic compositions evolved independently from the oxygen isotopic compositions.

8. Thermodynamic modeling of the fluid-rock interactions leading to the concentration of the REE in minerals such as monazite-(Ce) using Hch equilibrium modeling software. Aliquots of REE-bearing fluid (mainly Ce) were reacted with a phosphate-bearing carbonatite, depositing monazite-(Ce). The NaCl content of the fluid was assumed to be 10 wt.% NaCl and the pH 2.5. Thermodynamic data for monazite-(Ce) were taken from Popa et al. (2007) and for the aqueous REE species from Migdisov et al. (2009). The fluid was assumed to cool from 400°C to 300°C.

Thesis organization

This thesis has been written in manuscript format. In addition to the manuscript, there are two supporting chapters and eleven appendices (A-K). An introductory chapter, including a literature review and description of the research objectives and methodology, explains the motivation of the research. The second chapter is a journal manuscript entitled "The nature and origin of the REE mineralization in the Wicheeda Carbonatite, British Columbia, Canada" and is co-authored by Joel Trofanenko, Anthony E. Williams-Jones, and George J. Simandl. The manuscript describes the geology and mineralogy of the Wicheeda Carbonatite and fenite, and presents whole rock chemical data, mineral chemical data and whole rock carbon and oxygen isotopic data. The information is used to develop a model for the formation of the intrusion and the processes responsible for mineralization. Chapter 3 summarizes the conclusions of the study, identifies the

contributions to knowledge, and makes recommendations for future work. The appendices comprise: A. Locations of outcrops sampled; B. Locations of drill cores sampled; C. Counting times and standards used for each element analyzed with the electron microprobe; D. Results of electron microprobe analyses of dolomite; E. Results of electron microprobe analyses of biotite and biotite; F. Results of electron microprobe analyses of amphibole; G. Results of electron microprobe analyses of pyroxene; H. Results of electron microprobe analyses of albite and potassium feldspar; I. Results of electron microprobe analyses of apatite; J. Results of electron microprobe analyses of bastnäsite-(Ce), parisite-(Ce), synchysite-(Ce), cordylite-(Ce), and ancylite-(Ce); K. Results of electron microprobe analyses of monazite.

References

Andersen, T., 1984, Secondary processes in carbonatites - petrology of rodberg (hematite-calcite-dolomite carbonatite) in the Fen Central Complex, Telemark (South-Norway): Lithos, v. 17, p. 227-245.

Armstrong, J. E., Hoadley, J. W., Muller, J. E., and Tipper, H. W., 1969, Geology, McLeod Lake Map Area (93J), Geological Survey of Canada, p. Map 1204A.

Arzamastsev, A. A., Bea, F., Glaznev, V. N., Arzamastseva, L. V., and Montero, P., 2001, The Kola alkaline province in the Paleozoic: Evaluation of primary mantle magma composition and magma generation conditions: Russian Journal of Earth Sciences, v. 3, p. 1-32.

Barth, T. F. W., and Ramberg, I. B., 1966, The Fen circular complex: New York, NY, Interscience.

Betmanis, A. I., 1987, Report on geological, geochemical and magnetometer surveys on the Prince and George groups, cariboo mining division, in British Columbia Ministry of Energy, Mines, and Petroleum Resources, p. 1-86.

Brøgger, W. C., 1921, Die Eruptivgesteine des Kristianiagebietes. IV: Das fengebiet in Telemark, Norwegen: Vit. Seslk. Skr. I Mat. Nat. Klasse, v. 1.

Brooker, R. A., 1998, The effect of CO_2 saturation on immiscibility between silicate and carbonate liquids: an experimental study: Journal of Petrology, v. 39, p. 1905-1915.

Bruland, T., 2011, 2010 Diamond drilling on Carbo rare earth element property, p. 5-31.

Castor, S. B., 2008, The Mountain Pass rare-earth carbonatite and associated ultrapotassic rocks, California: Canadian Mineralogist, v. 46, p. 779-806.

Castor, S. B., and Hedrick, J. B., 2006, Rare earth elements, Society for Mining, Metallurgy and Exploration.

Chakhmouradian, A. R., and Zaitsev, A. N., 2012, Rare earth mineralization in igneous rocks: sources and processes, Elements, 8, p. 347-353.

Chao, E. C. T., Back, J. M., Minkin, J. A., Tatsumoto, M., Junwen, W., Conrad, J. E., and Mckee, E. H., 1997, The sedimentary Carbonate-Hosted Giant Bayan Obo REE-Fe-Nb Ore Deposit of Inner Mongolia, China: A Cornerstone Example for Giant Polymetallic Ore Deposits of Hydrothermal Origin: US Geological Survey Bulletin 2143.

Currie, K. L., and Ferguson, J., 1971, A study of fenitization around the alkaline carbonatite complex at Callander Bay, Ontario, Canada: Canadian Journal of Earth Sciences, v. 8, p. 498-517.

Dalsin, M. L., and Groat, L. A., 2011, The Geology and Mineralogy of the Carbo Property, Wicheeda Carbonatite Complex, BC, Roundup 2011: Vancouver, BC.

Dalsin, M. L., Groat, L. A., Creighton, S., and Evans, R. J., 2015, The mineralogy and geochemistry of the Wicheeda Carbonatite Complex, British Columbia Canada: Ore Geology Reviews, v. 64, p. 523-542.

Doroshkevich, A. G., Viladkar, S. G., Ripp, G. S., and Burtseva, M. V., 2009, Hydrothermal REE mineralization in the Amba Dongar carbonatite complex, Gujarat, India: The Canadian Mineralogist, v. 47, p. 1105-1116.

Drew, L. J., Qingrun, M., and Weijun, S., 1990, The Bayan Obo iron rare-earth niobium deposits, Inner Mongolia, China: Lithos, v. 26, p. 43-65.

Eggler, D. H., 1974, Effect of CO2 on the melting of peridotite: Carnegie Institution of Washington Yearbook, v. 73, p. 215-224.

Eggler, D. H., 1978, The effect of CO2 upon partial melting of peridotite in the system Na_2O-CaO-Al_2O_3-MgO-SiO_2-CO_2 to 35 kb, with an analysis of melting in a peridotite-H_2O-CO_2 system: American Journal of Science, v. 278, p. 305-343.

Eggler, D. H., 1989, Carbonatites, primary melts, and mantle dynamics, in Bell, K., ed., Carbonatites, Genesis and Evolution: London, UK, Unwin Hyman Ltd., p. 561-579.

Fortin-Bélanger, M., 1977, Le complexe annulaire, à carbonatite de St.-Honoré (P.Q., Canada) et sa minéralisation à niobium: étude pétrographique et géochimique, Université Claude Bernard, 308 p.

Fournier, A., 1993, Magmatic and hydrothermal controls of LREE mineralization of the St. Honoré carbonatite, Quebec: Unpub. Manuscript thesis, McGill University, 147 p.

Freestone, I. C., and Hamilton, D. L., 1980, The role of liquid immiscibility in the genesis of carbonatites - an experimental study: Contributions to Mineralogy and Petrology, v. 73, p. 105-117.

Garson, M. S., 1965, Carbonatites in Southern Malawi: Geological Survey Department Bulletin, v. 15, p. 128.

Gittins, J., Beckett, M. F., and Jago, B. C., 1990, Composition of the fluid phase accompanying carbonatite magma: a critical examination: American Mineralogist, v. 75, p. 1106-1109.

Gittins, J., and Harmer, R. E., 1997, What is ferrocarbonatite? A revised classification: Journal of African Earth Sciences, v. 25, p. 159-168.

Grenier, L., Tremblay, J.-F., and Sirois, R., 2013, NI 43-101 Technical report, surface diamond drilling exploration program for rare earth elements, IAMGOLD Corporation, p. 161.

Griffin, W. L., and Taylor, P. N., 1975, The Fen Damkjernite: Petrology of a "central-complex kimberlite": Physics and Chemistry of the Earth, v. 9, p. 163-177.

Hamilton, D. L., Bedson, P., and Esson, J., 1989, The behaviour of trace elements in the evolution of carbonatites, in Bell, K., ed., Carbonatites, Genesis and Evolution: London, UK, Unwin Hyman Ltd.

Harmer, R. E., and Gittins, J., 1998, The case for primary, mantle-derived carbonatite magma: Journal of Petrology, v. 39, p. 1895-1903.

Hatch, G. P., 2012, Dynamics in the global market for rare earths, Elements, 8, Mineralogical Society of America, p. 341-346.

Hu, Z. G., S., 2008, Upper crustal abundances of trace elements: A revision and update: Chemical Geology, v. 253, p. 205-221.

Kjarsgaard, B. A., 1998, Phase relations of a carbonated high-CaO nephelinite at 0.2 and 0.5 GPa: Journal of Petrology, v. 39, p. 2061-2075.

Kjarsgaard, B. A., and Hamilton, 1988, Liquid immiscibility and the origin of alkali-poor carbonatites: Mineralogical Magazine, v. 52, p. 43-55.

Kremers, H. E., 1958, Rare earths: Engineering and Mining Journal, v. 159, p. 145-146.

Kresten, P., 1976, A magmatic survey of the Alno Complex: Geologiska Foreningens I Stockholm Forhandlingar, v. 98, p. 361-362.

Kresten, P., 1979, The Alnö complex: discussion of the main features, bibliography and excursion guide, Nordic Carbonatite Symposium, p. 67.

Kresten, P., 1988, The chemistry of fenitization: examples from Fen, Norway: Chemical Geology, v. 68, p. 329-349.

Kresten, P., Printzlau, I., Rex, D. C., Vartiainen, H., and Woolley, A. R., 1977, New ages of carbonatitic and alkaline ultramafic rocks from Sweden and Finland: Geologiska Foreningens I Stockholm Forhandlingar, v. 99, p. 62-65.

Kynicky, J., Smith, M. P., and Xu, C., 2012, Diversity of rare earth deposits: The key example of China, Elements, 8, p. 361-367.

Lagache, M., and A. Weisbrod, 1977, The system: two alkali feldspars-KCl-NaCl-H2O at moderate to high temperatures and low pressures: Contributions to Mineralogy and Petrology, v. 62, p. 77-101.

Lane, R., 2009, Diamond drilling report on the Wicheeda property, p. 1-196.

Lane, R., 2010, 2009 Diamond drilling report on the Wicheeda rare earth property, p. 1-29.

Le Bas, M. J., 1977, Carbonatite-Nephelinite Volcanism: London, Wiley.

Le Bas, M. J., 1981, Carbonatite magmas: Mineralogical Magazine, v. 44, p. 133-140.

Le Bas, M.J., 2008, Fenite associated with carbonatites: Canadian Mineralogist, v. 46, p. 915-932.

Lee, W.-J., and Wyllie, P. J., 1994, Experimental data bearing on liquid immiscibility, crystal fractionation, and the origin of calciocarbonatites and natrocarbonatites: International Geology Reviews, v. 36, p. 797-819.

Lee, W.-J., and Wyllie, P. J., 1998, Processes of crustal carbonatite formation by liquid immiscibility and differentiation, elucidated by model systems: Journal of Petrology, v. 39, p. 2005-2013.

Mäder, U. K., and Greenwood, H. J., 1987, Carbonatites and related rocks of the Prince and George claims, northern rocky mountains (93I; 93J), Geological Fieldwork 1987, British Columbia Ministry of Energy, Mines and Petroleum Resources.

McKie, D., 1966, Fenitization, in Tuttle, O. F. G., J., ed., Carbonatites: New York, NY, Interscience, p. 261-294.

Meen, J. K., Ayers, J. C., and Fregeau, E. J., 1989, A model of upper mantle metasomatism by carbonated alkaline melts: trace element and isotopic compositions of mantle source regions of carbonatite and other continental igneous rocks, in Bell, K., ed., Carbonatites, Genesis and Evolution: London, UK, Unwin Hyman Ltd., p. 464-495.

Migdisov, A., and Williams-Jones, A. E., 2004, A spectrophotometric study of Palladium (II) complexation in chloride solutions: Geochimica et Cosmochimica Acta, v. 68, p. A289.

Migdisov, A., and Williams-Jones, A. E., 2006, An experimental study of solubility and speciation of NdF3 in F-bearing aqueous solutions: Geochimica et Cosmochimica Acta, v. 70, p. A419.

Migdisov, A., and Williams-Jones, A. E., 2007, An experimental study of the solubility and speciation of neodymium (III) fluoride in F-bearing aqueous solutions: Geochimica et Cosmochimica Acta, v. 71, p. 3056-3069.

Migdisov, A., Williams-Jones, A. E., van Hinsberg, V., and Salvi, S., 2011, An experimental study of the solubility of baddeleyite (ZrO_2) in fluoride-bearing solutions at elevated temperature: Geochimica et Cosmochimica Acta, v. 75, p. 7426-7434.

Migdisov, A., Williams-Jones, A. E., and Wagner, T., 2009, An experimental study of the solubility and speciation of the Rare Earth Elements (III) in fluoride- and chloride-bearing aqueous solutions at temperatures up to 300 degrees C: Geochimica et Cosmochimica Acta, v. 73, p. 7087-7109.

Mitchell, R. H., 2005, Carbonatites and carbonatites and carbonatites: Canadian Mineralogist, v. 43, p. 2049-2068.

Sims, J., and Blackman, B., 2012, Molycorp's Rare Earth Reserves at Mountain Pass Increase by 36%, Molycorp. Accessed 25 November 2014. http://www.molycorp.com/molycorps-rare-earth-reserves-at-mountain-pass-increase-by-36/

Moore, M., Chakhmouradian, A. R., Mariano, A. N., and Sidhu, R., 2015, Evolution of rare-earth mineralization in the Bear Lodge carbonatite, Wyoming: Mineralogical and isotopic evidence: Ore Geology Reviews, v. 64, 499-521.

Morogan, V., 1994, Ijolite versus carbonatite as sources of fenitization: Terra Nova, v. 6, p. 166-176.

Morogan, V., and A.R. Woolley, 1988, Fenitization at the Alno carbonatite complex, Sweden; distribution, mineralogy and genesis: Contributions to Mineralogy and Petrology, v. 100, p. 169-182.

Noble, A. C., Pickarts, J. T., and Larsen, R. K., 2013, Technical report on the mineral reserves and resources and development of the Bull Hill Mine, Rare Element Resources, p. 1-207.

Pearson, R. G., 1963, Hard and soft acids and bases: Journal of the American Chemical Society, v. 85, p. 3533-3539.

Popa, K., Konings, R. J. M., and Geisler, T., 2007, High-temperature calorimetry of $(La_{1-x}Ln_x)PO_4$ solid solutions: Journal of Chemical Thermodynamics, v. 39, p. 236-239.

Ray, J. S., and Ramesh, R., 2000, Rayleigh fractionation of stable isotopes from a multicomponent source: Geochimica et Cosmochimica Acta, v. 64, p. 299-306.

Roelofsen, J. N., 1997, The primary and secondary mafic silicates of two alkaline anorogenic complexes: Strange Lake (Quebec-Labrador) and Amba Dongar (Gujarat, India), McGill University, 321 p.

Rubie, D. C., and Gunter, W. D., 1983, The role of speciation in alkaline igneous fluids during fenite metasomatism: contributions to mineralogy and petrology, v. 82, p. 165-175.

Sæther, E., 1957, The alkaline rock province of the Fen area in southern Norway: Det Klonglige Norske Videnskabsselskaps Skrifter, v. 1, p. 150.

Slagel, M., 1997, Miscible silicate-carbonate liquids in the system K_2O-CaO-MgO-Al_2O_3-SiO_2-H_2O-CO_2, Geological Association of Canada-Mineralogical Association of Canada Ottawa '97, p. A-139.

Smith, M. P., and Henderson, P., 2000, Preliminary fluid inclusion constraints on fluid evolution in the Bayan Obo Fe-REE-Nb deposit, inner Mongolia, China: Economic Geology, v. 95, p. 1371-1388.

Sweeney, R. J., 1994, Carbonatite melt compositions in the earth's mantle: Earth and Planetary Science Letters, v. 128, p. 259-270.

Taylor, G. C., and Stott, D. F., 1979, Geology, Monkman Pass Map Area, British Columbia (93I), Geological Survey of Canada, p. Open File Map 630.

USGS, 2014, Mineral commodity summaries 2014, U.S. Geological Survey, p. 131-132.

Vartiainen, H., and Woolley, A. R., 1976, The petrography, mineralogy, and chemistry of the fenites of the Sökli carbonatite intrusion, Finland: Geological Survey of Finland Bulletin, v. 280.

Veksler, I. V., Dorfman, A. M., Dulski, P., Kamenetsky, V. S., Danyushevsky, L., Jeffries, T., and Dingwell, D. B., 2012, Partitioning of elements between silicate melt and miscible fluoride, chloride, carbonate, phosphate, and sulfate melts, with

implications to the origin of natro-carbonatite: Geochimica et Cosmochimica Acta, v. 79, p. 20-40.

Verschure, R. H., and Maijer, C., 1984, Pluri-metasomatic resetting of Rb-Sr whole-rock systems around the Fen peralkaline-carbonatitic ring complex, Telemark, south Norway: Terra Cognita, v. 4, p. 191-192.

Viladkar, S. G., 1981, The carbonatites of Amba Dongar, Gujarat, India: Geological Society of Finland Bulletin, v. 53, p. 17-28.

Viladkar, S. G., 1986, Fenitization at the Amba Dongar carbonatite-alkalic complex, India: Proceedings NEMIRAM (New Minerals and Raw Materials) Symposium, Czechoslovakia, 1986, p. 170-189.

von Eckermann, H., 1948, The alkaline district of Alnö island: Sveriges Geologiska Undersökning, v. 36, p. 1-176.

Williams-Jones, A. E., Migdisov, A. A., and Samson, I. M., 2012, Hydrothermal Mobilisation of the Rare Earth Elements - a Tale of "Ceria" and "Yttria", Elements, p. 26.

Williams-Jones, A. E., and Palmer, D. A. S., 2002, Fluid evolution of the Amba Dongar carbonatite complex, India: Chemical Geology, v. 185, p. 283-301.

Woolley, A. R., 1982, A discussion of carbonatite evolution and nomenclature, and the generation of sodic and potassic fenites: Mineralogical Magazine, v. 46, p. 13-17.

Woolley, A. R., and Kempe, D. R. C., 1989, Carbonatites: nomenclature, average chemical compositions, and element distribution, in Bell, K., ed., Carbonatites, Genesis and Evolution: London, UK, Unwin Hyman Ltd., p. 1-13.

Wu, C., 2007, Bayan Obo controversy: carbonatites versus Iron Oxide-Cu-Au-(REE-U): Resource Geology, v. 58, p. 348-354.

Wyllie, P. J., and Tuttle, O. F., 1960, The system $CaO-CO_2-H_2O$ and the origin of carbonatites: Journal of Petrology, v. 1, p. 1-46.

Zaitsev, A. N., Wall, F., and Le Bas, M. J., 1998, REE-Sr-Ba minerals from the Khibina carbonatites, Kola peninsula, Russia: their mineralogy, paragenesis and evolution: Mineralogical Magazine, v. 62, p. 225-250.

Zaitsev, A. N., Williams, C. T., Jeffries, T. E., Strekopytov, S., Moutte, J., Ivashchenkova, O. V., Spratt, J., Petrov, S. V., Wall, F., Seltmann, R., and Borozdin, A. P., 2014, Rare earth elements in phoscorites and carbonatites of the

Devonian Kola Alkaline Province, Russia: Examples from Kovdor, Khibina, Vuoriyarvi and Turiy Mys complexes: Ore Geology Reviews, v. 61, p. 204-225.

CHAPTER II: Journal Manuscript

The nature and origin of the REE mineralization in the Wicheeda Carbonatite, British Columbia, Canada

Joel Trofanenko, Anthony E. Williams-Jones, and George J. Simandl

Joel Trofanenko and Anthony E. Williams-Jones
Earth and Planetary Sciences, McGill University
3450 University Street, Montreal, QC
Canada H3A 0E8

George J. Simandl
British Columbia Geological Survey
Ministry of Energy and Mines, Victoria, BC
Canada V8W 9N3

Abstract

The Wicheeda Carbonatite is a small plug that hosts relatively high-grade LREE mineralization in the British Columbia alkaline province. It was emplaced within metasedimentary rocks belonging to the Kechika Group, which have been altered to potassic fenite near the intrusion and sodic fenite at greater distances from it. The intrusion comprises a ferroan dolomite carbonatite core, which passes outwards gradationally into calcite carbonatite. The potentially economic REE mineralization is hosted by the dolomite carbonatite. Three types of dolomite have been recognized. Dolomite 1 constitutes the bulk of the dolomite carbonatite, Dolomite 2 replaced Dolomite 1 near veins and vugs and Dolomite 3 occurs in veins in and vugs together with the REE mineralization. Carbon and oxygen isotope ratios indicate that the calcite carbonatite crystallized from a magma of mantle origin, that Dolomite 1 is of primary igneous origin, that Dolomite 2 has a largely igneous signature with a small hydrothermal input and that Dolomite 3 is of hydrothermal origin. The REE minerals comprise REE-fluorocarbonates, ancylite-(Ce), and monazite-(Ce) and in addition to Dolomite 3, also occur with barite, molybdenite, pyrite and thorite. Minor concentrations of niobium are present as magmatic pyrochlore in the calcite carbonatite.

A model is proposed in which calcite carbonatite was the earliest phase to crystallize and followed by dolomite carbonatite. During crystallization of the latter, an aqueous-carbonic fluid was exsolved, which mobilized the REE as chloride complexes into vugs and fractures in the dolomite carbonatite, where they precipitated, largely in response to the increase in pH that accompanied fluid-rock interaction. These fluids altered the host

metasedimentary rock to potassic fenite adjacent to the carbonatite and distal to it, they

mixed with formational waters to produce sodic fenite.

Introduction

It has been long known that carbonatites are enriched in the rare earth elements (REE), and in some cases host economic or potentially economic concentrations of these metals. Examples of the latter include Mountain Pass (Castor, 2008), Maoniuping (Xu, 2003; 2004; Kynicky et al., 2012), Kangankunde (Wall and Mariano, 1996), St. Honoré (Fortin-Bélanger, 1977; Fournier, 1993), Amba Dongar (Doroshkevich et al., 2009), and Bear Lodge (Moore et al., 2015). In rare cases, such as the Mountain Pass deposit, textural relationships indicate that the REE mineralization is magmatic in origin (Castor, 2008), but more commonly the available evidence suggests that it was the product of both magmatic and hydrothermal processes (e.g., Amba Dongar, Doroshkevich et al., 2009; Bear Lodge, Moore et al., 2015). In the latter deposits, the carbonatites were strongly overprinted by hydrothermal fluids resulting in remobilization and precipitation of the REE in vug- and vein-hosted assemblages. Although it is widely believed that these fluids originate from the carbonatite (Currie and Ferguson, 1971; Kresten 1988; Wyllie, 1989; Gittins et al., 1990) and fluid inclusion studies (e.g., Bühn and Rankin, 1999; Bühn et al., 2002; Williams-Jones and Palmer, 2002) have documented the nature of the fluids exsolving from carbonatites, the controls on the REE mineralization are poorly understood. In many carbonatite-hosted deposits, there is a close association of the REE mineralization with fluorite (e.g., Amba Dongar, Doroshkevich et al., 2009; Bear Lodge, Moore et al., 2015), and this has led some authors (Möller et al., 1980; Salvi and Williams-Jones, 1990; Williams-Jones et al., 2000) to suggest that the REE are transported as fluoride complexes, particularly as such complexes are known to be extremely stable (Migdisov et al., 2009). However, recent modeling has shown that

33

transport of REE as fluoride complexes is not feasible because of the low activity of fluoride ions at low pH due to their association in the weak acid, HF, and the very low solubility of REE minerals at higher pH (Williams-Jones et al., 2012). This modeling showed that REE-chloride complexes might be a plausible alternative transport medium for systems in which chlorinity is high, and that for such systems increasing pH and/or decreasing temperature could lead to REE mineralization. They also noted that the REE form strong complexes with sulphate ions and that such complexation could be another means of REE transport. Fluid inclusion studies of the Amba Dongar carbonatite show that fluids exsolving from carbonatites (aqueous-carbonic) can have high concentrations of both chloride and sulphate ions (Williams-Jones and Palmer, 2002). The fluids in this case were responsible for fenitization and likely also produced the REE mineralization, i.e., REE-fluorocarbonates that are associated with barite, fluorite, and quartz (Doroshkevich et al., 2009). For Bear Lodge, it has been proposed that the REE were concentrated as magmatic burbankite, and remobilized by carbo-hydrothermal fluids enriched in F^-, CO_2^-, and SO_4^{2-}, which deposited ancylite-(Ce), REE-fluorocarbonates, and monazite-(Ce) (Moore et al., 2015).

The Wicheeda Carbonatite, which is located in the Alkaline Igneous Province of British Columbia, Canada (Fig. 1) and is the subject of this paper, contains potentially exploitable concentrations of the REE (Pell, 1994; Lane, 2009; 2010). Like many intrusions in this Province (Pell, 1994), the Wicheeda Carbonatite has an extensive fenitization halo. Moreover, a preliminary study suggests that the REE mineralization may be hydrothermal in origin (Lane, 2009). The Wicheeda Carbonatite therefore

34

presents an excellent opportunity to better understand the controls on hydrothermal carbonatite-hosted REE mineralization. The intrusion (Fig. 1) was first described in British Columbia Geological Survey reports (Mäder and Greenwood, 1987; Pell, 1994) and explored by Teck Explorations Ltd. over 20 years ago (Betmanis, 1987), but received little attention until 2008, when Spectrum Mining Corp explored it by a variety of methods, including drilling. They reported that the carbonatite contains a resource of 11.3 million tons grading 1.95 wt.% TREO (Lane, 2010), making it the best prospect for an economic REE deposit in British Columbia (Pell, 1994; Lane, 2009, 2010). The REE mineralization is concentrated mainly in the carbonatite, largely as carbonate minerals, although it is also observed locally in the fenite. Carbonatite also occurs to the southeast of the main intrusion, as dikes and sills associated with alkaline igneous intrusions. Canadian International Minerals Inc. explored these bodies and reported the occurrence in them of sporadic carbonatite-hosted REE mineralization.
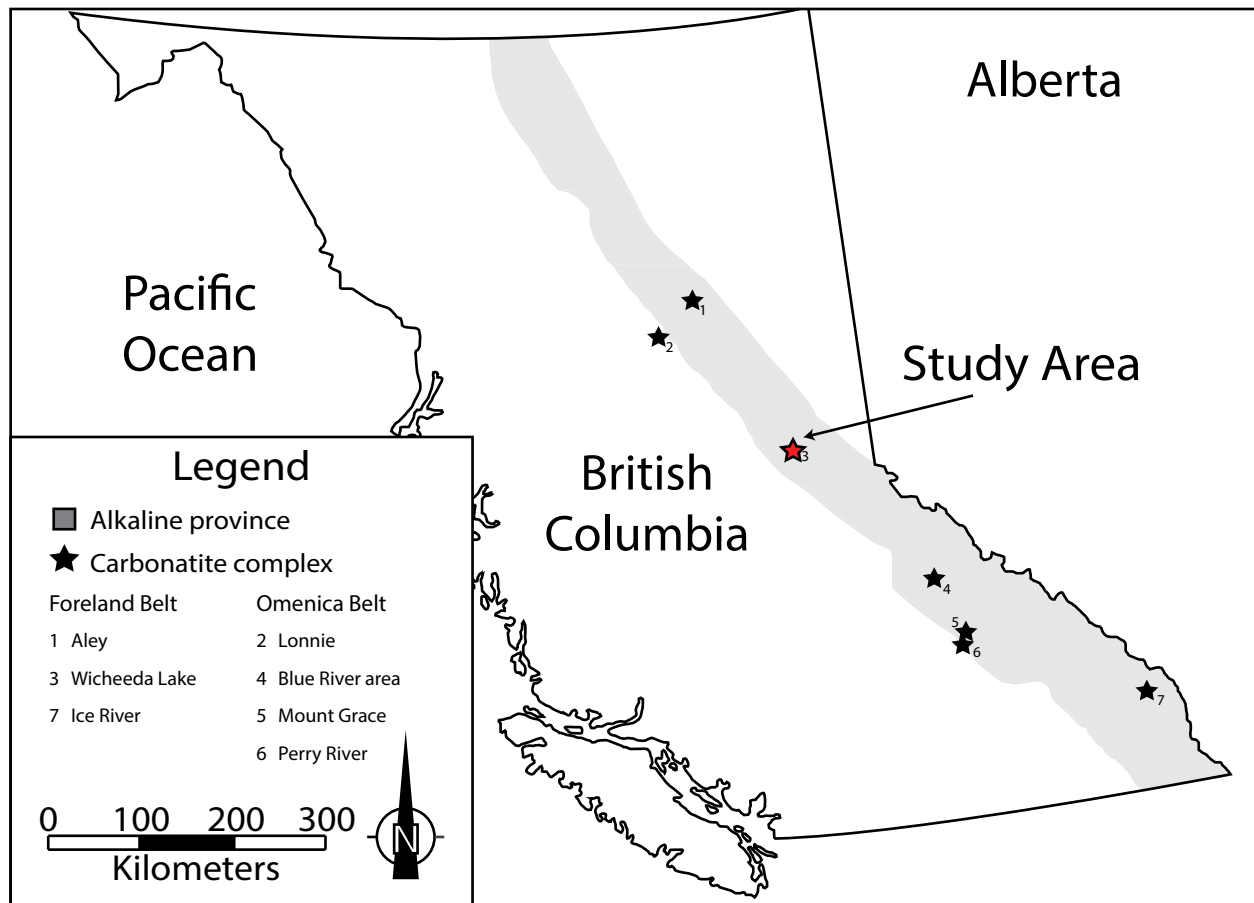
Fig. 1: A map of British Columbia showing the location of the British Columbia alkaline province and the most important rare-metal deposits.

In this paper, we use a combination of field and laboratory techniques to investigate the nature and genesis of the REE mineralization in the main Wicheeda Carbonatite. The scope of work included field mapping, outcrop description, drill core logging and sampling of the representative lithologies, optical and scanning electron microscopy, chemical analyses (including isotopic) of the bulk rock and minerals, and thermodynamic modeling. The results show that the REE mineralization is hydrothermal in origin. We have developed a model in which the REE were concentrated in fluids released from the carbonatite magma and precipitated REE carbonates in response to decreasing temperature and the increase in pH that accompanied interaction of the fluids with the crystallized carbonatite.

Geological Setting

The Wicheeda Carbonatite was emplaced in the Kechika Group metasedimentary rocks of the Foreland belt of the Canadian Cordillera, an imbricated fold and thrust assemblage of passive margin strata deposited along the ancestral margin of North America. The Foreland Belt contains a large alkaline province (Fig. 1), which stretches from the Canadian Cordillera to the southwestern United States (Millonig et al., 2012). It hosts the Aley, Ice River, Bear Paw, Rock Canyon, Frenchman Cap Dome, and Wicheeda alkaline complexes (Pell, 1994; Millonig et al., 2012; Dalsin et al., 2015). Among them, the Aley (niobium), Rock Canyon (REE), and Wicheeda (REE) alkaline complexes contain the highest concentrations of niobium and the REE.

The rocks underlying the alkaline province belong to the Middle Proterozoic Purcell Supergroup and comprise primary clastic and carbonate rocks >20 km thick deposited

between 1700 and 780 Ma (Monger et al., 1972; Sears and Price, 1978; Monger and Price, 1979). Late Proterozoic (780-570 Ma) strata comprising gritty feldspathic sandstones, locally also volcanic rocks, and carbonate rocks lie unconformably over the Purcell Supergroup. They show evidence of having been subjected to glacial activity, and are disconformably overlain by Early Cambrian to Late Jurassic sedimentary rocks (Monger, 1989). The latter comprise thin platform carbonates, which pass into thin, deeper-water argillaceous shales deposited along a complex passive margin.

On the basis of U-Pb and Th-Pb age determinations conducted on samples from various localities within the alkaline province, the latter is interpreted to have formed during three episodes of magmatism (e.g., Millonig et al., 2012). The first episode (800-700 Ma) coincided with the breakup of Rodinia, and the other two (500 Ma, 360-340 Ma) with subsequent periods of extension. Most of the alkaline complexes hosting economic mineralization were emplaced during the youngest of these three episodes.
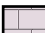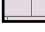
The rocks surrounding the Wicheeda Carbonatite and nearby dikes and sills comprise steeply dipping limestone, marble, siltstone, argillite, and calcareous sedimentary rocks belonging to the Upper Cambrian to Lower Ordovician Kechika Group (Fig. 2; Armstrong et al., 1969; Taylor and Stott, 1979). These rocks are in fault contact with Cambrian to Devonian carbonates, slates, and siltstones east of the complex, and to the west are in fault contact (McLeod Fault) with Upper Proterozoic to Permian Gog Group quartzites and unassigned Devonian to Permian felsic volcanic rocks (Lane, 2009). The faults bound the McGregor plateau in which the Wicheeda Complex is located; the

eastern fault is an extension of the Rocky Mountain Trench, and is the dominant structural feature in the area (Armstrong et al., 1969).
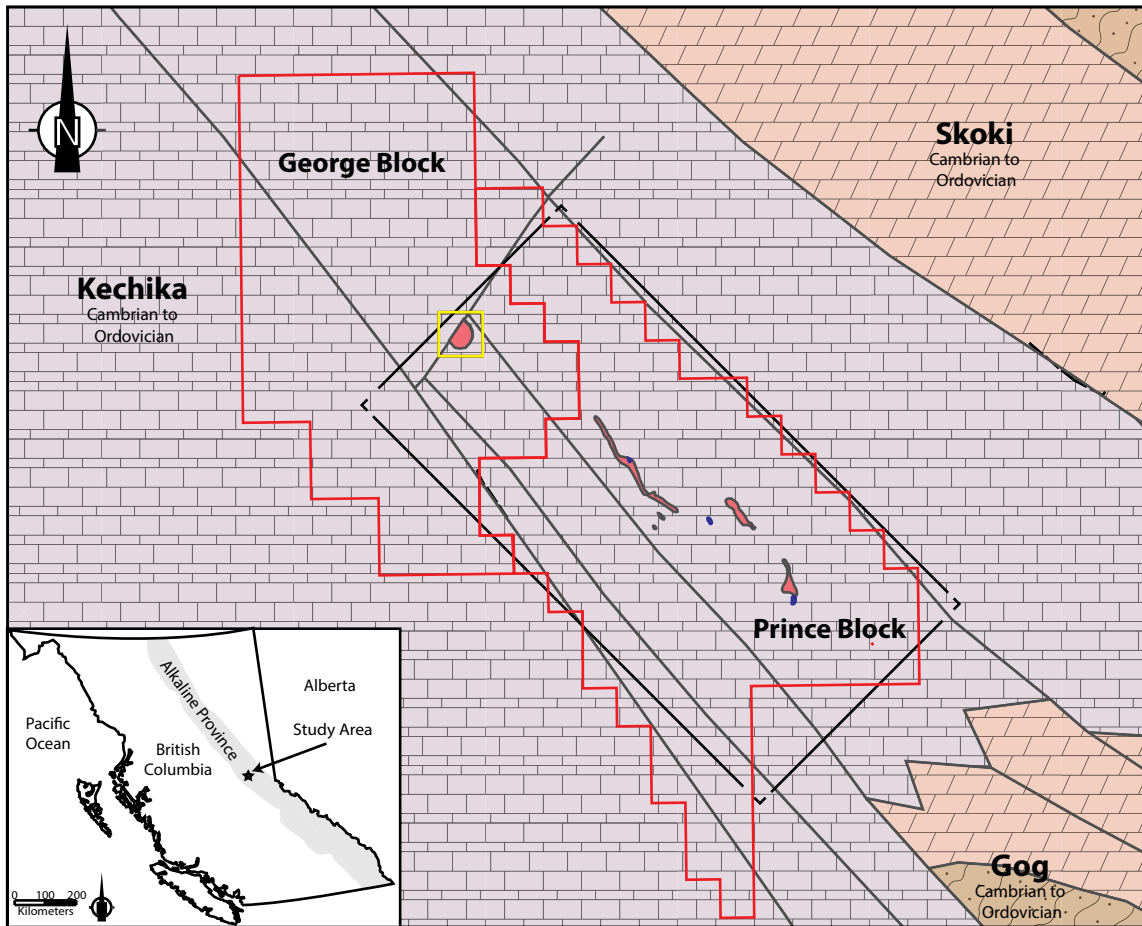
Stratified Rocks

Cambrian to Ordovician

Kechika Group
Limestone, marble, shale

Skoki Formation
Dolomitic sedimentary rocks

Upper Proterozoic to Cambrian

Gog Group
Quartz arenite, clastic sedimentary rocks

Intrusive Rocks

Carboniferous

Wicheeda Carbonatite
Calcite to dolomite carbonatite

Syenite
K-feldspar bearing syenite

— Fault

☐ Study Area

☐ Outline of exploration claims

⌐ ⌐ Outline of aeromagnetic map
⌙ ⌙ (Fig. 3)

0   5

Kilometers

Fig. 2: The location of the Wicheeda carbonatite and other nearby carbonatite and alkaline silicate dykes and sills within the Foreland belt sedimentary succession. The locations of the George and Prince claim blocks are outlined as are the limits of the aeromagnetic map shown (rectangle outlined with black dashed lines) in Figure 3. The inset image shows the location of the Wicheeda carbonatite in the British Columbia alkaline province.

The Wicheeda Carbonatite explored by Spectrum Mining Corporation, and the focus of the present study, is a 250 m diameter body inferred to be a plug, which was described by Mäder and Greenwood (1988) as a uniform ankerite carbonatite containing potassium feldspar and a "parisite-like" rare earth carbonate mineral. The intrusion is steeply dipping to the west and is in contact with fenite (Lane, 2009; 2010).

Exploration History

There has been limited exploration of the Wicheeda Complex until recently. A prospector, Kol Lovang, first sampled the area in the 1970s and staked claims based on elevated concentrations of several base metals. However, no follow up work was conducted and the claims were permitted to lapse. In the 1980s Teck Explorations Ltd. assayed Lovang's samples and obtained elevated niobium values, prompting the company to conduct a preliminary exploration program including geological and geophysical mapping, soil sampling, trenching, and stream sediment sampling. Based on the results of this exploration, Teck identified areas for further exploration and staked several blocks of claims including the George and Prince blocks, which are presently held by Spectrum Mining Corp. and Canadian International Minerals Inc., respectively (Fig. 2). Test pits and trenches were blasted on both claims. Soil samples analyzed from the George Grid yielded high TREE concentrations (up to 4.2 wt.%) and Nb concentrations up to 0.07 wt.%, whereas the Prince Grid samples contained low TREE concentrations (<0.2 wt.%) but higher Nb concentrations (up to 0.24 wt.%).

In 2008, Spectrum Mining Corp. began a diamond drilling exploration program on the Wicheeda Carbonatite (Lane, 2009). Four holes were drilled from a single drill set-up in

41

a fan-like pattern, with a total length of 866 m, and intersected dolomite carbonatite at surface, and carbonatite breccia and fenite at depth. One hole terminated in calcite carbonatite. Drill core logging and geochemical analyses showed that the dolomite carbonatite is strongly REE-enriched, preferentially in the light REE (LREE). Anomalous concentrations of Mo, Ba, Sr, Mn, As, P, Y, Th were observed (Lane, 2009). Petrographic examination of the dolomite carbonatite revealed the presence of accessory potassium feldspar and albite, and traces of niobian rutile, biotite, pyrochlore, thorite, pyrite, galena, and molybdenite (Lane, 2009). The dominant REE minerals identified were Ca-REE-fluorocarbonates interpreted to be parisite-(Ce), röntgenite-(Ce), or synchysite-(Ce); monazite-(Ce) was also observed. Allanite and euxenite were identified in one sample.

Additional drilling (14 holes for a total length of 1835 m) was carried out in 2009 from three drill sites, two within the Wicheeda Carbonatite and one located on a much smaller intrusion 400 m north of the Wicheeda Carbonatite. The drill holes within the Wicheeda Carbonatite, which were mainly inclined, intersected REE-mineralized dolomite carbonatite in their upper parts, calcite carbonatite at depth, and in most cases terminated in fenite (Lane, 2010). A single, northerly inclined drill hole (WI09-14) terminated in calcite carbonatite barren of REE. The three holes drilled to the north of the Wicheeda Carbonatite all intersected coarse-grained calcite carbonatite but no significant REE mineralization (<1% TREO). Based on the results of the drilling in 2008 and 2009, the Wicheeda Carbonatite was estimated to contain a resource of 11.3 million tons grading

1.95% Ce+La+Nd, mainly as coarse-grained bastnäsite-(Ce) and monazite-(Ce) (Lane, 2010).

In July 2010, Canadian International Minerals Inc. conducted a 566.1 line-km Helicopter-Borne AeroTEM System Electromagnetic, Magnetic, and Radiometric Survey of the Wicheeda Carbonatite and the Prince claims to the southeast. Magnetic and radiometric anomalies were observed on the George claims, including a small (<150 nT) ellipsoidal anomaly over the Wicheeda Carbonatite and linear anomalies on the Prince claims (Fig. 3; Bruland, 2011). Diamond drilling on the Prince claims by Canadian International Minerals Inc. revealed a series of carbonatite dikes and veins, and mafic dikes (Bruland, 2011; Dalsin and Groat, 2011). The best REE intersection was 4.68 wt.% TREO over 0.9 m (largely as Ca-REE-fluorocarbonates, Ba-REE-fluorocarbonates, ancylite-(Ce), monazite-(Ce), euxenite-(Y), and allanite-(Ce)) in calcio- to ferro-carbonatite dikes.
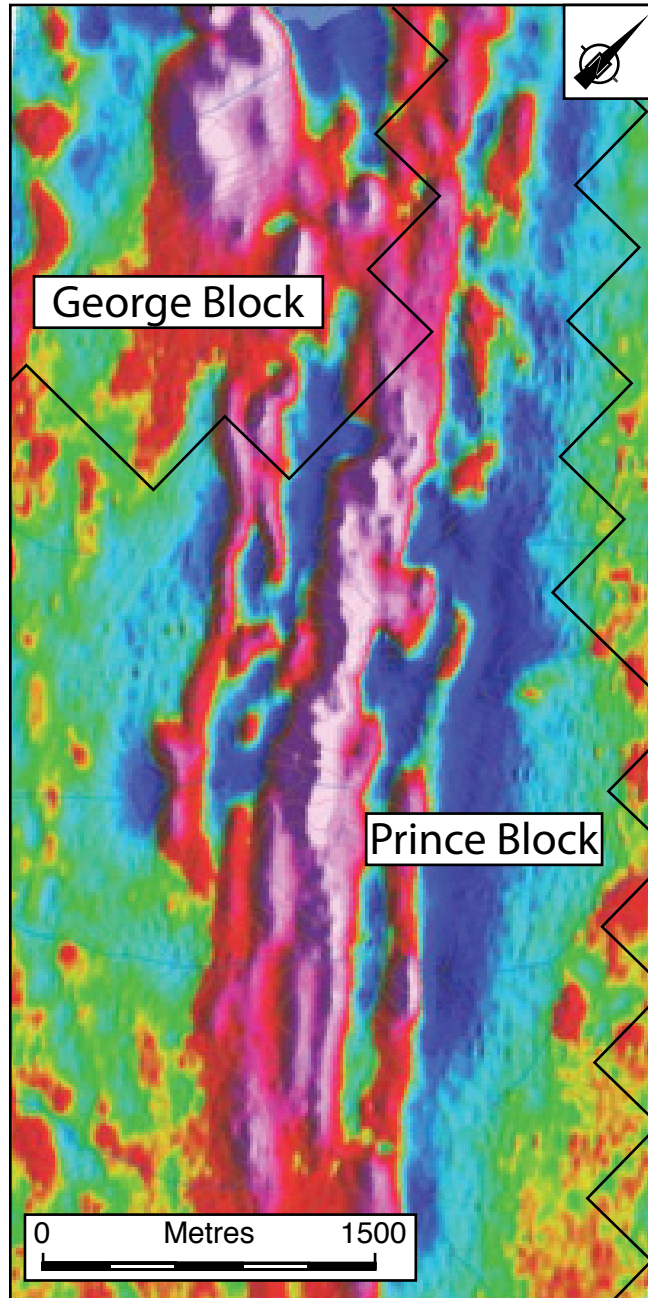
Fig. 3: A magnetic gradient map of the Wicheeda Complex from Bruland (2011a) prepared for Canadian International Minerals Inc. by Aeroquest International Ltd. The exploration rights to the George claims, on which the Wicheeda carbonatite is located, and the neighboring Prince claims are presently held by Spectrum Mining Corp., and Canadian International Minerals Inc., respectively.

Methodology

Bulk Lithochemistry

Samples of outcrop and drill core from four holes drilled by Spectrum Mining Corp. in 2008 and 2009 were analyzed by ALS Minerals in Vancouver for their bulk and trace element compositions. All samples were ground using a steel mill. Samples were subjected to lithium metaborate fusion, digested in 100 mL of 4% nitric acid/ 2% hydrochloric acid and analyzed by Inductively Coupled Plasma Emission Spectrometry for the major elements and Inductively Coupled Plasma Mass Spectrometry for the trace elements. Loss on ignition (LOI) was determined after fusion. The carbon and sulfur contents were determined using the LECO combustion method. The fluorine content was determined for a subset of samples by potassium hydroxide fusion followed by leaching in de-ionized water and analysis by an ion selective electrode. The results are summarized in Table 1.

Table 1: Bulk rock compositions of the Wicheeda carbonatites and fenites.

Sample Number	Lithology	SiO₂	Al₂O₃	Fe₂O₃	MgO	CaO	Na₂O	K₂O	TiO₂	P₂O₅	MnO
						wt.%					
	Detection Limit	0.01	0.01	0.01	0.01	0.01	0.01	0.01	0.01	0.01	0.01
WI-11-02	Dolomite carbonatite	4.45	1.41	8.23	13.55	26.20	0.37	0.47	b.l.	1.38	1.24
WI-11-03	Dolomite carbonatite	4.22	1.16	8.08	13.10	23.80	0.69	0.10	b.l.	0.21	1.07
WI-11-07	Dolomite carbonatite	3.45	0.96	6.31	13.05	23.30	0.66	b.l.	b.l.	1.39	0.82
WI-11-09	Dolomite carbonatite	2.00	0.53	6.91	13.80	21.00	0.26	0.04	b.l.	0.04	0.36
WI-11-11	Dolomite carbonatite	1.05	0.28	9.50	12.30	27.60	0.14	b.l.	b.l.	1.70	1.69
WI-11-12	Dolomite carbonatite	5.42	1.56	6.54	14.25	27.10	0.88	0.04	b.l.	1.44	0.87
WI-11-15	Sodic fenite (veined)	35.50	10.10	4.90	6.35	13.60	5.78	0.29	b.l.	1.78	0.40
WI-13-49	Dolomite carbonatite	3.55	0.31	10.65	12.80	27.90	0.18	0.02	b.l.	0.87	1.91
WI-13-50	Calcite carbonatite	6.33	1.78	4.22	2.24	44.90	0.44	0.70	0.22	2.46	0.83
WI-13-55	Sodic fenite	37.00	6.46	6.20	3.22	22.40	5.45	0.82	0.27	0.42	0.51
WI-13-57	Sodic fenite	20.00	5.86	7.74	8.55	20.80	0.37	4.44	0.20	1.34	1.36
WI-13-62	Dolomite carbonatite	1.48	0.28	10.00	13.40	29.70	0.04	0.13	b.l.	b.l.	1.90
WI-13-63	Potassic fenite	34.40	8.49	9.62	9.36	14.15	0.62	1.42	0.48	0.18	0.57
080105	Dolomite carbonatite	2.07	0.52	8.05	12.70	25.90	0.23	0.12	b.l.	0.17	1.19
080111	Potassic fenite	41.70	11.75	5.40	2.85	14.90	4.73	3.60	0.52	0.16	0.29
080112	Potassic fenite	35.90	7.65	4.52	2.25	22.20	6.09	0.83	0.36	0.30	0.40
080114	Potassic fenite	38.20	11.20	6.24	2.82	17.10	5.09	2.46	0.50	0.27	0.31
080115	Potassic fenite	47.00	13.40	5.04	3.20	13.70	4.05	3.93	0.57	0.16	0.14
090901	Dolomite carbonatite	5.88	0.72	7.86	10.45	24.30	0.25	0.27	b.l.	1.13	1.01
090903	Dolomite carbonatite	12.70	3.66	13.10	9.69	18.85	1.24	1.18	0.49	0.06	1.25
090904	Dolomite carbonatite	14.80	4.62	11.50	10.45	18.75	1.26	1.62	0.53	0.05	1.15
090905	Dolomite carbonatite	1.01	0.22	9.87	12.15	26.50	0.19	b.l.	b.l.	0.14	1.79
090907	Dolomite carbonatite	2.18	0.57	12.75	11.75	27.70	0.35	b.l.	b.l.	0.04	1.73
090909	Dolomite carbonatite	1.02	0.25	11.35	13.10	28.90	0.12	0.03	b.l.	0.18	2.29
090910	Dolomite carbonatite	1.16	0.28	11.30	12.65	29.20	0.18	0.01	b.l.	0.04	1.96
090912	Potassic fenite	22.90	6.45	4.86	2.14	30.30	3.80	0.14	0.24	2.10	0.86
090913	Potassic fenite	25.30	7.26	5.57	1.73	27.10	3.73	1.34	0.46	13.85	0.37
091005	Dolomite carbonatite	0.66	0.14	8.78	12.80	25.80	0.11	b.l.	b.l.	0.06	1.38
091011	Dolomite carbonatite	5.89	1.63	9.61	12.25	25.70	0.86	0.21	0.03	0.11	1.59

Notes:

n.a. Not analysed

b.l. Below detection limits as noted

46

Table 1: Bulk rock compositions of the Wicheeda carbonatites and fenites.

Name	Lithology	BaO	SrO	S Wt.%	C	LOI	F	Nb	Rb ppm	Sr	Ta
	Detection Limit	0.01	0.01	0.01	0.01	0.01	0.01	0.01	0.01	0.01	0.01
WI-11-02	Dolomite carbonatite	0.17	0.06	0.04	10.35	38.8	970	153	n.a.	n.a.	n.a.
WI-11-03	Dolomite carbonatite	0.61	0.17	0.88	10.95	36.8	7000	62.2	n.a.	n.a.	n.a.
WI-11-07	Dolomite carbonatite	0.81	0.2	0.26	10.7	37.6	6060	27.2	n.a.	n.a.	n.a.
WI-11-09	Dolomite carbonatite	b.l.	0.06	1.39	10.55	35.2	14500	191.5	n.a.	n.a.	n.a.
WI-11-11	Dolomite carbonatite	0.04	0.13	0.08	11.3	39.5	150	33.7	n.a.	n.a.	n.a.
WI-11-12	Dolomite carbonatite	0.01	0.05	0.03	11	39.2	720	4	n.a.	n.a.	n.a.
WI-11-15	Sodic fenite (veined)	0.04	0.05	1.05	5	16.3	1150	57	n.a.	n.a.	n.a.
WI-13-49	Dolomite carbonatite	0.03	0.11	0.03	12.2	40.1	b.l.	13.6	n.a.	n.a.	n.a.
WI-13-50	Calcite carbonatite	0.32	1.59	0.61	9.64	32.4	b.l.	2500	n.a.	n.a.	n.a.
WI-13-55	Sodic fenite	0.16	0.48	0.02	4.91	17.5	b.l.	29.3	n.a.	n.a.	n.a.
WI-13-57	Sodic fenite	0.07	0.13	0.05	8.26	27.7	0.01	559	n.a.	n.a.	n.a.
WI-13-62	Dolomite carbonatite	0.03	0.09	0.03	12.9	42.3	b.l.	219	n.a.	n.a.	n.a.
WI-13-63	Potassic fenite	b.l.	0.06	0.98	5.21	18.75	0.01	1720	n.a.	n.a.	n.a.
080105	Dolomite carbonatite	0.16	0.11	0.06	11.3	40.1	n.a.	4.8	2.4	618	b.l.
080111	Potassic fenite	0.26	0.42	0.11	3.25	12.25	n.a.	38.3	162.5	3640	0.6
080112	Potassic fenite	0.09	0.69	0.1	4.74	16.15	n.a.	160.5	21.7	5840	0.9
080114	Potassic fenite	0.3	0.12	0.71	3.67	12.9	n.a.	33.5	129.5	995	0.6
080115	Potassic fenite	0.03	0.11	0.06	1.84	7.29	n.a.	15.1	114.5	899	1
090901	Dolomite carbonatite	0.2	0.12	0.78	10.2	34.5	n.a.	313	5.6	776	2.1
090903	Dolomite carbonatite	0.22	0.16	3.97	8.31	23.8	n.a.	2500	29.9	1280	5.8
090904	Dolomite carbonatite	0.06	0.2	1.07	7.84	26.4	n.a.	2500	109.5	1580	6.4
090905	Dolomite carbonatite	0.75	0.31	0.13	11.8	40.7	n.a.	35	0.9	2460	0.2
090907	Dolomite carbonatite	0.03	0.2	1.44	11.55	37.3	n.a.	63.9	0.4	1715	0.3
090909	Dolomite carbonatite	0.04	0.21	0.03	12.2	42.1	n.a.	12	1.3	1785	b.l.
090910	Dolomite carbonatite	0.04	0.21	0.89	11.85	39.6	n.a.	4.1	0.5	1675	b.l.
090912	Potassic fenite	0.11	0.52	0.54	7.04	24.3	n.a.	235	3.4	4540	1.1
090913	Potassic fenite	0.08	0.61	1.12	3.12	9.54	n.a.	254	22.7	4930	2.3
091005	Dolomite carbonatite	0.81	0.26	0.3	11.3	40.6	n.a.	9.2	b.l.	2020	b.l.
091011	Dolomite carbonatite	0.14	0.17	0.1	11.2	38.9	n.a.	209	3.6	1365	0.6

Notes:
n.a. Not analyzed
b.l. Below detection limits as noted

47

Table 1: Bulk rock compositions of the Wicheeda carbonatites and fenites.

Name	Lithology	U	Zr	Ga	Th	Y	La	Ce	Pr	Nd	Sm
							ppm				
Detection Limit		0.05	2	0.03	0.05	0.5	0.5	0.5	0.03	0.1	0.03
WI-11-02	Dolomite carbonatite	2.78	b.l.	n.a.	301	130	11000	14500	1100	3340	311
WI-11-03	Dolomite carbonatite	2.35	b.l.	n.a.	898	102	22700	27900	2100	6340	450
WI-11-07	Dolomite carbonatite	0.98	b.l.	n.a.	1000	143	28300	37000	2800	8710	682
WI-11-09	Dolomite carbonatite	2.02	b.l.	n.a.	1000	190	40500	53200	4300	11900	900
WI-11-11	Dolomite carbonatite	0.5	b.l.	n.a.	422	117	11100	15400	1100	3670	334
WI-11-12	Dolomite carbonatite	0.34	b.l.	n.a.	252	136	6980	8620	844	3460	265
WI-11-15	Sodic fenite (veined)	1.46	b.l.	n.a.	405	126	4780	5980	261	1885	285
WI-13-49	Dolomite carbonatite	0.53	b.l.	n.a.	454	53.9	5720	9000	820	2520	281
WI-13-50	Calcite carbonatite	27.7	108	n.a.	54.7	62.5	1105	2040	177.5	522	55.4
WI-13-55	Sodic fenite	0.4	211	n.a.	33.6	38.5	229	402	147.5	115.5	15.95
WI-13-57	Sodic fenite	7.73	b.l.	n.a.	175.5	66.5	2110	3030	37.1	796	107.5
WI-13-62	Dolomite carbonatite	2.72	b.l.	n.a.	217	24.4	3650	5030	419	1225	127
WI-13-63	Potassic fenite	24	3	n.a.	82.8	31.2	1165	1685	n.a.	441	55.1
080105	Dolomite carbonatite	1.1	b.l.	119	1000	131.5	28000	42800	1000	9770	947
080111	Potassic fenite	0.47	104	17.9	21	25.9	246	411	37.3	111	14.7
080112	Potassic fenite	0.88	159	12.2	9.81	30.2	233	399	35.7	107.5	14.25
080114	Potassic fenite	1.45	120	18.8	29.1	85.9	353	677	69.7	236	39.1
080115	Potassic fenite	1.96	116	16.5	17.9	22.5	88	140.5	14.35	47.4	7.53
090901	Dolomite carbonatite	1.95	b.l.	125.5	1000	233	36700	50300	1000	9170	884
090903	Dolomite carbonatite	8.82	b.l.	38.8	328	48.2	7650	9830	797	2080	194.5
090904	Dolomite carbonatite	10.6	b.l.	55.6	498	70.3	14400	18700	1000	2980	285
090905	Dolomite carbonatite	1.73	b.l.	73.9	695	64.5	20400	27700	1000	5110	471
090907	Dolomite carbonatite	0.95	b.l.	40.2	365	53.3	9110	14000	1000	2880	276
090909	Dolomite carbonatite	0.24	b.l.	8.1	68.4	16.1	1430	2000	163	453	49
090910	Dolomite carbonatite	1.08	b.l.	35.2	400	29.3	8100	13400	904	2420	223
090912	Potassic fenite	2.1	164	20.2	72.5	190	1425	2040	171.5	494	71.6
090913	Potassic fenite	2.47	7	24.1	251	1155	771	1490	172.5	720	260
091005	Dolomite carbonatite	1.8	b.l.	96	884	73.1	27800	36200	1000	6490	611
091011	Dolomite carbonatite	1.48	b.l.	41.4	371	32.4	9450	14800	983	2580	235

Notes:
n.a. Not analyzed
b.l. Below detection limits as noted

48

Table 1: Bulk rock compositions of the Wicheeda carbonatites and fenites.

Name	Lithology	Eu	Gd	Tb	Dy	Ho	Er	Tm	Yb	Lu	Total
							ppm				
Detection Limit		0.03	0.1	0.01	0.01	0.05	0.05	0.01	0.03	0.01	0.01
WI-11-02	Dolomite carbonatite	88.4	162	16.6	62.5	7.2	11.15	0.9	3.79	0.41	96.3
WI-11-03	Dolomite carbonatite	86.1	175.5	13.65	43	4.79	6.79	0.54	2.73	0.34	90.02
WI-11-07	Dolomite carbonatite	143.5	280	21.4	66.6	7.06	9.12	0.72	3.64	0.47	88.56
WI-11-09	Dolomite carbonatite	178	390	27.2	84.4	9.08	12.05	0.9	4.1	0.53	80.22
WI-11-11	Dolomite carbonatite	86	164.5	15.35	53.9	6.08	9.26	0.79	3.79	0.47	93.93
WI-11-12	Dolomite carbonatite	71.9	145.5	13.55	50.5	6.26	10.4	0.93	4.19	0.49	97.36
WI-11-15	Sodic fenite (veined)	84.1	185.5	16.05	56	6.47	9.88	0.83	3.58	0.43	95.04
WI-13-49	Dolomite carbonatite	58.6	121.5	9.3	24.7	2.45	3.76	0.29	1.51	0.24	98.43
WI-13-50	Calcite carbonatite	14.85	27.7	3.21	14.05	2.34	5.73	0.65	4.19	0.56	98.43
WI-13-55	Sodic fenite	4.22	10.7	1.44	7.64	1.45	3.93	0.52	3.53	0.52	100.89
WI-13-57	Sodic fenite	32.6	70.6	7.9	28.9	3.45	5.42	0.4	1.63	0.17	98.56
WI-13-62	Dolomite carbonatite	30.2	58.7	4.64	12.65	1.18	1.62	0.11	0.63	0.09	99.37
WI-13-63	Potassic fenite	15.05	30.9	3.52	13.15	1.56	2.52	0.2	1.03	0.1	98.14
080105	Dolomite carbonatite	154	372	27.2	68.6	6.24	9.33	0.66	2.43	0.3	91.32
080111	Potassic fenite	3.42	8.63	1.13	5.3	0.91	2.74	0.32	2.18	0.25	98.84
080112	Potassic fenite	3.46	9.11	1.22	6.22	1.11	3.41	0.4	2.61	0.37	97.44
080114	Potassic fenite	8.86	24.6	3.14	15.75	2.85	8.32	1.01	6.39	0.82	97.52
080115	Potassic fenite	1.51	5.41	0.73	4.38	0.83	2.54	0.27	2.03	0.26	98.91
090901	Dolomite carbonatite	179	404	36.3	105.5	10.8	16.55	1.18	4.65	0.47	86.52
090903	Dolomite carbonatite	43.8	98	9.46	27.8	2.6	3.5	0.18	0.8	0.07	86.41
090904	Dolomite carbonatite	65.7	146	13.9	41.4	3.85	5.24	0.28	1.01	0.1	91.39
090905	Dolomite carbonatite	97.4	205	15.2	34.3	2.81	3.7	0.24	0.87	0.08	93.63
090907	Dolomite carbonatite	57	123.5	10.05	25.3	2.23	3.14	0.24	1.27	0.12	94.62
090909	Dolomite carbonatite	12.35	23.3	2.25	7.04	0.84	1.53	0.13	0.78	0.11	99.59
090910	Dolomite carbonatite	41.6	90.5	7.08	17.2	1.49	2.41	0.18	0.82	0.07	96.62
090912	Potassic fenite	21.8	57.3	7.69	39.5	6.66	17.4	1.83	10.2	1.19	98.72
090913	Potassic fenite	93.6	335	52	279	43.5	86.7	6.74	22.3	1.86	96.94
091005	Dolomite carbonatite	125	262	20.6	44.7	3.47	4.46	0.24	0.95	0.11	91.4
091011	Dolomite carbonatite	45.4	93.6	7.36	17.85	1.71	2.5	0.16	0.87	0.09	97.09

Notes:
n.a. Not analysed
b.l. Below detection limits as noted

49

Mineral Chemistry

Mineral compositions were determined at McGill University using a JEOL JXA-8900L electron microprobe equipped with five wavelength-dispersive spectrometers and a Si(Li) energy-dispersive detector. Spot analyses using wavelength-dispersive spectrometry, were conducted at 20 kV with a 30 nA beam current and a 10 μ m beam diameter for dolomite, feldspar, and the mafic minerals, and a 5 μ m beam diameter for apatite, the Sr-REE-carbonates, REE-fluorocarbonates, and REE-phosphates. Data reduction was performed using a ZAF correction procedure. The standards and counting times used are reported in Appendix C. Detection limits for each mineral are available with their analytical data in Appendices D-K. Table 2 lists the minerals mentioned in the text with their idealized chemical formulae.

Table 2: Structural formulae of the minerals mentioned in the text.

Mineral	Abbreviation	Formula
Silicates		
Aegirine	Aeg	$NaFe^{3+}Si_2O_6$
Aegirine-Augite	Agt	$(Ca,Na)(Mg,Fe^{2+},Fe^{3+})Si_2O_6$
Albite	Ab	$NaAlSi_3O_8$
Biotite	Bt	$K(Fe,Mg)_3AlSi_3O_{10}(OH)_2$
Chlorite	Chl	$(Mg,Fe)_5Al(AlSi_3O_{10})(OH)_8$
K-feldspar	K-fs	$KAlSi_3O_8$
Muscovite	Ms	$KAl_2(AlSi_3O_{10})(OH)_2$
Phlogopite	Phl	$KMg_3AlSi_3O_{10}(OH)_2$
Quartz	Qtz	SiO_2
Magnesioriebeckite	Rbk	$\square Na_2(Fe^{2+}{}_3Fe^{3+}{}_2)Si_8O_{22}(OH)_2$
Clinozoisite	Czo	$Ca_2Al_3(SiO_4)(Si_2O_7)O(OH)$
Oxides		
Hematite	Hem	Fe_2O_3
Ilmenite	Ilm	$FeTiO_3$
Pyrochlore	Pcl	$(Na,Ca)_2Nb_2O_6(OH,F)$
Rutile	Rut	$(Ti,Nb,Fe)O_2$
Thorite	Th	$(Th,U)SiO_4$
Sulphides		
Pyrite	Py	FeS_2
Molybdenite	Mo	MoS_2

Mineral		Formula
Carbonates		
Ancylite-(Ce)	Anc	$(Ce)(Sr,Ca)(CO_3)_2(OH)*H_2O$
Ankerite	Ank	$Ca(Fe,Mg,Mn)(CO_3)_2$
Bästnasite-(Ce)	Bsn	$CeCO_3F$
Burbankite-(Ce)	Bur	$(Na,Ca)_3(Sr,Ba,Ce)_3(CO_3)_5$
Calcite	Cal	$CaCO_3$
Cordylite-(Ce)	Cor	$(Na,Ca)BaCe_2(CO_3)_4F$
Dolomite	Dol	$Ca(Mg,Fe)(CO_3)_2$
Parisite-(Ce)	Par	$CaCe_2(CO_3)_3F_2$
Strontianite	Str	$SrCO_3$
Synchysite-(Ce)	Syn	$CaCe(CO_3)_2F$
Sulphates		
Barite	Brt	$BaSO_4$
Phosphates		
Fluorapatite	Ap	$Ca_5(PO_4)_3(F,OH)$
Monazite-(Ce)	Mnz	$CePO_4$
Fluorides		
Fluorite	Fl	CaF_2

Stable Isotopes

Samples of calcite and dolomite were analyzed for their contents of stable carbon (^{12}C and ^{13}C) and oxygen (^{16}O and ^{18}O) using a Nu instruments isotope-ratio mass spectrometer at McGill University. All samples were ground using a drill press. Carbon dioxide was released by reaction with phosphoric acid and transferred cryogenically to a dual micro inlet followed by isotopic measurement. The carbon isotopic ratios were standardized to Vienna Pee Dee Belemnite (V-PDB) and reported as $\delta\,^{13}C$ values and the oxygen isotopic ratios to Vienna Standard Mean Ocean Water (V-SMOW) and reported as $\delta\,^{18}O$. A total of 20 samples were analyzed.

Local Geology

The study area is centered on the Wicheeda Carbonatite, which is separated by a later NE-SW trending fault from Kechika Group slates to the west (Fig. 4). A second northwest-southeast trending fault identified by a photo-lineament is cut by this fault and does not appear to have displaced either the carbonatite or surrounding rocks. To the east, fenitized Kechika Group argillaceous limestones surround the Wicheeda Carbonatite. These comprise a proximal potassic fenite extending up to about 80 m from the carbonatite and a distal fenite that includes the most southerly and easterly outcrops in the study area exclusive of carbonatite and fenite. Small outcrops of carbonatite occur to the east and northeast of the Wicheeda Carbonatite and a felsic dyke is exposed in the northeast.
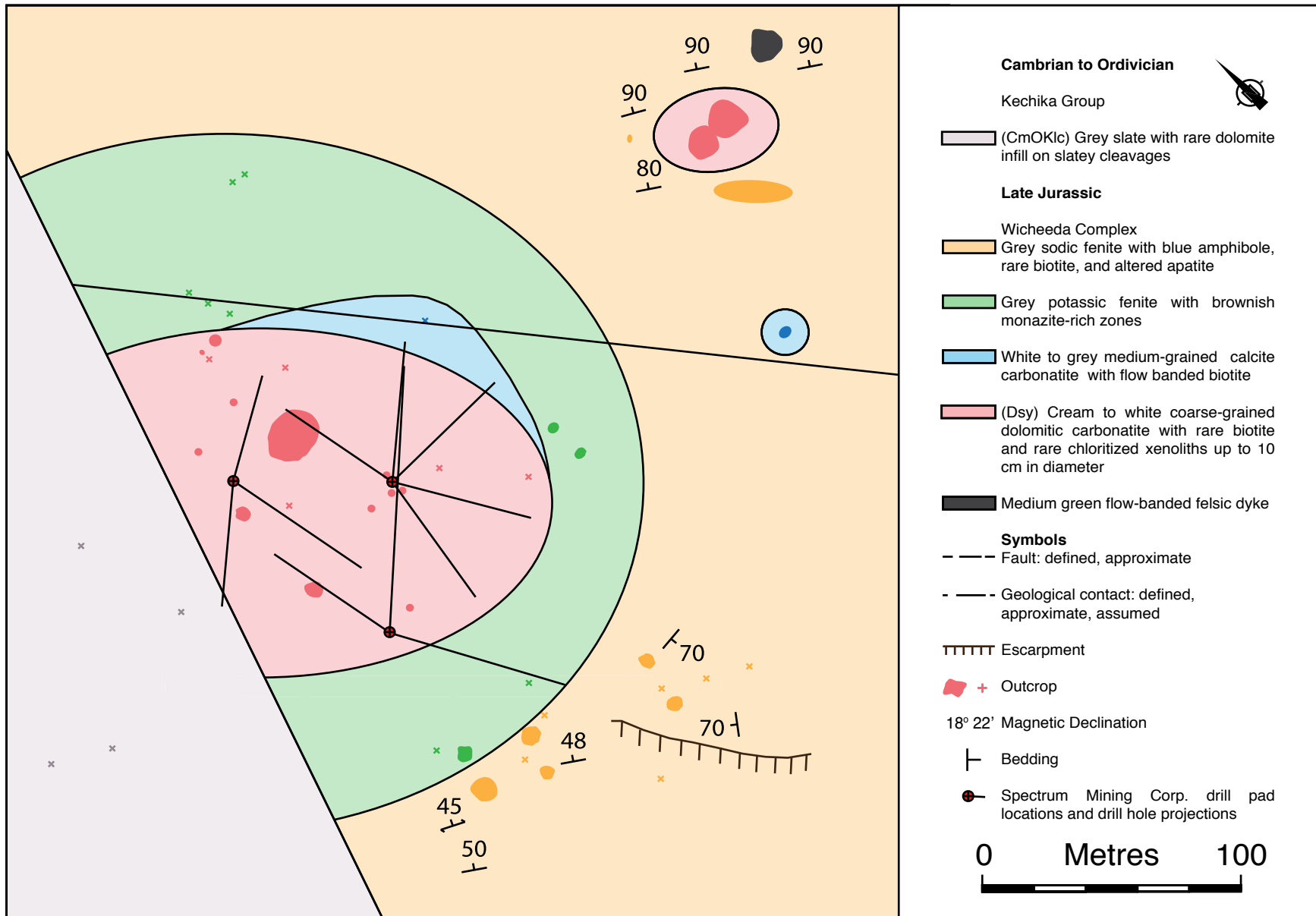
Fig. 4: Geological map of the Wicheeda carbonatite and environs.

Kechika Group Metasedimentary Rocks

The Kechika Group metasedimentary rocks exposed west of the NE-SW trending fault comprise weakly foliated grey slates with a well-developed cleavage and fractures infilled by dolomite. Elsewhere in the study area, as mentioned above, the Kechika Group rocks have been fenitized. To the north, east and south (east of the NE-SW trending fault) of the study area, they comprise thickly bedded limestone and argillaceous limestone striking from 320° to 350° and dipping from 45° to 90°. The beds typically show a fining-upward sequence of limestone to silty argillaceous limestone comprising millimeter-scale calcite-rich and silt- to clay-rich laminations, and are capped by clay rip-up clasts. The calcite-rich laminations are composed of clear anhedral, sutured calcite grains up to 300 μ m in diameter and subordinate zoned subhedral apatite crystals with inclusion-rich (calcite) cores and clear, inclusion-poor rims; the apatite is concentrated near the argillaceous silty laminations. The silt-/clay-rich laminations comprise subhedral quartz (100 μ m), clay minerals, and subordinate fine-grained (<100 μ m) anhedral calcite.

The Wicheeda Carbonatite

With the exception of a small zone on its northeastern flank where it passes gradationally into calcite (Fig. 4), the Wicheeda carbonatite is exclusively dolomitic. Small outcrops of dolomite carbonatite and calcite carbonatite are also present ~150 m northeast and 100 m east of the main intrusion, respectively (Fig. 4). The dolomite carbonatite is heavily oxidized to a dark orange or brown color in outcrop and to depths of up to 5 m in drill core. Where fresh, it is cream or white in color and is extremely vuggy with fractures

commonly infilled by dolomite and REE minerals (Fig. 5A to 5D). Near the contact with the potassic fenite, corroded clasts of albite + apatite up to 3 cm in diameter have been incorporated into the carbonatite. Large euhedral dolomite crystals up to 2 cm in diameter comprise 65 to 70 vol.% of the rock and are accompanied by vein and vug-filling potassium feldspar (5 to 10 vol.%), dark micas (5-10 vol.%), calcite (5 vol.%), hematite (2 to 5 vol.%), pyrite (1 to 3 vol.%), and barite (1-2 vol.%). Rare earth element-bearing carbonate minerals, including bastnäsite-(Ce), parisite-(Ce), synchysite-(Ce), ancylite-(Ce) and cordylite-(Ce), and monazite-(Ce) make up between 3 to 6 vol.% of the rock. Traces of molybdenite, niobian rutile, and thorite are also present. Three texturally distinct varieties of dolomite have been recognized (Fig. 5B and 5C). Dolomite 1 is characterized by relatively clear (inclusion-poor) euhedral rhombs up to 1 cm in diameter with well-developed cleavages and triple junction grain boundaries, which are locally lined by hematite. In very rare cases, the cleavages are curved and contain microcrystalline dolomite within them. Dolomite 1 makes up most (>90 vol.%) of the dolomite in the carbonatite. The second variety, Dolomite 2, comprises dusty micro-fluid inclusion-rich (<2 μm) cryptocrystalline carbonate surrounding vugs and veins (Fig. 5B). Large euhedral crystals of compositionally zoned Dolomite 3 occur in veins and as a cavity-lining phase with semi-continuous growth rims containing primary fluid micro-inclusions (<2 μm diameter) (Fig. 5B).
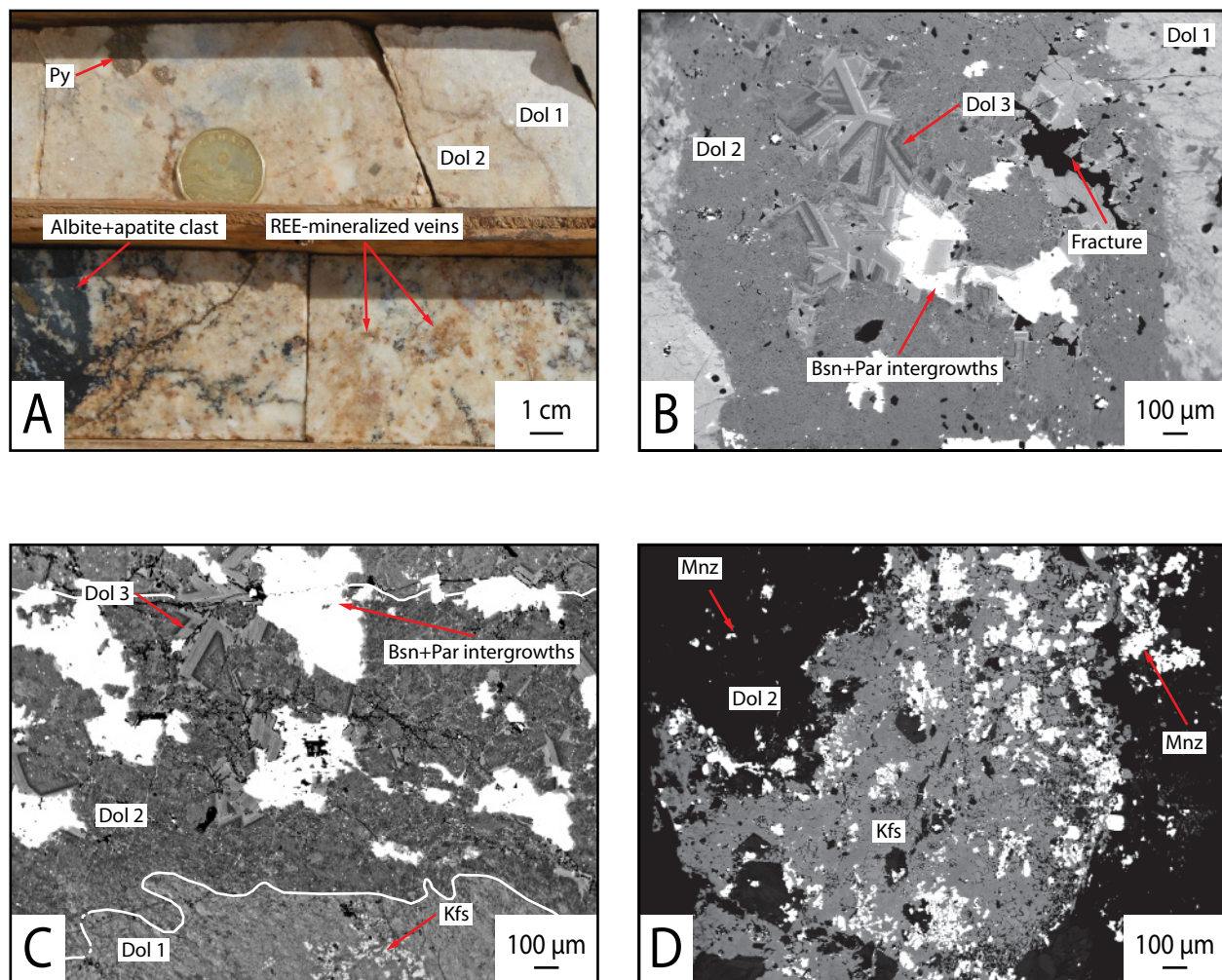
Fig. 5: A. White (Dolomite 1) to cream (Dolomite 2) dolomite carbonatite with bright orange REE-mineralized veinlets. Xenoliths of sodic fenite up to 30 cm have been incorporated into the carbonatite. Pyrite occurs in veinlets and as blebby subhedral grains. B. Back-scattered electron image of dolomite carbonatite (sample 080101) showing relatively clear Dolomite 1 (light grey) altered to Dolomite 2 near vugs infilled by Dolomite 3 and bastnäsite-(Ce) and parisite-(Ce) (bright). C. Back-scattered electron image of dolomite carbonatite (sample WI080101) showing Dolomite 1 altered to Dolomite 2 near vugs partially infilled by Dolomite 3 and bastnäsite-(Ce) and parisite-(Ce). D. Back-scattered electron image of dolomite carbonatite (sample WI090802) showing a vug infilled with K-feldspar and monazite-(Ce).

56

The calcite carbonatite comprises white, medium-grained, equigranular calcite (65 vol.%) replaced by Dolomite 1 (15-20 vol.%; Fig. 6A) with minor biotite (5 vol.%), albite (5 vol.%), aegirine-augite (2 vol.%), pyrite (2 vol.%), and pyrochlore (1 vol.%) and traces of apatite. It displays evidence of strong flow banding with alternating millimeter-thick layers of biotite and 5 mm-thick calcite-rich layers (Fig. 6B). Fine-grained (<100 µm) subhedral to anhedral albite commonly contains inclusions of rounded calcite (10 µm) and is locally altered to clinozoisite. Emerald-green, euhedral aegirine crystals up to 400 µm in diameter form clusters near the contact with the dolomite carbonatite and are commonly rimmed by brown euhedral biotite (Fig. 6C). Brown, euhedral pyrochlore grains up to 25 µm in diameter occur as inclusions in calcite and rarely in biotite (Fig. 6C). Pyrite and clinozoisite occur locally in cavities (Fig. 6D).
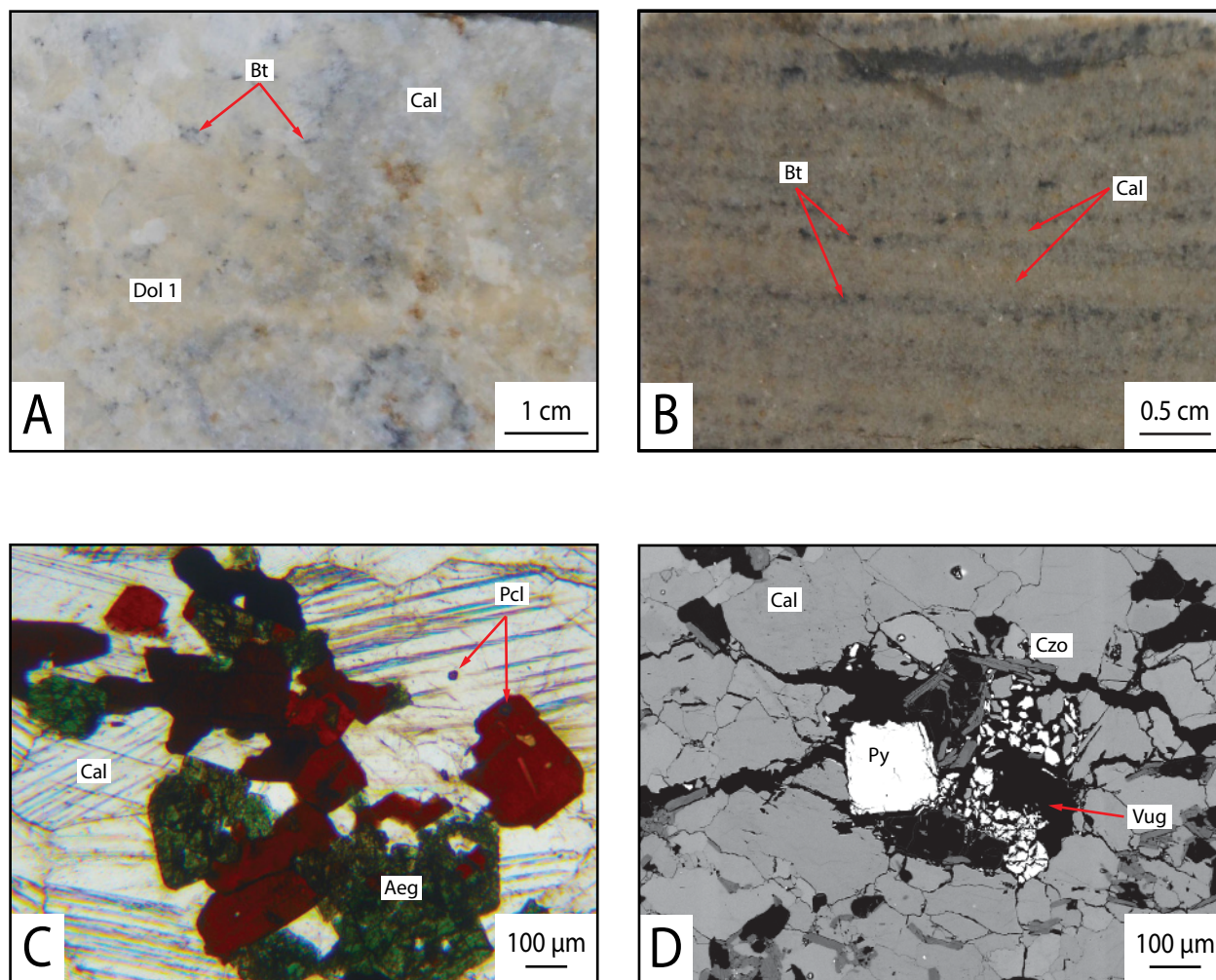
Fig. 6: A. Drill core from WI-09-08 (49 m depth) of grey calcite carbonatite comprising calcite (Cal), and containing white Dolomite 1 and dark Fe-rich biotite (Bt) grains. B. Photograph of calcite carbonatite with alternating dark grey biotite-rich and white to light grey calcite layers. C. Plane-polarized photomicrograph of calcite carbonatite (WI-09-08) with equigranular calcite, emerald-green aegirine (Aeg), and reddish-brown biotite (Bt). Traces of pyrochlore (Pcl) occur as inclusions in calcite and biotite. D. Back-scattered electron image showing fractured calcite carbonatite containing a vug partially infilled by pyrite, zoisite, and albite; albite is also disseminated in the matrix of the carbonatite.

Potassic Fenite

The potassic fenite outcrops poorly and descriptions of it come mainly from examination of the drill core. The fenite varies in color from beige (strongly altered) near the intrusion to grey (weakly altered) further from the carbonatite-fenite contact (Fig. 7A). Mineralogically, the potassic fenite comprises potassium feldspar (30 to 35 vol.%), biotite (15 to 20 vol.%), albite (15 to 25 vol.%), calcite (10-15 vol.%), and aegirine-augite (5-10 vol.%), together with traces of magnesioriebeckite, apatite, rutile, monazite-(Ce), and ancylite-(Ce). The potassium feldspar occurs as blebby, anhedral aggregates up to 0.5 mm in diameter in clots with fine-grained albite (Fig. 7B) and as larger crystals that clearly replaced albite. Fine-grained anhedral calcite is interstitial to potassium feldspar and albite, and is rimmed by dolomite. Aegirine-augite occurs locally and is found most commonly in the distal parts of the potassic fenite where it forms acicular crystals. Riebeckite commonly occurs with the aegirine-augite and shows evidence of replacement by biotite (Fig. 7C). Biotite also occurs as large, euhedral crystals rimmed by chlorite in veinlets with calcite. Subhedral niobian rutile with inclusions of albite and potassium feldspar is found in the altered biotite rims. Strongly zoned, blue to violet luminescent, subhedral to anhedral fine-grained apatite (Apatite 1) with albite inclusions is disseminated in the albite-potassium feldspar clots. This apatite is replaced by fine-grained monazite-(Ce); the latter occurs in contact with potassium feldspar and near dolomite veinlets (Fig. 7D).

59
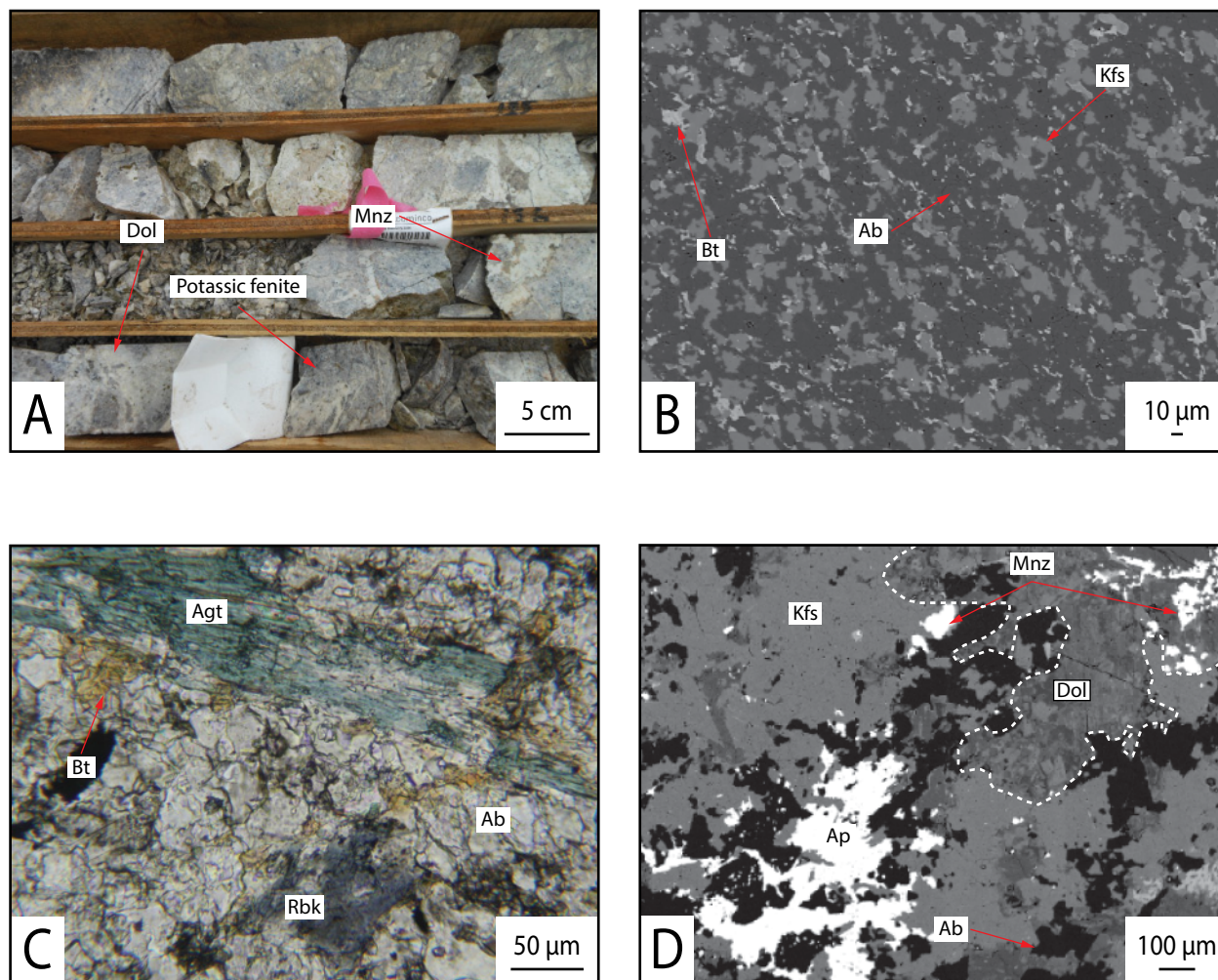
Fig. 7: A. Intensely altered potassic fenite from drill hole WI-09-08 (~135 m depth) with beige clots of monazite-(Ce) at the contact between the fenite and dolomite-filled fractures. B. Back-scattered electron image of mottled dark grey albite (Ab) in potassic fenite replaced by medium-grey K-feldspar (Kfs) and light grey biotite (Bt). C. Photomicrograph in plane-polarized light of outcrop sample of potassic fenite (WI-13-55) containing acicular blue-green acicular aegirine-augite (Agt) and blue-grey riebeckite that has been replaced by biotite in clear albite (Ab) and K-feldspar (Kfs). D. Back-scattered electron image of potassic fenite showing anhedral Apatite 1 (Ap) with inclusions of albite (Ab) near aggregates of monazite-(Ce) (Mnz) at the contact between K-feldspar and dolomite (dashed line).

Sodic Fenite

Macroscopically, the sodic fenite resembles the unaltered Kechika Group rocks and is distinguished from them by the presence of abundant calcite veinlets, particularly near the contact with the potassic fenite. The sodic fenite consists mainly of albite (25 to 35 vol.%), calcite (25 to 35 vol.%), aegirine (10 to 15 vol.%) and riebeckite (5 to 10 vol.%). Relict sedimentary bedding locally survived fenitization and is preserved as alternating albite + aegirine $\pm$ calcite, and calcite-rich laminations (Fig. 8A,B). In the former laminations, albite laths up to 100 μ m in length occur with bundles of acicular aegirine crystals up to 1 mm in length (Fig. 8B). The albite laths commonly contain inclusions of very fine-grained (5 μ m) anhedral calcite crystals. Within the aegirine + albite laminations, rare, pale blue-grey riebeckite forms spongy masses up to 200 μ m in diameter and fibrous needles after aegirine. Biotite occurs as fine-grained disseminated flakes and larger (200 μ m) crystals rimmed by chlorite (Fig. 8C,D) in veins with calcite and rare siderite (Fig. 8C). Apatite 2 (1 to 2 vol. %) forms euhedral to subhedral, weakly zoned crystals up to 200 μ m in diameter disseminated throughout the albite+calcite matrix and commonly forms aggregates (Fig. 8C). It has an albite-calcite inclusion-rich core and a clear rim, and is concentrated in the albitic laminations. Very fine-grained calcite and pyrite (oxidized in surface exposures) also occur in these laminations. The calcite-rich laminations are coarser-grained, consisting of sutured crystals up to 800 μ m in diameter, and only contain traces of REE mineralization. The latter occurs as microveinlets of ancylite-(Ce) in the albite + aegirine laminations or as monazite-(Ce),

which replaced Apatite 2. This mineralization is only found at or near the contact with the

potassic fenite.
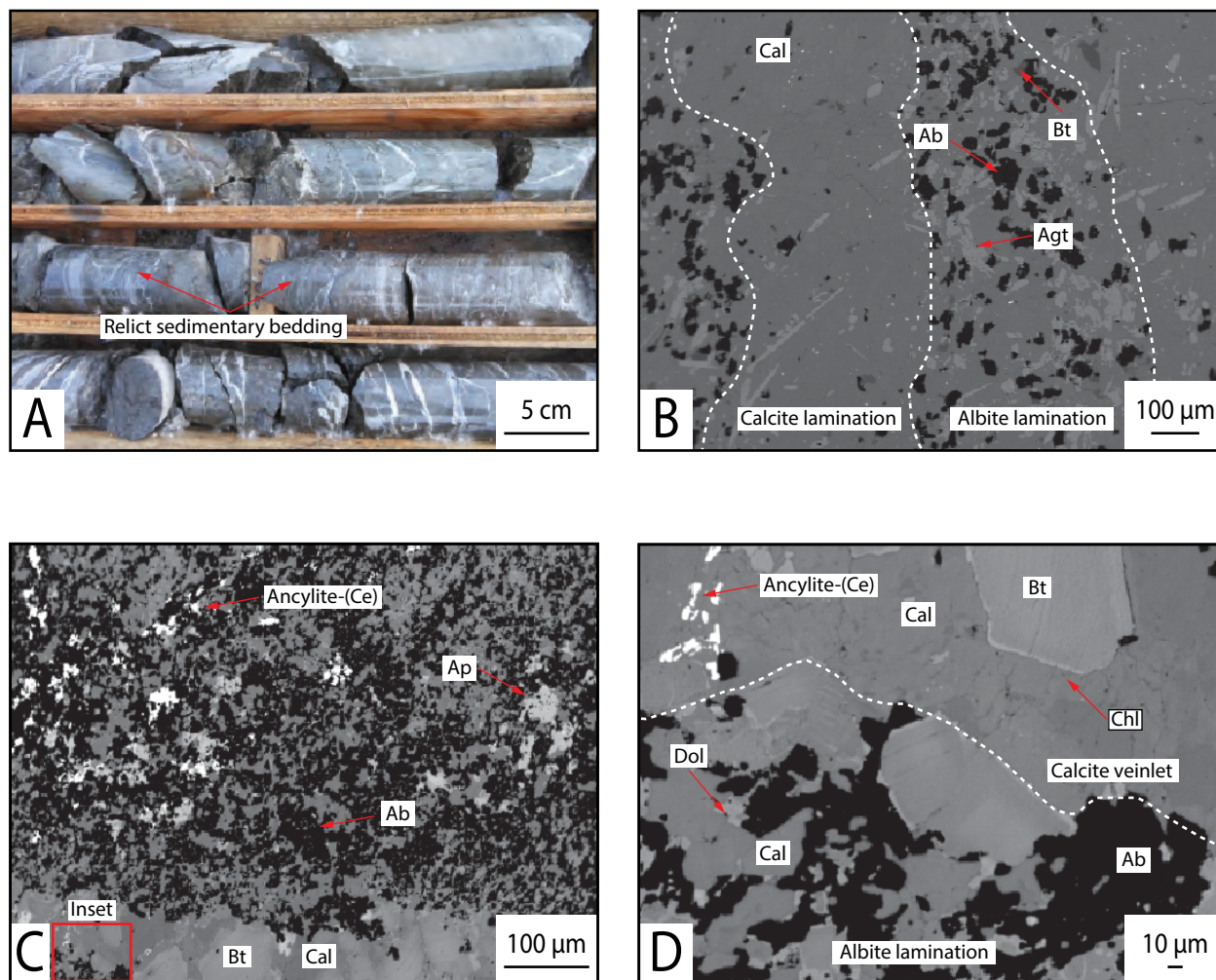
Fig. 8: A. Fractured sodic fenite from drill hole 08-WI-01 (180 m depth) displaying the relict sedimentary layering of the Kechika Group rocks as alternating pale blue and pale green-grey bands. B. Back-scattered electron image of sodic fenite showing thin alternating calcite-rich (Cal) laminations and aegirine-augite (Agt) - albite (Ab) -rich laminations (sample WI-13-07). Dashed lines indicate the boundaries of the laminations. C. Back-scattered electron image showing mottled albite and calcite and a crosscutting veinlet of calcite (Cal), biotite (Bt), and ancylite-(Ce) from sodic fenite sample WI-13-01. D. Inset of B. showing a calcite+biotite veinlet with biotite rimmed by chlorite (Chl), and traces of ancylite-(Ce).

Felsic Igneous Rock

A small outcrop of a felsic igneous rock was identified near the dolomite carbonatite northeast of the main intrusion. It comprises a felty, clay-altered albite matrix; 0.5 mm wide veinlets of potassium feldspar and a trace of strontianite (crystals up to 100 μm in diameter) are common. No REE mineralization was identified in this rock.

Rare Earth Element Mineralization

As has already been mentioned, the REE mineralization is restricted mainly to the dolomite carbonatite. There, it occurs mostly in veins and vugs, commonly with Dolomite 3 (Fig. 5C) and less commonly as very small grains of monazite-(Ce) disseminated in Dolomite 2 (Fig. 5D). Bastnäsite-(Ce) (2 vol. %) and parisite-(Ce) (2 vol. %) form large (1 mm) dark red and brownish-yellow pseudo-hexagonal crystals, respectively. More commonly, however, they occur as very fine (<2 μm wide) syntactic intergrowths in these large crystals (Fig. 9A). Rare synchysite-(Ce) (<1 vol. %) occurs as very fine lamellae exsolved from parisite-(Ce). Both bastnäsite-(Ce) and parisite-(Ce) replaced brownish anhedral masses of ancylite-(Ce) (<1 vol. %) (Fig. 9B) and cordylite-(Ce) (<1 vol.%). Elsewhere, cordylite-(Ce) was replaced by ancylite-(Ce) (Fig. 9C). Monazite-(Ce) (1 vol. %) forms narrow prisms (10 μm long) that occur as inclusions in Dolomite 3, bastnäsite-(Ce), and parisite-(Ce) (Fig. 9D) and as aggregates near albite-rich fenite xenoliths, commonly in association with Dolomite 3 (Fig. 9E). The xenoliths contain traces of niobian rutile, which occurs as inclusions in veinlets of molybdenite and pyrite; these veinlets also rim Dolomite 2 in the vugs (Fig. 9F). Traces of thorite occur as inclusions in bastnäsite-(Ce) and vug-filling potassium feldspar.

Taken together, these observations help establish a paragenesis for the mineralization (Fig. 10). Dolomite 3, barite, and sulfide minerals precipitated first as shown by their occurrence along the walls of the fractures and vugs, and were followed by precipitation of thorite and monazite-(Ce), later ancylite-(Ce) and cordylite-(Ce) and finally bastnäsite-(Ce), parisite-(Ce), and synchysite-(Ce) (Fig. 9A-F).
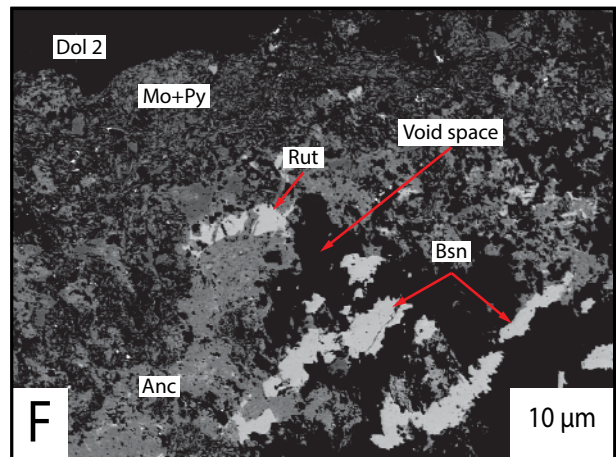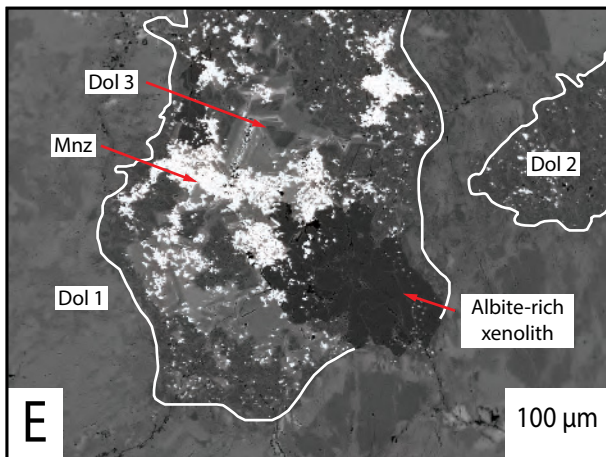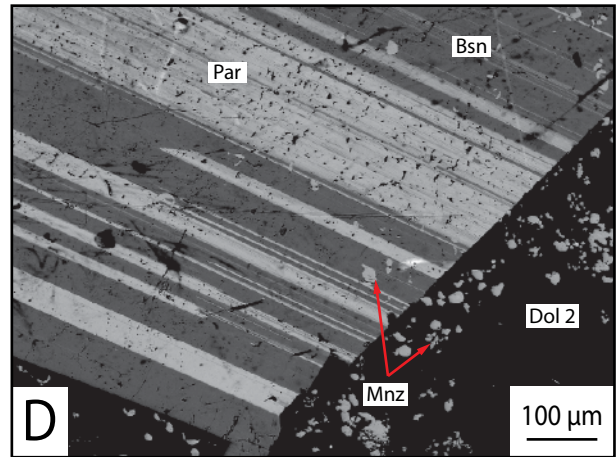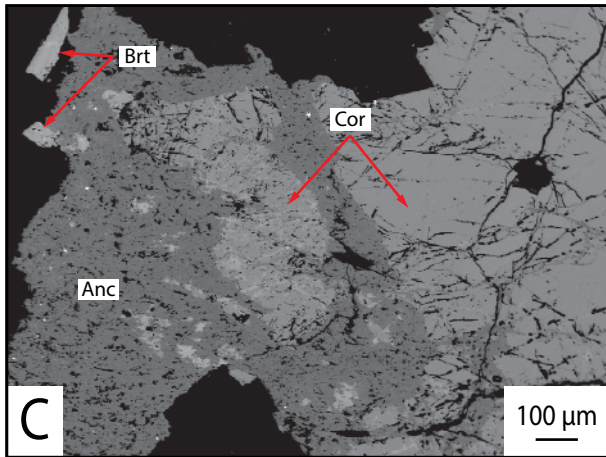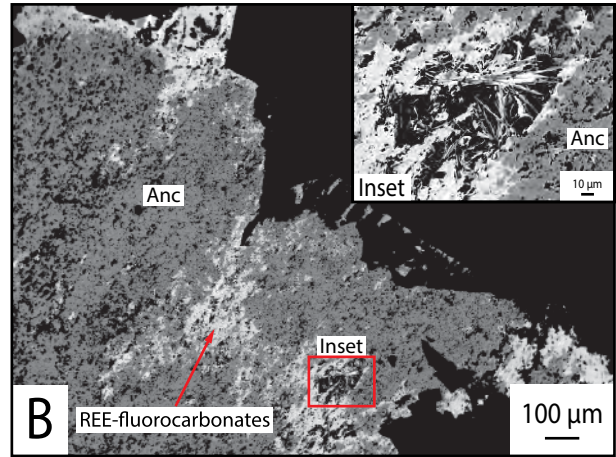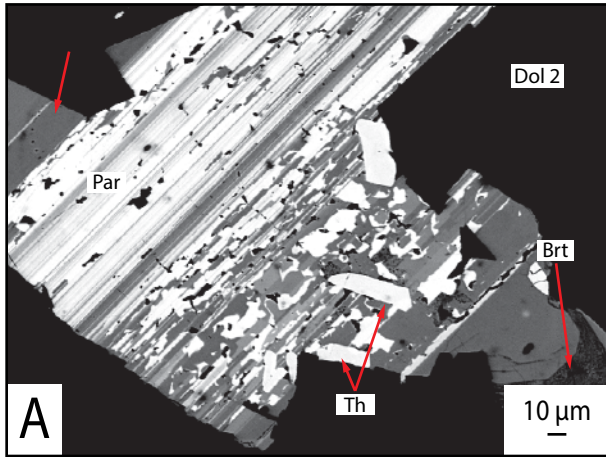
Fig. 9: A-F. Back-scattered electron images of dolomite carbonatite. A. Cross-section of a vein in which fractured Dolomite 2 was infilled by barite (Brt) and intergrowths of bastnäsite-(Ce) (Bsn) and parisite-(Ce) (Par) both containing inclusions of tabular thorite (Th). B. Cross-section of a fracture infilled by barite that was later replaced by ancylite-(Ce) (Anc). Inset of B.: Intergrowths of bastnäsite-(Ce) and parisite-(Ce) that replaced ancylite-(Ce). C. Cross-section of a vein of Dolomite 3 with inclusions of barite and cavity-lining cordylite-(Ce) (Cor) that was replaced by ancylite-(Ce) (Anc). D. Inclusions of monazite-(Ce) in intergrowths of bastnäsite-(Ce) and parisite-(Ce). E. Dolomite 1 altered to Dolomite 2 adjacent to a sodic fenite xenolith; an open space created by the alteration is infilled by Dolomite 3, which is cut by monazite-(Ce). F. A fracture partially infilled by molybdenite (Mo) and pyrite (Py), followed by ancylite-(Ce) containing inclusions of rutile (Rut); bastnäsite-(Ce) occupies open space adjacent to the ancylite-(Ce).

REE-BEARING MINERALS	Magmatic	Hydrothermal

Carbonatite:
Pyrochlore
Pyrite
Barite
Molybdenite
Thorite
Monazite-(Ce)
Cordylite-(Ce)
Ancylite-(Ce)
Bästnasite-(Ce)
Parisite-(Ce)
Synchysite-(Ce)

Fenite:
Apatite
Monazite
Niobian Rutile

Fig. 10: Paragenetic diagram showing the order of crystallization of the main REE-bearing and associated minerals in the Wicheeda carbonatite. The line widths indicate the relative abundances of the minerals.

Carbonatite Composition

A total of 19 samples of dolomite and calcite carbonatite from outcrop and drill core were analyzed for their major and trace element compositions using the methods described earlier (Methodology). The results are summarized in Table 1. According to the classification scheme of Gittins and Harmer (1997), carbonatites from the Wicheeda plug are mainly magnesio- and ferro-carbonatites, or ferruginous calcio-carbonatites with compositions near the MgO-rich/CaO-poor corner of the corresponding field; the one sample of calcite carbonatite that was analyzed, as expected, classifies as calcio-carbonatite (Fig. 11). The main non-volatile components of the calcite carbonatite are CaO (44.9 wt.%), MgO (2.24 wt.%), FeO (9.46 wt.%), and MnO (0.83 wt.%). There are also minor concentrations of SrO (1.59 wt.%), BaO (0.32 wt.%), P_2O_5 (2.46 wt.%), Th (55 ppm), Nb (2500 ppm), and ΣREE (0.4 wt.%). The dolomite carbonatite (n=18), by comparison, on average, contains less CaO (25.5 wt.%), more MgO (12.45 wt.%), more Fe_2O_3 (9.46 wt.%), and more MnO (1.4 wt.%). The contents of SrO (0.16 wt.%), BaO (0.23 wt.%), P_2O_5 (0.5 wt.%), and Nb (353 ppm) are much lower, whereas the Th and ΣREE contents are higher by an order of magnitude (564 ppm and 3.3 wt.%, respectively). Significantly, the magnesio-carbonatites are slightly more enriched in the REE than the ferro-carbonatites (Fig. 12). The chondrite-normalized trace element profiles (Fig. 13) show that relative to the calcite carbonatite, the dolomite carbonatite samples are enriched in Th and the REE (mainly the LREE) and depleted in Rb, U, Nb, and Ta. Both carbonatites have pronounced negative U, Ta, and Zr anomalies. The chondrite-normalized REE profiles (Fig. 14) of the dolomite carbonatite show a much greater degree of LREE-enrichment (La/Lu=6470) than the calcite carbonatite

69

(La/Lu=204). Indeed, the Yb and Lu contents of the calcite carbonatite correspond to the

upper limit of their contents in the dolomite carbonatite.
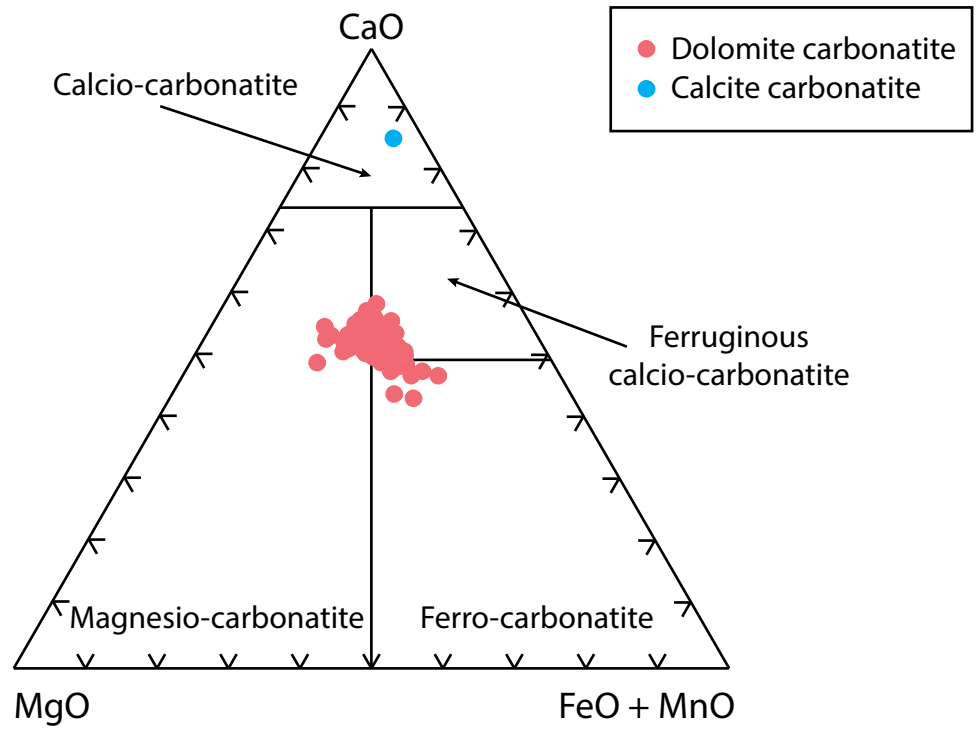
Fig. 11: The distribution of Wicheeda carbonatite compositions (molar proportions) on the CaO-MgO-(FeO+MnO) carbonatite classification diagram of Gittins and Harmer (1997).
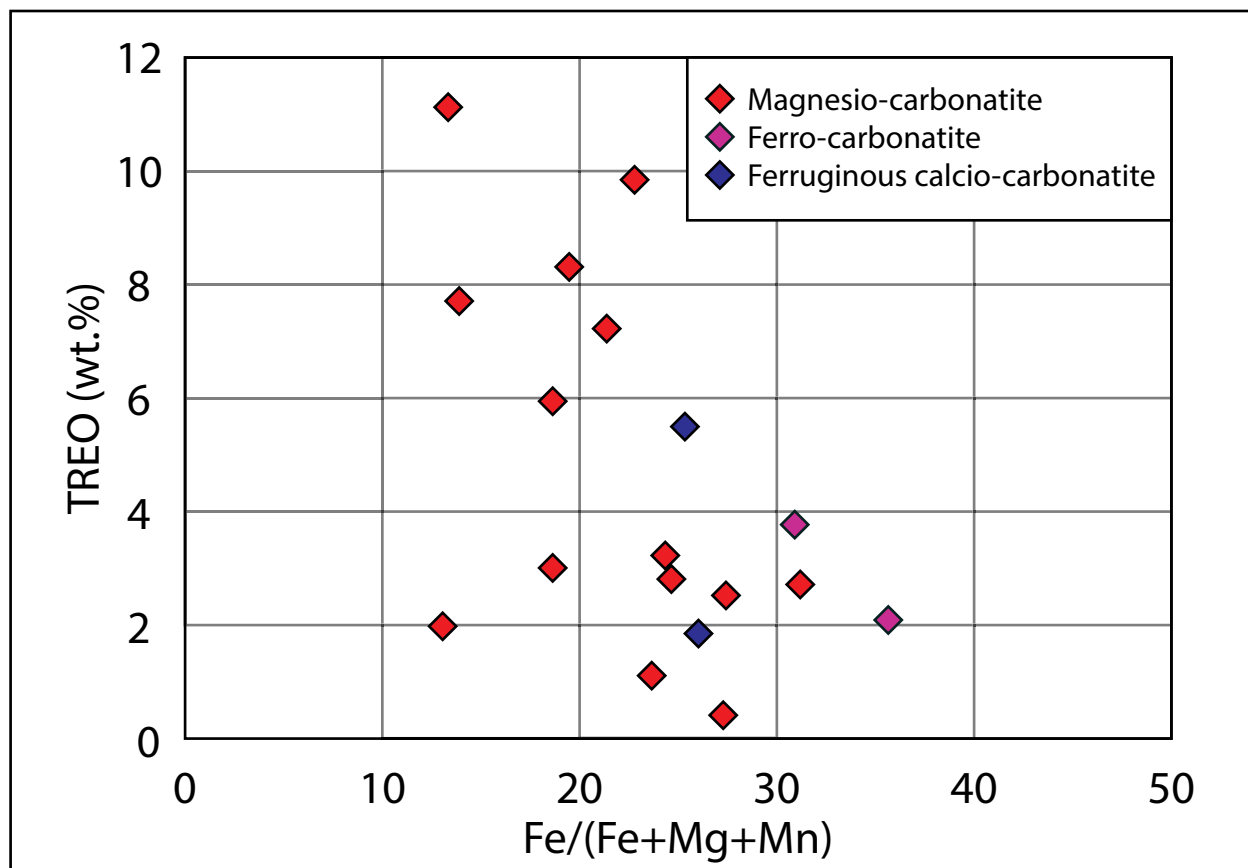
Fig. 12: The TREO content (wt.%) of the Wicheeda dolomite carbonatites as a function of the bulk molar ratio, Fe/(Fe+Mg+Mn).
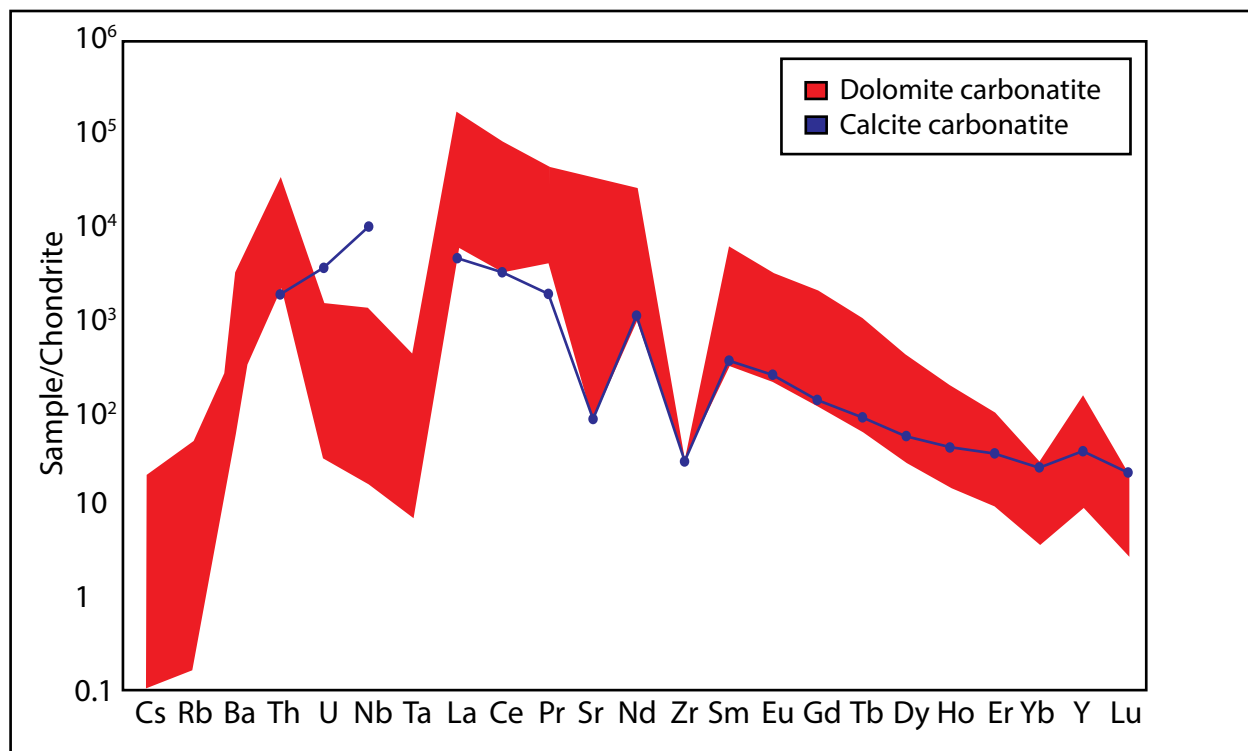
Fig. 13: A chondrite-normalized spider diagram illustrating the distribution of trace elements in the Wicheeda carbonatites. The data were normalized to CI chondrite (McDonough and Sun, 1995).
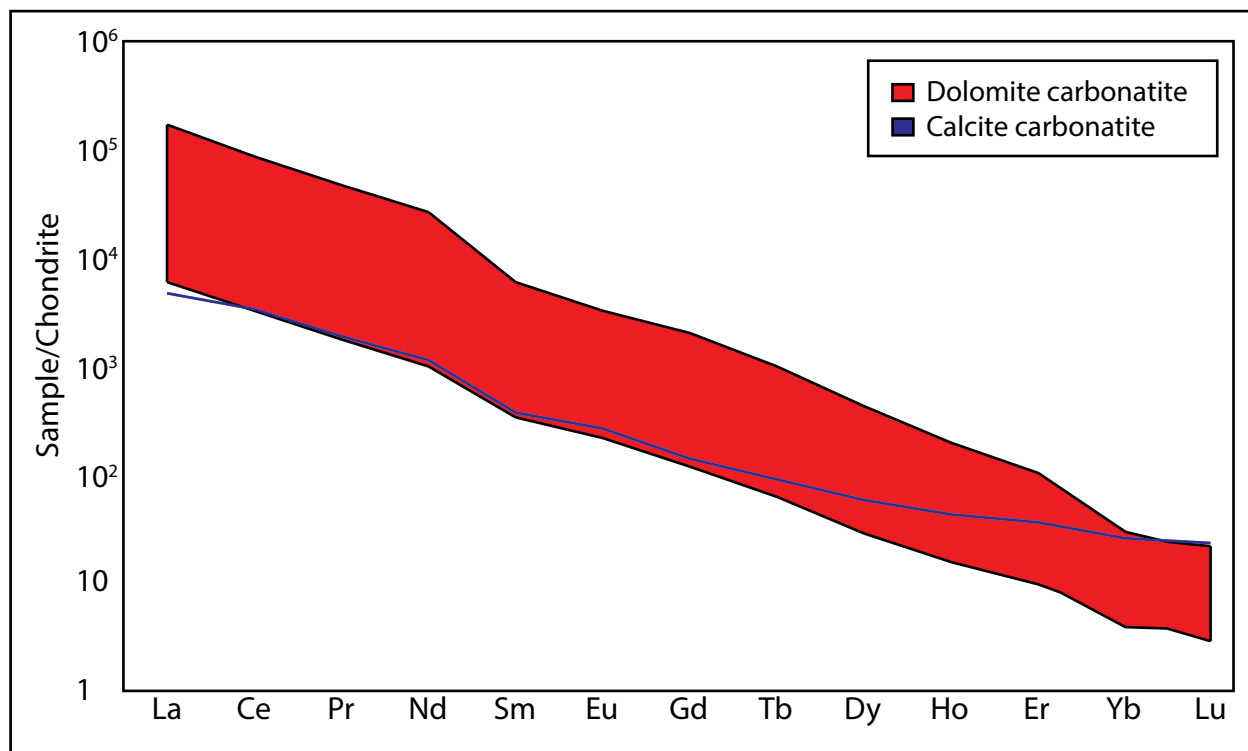
Fig. 14: A chondrite-normalized REE diagram for the Wicheeda dolomite carbonatite (n=18) and calcite carbonatite (n=1). The data were normalized to CI chondrite (McDonough and Sun, 1995).

Fenite Composition

A small number of samples of potassic fenite (5) and sodic fenite (3) were analyzed for their bulk chemical composition in order to distinguish them chemically. As is evident from Figure 15, they are clearly distinguishable by their relative proportions of Al_2O_3, Na_2O and K_2O, which confirms the mineralogical classification of these two fenite types. The potassic fenite contains an average of 30.4 wt.% SiO_2, 8.9 wt.% Al_2O_3, 3.1 wt.% Na_2O, 2.2 wt.% K_2O, 6.9 wt.% Fe_2O_3, 5.1 wt.% MgO, 0.8 wt.% P_2O_5, 0.81 wt.% SrO, and 0.14 wt.% BaO (Table 1). The average ΣREE content is 0.34 wt.%, the Nb content 473 ppm, and the S content 0.6 wt.%. The F content is below its limit of detection.

On average, the sodic fenite contains more SiO_2 (36.1 wt.%), Na_2O (5.8 wt.%) and SrO (0.42 wt.%) than the potassic fenite and less Al_2O_3 (8.1 wt.%), K_2O (0.7 wt.%), Fe_2O_3 (5.2 wt.%), and MgO (3.9 wt.%) (Table 1). It also has very much lower ΣREE (0.08 wt.%), and Nb (82 ppm) contents than the latter. The P_2O_5 (0.83 wt.%) and BaO (0.10 wt.%) contents are similar to those of the potassic fenite, however, the S content (0.4 wt.%) is slightly lower. The F content is below the detection limit.

Although the carbonatites and fenites have quite different major element compositions, their trace element composition profiles are relatively similar (Figs. 13, and 16). Both the potassic and sodic fenite are enriched in Th, Nb, REE, and Y and have negative U, Ta, and Zr anomalies; the Kechika metasedimentary rocks are depleted in Nb and enriched in U. The potassic fenite samples generally have higher Th, U, Nb and REE contents than the sodic fenite (Figs. 16 and 17). Moreover, the Yb and Lu contents of the most REE-

enriched potassic fenites are greater than those of any of the rocks in the study area (Table 1). Fresh Kechika Group argillaceous limestone has a lower REE content than either of the fenite types and a lower La/Lu ratio.
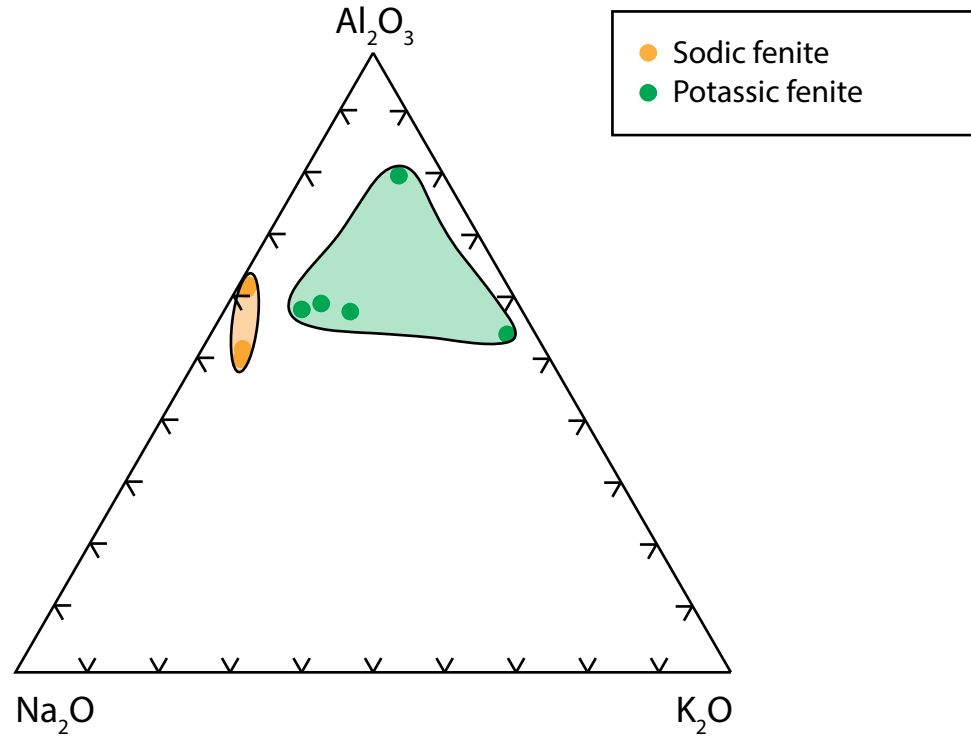
Fig. 15: A plot showing the compositions (wt. %) of potassic and sodic fenites in terms of the components, Al_2O_3, Na_2O, and K_2O.
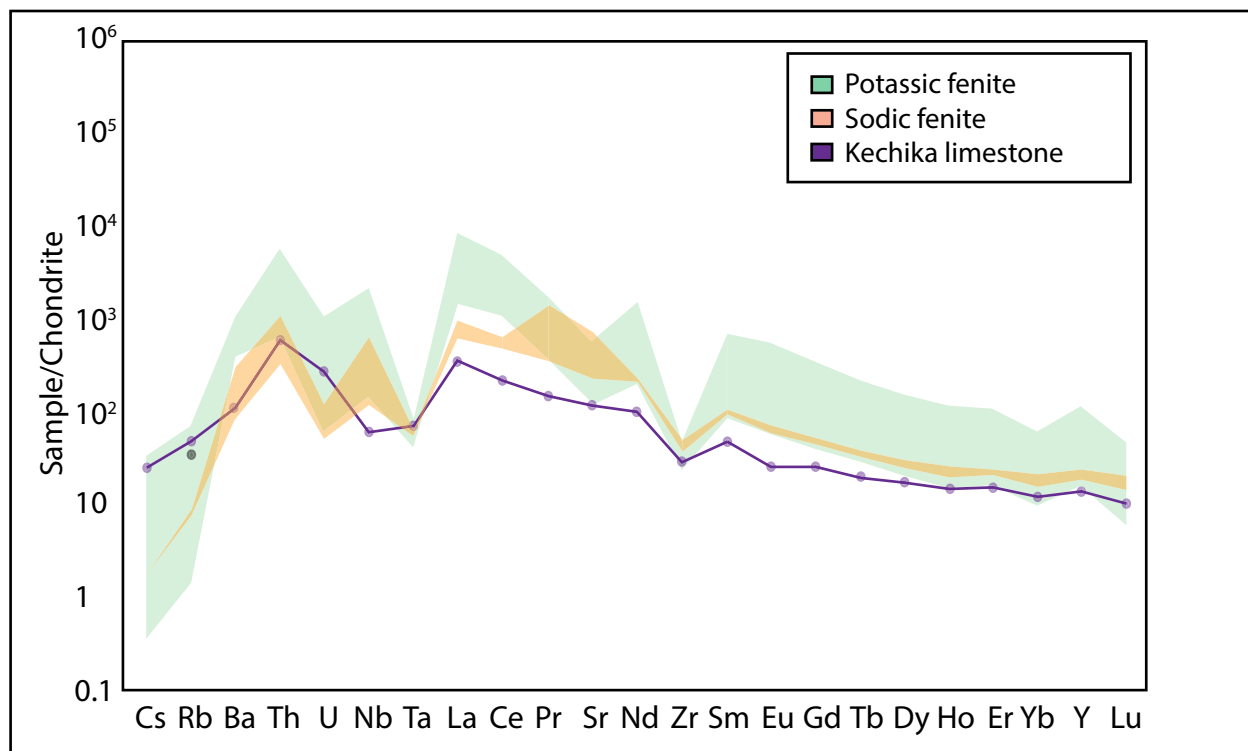
Fig. 16: A chondrite-normalized spider diagram illustrating the distribution of trace elements in the Wicheeda fenites and Kechika argillaceous limestone.
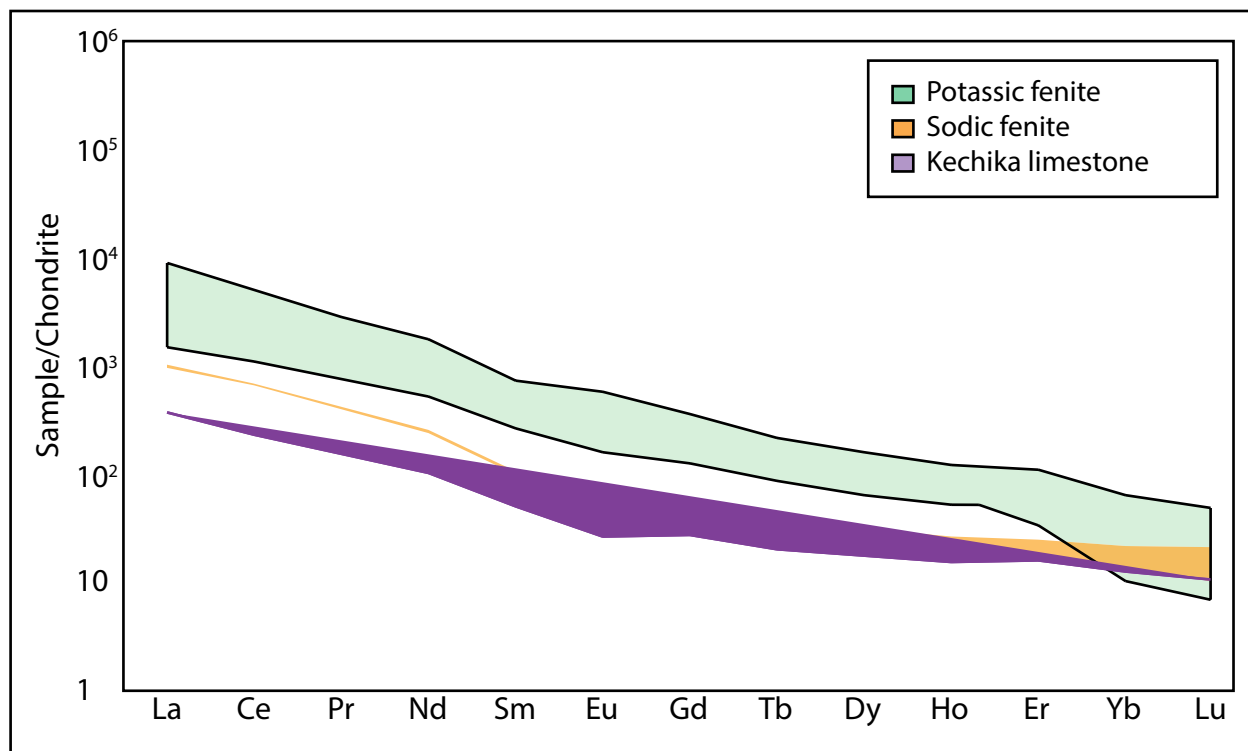
Fig. 17: A chondrite-normalized REE diagram for the potassic fenite (n=6), sodic fenite (n=3), and
Kechika argillaceous limestone (n=1). The data were normalized to CI chondrite (McDonough and
Sun, 1995).

Bulk distribution of the REE

As will be evident from the preceding sections, the potentially economic REE mineralization is concentrated in the carbonatites and particularly the dolomite carbonatite. This is borne out by Figure 18A, which shows the total REE content (TREO) of the different carbonatite types and fenites compiled from company drill core assay data and an assumed economic cutoff grade of 1 wt.% TREO. Elevated niobium concentrations (>500 ppm) were observed mainly in the calcite carbonatite and potassic fenite (Fig. 18B). As the REE are present dominantly as REE fluorocarbonate minerals and phosphates, we have also evaluated their distribution in the dolomite carbonatite as a function of the contents of fluorine and phosphorous (Fig. 19A and 19B; Table 1). The importance of fluorine to the REE mineralization is clearly demonstrated by the strong linear correlation of F and LREE bulk rock contents (Fig. 19A). Significantly, and in contrast to the behavior of the LREE with fluorine, the data for LREE versus phosphorous, indicate the presence of two populations, one with a low P content (<0.5 wt.%) and another with a relatively elevated P content (0.8-1.7 wt.%). In further contrast to the data for F, the LREE content in both the populations appears to be independent of the phosphorous content. The likely explanation for these observations is that in some samples the REE mineralization was largely in the form of REE fluorocarbonate and Sr-REE carbonate minerals (low P population), whereas in others it also comprised appreciable concentrations of monazite-(Ce) (high P population); some of the samples of the high P population also have elevated concentrations of alkalis and Al, and may therefore contain small proportions of apatite-bearing fenite xenoliths not detected during sampling (see earlier descriptions of rock units).

80
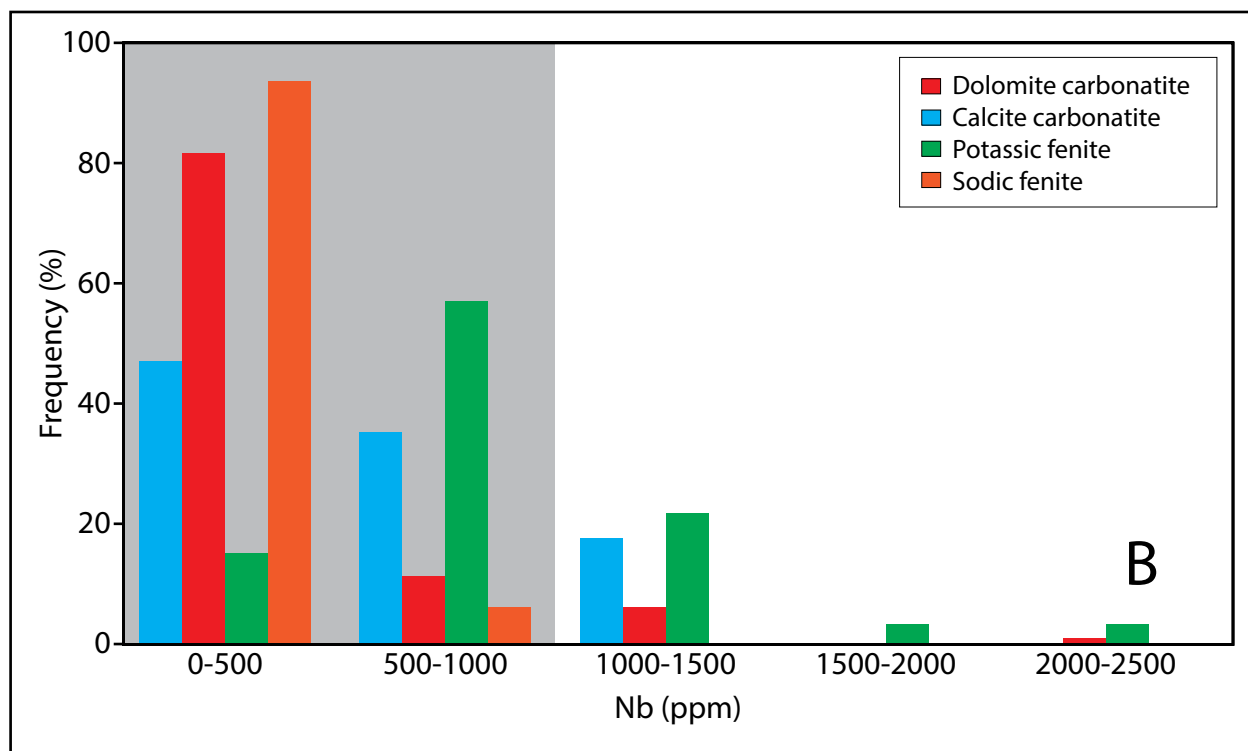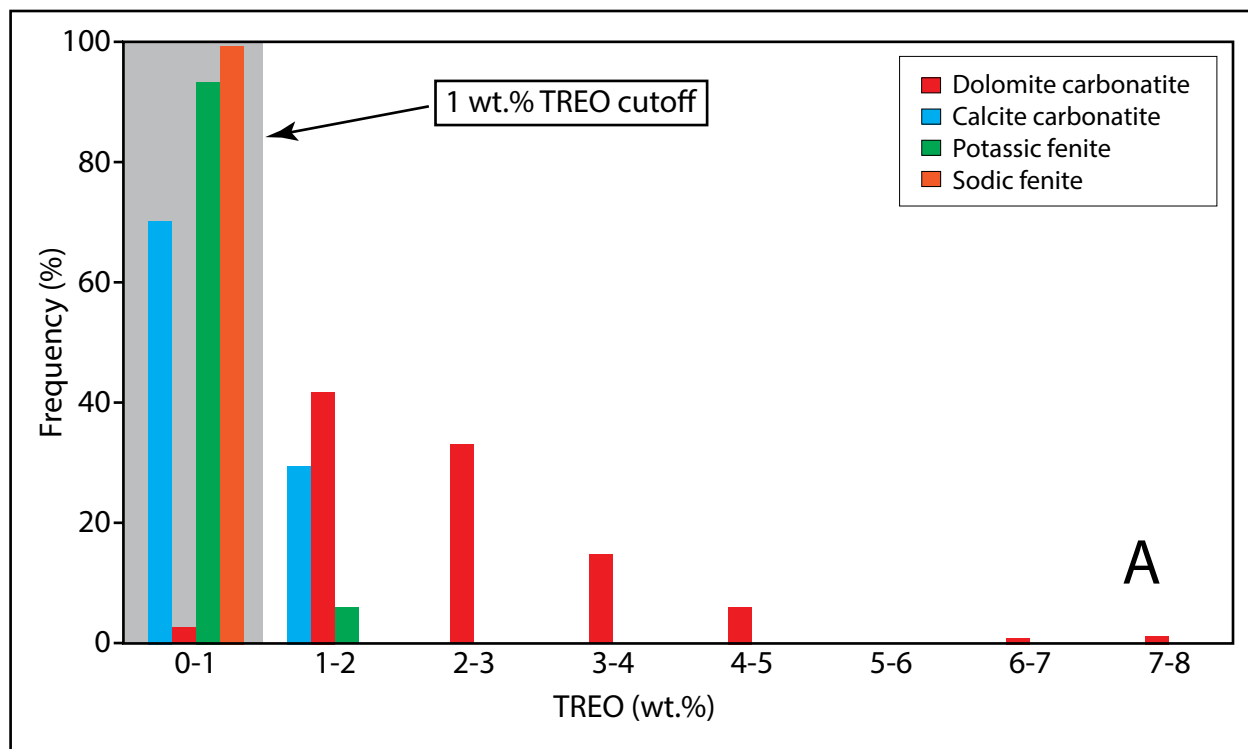
Fig. 18: A. A bar graph showing the total REE content in weight percent of the carbonatites and fenites. B. A bar graph showing the total niobium content in weight percent of the carbonatites and fenites. The graphs were constructed from company drill core assay data (Lane, 2009; 2010).
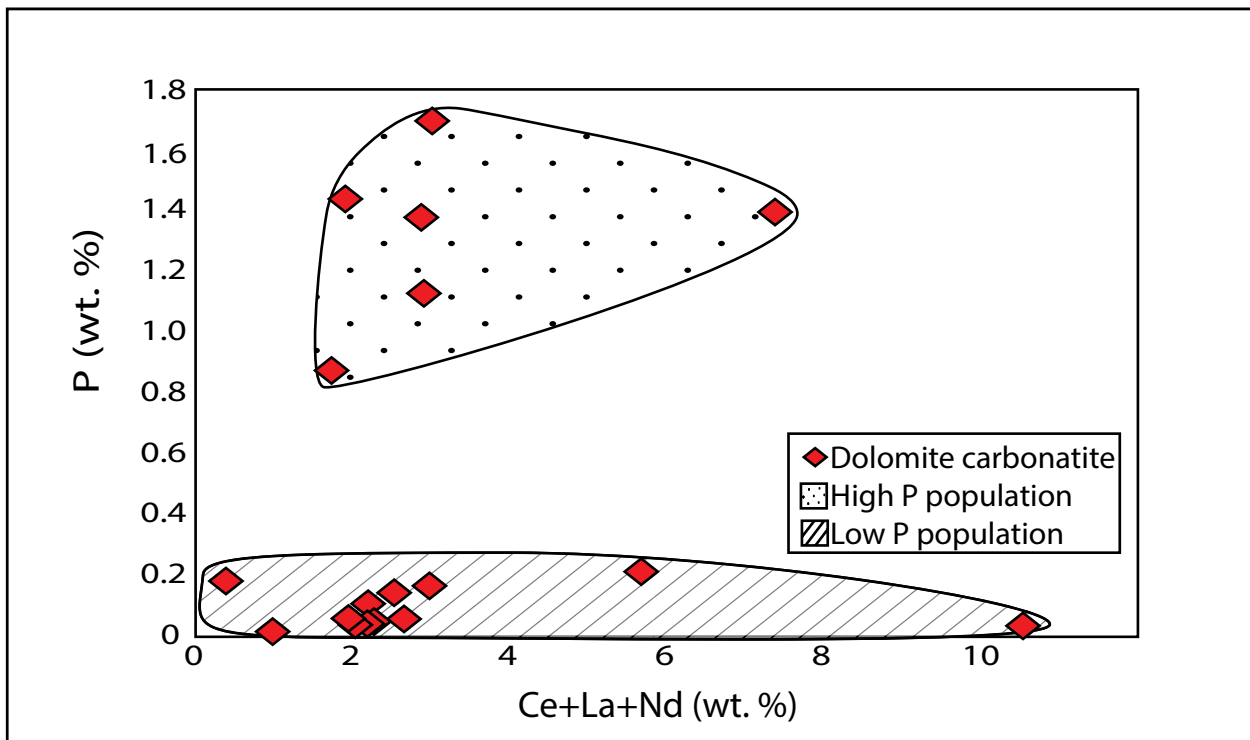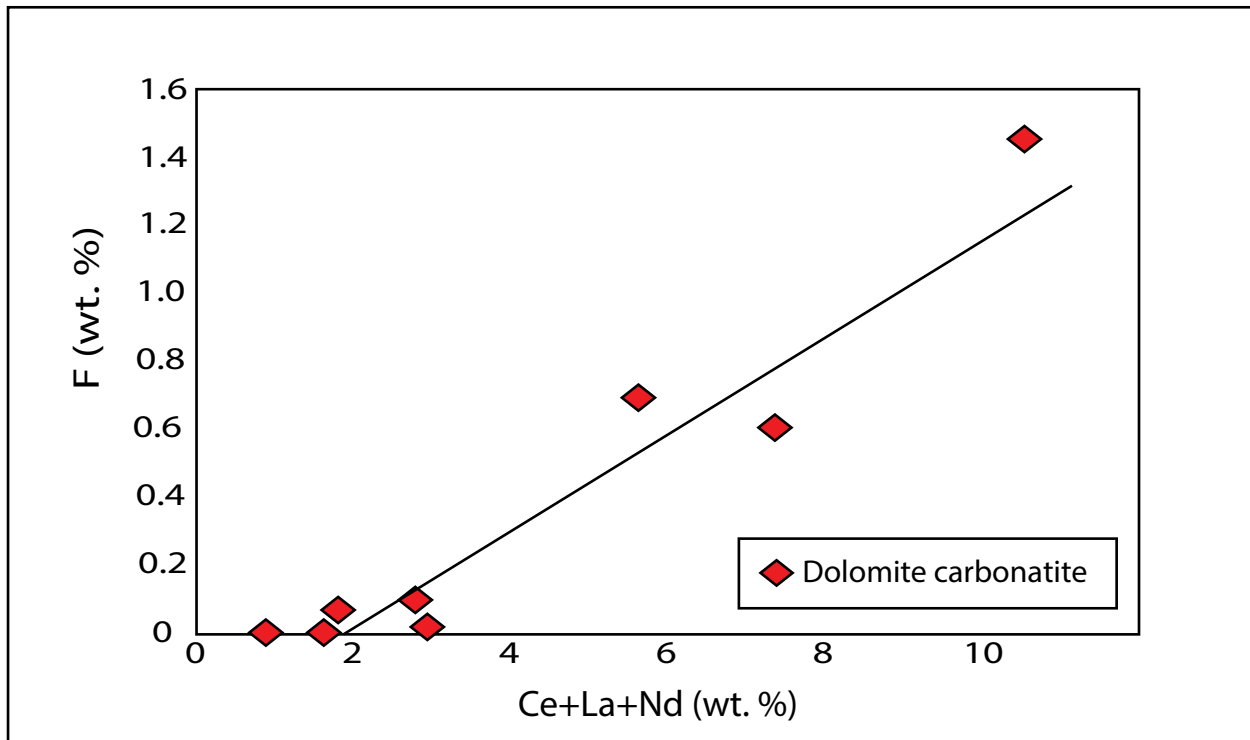
Fig. 19: A. The concentration of Ce+La+Nd (wt.%) as a function of F concentration (wt. %) in the dolomite carbonatite. The trend line illustrates the linear relationship between F and LREE contents. B. The concentration of Ce+La+Nd (wt.%) as a function of P concentration in the dolomite carbonatite. The data indicate the presence of a high P population (representing fluorapatite-bearing fenite xenoliths), and a low P population (xenolith-free).

Mineral Chemistry

Carbonates

Electron microprobe analyses were conducted on crystals of Dolomite 1, 2, and 3 in samples collected from the main intrusion (WI-11-02, WI-11-07, WI-11-09, and WI-11-12) and the carbonatite outcrop northeast of the main intrusion (WI-13-11). The average compositions of Dolomite 1 and 2 are quite similar (Table 3). Dolomite 1 has average CaO, FeO, MgO, MnO contents of 29.6, 18.4, 5.1, and 0.6 wt.%, respectively, and Dolomite 2 has average concentrations for these oxides of 29.6, 17.0, 6.7, and 0.8 wt.%, respectively. However, FeO:MgO ratios of Dolomite 1 are on average lower and have a more limited range (average XFe_{Dol1}=0.24; Fig. 20A) than those of Dolomite 2 (average XFe_{Dol2}=0.31; Fig. 20A) 2. Dolomite 3 has a similar CaO content (29.33 wt.%) to Dolomite 1 and Dolomite 2, but on average, it contains less MgO (14.69 wt.%), and more FeO (9.26 wt.%) and MnO (1.14 wt.%). Moreover, it is progressively enriched in FeO and MnO inwards from its contacts with Dolomite 2 or from the walls of the cavities (in which it commonly occurs) to their centers (Figure 20B and C).The three dolomite types display a distribution of CaO, FeO and MgO contents that broadly mimics that of the corresponding bulk rock, although the latter are displaced to higher FeO and higher CaO (Table 1, Table 3; Figure 21). The Ba and Sr contents of both Dolomite 1 and Dolomite 2 are below the corresponding detection limits. By comparison, Dolomite 3 contains elevated SrO (0.16 wt.%).

83

Table 3: Average composition of carbonates in the Wicheeda carbonatite.

Mineral		Dolomite			Calcite
Rock type		Dolomite carbonatite			Calcite carbonatite
Classification		Dol 1	Dol 2	Dol 3	
		n=28	n=82	n=44	n=18
CaO	wt.%	29.55	29.57	29.33	53.36
MgO		18.39	17.00	14.69	0.36
FeO		5.13	6.65	9.26	1.84
MnO		0.57	0.83	1.14	1.19
SrO		b.l.	b.l.	0.16	b.l.
CO_2		46.24	46.01	45.87	43.15
Total		99.88	100.06	100.45	99.90
Cations		O=6			O=3
Ca	apfu	1.01	1.01	1.00	0.95
Mg		0.86	0.81	0.71	0.01
Fe^{2+}		0.14	0.18	0.25	0.03
Mn		0.02	0.02	0.03	0.02
Sr		0.00	0.00	0.00	0.00
C		1.99	2.00	2.01	0.98
Total		4.01	4.00	3.99	1.99

Notes: b.l. Below detection limits for oxides (wt.%), as noted in Appendix D
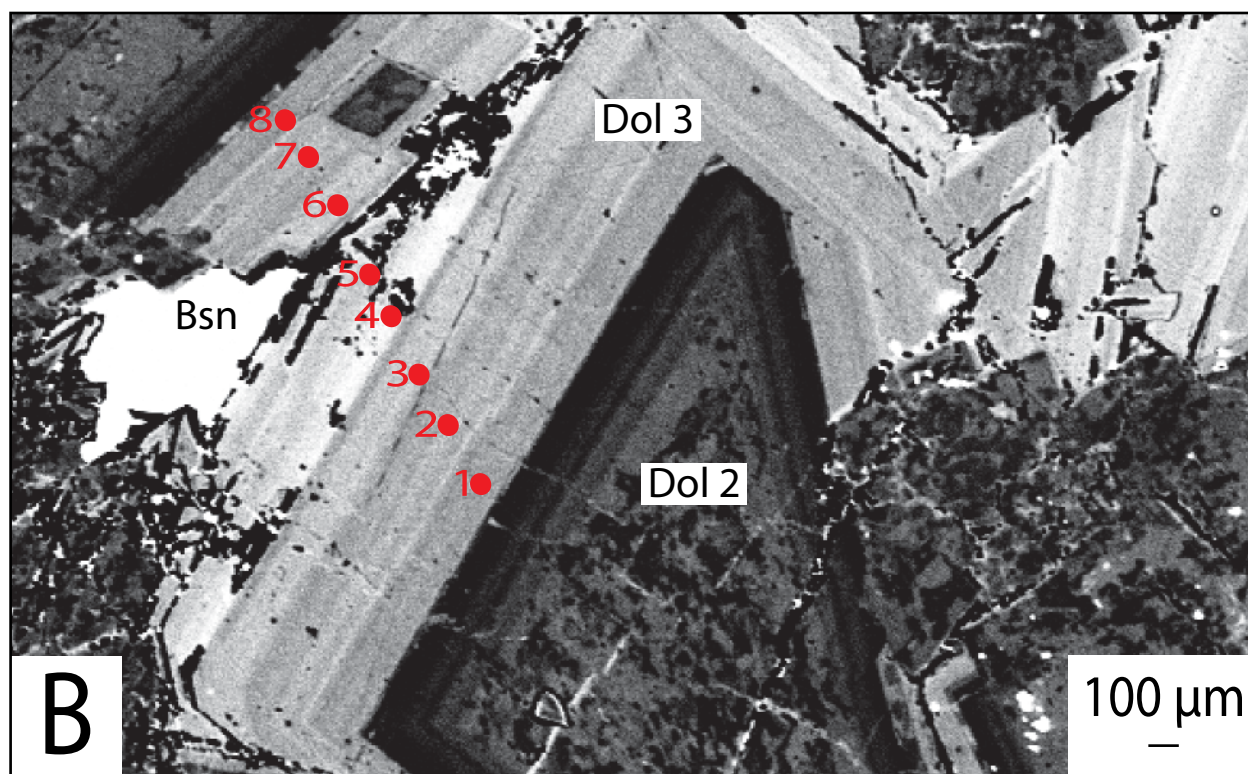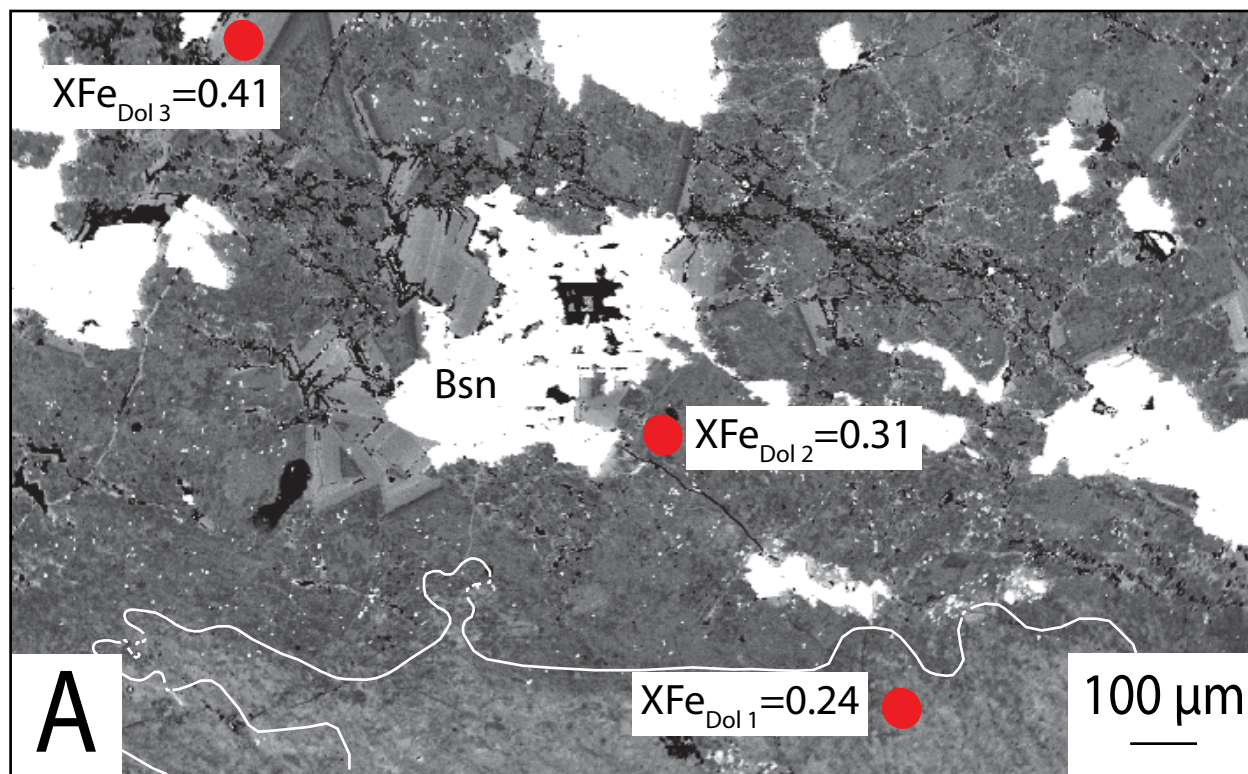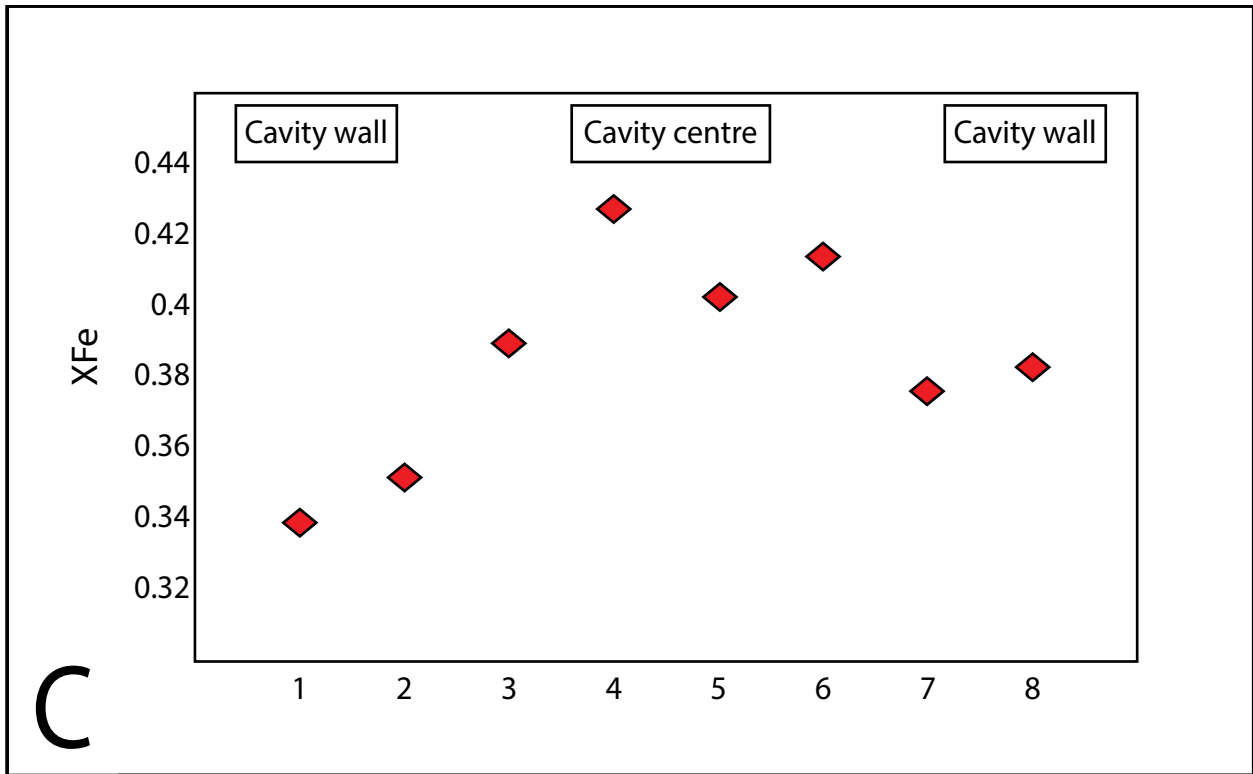
Fig. 20: A. Back-scattered electron image of dolomite carbonatite (WI-13-11). Iron-poor Dolomite 1 (light grey) was altered to iron-rich Dolomite 2 (dark grey) near a fracture partially infilled by compositionally zoned Dolomite 3 and bastnäsite-(Ce) (Bsn). The three red filled circles show the locations of analyses of Dolomite 1, Dolomite 2 and Dolomite 3 and the adjacent text boxes the corresponding mole fraction of Fe (XFe) B. Back-scattered electron image showing the location of an electron-microprobe traverse across Dolomite 3 from a cavity wall to the cavity centre. C. The XFe value for each of the locations in Dolomite 3 indicated in B.
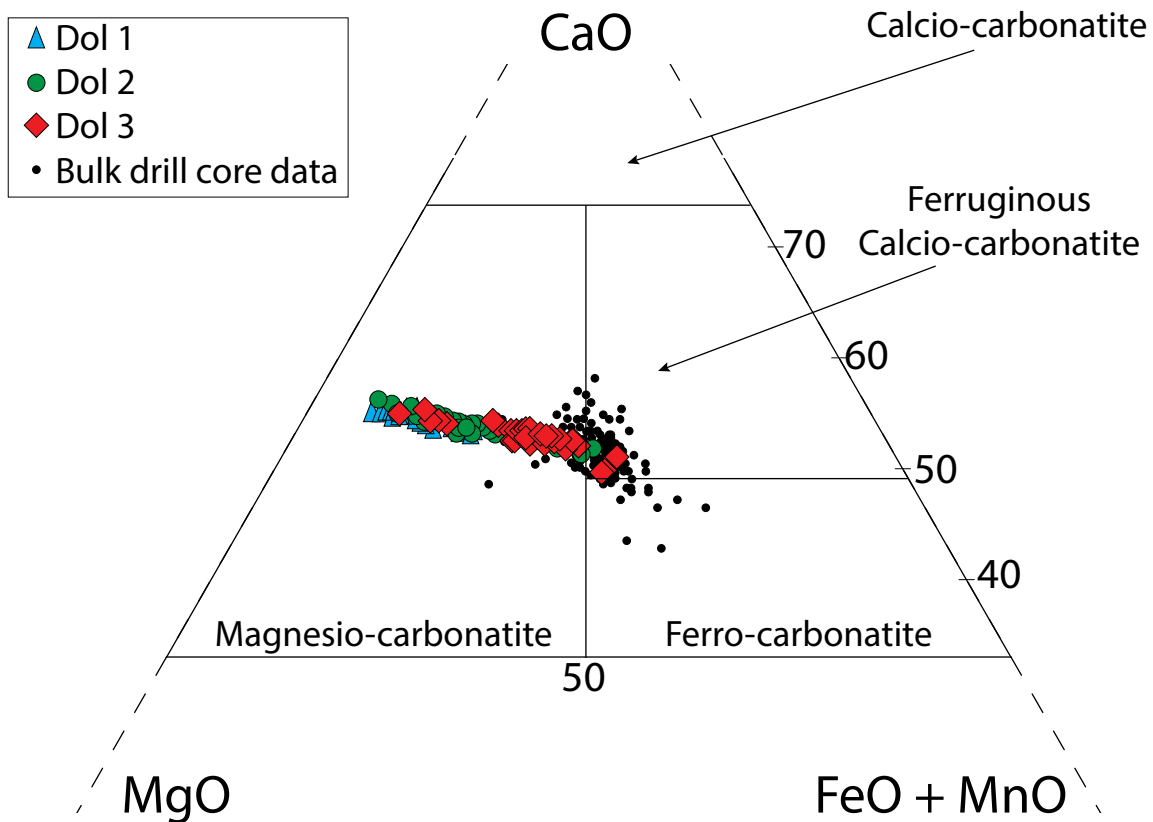
Fig. 21: The composition of Dolomite 1, Dolomite 2 and Dolomite 3 in terms of the components CaO, MgO, and FeO (molar proportions). The bulk rock compositions and fields of the carbonatite types of Gittins and Harmer (1997) are shown for comparison (see main text for further detail).

Calcite grains were analyzed in a single sample of calcite carbonatite. This mineral is close to the end-member composition with 53.4 wt.% CaO and 43.2 wt.% CO_2. There are minor concentrations of MgO (0.36 wt.%), FeO (1.84 wt.%), Mn (1.19 wt.%), SrO (0.03 wt.%). Barium is below its limit of detection.

Silicates

Mica

The compositions of micas from the dolomite and calcite carbonatites (Table 4) identify them as members of the phlogopite-biotite series (e.g., Fig. 22). Mica in the dolomite carbonatite has a composition ranging from 54 to 60% of the phlogopite component and appreciable contents of TiO_2 (1.87 wt.%) and F (2.9 wt.%), whereas mica in the calcite carbonatite contains between 75 and 78% of the biotite component. In addition to its higher biotite content, mica in the calcite carbonatite contains more TiO_2 (3.74 wt.%) and less F (0.19 wt.%) than in the dolomite carbonatite.

The major element chemistry of the mica in potassic and sodic fenite is very similar (Table 4). There is from 52 to 62% phlogopite and appreciable TiO_2 (1.9 wt.%) and F (2.8 wt.%). Compositionally, this mica is similar to mica in the dolomite carbonatite (Fig. 22).
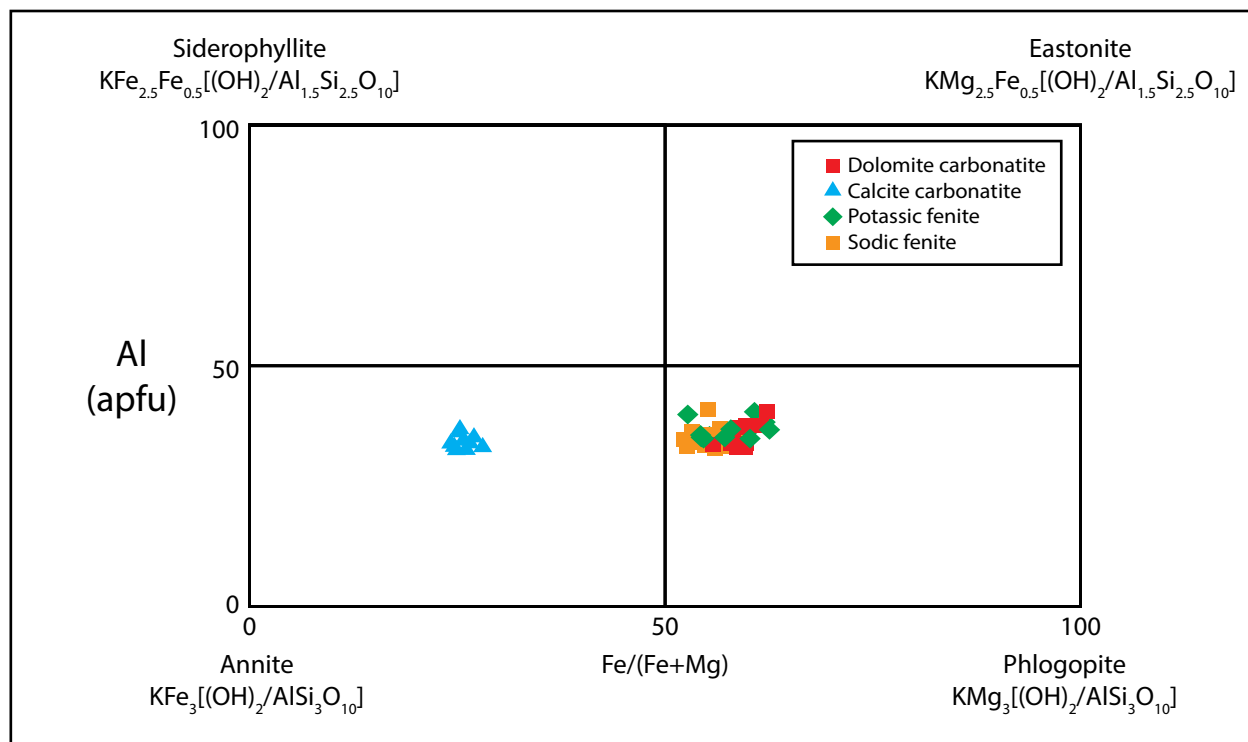
Fig. 22: The composition of mica in the dolomite carbonatite, calcite carbonatite, potassic fenite, and sodic fenite in terms of the end member components, siderophyllite, eastonite, phlogopite, and annite after Rieder et al. (1998).

Table 4: Average composition of biotite, amphibole and pyroxene in sodic fenite (AFEN), potassic fenite (KFEN), dolomite carbonatite (Cd), and calcite carbonatite (Cc).

Mineral		Biotite					Magnesioriebeckite	Aegirine		Aegirine-Augite
Rock Type		AFEN	KFEN	KFEN	Cd	Cc	KFEN	KFEN	KFEN	Cc
Sample		WI-13-01	WI-13-35	WI-13-37	WI080101	WI090806	WI-13-37	WI-13-37	08-WI-01-12	WI-09-08-06
		n=18	n=9	n=17	n=15	n=13	n=17	n=15	n=10	n=18
SiO_2	wt.%	38.97	38.37	38.96	39.06	35.08	54.94	52.10	52.41	50.94
TiO_2		1.97	1.75	1.91	1.87	3.74	0.53	1.87	1.43	0.35
Al_2O_3		10.94	11.83	11.53	11.17	10.02	0.87	0.84	1.28	0.58
FeO		19.37	19.17	18.92	18.82	31.11	16.55	26.84	27.35	26.33
MnO		0.19	0.17	0.16	0.16	0.53	0.04	0.08	b.l.	0.39
MgO		13.58	13.19	13.58	13.87	6.16	12.99	0.56	0.45	2.81
CaO		0.06	0.06	0.05	0.07	0.09	0.53	0.38	0.22	10.10
Na_2O		0.17	0.12	0.14	0.19	0.107	7.82	13.80	13.93	7.77
K_2O		10.16	10.17	10.27	10.20	9.67	1.65	b.l.	b.l.	b.l.
F		2.78	2.66	2.83	2.90	0.19	1.72	b.l.	b.l.	b.l.
Total		98.18	97.49	98.36	98.31	94.62	97.64	96.50	97.11	99.87
Cations	apfu			O=12			O=23	O=6		O=6
Si		2.99	2.95	3.04	2.99	2.99	8.02	1.97	1.96	1.97
Ti		0.12	0.11	0.11	0.12	0.24	0.06	0.06	0.04	0.01
Al		1.08	1.17	1.15	1.10	1.03	0.15	0.04	0.06	0.03
Fe^{2+}		-	-	-	-	1.05	2.05	0.09	0.09	-
Fe^{3+}		1.35	1.35	1.26	1.31	1.23	0.25	0.84	0.85	0.76
Mn		0.00	0.00	0.00	0.00	0.04	0.00	0.00	0.00	0.01
Mg		1.69	1.65	1.62	1.72	0.79	2.88	0.03	0.03	0.16
Ca		0.00	0.00	0.00	0.00	0.17	0.08	0.02	0.01	0.41
Na		0.03	0.02	0.09	0.03	0.02	2.25	1.10	1.11	0.58
K		1.08	1.09	1.05	1.08	1.04	0.31	0.00	0.00	0.00
F		0.69	0.67	0.67	0.72	0.05	0.78	0.00	0.00	0.00

Notes: b.l. Below detection limits for oxides (wt.%), as noted in Appendix D

Below detection limits for oxides (wt.%), which are as follows: Si, 0.04; Ti, 0.05; Al, 0.03; Fe, 0.04; Mn, 0.04; Mg, 0.02; Ca, 0.03; Na, 0.03; K, 0.02; F, 0.17; Cl, 0.03.

Amphibole

Amphibole was only observed in one sample (WI-13-37), a potassic fenite, in which it replaced aegirine. Its composition (Table 4) classifies it as magnesioriebeckite (Fig. 23; Hawthorne et al., 2012).

Pyroxene

Pyroxene was observed in two samples of potassic fenite (WI-13-37, 08-WI-01-12) and one sample of calcite carbonatite (WI-09-08-06). In the potassic fenite, the pyroxene classifies as aegirine on the sodic pyroxene ternary diagram (e.g., Fig. 24) of Morimoto et al. (1988). It contains from 70 to 74% of the aegirine end-member and from 0.5 to 3.8% of the jadeite end-member, and is characterized by a high content of Na_2O (13.85 wt.%), and low Al_2O_3 (1 wt.%), and CaO (0.5 wt.%) contents (Table 4). Its manganese content is below the detection limit and the TiO_2 content is comparable to that in the mica (1.69 wt.%). The pyroxene in the calcite carbonatite contains more calcium (10.1 wt.% CaO), magnesium (2.81 wt.% MgO), and manganese (0.39 wt.% MnO), and less Na_2O (7.77 wt.%) and TiO_2 (0.35 wt.%). Its composition defines a linear trend straddling the boundary between aegirine and aegirine-augite (Fig. 24).
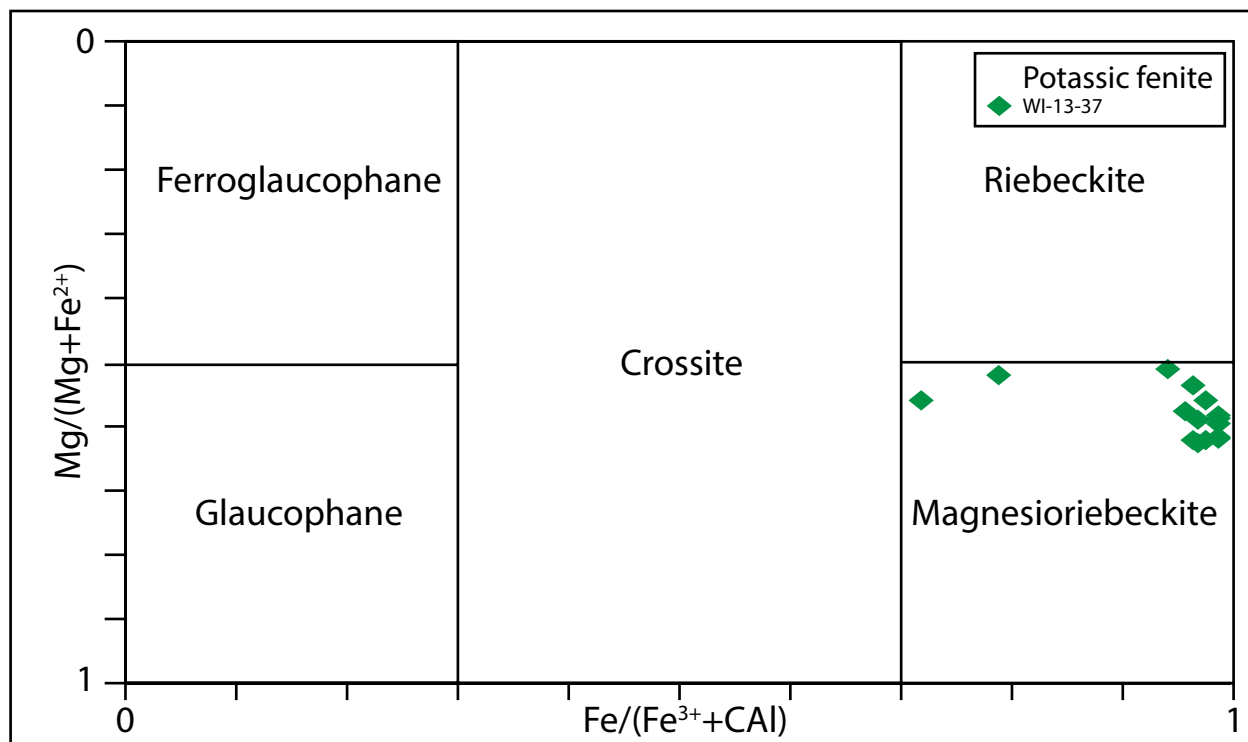
Fig. 23: The composition of amphibole in the potassic fenite represented on the classification diagram of Hawthorne et al. (2012).
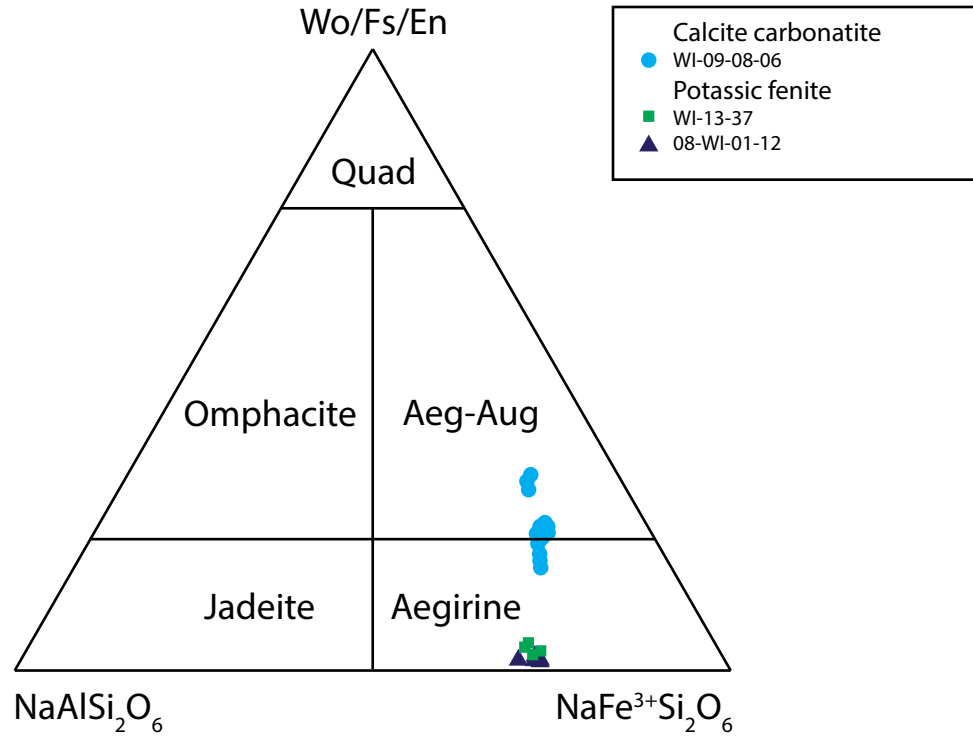
Fig. 24: The composition of pyroxene in calcite carbonatite and potassic fenite represented on the classification diagram of Morimoto et al. (1988). Wo/Fs/En refer to wollastonite ($CaSiO_3$), forsterite (Mg_2SiO_4), and enstatite ($FeSiO_3$), respectively.

Alkali feldspar

Alkali feldspar is observed in both the carbonatites and fenites. It occurs as potassium feldspar (Or_{98}) in the dolomite carbonatite and contains minor BaO (2.77 wt.%); SrO and Rb_2O are at or below their detection limits (Table 5). The calcite carbonatite only contains albite (Ab_{92} to Ab_{99}); BaO, SrO, and Rb_2O concentrations are at or below the detection limits.

Feldspars in the potassic and sodic fenite are near the potassium feldspar and albite end-members on an anorthite-albite-orthoclase ternary diagram, respectively (Table 5, Fig. 25). Feldspar in the potassic fenite contains both potassium feldspar, which has a composition of Or_{78-99}, and albite (Ab_{90-99}). The albite has low concentrations of FeO (0.4 wt.%) and CaO (0.32 wt.%). The SrO and Rb_2O contents of the feldspars are at or below their detection limits; minor concentrations of BaO were observed in the albite (0.68 wt.%). In the sodic fenite, the feldspar is exclusively albite with a much narrower range in composition than in the potassic fenite (Ab_{98} to Ab_{99}) and has low concentrations of FeO (up to 1.6 wt.%) and CaO (up to 1.5 wt.%). The BaO, SrO, and Rb_2O contents are at or below their detection limits.

Table 5: Average composition of alkali feldspar in sodic fenite (AFEN), potassic fenite (KFEN), dolomite carbonatite (Cd), and calcite carbonatite (Cc).

Mineral		Feldspar								
Rock Type		*AFEN*	*KFEN*	*KFEN*	*KFEN*	*KFEN*	*KFEN*	*KFEN*	*Cc*	*Cd*
Sample		WI-13-01	WI-13-09	WI-13-09	WI-13-55	WI-13-55	WI-13-57	WI-13-57	WI-13-38	WI090902
		n=9	n=30	n=10	n=17	n=21	n=11	n=11	n=15	n=7
SiO_2	wt.%	68.40	67.48	64.45	66.09	65.87	68.38	63.15	67.70	62.79
Al_2O_3		19.65	19.29	18.43	19.51	18.82	19.08	19.23	19.44	19.40
Na_2O		11.37	11.29	0.50	6.81	4.23	11.18	0.36	11.35	0.35
K_2O		0.09	0.08	15.89	0.14	10.46	0.06	15.56	0.07	15.09
BaO		b.l.	b.l.	b.l.	1.16	0.10	b.l.	0.21	b.l.	2.77
CaO		0.04	0.32	0.09	0.12	0.17	b.l.	0.11	0.51	b.l.
FeO		b.l.	0.44	0.07	0.11	0.07	0.08	0.15	b.l.	0.10
Total		99.63	98.98	99.52	100.15	99.78	98.87	98.83	99.18	100.57
Cations					O=8					
Si	apfu	2.99	2.96	2.91	2.99	2.95	3.10	2.95	2.98	2.90
Al		1.01	1.00	0.98	1.01	1.03	0.90	1.07	1.01	1.06
Na		0.97	0.96	0.04	0.96	0.05	0.87	0.03	0.97	0.03
K		0.00	0.00	0.91	0.01	0.91	0.00	0.93	0.00	0.90
Ba		0.00	0.00	0.00	0.00	0.02	0.00	0.00	0.00	0.04
Ca		0.00	0.09	0.22	0.01	0.01	0.00	0.01	0.03	0.00
Fe		0.00	0.02	0.01	0.00	0.04	0.00	0.01	0.00	0.10

Notes: b.l. Below detection limits for oxides (wt.%), as noted in Appendix D
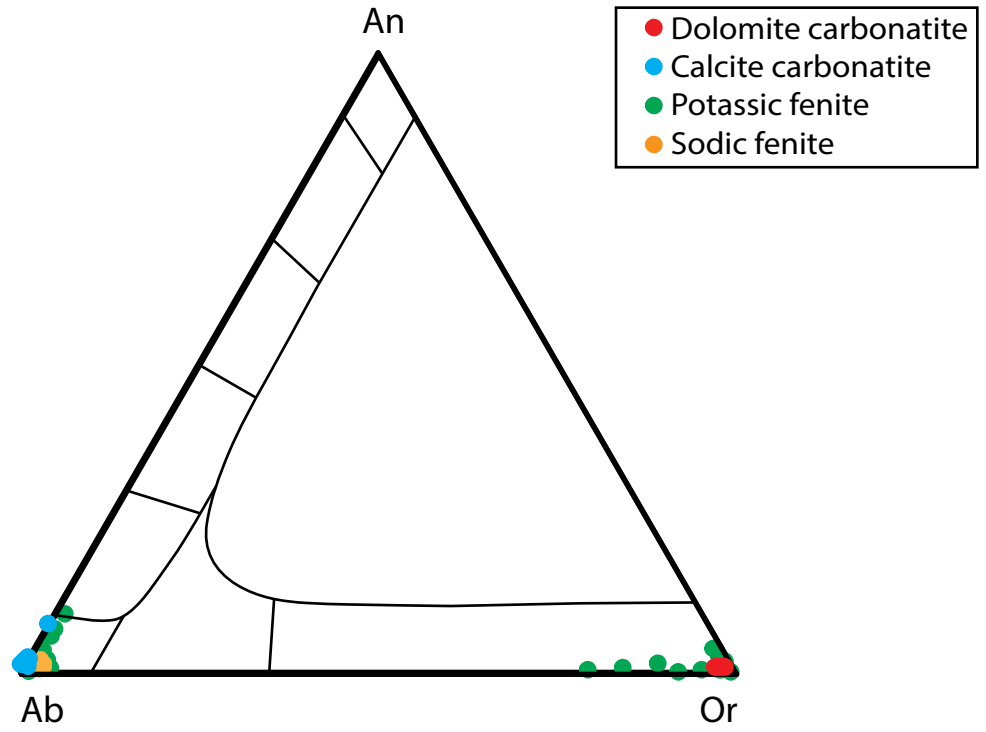
Fig. 25: The composition of feldspar in sodic fenite, potassic fenite, and calcite carbonatite in terms of the components, anorthite, albite and orthoclase.

REE and HFSE Minerals

The REE are concentrated mainly in the dolomite carbonatite as REE-fluorocarbonate minerals, Sr-REE-carbonate minerals, and monazite-(Ce); they are also concentrated to a much smaller degree as monazite-(Ce) and apatite in the fenites. Niobium is present as pyrochlore in the calcite carbonatite and mainly as niobian rutile in the dolomite carbonatite. Thorite is the main thorium-bearing mineral, however, minor concentrations of Th are also present in ancylite-(Ce) and monazite-(Ce).

REE-carbonate minerals

The REE-fluorocarbonate and Sr-REE-carbonate minerals are the most abundant REE-bearing minerals in the Wicheeda Carbonatite. They comprise (in order of decreasing abundance) bastnäsite-(Ce), parisite-(Ce), ancylite-(Ce), cordylite-(Ce), and synchysite-(Ce). Cordylite-(Ce) (Ba-REE-fluorocarbonate) replaced barite in fractures and vugs containing Dolomite 3, and was later replaced by ancylite-(Ce) (Sr-REE-fluorocarbonate), and in turn by bastnäsite-(Ce), parisite-(Ce), and synchysite-(Ce); synchysite-(Ce) replaced parisite-(Ce). The results of electron microprobe analyses of the REE-fluorocarbonate and Sr-REE-carbonate minerals are summarized in Table 6.

Table 6: Average composition of REE-fluorocarbonate and REE-carbonate minerals in dolomite carbonatite.

Mineral		Bastnäsite-(Ce) n=43	Parisite-(Ce) n=41	Synchysite-(Ce) n=4	Cordylite-(Ce) n=8	Ancylite-(Ce) n=8
CaO	wt.%	0.25	10.21	18.98	2.73	2.45
La_2O_3		28.19	21.07	18.13	15.99	18.67
Ce_2O_3		35.52	29.14	23.21	22.08	24.93
Pr_2O_3		2.91	2.71	1.95	0.44	2.18
Nd_2O_3		7.25	7.44	5.10	3.62	5.38
Sm_2O_3		b.l.	0.25	0.38	0.14	b.l.
Gd_2O_3		0.18	0.30	0.16	b.l.	0.21
Y_2O_3		0.06	0.12	0.08	b.l.	0.09
CO_2^1		16.91	21.05	25.58	29.39	20.87
SrO		0.04	0.30	0.53	2.68	14.92
BaO		0.04	0.04	0.05	19.76	0.60
ThO_2		0.19	0.36	0.23	b.l.	1.67
SiO_2		0.06	0.04	0.06	0.02	0.51
Na_2O		b.l.	b.l.	b.l.	3.25	b.l.
Al_2O_3		0.02	0.03	b.l.	0.16	0.02
UO_2		0.01	0.01	0.01	0.01	0.02
F		8.22	6.88	5.53	2.72	0.86
Cl		b.l.	b.l.	b.l.	b.l.	0.02
H_2O^1						6.41
Total		100.00	100.00	100.00	100.00	100.00
Cations		O=3	O=9	O=6	O=12	O=8
Ca	apfu	0.01	1.01	1.17	0.33	0.18
La		0.38	0.71	0.38	0.66	0.48
Ce		0.47	0.98	0.49	0.91	0.64
Pr		0.04	0.09	0.04	0.02	0.06
Nd		0.09	0.24	0.10	0.15	0.13
Sm		0.00	0.01	0.01	0.01	0.00
Gd		0.00	0.01	0.00	0.00	0.00
Y		0.00	0.00	0.00	0.00	0.00
Sr		0.00	0.02	0.02	0.17	0.61
Ba		0.00	0.00	0.00	0.87	0.02
Th		0.00	0.01	0.00	0.00	0.02
Si		0.00	0.00	0.00	0.00	0.04
Na		0.00	0.00	0.00	0.71	0.00
Al		0.00	0.00	0.00	0.02	0.00
U		0.00	0.00	0.00	0.00	0.00
F		0.74	1.67	1.00	0.96	0.19
Cl		0.00	0.00	0.00	0.00	0.00
C^2		1.00	3.00	2.00	4.00	2.00
H^2						3.00

Notes: b.l. Below detection limits for oxides (wt.%), as noted in Appendix D
1 Calculated.
2 Based on ideal chemical formula.

Bastnäsite-(Ce) has a near-ideal composition with 74.2 wt.% TREO and 8.2 wt.% F. It is strongly LREE-selective (mainly Ce) with an average Ce/Y ratio of 592 and contains trace amounts of Gd_2O_3 (0.18 wt.%) and Y (0.06 wt.%) as well as CaO (0.25 wt.%), ThO_2 (0.19 wt.%), BaO (0.04 wt.%), and SrO (0.04 wt.%). In some samples there is a small positive chondrite-normalized Eu anomaly (Fig. 26A).

Parisite-(Ce), which occurs as syntactic intergrowths in bastnäsite-(Ce), has TREO and F contents of 60.98 wt.% and 6.88 wt.%, respectively and a Ce/Y ratio of 242. The average CaO content is 10.2 wt.%, and there are traces of Sm_2O_3 (0.25 wt.%), Gd_2O_3 (0.30 wt.%), and Y (0.12 wt.%) as well as ThO_2 (0.36 wt.%), SrO (0.3 wt.%), and BaO (0.04 wt.%).

Synchysite-(Ce) was only observed in one sample (WI091006; 90.6 m depth) and has average REE and F contents of 48.97 and 5.53 wt.%, respectively. The average Ce/Y ratio is 292 and the Sm_2O_3 (0.38 wt.%), Eu_2O_3 (0.04 wt.%), Gd_2O_3 (0.16 wt.%), and Y (0.08 wt.%) contents are comparable to those of bastnäsite-(Ce) and parisite-(Ce). However, the Dy_2O_3 content (below the detection limit) is the lowest of any of the REE minerals. The average CaO content is 18.98 wt.%, and there are traces of ThO_2 (0.23 wt.%), SrO (0.52 wt.%), and BaO (0.05 wt.%). Like bastnäsite-(Ce), synchysite-(Ce) displays a slightly positive chondrite-normalized Eu anomaly (Fig. 26C).

Ancylite-(Ce) and cordylite-(Ce) are strongly LREE-enriched. Indeed, with a Ce:Y ratio of 3360, ancylite-(Ce) is the most strongly LREE-enriched mineral in the Wicheeda

99

system (Fig. 26D) . It contains an average of 51.62 wt.% TREO, 14.92 wt.% SrO and

2.45 wt.% CaO. As for the REE fluorocarbonate minerals, it contains traces of Gd_2O_3

(0.21 wt.%), and Y (0.09 wt.%) as well as small proportions of SiO_2 (0.51 wt.%) and

BaO (0.6 wt.%), and has the highest ThO_2 (1.67 wt.%) content of any of the REE

minerals.

Cordylite-(Ce) has the lowest TREO content of any of the REE minerals (42.43 wt.%;

Fig. 26E), and an average BaO content of 19.76 wt.%, CaO content of 2.73 wt.%, Na_2O

content of 3.25 wt.%, and F content of 2.72 wt.%. The Ce/Y ratio averages 816 and there

are traces of Sm_2O_3 (0.14 wt.%), Gd_2O_3 (0.12 wt.%), Y (0.03 wt.%), and ThO_2 (0.09

wt.%).

The chondrite-normalized REE-profiles of ancylite-(Ce) and cordylite-(Ce) (Fig. 26D and

E) are very similar to those of bastnäsite-(Ce) and synchysite-(Ce), although the HREE

contents of ancylite-(Ce) and cordylite-(Ce) are higher. In some samples both ancylite-

(Ce) and cordylite-(Ce) display small positive Eu anomalies.

Monazite-(Ce)

As discussed earlier, monazite-(Ce) occurs mainly as fine-grained euhedral lath-like

inclusions in albite+apatite xenoliths in dolomite carbonatite and as inclusions in the

REE-fluorocarbonates, and to a much lesser extent near apatite in the potassic fenite.

Like the other REE minerals, monazite-(Ce) is strongly enriched in the LREE (Table 7;

Ce/Y of 565) and contains traces of Sm_2O_3 (0.55 wt.%), Gd_2O_3 (0.42 wt.%), and Y (0.11

wt.%). There are also minor concentrations of SiO_2 (0.17 wt.%), ThO_2 (0.09 wt.%), CaO

(0.22 wt.%), and Sr (0.23 wt.%). The slopes of the chondrite-normalized REE profiles are much lower than those of bastnäsite-(Ce), ancylite-(Ce), and cordylite-(Ce), and are comparable to those of parisite-(Ce) and synchysite-(Ce) (Fig. 26A to F), which reflects the higher HREE content of monazite-(Ce), parisite-(Ce), and synchysite-(Ce) (Table 6 and Table 7).
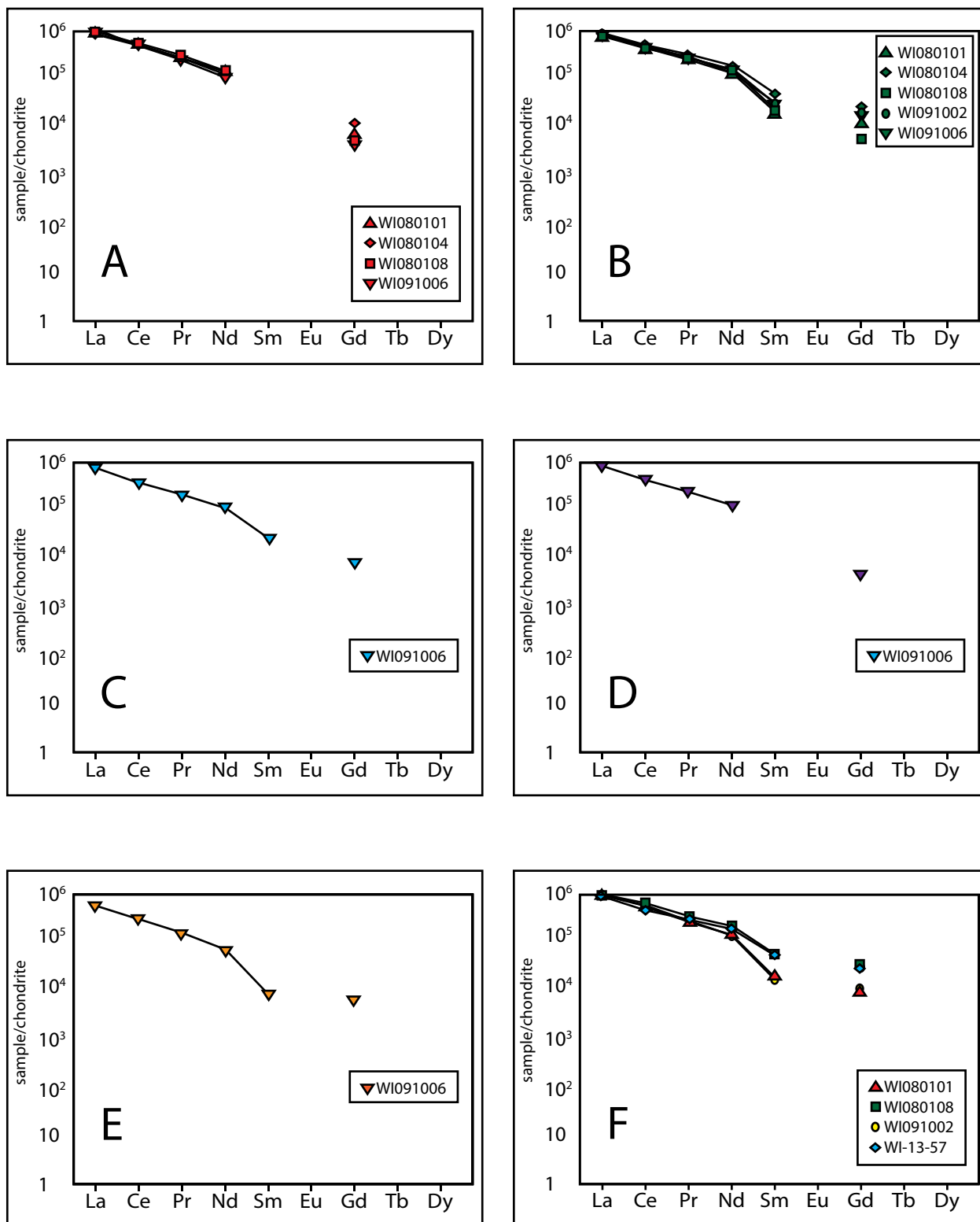
Fig. 26: A-F: Chondrite-normalized REE-profiles for the major REE-bearing minerals in the Wicheeda carbonatite. A. Bastnäsite-(Ce). B. Parisite-(Ce). C. Synchysite-(Ce). D. Ancylite-(Ce) E. Cordylite-(Ce). F. Monazite-(Ce). The chondrite values were taken from McDonough and Sun (1995).

102

Table 7: Average composition of monazite-(Ce) in potassic fenite (KFEN) and dolomite carbonatite (Cd).

Mineral		Monazite-(Ce)			
Rock Type		*KFEN*	*Cd*	*Cd*	*Cd*
Sample		WI-13-57	WI080101	WI080108	WI091002
		n=19	n=4	n=20	n=14
La$_2$O$_3$	wt.%	22.23	24.81	22.92	24.12
Ce$_2$O$_3$		32.60	33.74	31.73	34.79
Pr$_2$O$_3$		3.00	2.86	2.96	2.81
Nd$_2$O$_3$		8.63	6.91	8.89	6.67
Sm$_2$O$_3$		0.78	0.28	0.89	0.26
Gd$_2$O$_3$		0.62	0.20	0.64	0.22
Y$_2$O$_3$		b.l.	0.20	0.03	0.16
P$_2$O$_5$		29.54	30.26	28.74	29.09
CaO		0.28	0.21	0.28	0.11
SrO		0.31	0.09	0.45	0.07
ThO$_2$		0.87	1.08	0.50	0.58
SiO$_2$		0.19	0.24	0.09	0.16
F		0.24	0.28	0.21	0.20
Total		99.84	98.82	100.33	100.54
Cations		O=4			
La	apfu	0.32	0.35	0.34	0.35
Ce		0.47	0.48	0.47	0.51
Pr		0.04	0.04	0.04	0.04
Nd		0.12	0.10	0.13	0.10
Sm		0.01	0.00	0.01	0.00
Gd		0.01	0.00	0.01	0.00
Y		0.00	0.00	0.01	0.00
P		0.99	0.99	0.98	0.98
Ca		0.01	0.01	0.01	0.00
Sr		0.00	0.00	0.01	0.00
Th		0.01	0.00	0.00	0.01
Si		0.01	0.01	0.00	0.01
F		0.03	0.03	0.03	0.02

Notes: b.l. Below detection limits for oxides (wt.%), as noted in Appendix D

Apatite

Electron microprobe analyses of grains from the potassic (WI-13-37; WI-13-55) and sodic (WI-13-01) fenite revealed the mineral referred to earlier as apatite is in fact fluorapatite. Fluorapatite from the potassic fenite (Apatite 1) contains 0.14 wt.% Na_2O, 0.53 wt.% SrO, 0.86 wt.% LREE and minor concentrations of HREE (e.g., Y_2O_3 = 0.04 wt.%); ThO_2 is near the detection limit (Table 8). By contrast, fluorapatite from the sodic fenite (Apatite 2) has higher Na_2O (0.25 wt.%), SrO (1.03 wt.%), and HREE (e.g., Y_2O_3 = 0.42 wt.%) contents but lower LREE (0.7 wt.%). The ThO_2 contents are near the detection limit. The REE-profiles of Apatite 1 (e.g., Fig. 27A) are relatively flat with very modest HREE-enrichment whereas those of Apatite 2 (e.g., Fig. 28B) are flat or slightly LREE-enriched. In addition, Apatite 1 is compositionally zoned with a REE-poor core and a REE-enriched rim, whereas Apatite 2 is unzoned.

Table 8: Average composition of fluorapatite in sodic fenite (AFEN) and potassic fenite (KFEN).

Mineral		Apatite		
Rock Type		*AFEN*	*KFEN*	*KFEN*
Sample		WI-13-01	WI-13-37	WI-13-55
		n=10	n=9	n=10
CaO	wt.%	53.84	54.37	54.29
P_2O_5		40.89	40.93	41.72
Na_2O		0.25	0.12	0.16
SrO		1.03	0.43	0.62
SiO_2		b.l.	0.41	0.12
ThO_2		b.l.	0.05	b.l.
La_2O_3		b.l.	0.14	0.20
Ce_2O_3		0.20	0.38	0.42
Nd_2O_3		0.13	0.18	0.14
Y_2O_3		0.42	b.l.	b.l.
F		3.86	3.50	3.77
Cl		b.l.	0.10	b.l.
Total		99.42	99.28	100.06
Cations				
Ca	apfu	4.84	4.95	4.93
P		2.89	2.94	2.98
Na		0.08	0.02	0.03
Sr		0.05	0.02	0.03
Si		0.00	0.04	0.01
Th		0.00	0.00	0.00
La		0.00	0.00	0.01
Ce		0.01	0.01	0.01
Nd		0.00	0.01	0.00
Y		0.02	0.00	0.00
F		0.96	0.87	0.94
Cl		0.00	0.01	0.00

Notes: b.l. Below detection limits for oxides (wt.%), as noted in Appendix D
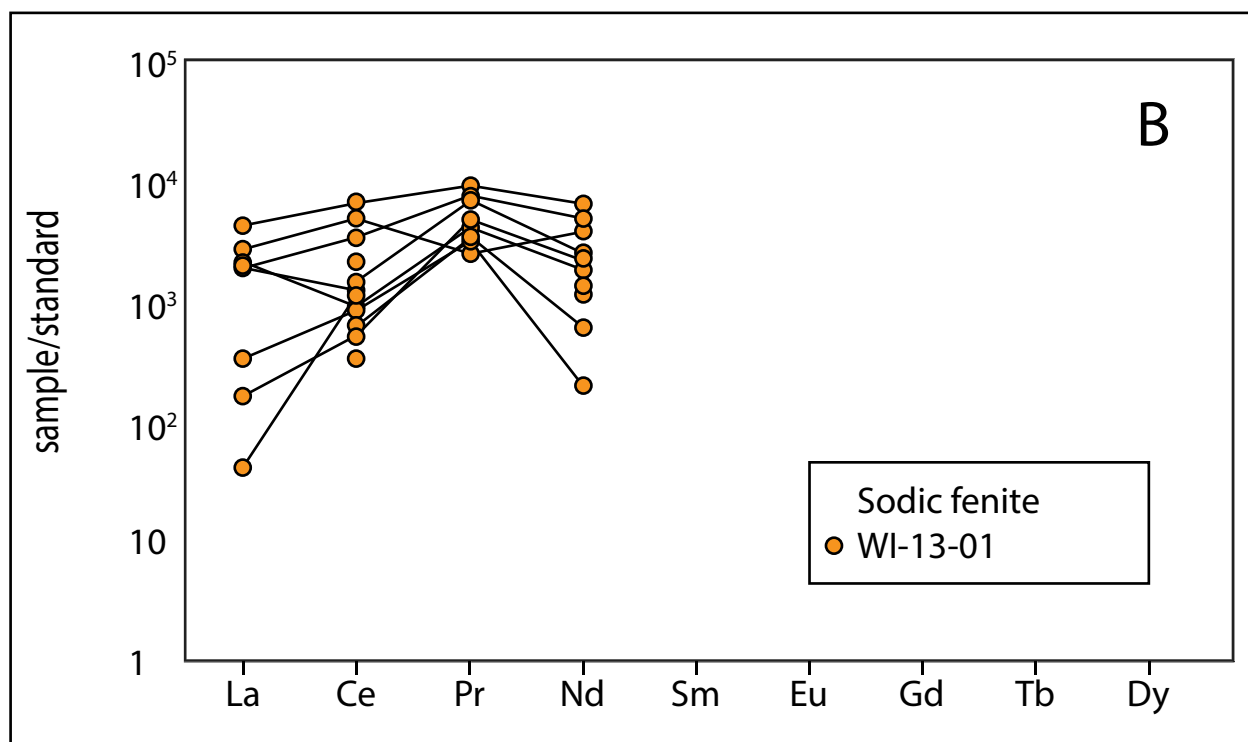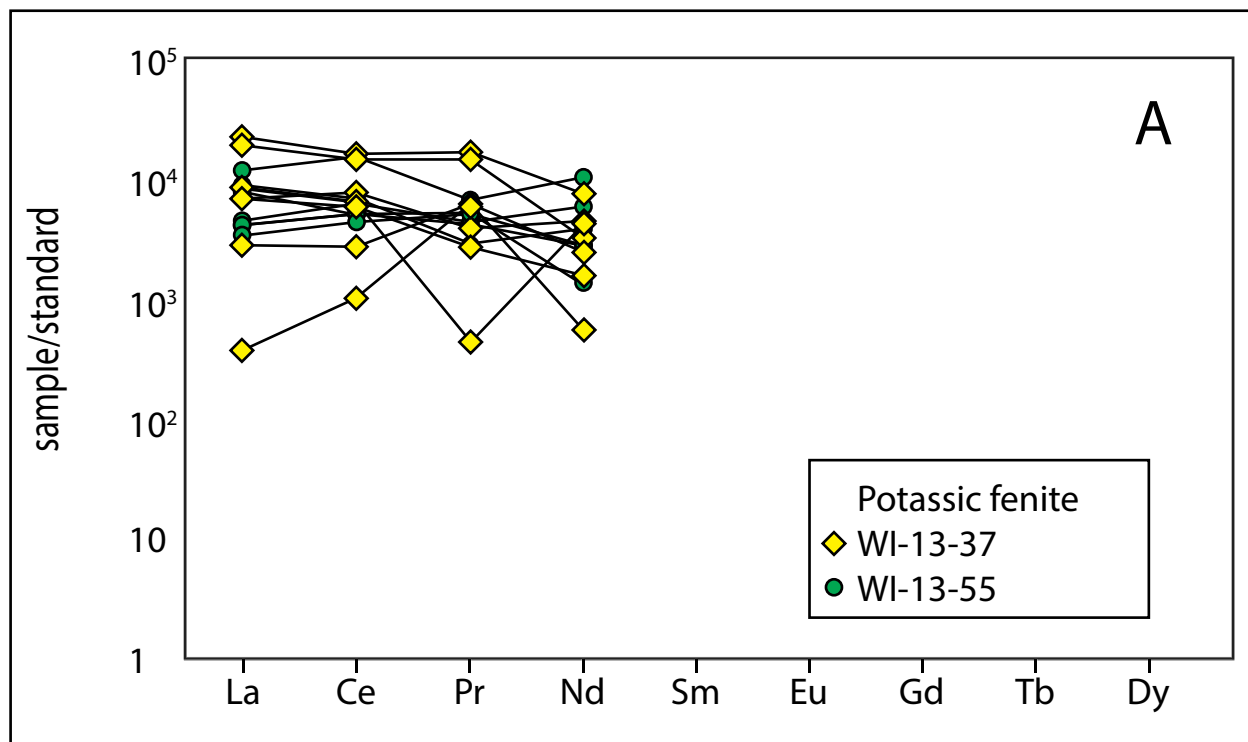
Fig. 27: Chondrite-normalized REE-profiles for fluorapatite samples from potassic fenite, A, and sodic fenite, B. The chondrite values were obtained from McDonough and Sun (1995).

106

Stable Isotope Geochemistry

A total of 20 samples of calcite, Dolomite 1, Dolomite 2, and Dolomite 3 were analyzed for their oxygen and carbon isotopes and standardized to $\delta\,^{13}C$ V-PDB and $\delta\,^{18}O$ V-SMOW, the results of which are summarized in Table 9. The $\delta\,^{13}C$ values of calcite in calcite carbonatite range from -6.31 to -6.27 ‰ and the $\delta\,^{18}O$ values from 6.91 to 6.97 ‰. Samples from the dolomite carbonatite have much higher values. The $\delta\,^{13}C$ and $\delta\,^{18}O$ values of Dolomite 1 range from -5.67 to -5.48 ‰ and from 9.35 to 10.02 ‰, respectively. Dolomite 2 has similar $\delta\,^{13}C$ and $\delta\,^{18}O$ values of -5.59 to -5.38 ‰ and 9.91 to 10.22 ‰, respectively. The $\delta\,^{13}C$ and $\delta\,^{18}O$ values of Dolomite 3, however, are significantly higher, ranging from -5.41 to -4.66 ‰ and from 11.05 to 12.03 ‰, respectively.

Table 9: Carbon and oxygen isotopic compositions of calcite carbonatite (Cc), Dol 1, Dol 2, and Dol 3.

Sample Name	std.	$\delta\ ^{13}C$ V-PDB[1]	$\delta\ ^{18}O$ V-SMOW[2]	Mineral
08010101		-5.38	9.92	Dol 2
08010102		-5.28	11.70	Dol 3
08010103		-5.15	11.85	Dol 3
08010113		-5.19	11.05	Dol 3
08010114		-4.66	12.03	Dol 3
08010804		-5.57	10.15	Dol 2
09080601		-6.31	6.97	Cc
09080602		-6.27	6.91	Cc
09082201		-5.67	9.57	Dol 1
09082202		-5.49	10.22	Dol 2
09090801		-5.61	10.02	Dol 1
09090901		-5.48	9.36	Dol 1
09090902		-5.59	9.94	Dol 1
09100601		-5.04	11.14	Dol 3
09100602		-5.15	11.12	Dol 3
09100603		-4.96	11.32	Dol 3
09100604		-4.96	11.34	Dol 3
09100901		-5.59	9.91	Dol 2
09101101		-5.48	10.17	Dol 2
09101102		-5.41	11.82	Dol 3

Notes: 1 Data standardized to Vienna Pee Dee Belemnite.
2 Data standardized to Standard Mean Ocean Water.

Discussion

Magmatic Evolution

As is the case for carbonatites elsewhere (Woolley and Kempe, 1989), the Wicheeda Carbonatite is characterized by high concentrations of HFSE and the REE, and elevated concentrations of F and the large ion lithophile element, Ba. These elements are incompatible, and concentrate in carbonatites because they are either the products of very small degrees of melting of a carbonated mantle or because they represent the end stages of evolution of an alkaline silicate mantle melt (Freestone and Hamilton, 1980; Kjarsgaard and Hamilton, 1988; Hamilton et al., 1989; Lee and Wyllie, 1998) or a liquid exsolved from that melt (von Eckermann, 1948; Eggler, 1974; Eggler, 1978; Eggler, 1989; Sweeney, 1994; Gittins and Harmer, 1998). The carbon and oxygen isotopic data discussed below indicate that the calcite carbonatite had a mantle origin, whereas the dolomite carbonatite likely originated from a more evolved source. The dolomite carbonatite also differs from the calcite carbonatite in being much more enriched in the REE and relatively depleted in Nb. If emplacement of the calcite carbonatite preceded emplacement of the dolomite carbonatite, which is a common characteristic of other carbonatites including Ngualla and Panda Hills, Tanzania (Van Straaten, 1989; Le Bas, 1977), Khibina, Russia (Le Bas, 1981; Zaitsev 1998; Zaitsev et al., 2014), and St. Honoré, Quebec (Fortin-Bélanger, 1977; Fournier, 1993) and a reasonable assumption given its location at the margins of the intrusion, then it follows that Nb enrichment occurred early and was followed by later REE enrichment. This interpretation is supported by experimental evidence demonstrating that, although Nb is typically more incompatible than the REE in igneous systems, pyrochlore, the principal niobium-bearing

109

mineral in carbonatites has a very low solubility in carbonatite magmas (Jago and Gittins, 1993; Mitchell and Kjarsgaard, 2002; 2004) compared to the REE (Jones and Wyllie, 1983; 1986). Indeed, as discussed earlier, the Wicheeda pyrochlore occurs as euhedra in calcite (calcite carbonatite), suggesting an early magmatic origin, whereas the REE mineralization (largely in the dolomite carbonatite) was clearly later. The proposed evolution from calcite carbonatite to dolomite carbonatite is predicted by experimental data for the system CaO-MgO-FeO showing that calcite is the first mineral to appear on the liquidus (Irving and Wyllie, 1975; Byrnes and Wyllie, 1981; Shatskiy et al., 2014). The extent to which the dolomite carbonatite evolved is less clear. Inspection of Figure 11 shows that the bulk rock compositions of most samples of dolomite carbonatite cluster near the MgO-rich and CaO-poor limit of the field of ferruginous calcio-carbonatite but that there is a weak trend from magnesio-carbonatite to ferrocarbonatite. Consistent with the experimental studies referred to above and the magnesium-rich nature of Dolomite 1 relative to the later dolomite types (Fig. 21), we propose that this trend is magmatic and represents the fractionation of a magnesio-carbonatite magma to a ferrocarbonatite composition. Significantly, REE mineralization occurred relatively early in this evolution as shown by the fact that the magnesio-carbonatite is more enriched in REE than the ferro-carbonatite.

Subsolidus Evolution

Carbon and oxygen isotopes

The carbon and oxygen isotopic composition of the calcite in the calcite carbonatite is consistent with a mantle origin as discussed in the previous section (Fig. 28). However, the carbon and oxygen isotopic composition of Dolomite 1 plots outside the mantle field, although largely within the primary igneous carbonatite field, and that of Dolomite 2 straddles the boundary between the field of primary igneous carbonatite and the field of carbonates of secondary origin. Indeed, the abundance of fluid inclusions in Dolomite 2 suggests a contribution to its isotopic composition from hydrothermal or carbo-hydrothermal fluids. In contrast to Dolomite 1 and Dolomite 2, the composition of Dolomite 3 plots entirely in the field of secondary carbonate, well removed from the field of primary igneous carbonatite, consistent with its occurrence as a vug-filling phase. A potentially significant feature of the isotopic compositions of the three dolomite types and calcite of the calcite carbonatite is that they are linearly distributed with a trend roughly parallel to that reflecting interaction between carbonatite and a hydrothermal or carbo-hydrothermal fluid (Fig. 28).
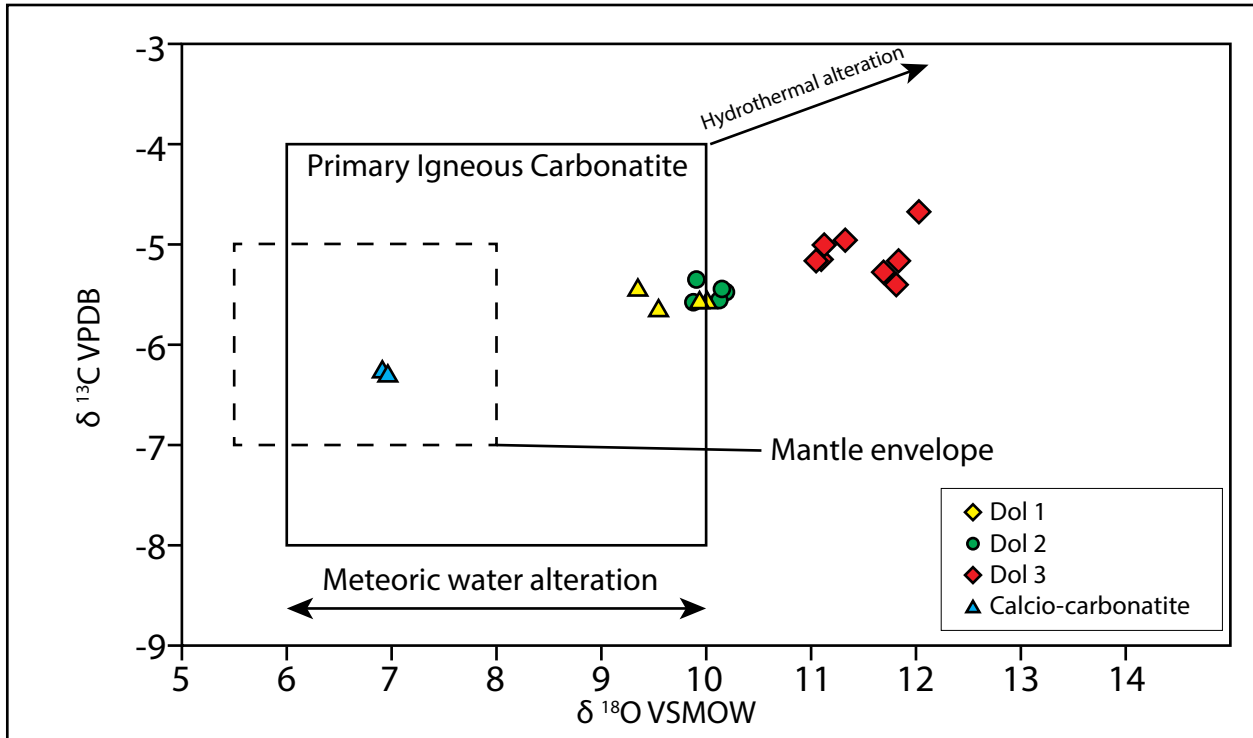
Fig. 28: A plot of $\delta^{18}O$ VSMOW versus $\delta^{13}C$ VPDB showing the distribution of oxygen and carbon isotopic ratios in the dolomite carbonatite (Dolomite 1, Dolomite 2, Dolomite 3) and calcite carbonatite. The data were normalized to V-SMOW and V-PDB, respectively. Also shown are the fields of mantle-derived carbonatite, primary magmatic carbonatite, and secondary carbonate resulting from interaction of the carbonatite with hydrothermal fluids and meteoric water after Taylor et al. (1969), Deines (1989), and Keller and Hoefs (1995).

Assuming that the trend referred to above might have resulted from equilibration of the carbonatites with a fluid exsolved from the magma, we have interpreted the isotopic data using the Rayleigh fractionation model developed by Pineau et al. (1973) and Deines (1989) and revised by Ray and Ramesh (2000). The carbon isotopic evolution of carbonatite is given by:

$$\delta\ ^{13}C = \alpha\ ^c\left(1000 + \delta\ ^{13}C_s^i\right)[f_c]^{(\alpha\ ^c - 1)} - 1000$$

where $\alpha\ ^c$ is the fractionation factor of carbon between carbonate (dolomite) and CO_2, f_c is the fraction of remaining carbon in the source, and $\delta\ ^{13}C_s^i$ is the initial carbon isotopic composition of the source. The oxygen isotopic composition is given by:

$$\delta^{18}O_{dol} = 10^3\left(\frac{\alpha_{d-1}^O}{a - \dfrac{b}{f_o}} - 1\right) + \left(\frac{\alpha_{d-1}^O}{a - \dfrac{b}{f_o}}\right)(\delta^{18}O_S)$$

where $\alpha\ ^o_{d-1}$ is the isotopic fractionation factor for oxygen between dolomite and the largest source component (i.e., CO_2 or H_2O), f_o is the fraction of oxygen remaining in the reservoir, a and b are the number of atoms contributed by the sources and $\delta^{18}O_S$ is the oxygen isotopic composition of the source. If we assume that H_2O is the largest source component (see below), the value of f_o for which CO_2 is exhausted is given by:

$$f_{CO_2} = \frac{1 - r_{CO_2-H_2O}}{1 + 2r_{CO_2-H_2O}}$$

$$a = 1 + \frac{2}{3}(\alpha_{CO_2-H_2O} - 1)$$

$$b = \frac{2}{3}(\alpha_{CO_2-H_2O} - 1)\left(\frac{1 - r_{CO_2-H_2O}}{1 + 2r_{CO_2-H_2O}}\right)$$

where $r_{CO_2-H_2O}$ is the ratio of CO_2 to H_2O in the fluid and $\alpha_{CO_2-H_2O}$ is the isotopic fractionation factor for oxygen between CO_2 and H_2O. The value of $\delta\,^{18}O_s$ is determined by the relationship:

$$(\delta^{18}O_s - \delta^{18}O_s^i) = 10^3\left\{\left(\frac{\alpha_{d-1}^O}{a}\right) * \ln\left(\frac{af_O - b}{a - b}\right) - \ln(f_O)\right\}$$

In order to correlate the carbon isotopic composition to that of oxygen in the carbonatite, the fraction of carbon remaining in the source (f_c) is related to that of oxygen remaining in the source (f_o) by the equation:

$$f_c = \left(\frac{1 - r_{H_2O-CO_2}}{3}\right) + f_O\left(\frac{2 + r_{H_2O-CO_2}}{3}\right)$$

Application of the above equations in modeling the trend shown in Figure 28 requires an estimate for the initial isotopic composition of the source fluid and estimates for either the temperature or the molar ratio of CO_2 to H_2O (r) in this fluid. Although the REE mineralization is hosted by the dolomite carbonatite, we have assumed that the exsolved

114

fluid had the same carbon and oxygen isotopic composition as the calcite carbonatite, i.e., a $\delta^{13}C$ value of -6.27 and a $\delta^{18}O$ value of 6.91 ‰. The reasons for this are: 1) judging by its carbon and oxygen isotopic composition, even the least evolved dolomite carbonatite may have been altered; 2) the contact between the calcite carbonatite and the dolomite carbonatite is gradational; and 3) the C and O isotopic ratios plot along a line extending from calcite in the calcite carbonatite to Dolomite 3 (Fig. 28). The fluid inclusion studies referred to earlier indicate that fluids exsolved from carbonatites contain appreciable proportions of both CO_2 and H_2O. On the basis of visual estimates of the volumetric proportions of CO_2 and H_2O in large numbers of fluid inclusions, Bühn and Rankin (1999) concluded that the fluids exsolved from the REE-bearing Kalkfeld carbonatite, Namibia, contained equal weight proportions of CO_2 and H_2O, corresponding to a molar ratio of 0.41:1. Bühn et al. (2002) reached a similar conclusion for the Okorusu carbonatite, Namibia. We have therefore modeled the data for a value of r of 0.41 (molar $CO_2:H_2O$). The fractionation factors were determined using the thermodynamic data of Richet et al. (1977), Chacko et al. (1991), Rosenbaum (1994), Zheng (1999), and Horita (2014). By fixing the value of r, we were able to vary temperature until the model curve fitted the measured distribution of $\delta^{13}C$ and $\delta^{18}O$ values in dolomite. This was achieved when the temperature was set to a value of 310 °C (Fig. 29). Significantly, the highest temperature that fitted any value of r was 400 °C, and was obtained when the data were modeled with a value of r of 0.47. We therefore conclude, on the basis of the C and O isotopic data, that the carbonatite evolved by reaction with its exsolved fluid in a closed system, culminating in the precipitation of Dolomite 3 and the REE minerals at a temperature between 300 and 400 °C.
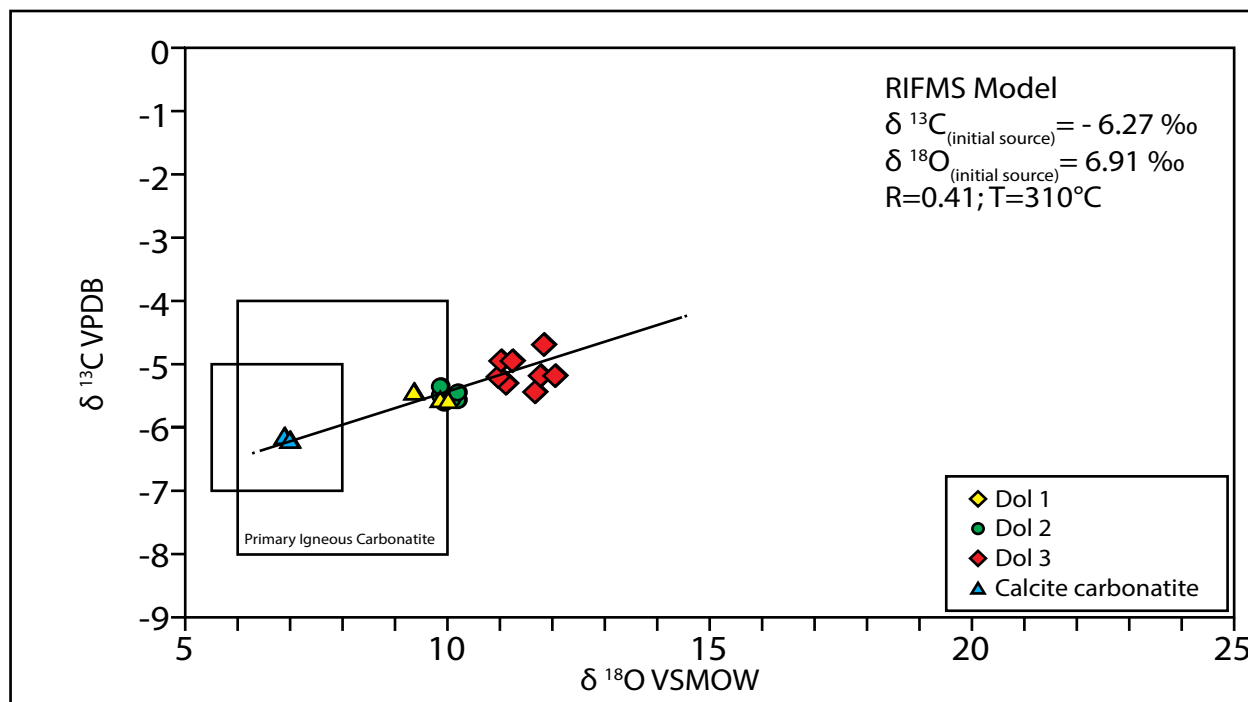
115

Fig. 29: A plot of δ 18O VSMOW versus δ 13C VPDB showing the distribution of oxygen and carbon isotopic ratios in the dolomite carbonatite (Dolomite 1, Dolomite 2, Dolomite 3) and calcite carbonatite. The black dashed line represents the trend in isotopic composition of the carbonate minerals resulting from closed system Raleigh-type fractionation of the carbonatite with its exsolved fluid. The fluid was assumed to have an initial composition of $\delta18O = 6.91$ ‰ and $\delta13C = -6.27$ ‰ and to have a molar $CO2:H2O$ ratio of 0.41. The calculated line replicates the measured isotopic values if the temperature is 310 °C. See the main text for details of the calculation.

Dolomite alteration

On the basis of its textural relationships and C and O isotopic composition, we interpret Dolomite 1 to be of magmatic origin, although it may have been partially altered by hydrothermal fluids. Dolomite 2 inherited a largely magmatic signature but textural relationships indicate that it replaced Dolomite 1. This, and the abundance of fluid inclusions in Dolomite 2 are interpreted to indicate that it is a secondary mineral (hydrothermal), an interpretation supported by the observation that its C and O isotopic ratios are slightly higher than those of Dolomite 1. Dolomite 3, which, as already noted, occupies vugs and fractures, clearly precipitated from hydrothermal or carbo-hydrothermal fluids; this interpretation is supported by the C and O isotopic data. Significantly, Dolomite 3 is accompanied by REE mineralization. The replacement of Dolomite 1 by Dolomite 2 was accompanied by an increase in the (FeO+MnO):MgO ratio. We interpret this to indicate that formation of Dolomite 2 resulted from the interaction of Dolomite 1 with a fluid that partially dissolved Dolomite 1, and substituted Fe and Mn for Mg. This fluid eventually saturated with dolomite and precipitated Dolomite 3, which has the highest (FeO+MnO)/MgO ratio of the three dolomite types.

Fenitization

Whereas primary sedimentary features (e.g., laminations), euhedral fluorapatite grains, and a low frequency of veining are observed in the sodic fenite, the potassic fenite is characterized by the complete destruction of sedimentary features, the occurrence of anhedral fluorapatite grains, and a much greater proportion of veins including some containing monazite-(Ce). This is consistent with the distal and proximal locations of the sodic and potassic fenite, respectively. In principle, the two fenites could be products of a

single fluid emanating from the carbonatite. However, for a fixed fluid composition, albite formation is favored by increasing temperature and potassium feldspar formation by decreasing temperature (Lagache and Weisbrod, 1977). Assuming, as seems reasonable, that temperature decreased with increasing distance from the Wicheeda Carbonatite, it therefore follows that different fluids produced the sodic and potassic fenites. The distribution of the REE in fluorapatite, a mineral occurring in both fenites, provides important clues about the source of the fluids. The chondrite-normalized REE profiles of fluorapatite from the potassic fenite (Apatite 1) generally have negative slopes, indicating preferential enrichment in the LREE, whereas the slopes of the profiles for fluorapatite from the sodic fenite (Apatite 2) are horizontal to positive (Fig. 27). Moreover the LREE content (specifically La and Ce) of the potassic fenite samples, on average, is about an order of magnitude higher than that of the sodic fenite. Given the LREE enrichment of the carbonatite, this suggests strongly that the fluid which produced the potassic fenite originated in the carbonatite, and that the fluid which produced the sodic fenite had another source.

As potassic fenite (mainly potassium feldspar) has been shown elsewhere to be the product of saline aqueous-carbonic fluids released by a carbonatite magma (e.g., Williams-Jones and Palmer, 2002), we propose that such fluids were also responsible for the formation of potassic fenite around the Wicheeda Carbonatite. This interpretation is consistent with the observation that albite and aegirine in the Kechika metasedimentary rocks were replaced by potassium feldspar and biotite. Although we cannot confidently identify the fluid responsible for the formation of the sodic fenite, the most plausible

118

explanation is that it was formational water that was heated by the Wicheeda Carbonatite. If this were the case, and the fluids were initially in equilibrium with potassium feldspar and plagioclase (these minerals commonly occur together in clastic metasedimentary rocks), then their heating would have caused them to reach equilibrium with albite alone (Fig. 30).
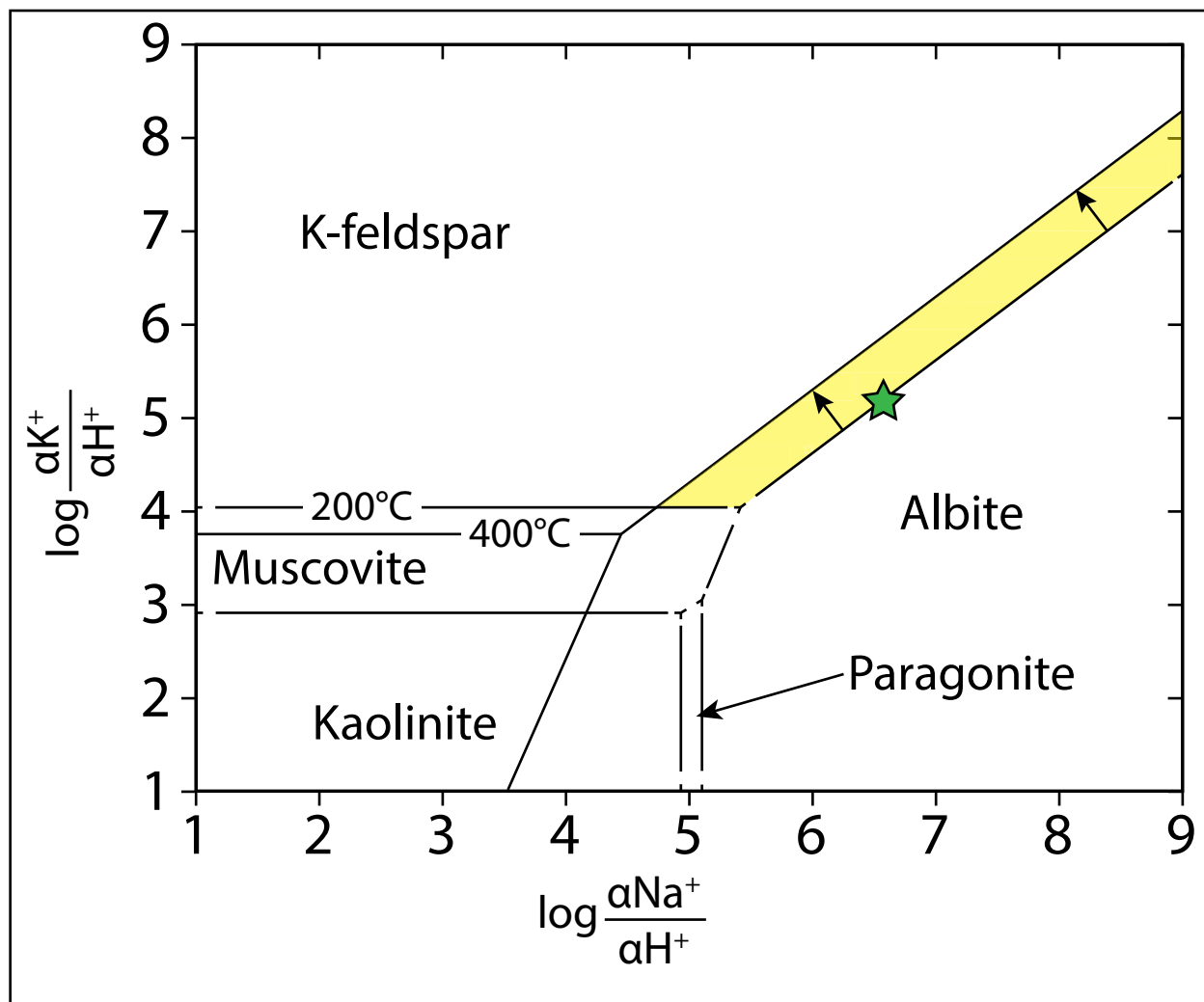
Fig. 30: Stability relationships of minerals in the system K-Na-Al-Si-OH as a function of log aK^+/aH^+ and log aNa^+/aH^+. The stability field for albite expands with increasing temperature at the expense of the stability fields for K-feldspar and muscovite. For example, formational waters in the Kechika argillaceous limestone (represented by the green star) are in equilibrium with both K-feldspar and albite at 200 °C but when heated to 400 °C are only in equilibrium with albite (sodic fenite).

HFSE mineralization

Magmatic concentration

Earlier in the discussion, we noted that as the REE are incompatible under most igneous conditions, they are readily incorporated in magmas like carbonatites, which are the products of very small degrees of partial melting, extreme fractionation or liquid immiscibility. As the compatibility of an element in a melt is controlled largely by its charge/radius ratio (i.e., Z/r), we can also predict that the LREE will be more incompatible than the HREE because of their larger radii (with the exception of Ce and Eu, which also can occur as +4 and +2, respectively, the REE occur exclusively as 3+ ions) and will therefore concentrate preferentially in carbonatites. The importance of magmatic processes in concentrating the REE in carbonatites has been demonstrated at Mountain Pass (California), where magmatic bastnäsite-(Ce) and monazite-(Ce) are the main REE-bearing minerals (Castor, 2008). However, although magmatic processes undoubtedly enriched the Wicheeda Carbonatite in the REE, the textural observations discussed below, show clearly that the REE mineralization, which is concentrated largely in the dolomite carbonatite, is hydrothermal in origin. By contrast, the occurrence of niobium as small euhedral crystals disseminated in the calcite carbonatite (as inclusions in calcite) provides compelling evidence that the niobium mineralization is entirely magmatic in origin. We conclude that the dominance of magmatic processes in causing the niobium mineralization and the limited role of magmatic processes in the REE mineralization reflect the very low solubility of Nb in carbonatite magmas and the much

greater solubility of the REE in these magmas (see Jones and Wyllie, 1983 for evidence of the latter).

Hydrothermal Transport

Carbonatite magmas exsolve aqueous fluids, which are commonly enriched in F^-, CO_2, SO_4^2, and PO_4^{3-}, ligands that can potentially mobilize the REE and alter the adjacent host rocks (Currie and Ferguson, 1971; Kresten and Morogan, 1986; Gittins et al., 1990; Bühn and Rankin, 1999; Williams-Jones and Palmer, 2002). The behavior of the REE in hydrothermal systems containing these anions is readily predicted by hard-soft acid-base principles (Pearson, 1963). These principles predict that, in the case of monovalent anions, the REE should form their most stable aqueous complexes with F^- followed by OH^-, NO_3^- and Cl^-. In the case of the divalent anions, the order is $CO_3^{2-} > SO_4^{2-} > PO_4^{3-}$. This is supported by recent experimental studies (e.g., Migdisov and Williams-Jones, 2002; 2007; 2008; Migdisov et al., 2009). At low pH, fluoride activity is very low because HF is a weak acid, and at higher pH fluoride activity is buffered to very low values because of the very low solubility of REE-fluoride minerals. Consequently, this precludes the transport of the REE as fluoride complexes (Williams-Jones et al., 2012). However, relatively high concentrations of the REE can be transported as REE-chloride complexes at low pH in fluids with salinities typical of those exsolving from carbonatite magmas and at higher pH as REE-sulphate complexes from sulphate-rich fluids (Williams-Jones et al., 2012). By contrast F^- acts as a depositional ligand, promoting the formation of minerals like bastnäsite-(Ce) (Williams-Jones et al., 2012).

REE-mineral precipitation

In the preceding section, we summarized our current understanding of the transport of REE by hydrothermal fluids. Here, we consider the controls on REE mineral deposition. The most important of REE mineral in the Wicheeda Carbonatite is bastnäsite-(Ce) (REECO$_3$F) which forms via the reaction:

$$REECl^{2+} + HF + HCO_3^{-} = REECO_3F + 2H^+ + Cl^-$$
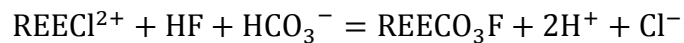
According to this reaction, bastnäsite-(Ce) deposition is favored by a high activity of HF and HCO$_3$⁻ and high pH. Interaction of acidic REE-bearing hydrothermal fluids with carbonate rocks would be particularly effective in increasing aHCO$_3$⁻ and pH as a result of the reaction:

$$2H^+ + CaMg(CO_3)_2 = Ca^{2+} + Mg^{2+} + 2HCO_3^{-}$$
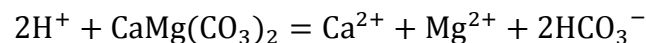
Unfortunately, thermodynamic data are currently lacking for bastnäsite-(Ce) and we are therefore unable to quantitatively evaluate its deposition. Another important REE mineral in the carbonatite, for which thermodynamic data are available, is monazite-(Ce). We modeled its formation by interacting a hypothetical REE-brine containing 10 wt.% NaCl (cf. Smith and Henderson, 2000; Williams-Jones et al., 2000) with dolomite carbonatite using the HCh equilibrium modeling software package (Shvarov, 2013). The carbonatite was assumed to contain 1 wt.% apatite in order to provide a source for

123

phosphorus. The initial temperature of the fluid was 400 °C (similar to that at Bayan Obo; Smith and Henderson, 2000), the pH 2.5 and the initial Ce content was 100 ppm. Thermodynamic data for monazite-(Ce) were taken from Popa et al. (2007) and for the aqueous Ce species from Migdisov et al. (2009). The fluid was cooled to 300 °C as milligram aliquots of carbonatite were added to 1 kg of REE-bearing fluid to simulate the reaction.

Reaction of carbonatite with the fluid consumed dolomite leading to a minor increase in pH (Fig. 31A) and also consumed apatite, adding phosphorus to the solution, which reacted with the dissolved cerium to produce monazite-(Ce). Owing to the very low solubility of monazite-(Ce) under the model conditions, the concentration of Ce in solution dropped sharply and at 340°C, after addition of only 1200 mg of apatite, more than 99% of the Ce initially in solution had been deposited as monazite-(Ce) (Fig. 31B). The model elegantly explains the intimate spatial association of the fluorapatite-bearing xenoliths with monazite-(Ce) and Dolomite 3 (e.g. Fig. 9E) in the Wicheeda Carbonatite.
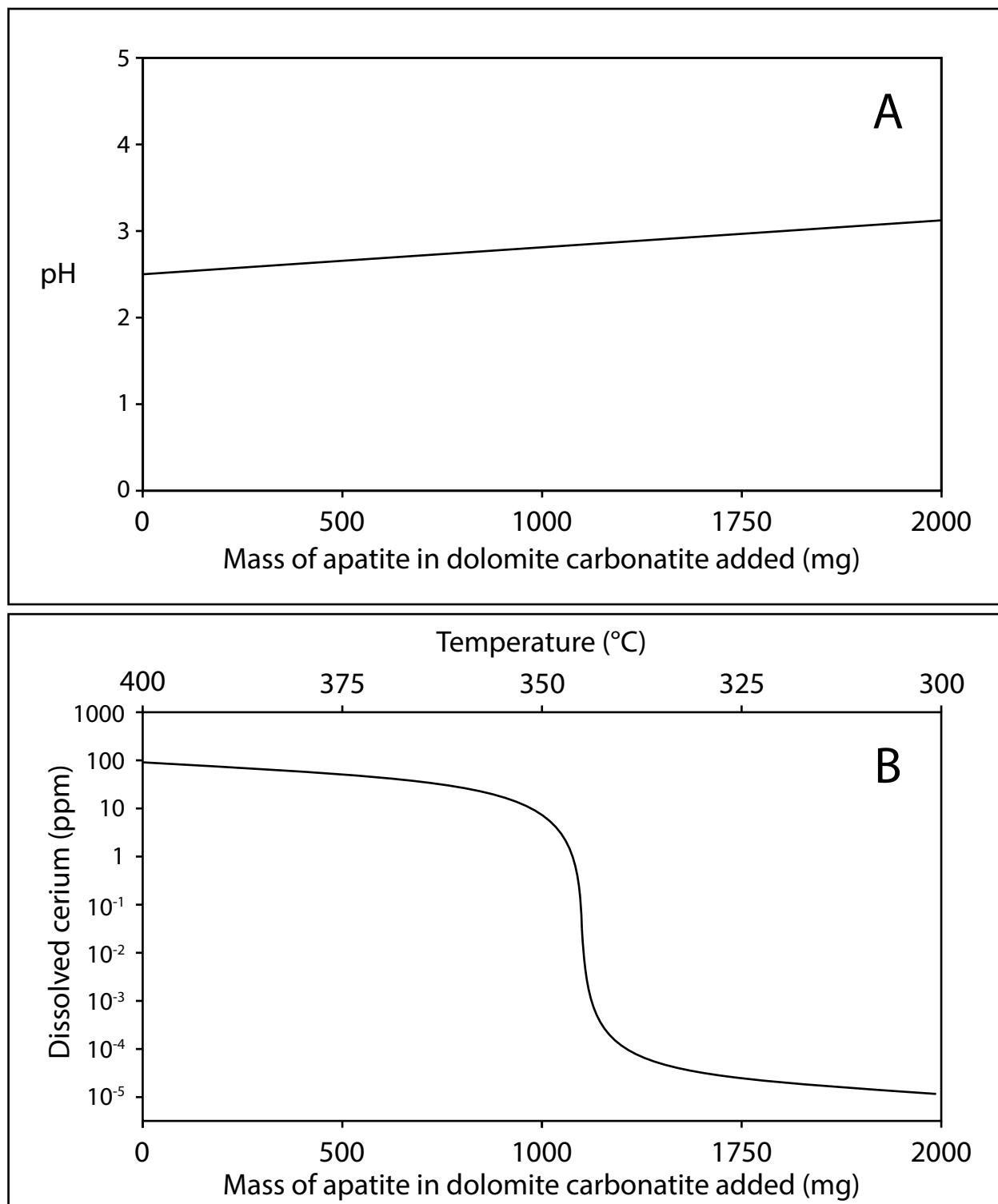
Fig. 31: Results of a model in which a hydrothermal fluid containing 10 wt.% NaCl and 100 ppm Ce reacted with apatite-bearing dolomite carbonatite (1 wt.% apatite) to form monazite-(Ce) while cooling from 400 to 300 °C. A. A plot of pH versus the mass of apatite in dolomite carbonatite (mg) added to the fluid. B. A plot of dissolved cerium concentration (mg) versus the mass of apatite in dolomite carbonatite (mg) added to the fluid. See the main text for details of the calculations.

125

Comparison to the REE mineralization in the Prince Claim Block

Earlier in this paper, we mentioned that carbonatite intrusions with sporadic REE mineralization (mainly dikes and sills) and associated alkaline intrusions are found immediately to the southeast of the main Wicheeda Carbonatite (George claims). Dalsin et al. (2015) studied these dikes and reported the occurrence of calcio- to ferruginous calcio-carbonatites comprising calcite, ankerite, and minor dolomite. The small amount of REE mineralization observed in the dikes occurs mainly as very fine-grained aggregates with calcite and strontianite, in which monazite-(Ce) was the earliest phase to form and is intergrown with later Ca-REE-fluorocarbonates and Ba-REE-fluorocarbonates. Dalsin et al. (2015) interpreted the aggregates, and the REE-fluorocarbonates in particular, to represent eutectic crystallization during rapid cooling of the dikes. Although we cannot rule out this possibility, the textures illustrated in their Figure 6 (e.g., Fig. 6b) and their description of Ca-REE fluorocarbonate minerals infilling fractures together with the occurrence of euhedral bastnäsite-(Ce) "more commonly …in rocks that are slightly altered" seems more consistent with a hydrothermal origin for the REE mineralization, as we have proposed for the Wicheeda Carbonatite. We thus consider it possible that the aggregates described by Dalsin et al. (2015) may represent vug fillings similar to those in the Wicheeda Carbonatite, and note that such aggregates (involving parasite, synchysite and bastnäsite) have been reported for the Bear Lodge carbonatite by Moore et al. (2015) and interpreted by them to fill miarolitic cavities and be hydrothermal or carbo-hydrothermal in origin.

Genetic Model

The Wicheeda Carbonatite is part of a NW-SE trending series of carbonatite and syenite plugs, dikes, and sills that make up the Wicheeda Carbonatite complex. Carbonatites in the complex vary from calcio- to ferro-carbonatites. To the southeast, they are predominantly calcitic, whereas the plug to the northwest (the focus of this study) comprises a marginal calcite facies and a dolomitic core. The occurrence of calcite carbonatite at the margin of the Wicheeda Carbonatite suggests that it represents the earliest magmatic phase to crystallize, an interpretation that is supported by experimental studies of phase relationships in the system CaO-MgO-FeO (Byrnes and Wyllie, 1983; Shatskiy et al., 2014) and carbon/oxygen isotopic data (Fig. 28). As the calcite carbonatite cooled, it saturated relatively early in niobium and crystallized primary pyrochlore. This was followed by intrusion of dolomite carbonatite with a more evolved carbon and oxygen isotopic composition (Fig. 28). Sometime after emplacement, the dolomite carbonatite exsolved an aqueous-carbonic fluid, evident as very small fluid inclusions in Dolomite 2, which mobilized the REE into vugs and veins, and altered the adjacent host rocks to potassic fenite. Distal to the carbonatite, this fluid mixed locally with formational waters that had been heated by the intrusive activity. The latter fluids produced sodic fenite further from the intrusion. As the exsolving fluid, which is interpreted to have been highly acidic, interacted with the carbonatite, it fractured and partially dissolved the host dolomite, creating vugs; the vugs may also represent miarolitic cavities. Barite, molybdenite, pyrite, thorite, and monazite-(Ce) were the earliest fracture and vug filling minerals to form. With progressive fluid-rock interaction cordylite-(Ce) replaced barite, and was in turn replaced by ancylite-(Ce). As the supply

of Ba and Sr from the barite was exhausted, they were followed by precipitation of bastnäsite-(Ce) and later parisite-(Ce) and synchysite-(Ce). Whether there were primary magmatic REE minerals is unknown. However, all the observable REE mineralization is clearly hydrothermal and is interpreted to be the product of the transport of the REE as chloride complexes in highly acidic aqueous-carbonic fluids and the precipitation of REE minerals in response to the increase in pH, which accompanied interaction of these fluids with the dolomite carbonatite. Monazite-(Ce) deposited in response to an increase in phosphate activity due to dissolution of fluorapatite-bearing xenoliths in the dolomite carbonatite.

References

Armstrong, J. E., Hoadley, J. W., Muller, J. E., and Tipper, H. W., 1969, Geology, McLeod Lake Map Area (93J), Geological Survey of Canada, p. Map 1204A.

Betmanis, A. I., 1987, Report on geological, geochemical and magnetometer surveys on the Prince and George groups, cariboo mining division, in British Columbia Ministry of Energy, Mines, and Petroleum Resources, p. 1-86.

Bruland, T., 2011, 2010 Diamond drilling on Carbo rare earth element property, p. 5-31.

Bühn, B., Rankin, A.H., 1999, Composition of natural, volatile-rich Na-Ca-REE-Sr carbonatitic fluids trapped in fluid inclusions, Geochimica et Cosmochimica Acta, v. 63, p. 3781-3797.

Bühn, B., Rankin, A.H., Schneider, J., Dulski, P., 2002, The nature of orthomagmatic, carbonatitic fluids precipitating REE,Sr-rich fluorite: fluid inclusion evidence from the Okorusu fluorite deposit, Namibia, Chemical Geology, v. 186, p. 79-98.

Byrnes, A. P., and Wyllie, P. J., 1981, Subsolidus and melting relations for the join $CaCO_3$-$MgCO_3$ at 6 kbar: Geochimica et Cosmochimica Acta, v. 45, p. 321-328.

Castor, S. B., 2008, The mountain pass rare-earth carbonatite and associated ultrapotassic rocks, California: Canadian Mineralogist, v. 46, p. 779-806.

Chacko, T., Mayeda, T. K., Clayton, R. N., and Goldsmith, J. R., 1991, Oxygen and carbon isotope fractionation between CO_2 and calcite: Geochimica et Cosmochimica Acta, v. 55, p. 2867-2882.

Currie, K. L., and Ferguson, J., 1971, A study of fenitization around the alkaline carbonatite complex at Callander Bay, Ontario, Canada: Canadian Journal of Earth Sciences, v. 8, p. 498-517.

Dalsin, M. L., and Groat, L. A., 2011, The geology and mineralogy of the Carbo property, Wicheeda Carbonatite Complex, BC, Roundup 2011: Vancouver, BC.

Dalsin, M. L., Groat, L. A., Creighton, S., and Evans, R. J., In press, The mineralogy and geochemistry of the Wicheeda Carbonatite Complex, British Columbia Canada: Ore Geology Reviews, v. 64, p. 523-542.

Deines, P., 1989, Stable isotope variations in carbonatites, in Bell, K., ed., Carbonatites Genesis and Evolution: London, UK, Unwin Hyman Ltd., p. 301-359.

Doroshkevich, A. G., Viladkar, S. G., Ripp, G. S., and Burtseva, M. V., 2009, Hydrothermal REE mineralization in the Amba Dongar carbonatite complex, Gujarat, India: The Canadian Mineralogist, v. 47, p. 1105-1116.

Eggler, D. H., 1974, Effect of CO_2 on the melting of peridotite: Carnegie Institution of Washington Yearbook, v. 73, p. 215-224.

Eggler, D. H., 1978, The effect of CO_2 upon partial melting of peridotite in the system Na_2O-CaO-Al_2O_3-MgO-SiO_2-CO_2 to 35 kb, with an analysis of melting in a peridotite-H_2O-CO_2 system: American Journal of Science, v. 278, p. 305-343.

Eggler, D. H., 1989, Carbonatites, primary melts, and mantle dynamics, in Bell, K., ed., Carbonatites, Genesis and Evolution: London, UK, Unwin Hyman Ltd., p. 561-579.

Fortin-Bélanger, M., 1977, Le complexe annulaire, à carbonatite de St.-Honoré (P.Q., Canada) et sa minéralisation à niobium: étude pétrographique et géochimique, Université Claude Bernard, 308 p.

Fournier, A., 1993, Magmatic and hydrothermal controls of LREE mineralization of the St. Honoré carbonatite, Quebec: Unpub. Manuscript thesis, McGill University, 147 p.

Freestone, I. C., and Hamilton, D. L., 1980, The role of liquid immiscibility in the genesis of carbonatites - an experimental study: Contributions to Mineralogy and Petrology, v. 73, p. 105-117.

Gittins, J., Beckett, M. F., and Jago, B. C., 1990, Composition of the fluid phase accompanying carbonatite magma: a critical examination.: American Mineralogist, v. 75, p. 1106-1109.

Gittins, J., and Harmer, R. E., 1997, What is ferrocarbonatite? A revised classification: Journal of African Earth Sciences, v. 25, p. 159-168.

Hamilton, D. L., Bedson, P., and Esson, J., 1989, The behaviour of trace elements in the evolution of carbonatites, in Bell, K., ed., Carbonatites, Genesis and Evolution: London, UK, Unwin Hyman Ltd.

Hawthorne, F. C., Oberti, R., Harlow, G. E., Maresch, W. V., Martin, R. F., Schumacher, J. C., and Welch, M. D., 2012, Nomenclature of the amphibole supergroup: American Mineralogist, v. 97, p. 2031-2048.

Horita, J., 2014, Oxygen and carbon isotope fractionation in the system dolomite-water-CO_2 to elevated temperatures: Geochimica et Cosmochimica Acta, v. 129, p. 111-124.

Irving, A. J., and Wyllie, P. J., 1975, Subsolidus and melting relationships for calcite magnesite and the join $CaCO_3$-$MgCO_3$ to 36 kbar: Geochimica et Cosmochimica Acta, v. 39, p. 35-53.

Jago, B. C., and Gittins, J., 1993, Pyrochlore crystallization in carbonatites: the role of fluorine: South African Journal of Geology, v. 96, p. 149-159.

Jones, A. P., and Wyllie, P. J., 1983, Low-temperature glass quenched from a synthetic, rare earth carbonatite: implications for the origin of the Mountain Pass Deposit, California: Economic Geology, v. 78, p. 1721-3.

Jones, A. P., and Wyllie, P. J., 1986, Solubility of rare earth elements in carbonatite magmas, indicated by the liquidus surface in $CaCO_3$-$Ca(OH)_2$-$La(OH)_3$ at 1 kbar pressure: Applied Geochemistry, v. 1, p. 95-102.

Keller, J., and Hoefs, J., 1995, Stable isotope characteristics of recent natrocarbonatites from Oldoinyo Lengai, IAVCEI Proceedings Volcanology.

Kjarsgaard, B. A., and Hamilton, 1988, Liquid immiscibility and the origin of alkali-poor carbonatites: Mineralogical Magazine, v. 52, p. 43-55.

Kresten, P., 1988, The chemistry of fenitization: examples from Fen, Norway: Chemical Geology, v. 68, p. 329-349.

Kresten, P. and V. Morogan, 1986, Fenitization at the Fen complex, southern Norway, Lithos, v. 19, p. 27-42.

Lagache, M. and A. Weisbrod, 1977, The system: two alkali feldspars-KCl-NaCl-H_2O at moderate to high temperatures and low pressures: Contributions to Mineralogy and Petrology, v. 62, p. 77-101.

Lane, R., 2009, Diamond drilling report on the Wicheeda property, p. 1-196.

Lane, R., 2010, 2009 Diamond drilling report on the Wicheeda rare earth property, p. 1-29.

Le Bas, M. J., 1977, Carbonatite-Nephelinite Volcanism: London, Wiley.

Le Bas, M. J., 1981, Carbonatite magmas: Mineralogical Magazine, v. 44, p. 133-140.

Lee, W.-J., and Wyllie, P. J., 1998, Processes of crustal carbonatite formation by liquid immiscibility and differentiation, elucidated by model systems: Journal of Petrology, v. 39, p. 2005-2013.

Mäder, U. K., and Greenwood, H. J., 1987, Carbonatites and related rocks of the Prince and George claims, northern rocky mountains (93I; 93J), Geological Fieldwork 1987, British Columbia Ministry of Energy, Mines and Petroleum Resources.

131

Migdisov, A., and Williams-Jones, A. E., 2002, A spectrophotometric study of neodymium(III) complexation in chloride solutions: Geochimica et Cosmochimica Acta, v. 66, p. 4311-4323.

Migdisov, A., and Williams-Jones, A. E., 2007, An experimental study of the solubility and speciation of neodymium (III) fluoride in F-bearing aqueous solutions: Geochimica et Cosmochimica Acta, v. 71, p. 3056-3069.

Migdisov, A., and Williams-Jones, A. E., 2008, spectrophotometric study of Nd(III), Sm(III), and Er(III) complexation in sulfate-bearing solutions at elevated temperatures: Geochimica et Cosmochimica Acta, v. 72, p. 5291-5303.

Migdisov, A., Williams-Jones, A. E., and Wagner, T., 2009, An experimental study of the solubility and speciation of the Rare Earth Elements (III) in fluoride- and chloride-bearing aqueous solutions at temperatures up to 300 °C: Geochimica et Cosmochimica Acta, v. 73, p. 7087-7109.

Millonig, L. J., Gerdes, A., and Groat, L. A., 2012, U-Th-Pb geochronology of meta-carbonatites and meta-alkaline rocks in the southern Canadian Cordillera: A geodynamic perspective: Lithos, v. 152, p. 202-217.

Mitchell, R. H., and Kjarsgaard, B. A., 2002, Solubility of niobium in the system $CaCO_3$-$Ca(OH)_2$-$NaNbO_3$ at 0.1 GPa pressure: Contributions to Mineralogy and Petrology, v. 144, p. 93-97.

Mitchell, R. H., and Kjarsgaard, B. A., 2004, Solubility of niobium in the system $CaCO_3$-CaF_2-$NaNbO_3$ at 0.1 GPa pressure: implications for the crystallization of pyrochlore from carbonatite magma: Contributions to Mineralogy and Petrology, v. 148, p. 281-287.

Möller, P., Morteani, G., and Schley, F., 1980, Discussion of REE distribution patterns of carbonatites and alkalic rocks: Lithos, v. 13, p. 171-179.

Monger, J. W. H., Gabrielse, H., and Souther, J. G., 1972, Evolution of the Canadian Cordillera: a plate-tectonic model: American Journal of Science, v. 272, p. 577-602.

Monger, J. W. H., and Price, R. A., 1979, Geodynamic evolution of the Canadian Cordillera - progress and problems: Canadian Journal of Earth Sciences, v. 16, p. 770-791.

Monger, J.W.H., 1989, Chapter 2, Overview of Cordilleran Geology, in Ricketts, B.D., ed., Western Canada Sedimentary Basin: A Case History: Calgary, Canadian Society of Petroleum Geologists, p. 9-32.

Moore, M., Chakhmouradian, A. R., Mariano, A. N., and Sidhu, R., In press, Evolution of rare-earth mineralization in the Bear Lodge carbonatite, Wyoming: Mineralogical and isotopic evidence: Ore Geology Reviews, v. 64, 499-521.

Morimoto, N. Fabries, J., Ferguson, A.K., Ginzburg, I.V., Ross, M., Seifert, F.A., Zussman, J., Aoki, K, and G. Gottardi, 1988, Nomenclature of Pyroxenes: Mineralogy and Petrology, v. 39, p. 55-76.

Pearson, R. G., 1963, Hard and soft acids and bases: Journal of the American Chemical Society, v. 85, p. 3533-3539.

Pell, J., 1994, Carbonatites, nepheline syenites, kimberlites and related rocks in British Columbia, British Columbia Ministry of Energy, Mines and Petroleum Resources, p. 1-44.

Pineau, F., Javoy, M., and Allégre, C. J., 1973, Etude systématique des isotopes de l'oxygéne, du carbone et du strontium dans les carbonatites: Geochimica et Cosmochimica Acta, v. 37, p. 2363-2377.

Popa, K., Konings, R. J. M., and Geisler, T., 2007, High-temperature calorimetry of $(La_{1-x}Lnx)PO_4$ solid solutions: Journal of Chemical Thermodynamics, v. 39, p. 236-239.

Ray, J. S., and Ramesh, R., 2000, Rayleigh fractionation of stable isotopes from a multicomponent source: Geochimica et Cosmochimica Acta, v. 64, p. 299-306.

Richet, P., Bottinga, Y., and Javoy, M., 1977, A review of hydrogen, carbon, nitrogen, oxygen, sulphur, and chlorine stable isotope fractionation among gaseous molecules: Annual Review of Earth and Planetary Sciences, p. 65-110.

Rieder, M., Cavazzini, G., D'Yakonov, Y.S., Frank-Kamenetskii, V.A., Gottardi, G., Guggenheim, S., Koval, P.V., Müller, G., Neiva, A.M.R., Radoslovich, E.W., Robert, J-L., Sassi, F.P., Takeda, H., Weiss, Z., and Wones, D.R., 1998, Nomenclature of the micas, The Canadian Mineralogist, 36, p. 905-912.

Rosenbaum, J. M., 1994, Stable isotope fractionation between carbon dioxide and calcite at 900°C: Geochimica et Cosmochimica Acta, v. 58, p. 3747-3753.

Salvi, S., and Williams-Jones, A.E., 1990, The role of hydrothermal processes in the granite-hosted zirconium, yttrium, REE deposit at Strange Lake, Quebec/Labrador: evidence from fluid inclusions: Geochimica et Cosmochimica Acta, v. 54, p. 2403-2418.

Sears, J.W., Price, R.A., 1978, The Siberian connection- a case for Precambrian separation of the North American and Siberian cratons, Geology, v. 6, p. 267-270.

Shatskiy, A., Borzdov, Y.M., Litasov, K.D., Kupriyanov, I.N., Ohtani, E., Palyanov, Y.N., 2014, Phase relations in the system $FeCO_3$-$CaCO_3$ at 6 GPa and 900-1700 °C and its relation to the system $CaCO$-$FeCO_3$-$MgCO_3$, American Mineralogist, v. 99, 773-785.

Shvarov, Y., 2013, HCh for Windows, A software package for thermodynamic modeling. http://www.geol.msu.ru/deps/geochems/soft/index_e.html

Smith, M. P., and Henderson, P., 2000, Preliminary fluid inclusion constraints on fluid evolution in the Bayan Obo Fe-REE-Nb deposit, inner Mongolia, China: Economic Geology, v. 95, p. 1371-1388.

Taylor, G. C., and Stott, D. F., 1979, Geology, Monkman Pass Map Area, British Columbia (93I), Geological Survey of Canada, p. Open File Map 630.

Taylor, H. P. J., Frechen, J., and Degens, E. T., 1967, Oxygen and carbon isotope studies of carbonatites from the Laacher See District, West Germany, and the Alnö District, Sweden: Geochimica et Cosmochimica Acta, v. 31, p. 407-430.

Van Straaten, P., 1989, Nature and structural relationships of carbonatites from southwest and west Tanzania, in Bell, K., ed., Carbonatites, Genesis and Evolution: London, UK, Unwin Hyman Ltd., p. 177-199.

von Eckermann, H., 1948, The alkaline district of Alnö island: Sveriges Geologiska Undersökning, v. 36, p. 1-176.

Wall, F., and Mariano, A. N., 1996, Rare earth minerals in carbonatites: a discussion centred on the Kangankunde Carbonatite, Malawi.: London, Chapman and Hall, 193-225.

Williams-Jones, A. E., Migdisov, A. A., and Samson, I. M., 2012, Hydrothermal Mobilisation of the Rare Earth Elements - a Tale of "Ceria" and "Yttria", Elements, v. 8, 355-360.

Williams-Jones, A. E., and Palmer, D. A. S., 2002, Fluid evolution of the Amba Dongar carbonatite complex, India: Chemical Geology, v. 185, p. 283-301.

Williams-Jones, A. E., Samson, I. M., and Olivo, G. R., 2000, The genesis of hydrothermal fluorite-REE deposits in the Gallinas Mountains, New Mexico: Economic Geology, v. 95, p. 327-342.

Woolley, A. R., and Kempe, D. R. C., 1989, Carbonatites: nomenclature, average chemical compositions, and element distribution, in Bell, K., ed., Carbonatites, Genesis and Evolution: London, UK, Unwin Hyman Ltd., p. 1-13.

Xu, C., Huang, Z.-L., Liu, C. Q., Qi, L., Li, W.-B., and Guan, T., 2003, Sources of ore-forming fluids in the Maoniuping REE deposit, Sichuan Province, China: Evidence from REE, radiogenic Sr, Nd, and stable-isotopes studies.: International Geology Reviews, v. 45, p. 635-645.

Xu, C., Zhilong, H., Congqiang, L., Liang, Q., Wenbo, L., and Guan, T., 2004, Genesis of the carbonatite-syenite complex and REE deposit at Maoniuping, Sichuan Province, China: Evidence from Pb isotope geochemistry: Geochemical Journal, v. 38, p. 67-76.

Zaitsev, A. N., Wall, F., and Le Bas, M. J., 1998, REE-Sr-Ba minerals from the Khibina carbonatites, Kola peninsula, Russia: their mineralogy, paragenesis and evolution: Mineralogical Magazine, v. 62, p. 225-250.

Zaitsev, A. N., Williams, C. T., Jeffries, T. E., Strekopytov, S., Moutte, J., Ivashchenkova, O. V., Spratt, J., Petrov, S. V., Wall, F., Seltmann, R., and Borozdin, A. P., 2014, Rare earth elements in phoscorites and carbonatites of the Devonian Kola Alkaline Province, Russia: Examples from Kovdor, Khibina, Vuoriyarvi and Turiy Mys complexes: Ore Geology Reviews, v. 61, p. 204-225.

Zheng, Y.-F., 1999, Oxygen isotope fractionation in carbonate and sulfate minerals: Geochemical Journal, v. 33, p. 109-126.

CHAPTER III: Conclusions

Conclusions

The Wicheeda Carbonatite comprises a ferroan dolomite core, which passes gradationally into calcite carbonatite at depth and at the margins of the intrusion. It is surrounded by potassic fenite (mainly potassium feldspar) near the intrusion and sodic fenite (albite+aegirine) at greater distances from it. Textural and stable isotopic evidence indicate that calcite carbonatite was the earliest magmatic phase to crystallize. As it cooled, the magma became saturated with respect to niobium and precipitated primary pyrochlore. Some time later, dolomite carbonatite magma was emplaced which, upon cooling, exsolved an aqueous-carbonic fluid, fracturing the carbonatite and altering its isotopic carbon and oxygen composition. On the basis of the carbon and oxygen isotopic data, the alteration took place at a temperature between 300 and 400 °C. This fluid also mobilized REE into fractures and vugs (miarolitic cavities and dissolution cavities), and altered the nearby Kechika Group metasedimentary rocks to potassic fenite. Sodic fenite formed as a result of the mixing of this fluid with formational waters heated by intrusive activity further from the carbonatite. The fractures and vugs in the dolomite carbonatite were filled by hydrothermal dolomite barite, molybdenite, pyrite and REE minerals. Barite was replaced by cordylite-(Ce) and ancylite-(Ce), and these minerals in turn by bastnäsite-(Ce), parisite-(Ce), and synchysite-(Ce).

As is evident from the preceding paragraphs and from Chapter 2, the REE mineralization in the Wicheeda Carbonatite is entirely hydrothermal in origin. This interpretation departs greatly from that proposed by Dalsin et al (2015) for REE mineralization in carbonatite dikes to the south of the main carbonatite intrusion.

Contributions to Knowledge

From a local perspective, this study provides an important contribution to one of the most promising REE prospects in the relatively unexplored British Columbia alkaline province. The research undertaken generated the first local geological maps of the intrusion, described the various rock units, and developed a model to explain its magmatic and hydrothermal evolution.

In a broader geological context, the study showed how magmatic hydrothermal fluids alter host rocks to sodic and potassic fenite, and that the concentration of REE by post-magmatic hydrothermal fluid in carbonates, fluorocarbonates, and in monazite-(Ce) is largely dependent on pH and the availability of F and P as depositional ligands. Also in this context, this study demonstrates that rare Sr- and Ba-REE-minerals such as ancylite-(Ce) and cordylite-(Ce), are concentrated by hydrothermal processes. Finally, this thesis has provided an important body of information that will help guide further exploration of this intrusion and other similar intrusions elsewhere.

Future research on the Wicheeda Carbonatite should focus on constraining the limits of fenitized haloes and the geometry of the intrusion. Based on existing drill core information, it is a plug-like intrusion with undefined roots and it is likely that these roots are important to better understanding the emplacement and post-emplacement history of the intrusion. Equally important is future research focused on understanding the composition and evolution of the fluids responsible for depositing the REE.

Appendices

Appendix A

Locations of outcrops sampled

Appendix A: Locations of outcrops sampled

Outcrop Number	UTM X Nad 83	UTM Y Nad 83	Outcrop Number	UTM X Nad 83	UTM Y Nad 83
WI-13-01	0558290	6042865	WI-13-33	0558361	6043254
WI-13-02	0558308	6043017	WI-13-34	0558364	6043270
WI-13-04	0558358	6043086	WI-13-35	0558363	6043285
WI-13-05	0558397	6043073	WI-13-36	0558438	6043320
WI-13-06	0558470	6043036	WI-13-37	0558448	6043318
WI-13-07	0558481	6043010	WI-13-38	0558463	6043152
WI-13-08	0558634	6042968	WI-13-39	0558341	6042805
WI-13-09	0558634	6042968	WI-13-40	0558384	6042846
WI-13-10	0558678	6043070	WI-13-41	0558386	6042837
WI-13-11	0558715	6043108	WI-13-42	0558386	6042853
WI-13-12	0558689	6043104	WI-13-43	0558395	6042866
WI-13-13	0558768	6043122	WI-13-44	0558468	6042806
WI-13-14	0558681	6043132	WI-13-45	0558443	6042815
WI-13-15	0558654	6043144	WI-13-46	0558415	6042851
WI-13-16	0558287	6042881	WI-13-47	0558400	6042885
WI-13-17	0558346	6043080	WI-13-49	0558434	6043024
WI-13-18	0558364	6043080	WI-13-50	0558327	6042917
WI-13-19	0558342	6043086	WI-13-51	0558317	6042895
WI-13-20	0558302	6043127	WI-13-52	0558304	6042886
WI-13-21	0558299	6043176	WI-13-53	0558294	6042898
WI-13-22	0558270	6043188	WI-13-54	0558253	6042888
WI-13-23	0558220	6043254	WI-13-55	0558260	6042916
WI-13-24	0558182	6043214	WI-13-56	0558247	6042937
WI-13-25	0558053	6043117	WI-13-57	0558272	6043076
WI-13-26	0558092	6043092	WI-13-58	0558275	6043147
WI-13-27	0558196	6043128	WI-13-59	0558338	6043163
WI-13-29	0558272	6043122	WI-13-60	0558327	6043198
WI-13-30	0558327	6043210	WI-13-61	0558367	6043201
WI-13-31	0558337	6043242	WI-13-62	0558333	6043158
WI-13-31a	0558337	6043242	WI-13-63	0558286	6043120
WI-13-32	0558347	6043225	WI-13-68	0557757	6043279

Appendix B

Locations of drill cores sampled

Appendix B: Locations of drill cores sampled

Drill Hole	Sample ID	Depth (m)	Drill Hole	Sample ID	Depth (m)
08WI01	080101	10.4	WI-09-09	090901	7.5
	080102	19.1		090902	27.1
	080103	22.8		090903	27.5
	080104	30.5		090904	35.1
	080105	33.0		090905	48.4
	080106	42.0		090906	52.4
	080107	43.3		090907	71.5
	080108	50.5		090908	84.4
	080109	61.6		090909	84.7
	080110	84.3		090910	103.6
	080111	85.2		090911	118.4
	080112	88.6		090912	146.7
	080113	90.6		090913	147.8
	080114	102.7	WI-09-10	091001	8.0
	080115	158.3		091002	10.0
WI-09-08	090801	5.6		091003	18.4
	090802	10.6		091004	64.1
	090803	17.6		091005	74.2
	090804	18.8		091006	90.6
	090805	22.0		091007	74.2
	090806	27.6		091008	93.1
	090807	30.0		091009	115.8
	090808	49.0		091010	118.5
	090809	90.6		091011	120.5
	090810	100.0		091012	121.7
	090811	127.7			
	090812	134.9			
	090813	146.9			

Appendix C

Counting times and standards used for each element analyzed with the electron microprobe

Appendix C: Counting times and standards used for each element analyzed with the electron microprobe

Element	Counting Time	Standard
Al	20	cameca orth
Ba	20	Ba-feld
Ba	50	Ba-feld
Ca	20	Cal1
Ca	20	diopside
Ca	20	Flap
Ce	20	Mac-Ce
Cl	20	vana2
Dy	50	Mac-Dy
Eu	100	Mac-Eu
F	20	CaF2
F	20	Flap
Fe	20	Fe2O3
Fe	20	sid1
Gd	50	Mac-Gd
K	20	cameca orth
La	20	Mac-La
Mg	20	diopside
Mg	20	Dol1
Mn	20	sid1
Mn	20	spessartine
Na	20	cameca albite
Nb	20	Na2Nb2O6
Nd	20	Mac-Nd
Nd	50	Mac-Nd
P	20	Flap
Pb	20	vana2
Pr	50	Mac-Pr
Rb	20	Rb-feld
Si	20	cameca orth
Si	20	diopside
Sm	50	Mac-Sm
Sr	20	Sr-feld
Sr	50	Sr-feld
Th	20	ThO2
Th	100	ThO2
Ti	20	tiO2
Y	20	Mac-Y
Zr	20	zircon

Appendix D

Results of electron microprobe analyses of dolomite and calcite

Appendix D: Results of electron microprobe analyses of dolomite and calcite

Name	Classification	CaO	MgO	FeO	MnO	CO₂¹	SrO	BaO	K₂O	P₂O₅	TiO₂	ThO₂	ZrO₂	Nb₂O₅	Y₂O₃	La₂O₃	Ce₂O₃	Nd₂O₃	Total
WI-11-02-01a	Dol 1	29.80	18.22	5.664	0.442	45.81	0.00	0.009	0.010	0.00	0.027	0.003	0.00	0.00	0.00	0.007	0.00	0.007	100.00
WI-11-02-01b	Dol 1	29.31	18.88	4.769	0.554	46.39	0.00	0.00	0.00	0.018	0.00	0.00	0.00	0.009	0.016	0.00	0.046	0.00	100.00
WI-11-02-02	Dol 1	29.70	19.16	4.491	0.298	46.23	0.00	0.00	0.00	0.023	0.00	0.00	0.00	0.038	0.00	0.00	0.055	0.00	100.00
WI-11-02-03	Dol 1	29.87	19.96	3.460	0.146	46.48	0.00	0.031	0.004	0.008	0.002	0.00	0.014	0.015	0.00	0.00	0.016	0.00	100.00
WI-11-02-04	Dol 2	29.59	17.09	6.621	0.828	45.80	0.017	0.008	0.006	0.020	0.00	0.035	0.00	0.00	0.022	0.008	0.009	0.00	100.00
WI-11-02-05a	Dol 1	29.44	17.38	6.837	0.766	45.49	0.00	0.00	0.003	0.014	0.00	0.035	0.00	0.025	0.00	0.007	0.009	0.00	100.00
WI-11-02-05b	Dol 1	29.42	18.55	5.150	0.669	46.10	0.00	0.018	0.010	0.00	0.00	0.088	0.00	0.00	0.00	0.00	0.005	0.005	100.00
WI-11-02-05c	Dol 1	29.46	18.02	5.956	0.669	45.73	0.00	0.00	0.007	0.023	0.009	0.00	0.043	0.047	0.00	0.00	0.00	0.042	100.00
WI-11-02-6	Dol 1	29.75	17.44	6.458	0.754	45.33	0.00	0.036	0.00	0.044	0.00	0.00	0.016	0.040	0.014	0.005	0.007	0.110	100.00
WI-11-02-12	Dol 1	29.75	18.44	5.395	0.532	45.76	0.00	0.017	0.012	0.001	0.00	0.00	0.00	0.027	0.00	0.021	0.039	0.00	100.00
WI-11-02-13	Dol 1	29.56	17.18	6.733	0.911	45.48	0.00	0.00	0.004	0.039	0.021	0.058	0.00	0.015	0.00	0.007	0.00	0.00	100.00
WI-11-02-14	Dol 1	29.65	17.88	6.404	0.639	45.27	0.00	0.026	0.00	0.022	0.00	0.00	0.00	0.002	0.059	0.007	0.022	0.021	100.00
WI-11-02-15	Dol 2	29.63	18.99	4.648	0.421	46.24	0.026	0.008	0.005	0.00	0.020	0.00	0.00	0.015	0.005	0.00	0.00	0.00	100.00
WI-11-02-16	Dol 2	29.57	18.15	5.602	0.600	45.92	0.024	0.040	0.010	0.011	0.010	0.00	0.00	0.00	0.052	0.004	0.012	0.00	100.00
WI-11-02-17	Dol 2	29.48	17.20	6.808	0.749	45.71	0.002	0.00	0.002	0.00	0.015	0.00	0.00	0.00	0.036	0.004	0.004	0.00	100.00
WI-11-02-18	Dol 2	29.39	17.06	6.986	0.899	45.38	0.030	0.00	0.010	0.00	0.011	0.00	0.005	0.031	0.014	0.046	0.059	0.125	100.00
WI-11-02-19	Dol 3	29.11	18.25	5.363	0.284	46.80	0.041	0.051	0.00	0.00	0.00	0.027	0.00	0.00	0.021	0.048	0.008	0.00	100.00
WI-11-02-20	Dol 2	29.41	18.70	4.823	0.489	46.44	0.001	0.042	0.005	0.005	0.00	0.00	0.00	0.019	0.00	0.048	0.020	0.00	100.00
WI-11-07-01	Dol 2	29.80	18.19	5.460	0.512	45.81	0.025	0.00	0.00	0.007	0.040	0.055	0.024	0.032	0.007	0.00	0.045	0.00	100.00
WI-11-07-02a	Dol 2	29.51	16.55	7.800	1.005	45.03	0.00	0.006	0.011	0.012	0.009	0.00	0.046	0.00	0.00	0.00	0.019	0.00	100.00
WI-11-07-02b	Dol 2	29.59	17.33	6.880	0.618	45.32	0.031	0.018	0.014	0.025	0.001	0.022	0.00	0.061	0.024	0.00	0.040	0.023	100.00
WI-11-07-02c	Dol 2	27.68	15.57	6.631	0.960	48.94	0.040	0.048	0.013	0.00	0.00	0.00	0.00	0.00	0.00	0.00	0.001	0.018	100.00
WI-11-07-02d	Dol 2	29.43	18.15	6.371	0.431	45.54	0.00	0.00	0.007	0.016	0.00	0.106	0.00	0.00	0.00	0.018	0.021	0.016	100.00
WI-11-07-02e	Dol 2	29.14	16.61	8.030	0.703	45.41	0.025	0.00	0.00	0.005	0.011	0.002	0.00	0.030	0.011	0.006	0.001	0.023	100.00
WI-11-07-07	Dol 3	29.76	18.15	5.129	0.601	46.16	0.062	0.00	0.00	0.017	0.00	0.00	0.022	0.00	0.006	0.00	0.019	0.071	100.00
WI-11-07-08	Dol 2	29.43	17.14	7.141	0.855	45.20	0.009	0.019	0.00	0.020	0.002	0.00	0.00	0.020	0.00	0.00	0.024	0.087	100.00
WI-11-07-09	Dol 2	29.76	18.43	5.134	0.587	45.91	0.016	0.005	0.00	0.00	0.007	0.00	0.00	0.020	0.005	0.00	0.029	0.093	100.00
WI-11-07-10	Dol 2	29.72	17.96	5.987	0.679	45.55	0.007	0.014	0.007	0.00	0.007	0.00	0.00	0.008	0.00	0.00	0.00	0.061	100.00
WI-11-07-11	Dol 2	29.12	14.52	9.955	1.745	44.40	0.023	0.00	0.00	0.030	0.00	0.006	0.00	0.042	0.00	0.009	0.026	0.072	100.00
WI-11-07-12	Dol 3	29.07	14.02	10.29	2.106	44.26	0.199	0.00	0.00	0.022	0.00	0.073	0.008	0.00	0.043	0.00	0.007	0.027	100.00
WI-11-12-01	Dol 2	29.52	16.73	7.260	0.853	45.37	0.00	0.00	0.00	0.00	0.00	0.023	0.043	0.042	0.043	0.007	0.00	0.020	100.00
WI-11-12-02	Dol 3	29.48	15.23	8.585	1.359	45.16	0.049	0.00	0.001	0.00	0.024	0.074	0.011	0.078	0.00	0.034	0.037	0.020	100.00
WI-11-11-03a	Dol 3	29.24	15.67	8.191	1.442	45.25	0.069	0.003	0.002	0.008	0.00	0.00	0.033	0.016	0.003	0.015	0.058	0.020	100.00
WI-11-11-03b	Dol 3	29.65	17.52	6.776	0.459	45.40	0.00	0.00	0.00	0.020	0.030	0.043	0.033	0.00	0.00	0.00	0.014	0.020	100.00
WI-11-11-03c	Dol 2	29.57	16.89	7.533	0.603	45.19	0.003	0.026	0.002	0.011	0.00	0.076	0.016	0.024	0.022	0.00	0.00	0.078	100.00
WI-11-11-03d	Dol 2	29.84	17.04	6.796	0.859	45.31	0.011	0.00	0.00	0.015	0.007	0.043	0.005	0.00	0.007	0.013	0.003	0.097	100.00
WI-11-12-07	Dol 2	29.64	16.88	6.798	0.813	45.78	0.00	0.051	0.003	0.008	0.00	0.004	0.005	0.00	0.027	0.00	0.004	0.00	100.00
WI-11-12-08	Dol 2	29.61	18.86	4.082	0.412	46.84	0.027	0.018	0.00	0.031	0.003	0.00	0.005	0.00	0.014	0.00	0.052	0.00	100.00
WI-11-12-09	Dol 2	29.61	19.46	3.078	0.248	47.24	0.00	0.033	0.00	0.014	0.00	0.049	0.022	0.015	0.00	0.051	0.031	0.065	100.00
WI-11-09-01	Dol 3	29.52	19.50	3.762	0.319	46.60	0.067	0.00	0.002	0.042	0.00	0.137	0.081	0.00	0.048	0.027	0.026	0.00	100.00
WI-11-09-02	Dol 3	29.82	18.87	4.438	0.247	46.41	0.028	0.006	0.023	0.042	0.017	0.045	0.027	0.00	0.016	0.00	0.00	0.034	100.00
WI-11-09-03	Dol 1	29.71	20.32	2.869	0.132	46.93	0.009	0.00	0.008	0.013	0.00	0.022	0.005	0.00	0.00	0.00	0.00	0.00	100.00
WI-11-09-04	Dol 1	29.69	19.72	3.578	0.193	46.76	0.004	0.00	0.005	0.010	0.015	0.00	0.016	0.010	0.00	0.00	0.00	0.00	100.00
WI-11-09-05	Dol 1	29.62	19.68	3.469	0.296	46.83	0.00	0.00	0.00	0.005	0.00	0.00	0.00	0.00	0.00	0.00	0.042	0.056	100.00
WI-11-09-06	Dol 1	29.74	19.45	4.022	0.306	46.40	0.00	0.022	0.00	0.012	0.00	0.001	0.00	0.036	0.00	0.00	0.00	0.00	100.00
WI-11-09-07	Dol 1	29.63	19.44	3.685	0.254	46.76	0.013	0.016	0.00	0.023	0.001	0.010	0.00	0.033	0.00	0.029	0.008	0.033	100.00
WI-11-09-08a	Dol 1	29.38	18.92	4.468	0.474	46.70	0.009	0.00	0.006	0.027	0.00	0.074	0.00	0.00	0.011	0.00	0.010	0.00	100.00
WI-11-09-08b	Dol 1	29.58	18.56	4.100	0.509	47.09	0.00	0.00	0.026	0.018	0.00	0.00	0.038	0.016	0.00	0.00	0.051	0.012	100.00
WI-11-09-10	Dol 1	29.42	18.78	3.752	0.353	47.53	0.021	0.051	0.002	0.022	0.00	0.00	0.011	0.00	0.00	0.047	0.00	0.009	100.00
WI-11-09-11	Dol 1	29.75	20.63	2.737	0.215	46.45	0.038	0.052	0.00	0.021	0.00	0.00	0.022	0.058	0.00	0.00	0.006	0.022	100.00
WI-11-09-12	Dol 1	29.49	19.73	3.128	0.167	47.41	0.00	0.013	0.015	0.019	0.00	0.00	0.00	0.00	0.006	0.00	0.00	0.025	100.00
WI-11-09-13	Dol 1	29.63	19.77	3.477	0.278	46.67	0.017	0.071	0.044	0.014	0.00	0.00	0.00	0.027	0.002	0.00	0.00	0.00	100.00
WI-11-09-14	Dol 1	29.43	18.89	4.357	0.207	46.96	0.00	0.00	0.048	0.006	0.00	0.00	0.024	0.040	0.002	0.006	0.027	0.00	100.00

Notes: The detection limits for oxides (wt.%), which are as follows: Ca, 0.03; Mg, 0.03; Fe, 0.07; Sr, 0.09; La, 0.09; La, 0.11; K, 0.03; Mn, 0.12; P, 0.04; Ce, 0.1; Th, 0.14; Nb, 0.09; Nd, 0.19; Ti, 0.19; Y, 0.06; Ba, 0.09; Zr, 0.09.

n.a. Not analysed

1 Calculated.

148

Appendix D: Results of electron microprobe analyses of dolomite and calcite

Name	Classification	CaO	MgO	FeO	MnO	CO₂¹	SrO	BaO	K₂O	P₂O₅	TiO₂	ThO₂	ZrO₂	Nb₂O₅	Y₂O₃	La₂O₃	Ce₂O₃	Nd₂O₃	Total
WI1311-65	Dol 1	29.01	13.16	10.86	2.160	44.79	0.022	0.00	n.a.	n.a.	n.a.	n.a.	n.a.	n.a.	n.a.	n.a.	n.a.	n.a.	100.00
WI1311-66	Dol 1	29.89	18.45	4.673	0.498	46.46	0.00	0.027	n.a.	n.a.	n.a.	n.a.	n.a.	n.a.	n.a.	n.a.	n.a.	n.a.	100.00
WI1311-67	Dol 1	29.69	18.04	5.426	0.577	46.25	0.014	0.003	n.a.	n.a.	n.a.	n.a.	n.a.	n.a.	n.a.	n.a.	n.a.	n.a.	100.00
WI1311-68	Dol 1	29.07	15.03	8.878	1.581	45.37	0.075	0.00	n.a.	n.a.	n.a.	n.a.	n.a.	n.a.	n.a.	n.a.	n.a.	n.a.	100.00
WI1311-69	Dol 1	29.07	15.16	8.861	1.519	45.38	0.006	0.00	n.a.	n.a.	n.a.	n.a.	n.a.	n.a.	n.a.	n.a.	n.a.	n.a.	100.00
WI1311-01	Dol 2	29.07	14.01	10.27	1.004	45.55	0.094	0.00	n.a.	n.a.	n.a.	n.a.	n.a.	n.a.	n.a.	n.a.	n.a.	n.a.	100.00
WI1311-02	Dol 2	29.13	15.20	8.519	1.377	45.69	0.090	0.00	n.a.	n.a.	n.a.	n.a.	n.a.	n.a.	n.a.	n.a.	n.a.	n.a.	100.00
WI1311-03	Dol 2	29.33	18.18	5.023	0.626	46.83	0.00	0.011	n.a.	n.a.	n.a.	n.a.	n.a.	n.a.	n.a.	n.a.	n.a.	n.a.	100.00
WI1311-04	Dol 2	29.22	18.32	4.620	0.583	47.25	0.009	0.00	n.a.	n.a.	n.a.	n.a.	n.a.	n.a.	n.a.	n.a.	n.a.	n.a.	100.00
WI1311-10	Dol 2	30.15	18.63	4.795	0.582	45.80	0.047	0.00	n.a.	n.a.	n.a.	n.a.	n.a.	n.a.	n.a.	n.a.	n.a.	n.a.	100.00
WI1311-11	Dol 2	29.27	15.55	8.215	1.190	45.73	0.040	0.00	n.a.	n.a.	n.a.	n.a.	n.a.	n.a.	n.a.	n.a.	n.a.	n.a.	100.00
WI1311-14	Dol 2	29.60	15.25	8.250	1.380	45.42	0.082	0.020	n.a.	n.a.	n.a.	n.a.	n.a.	n.a.	n.a.	n.a.	n.a.	n.a.	100.00
WI1311-21	Dol 2	29.64	17.71	5.551	0.639	46.41	0.051	0.00	n.a.	n.a.	n.a.	n.a.	n.a.	n.a.	n.a.	n.a.	n.a.	n.a.	100.00
WI1311-22	Dol 2	29.55	17.41	5.956	0.782	46.29	0.016	0.00	n.a.	n.a.	n.a.	n.a.	n.a.	n.a.	n.a.	n.a.	n.a.	n.a.	100.00
WI1311-23	Dol 2	29.27	19.35	3.571	0.339	47.47	0.00	0.00	n.a.	n.a.	n.a.	n.a.	n.a.	n.a.	n.a.	n.a.	n.a.	n.a.	100.00
WI1311-24	Dol 2	29.37	16.58	7.541	1.077	45.38	0.045	0.00	n.a.	n.a.	n.a.	n.a.	n.a.	n.a.	n.a.	n.a.	n.a.	n.a.	100.00
WI1311-25	Dol 2	29.19	15.24	8.365	1.396	45.73	0.081	0.00	n.a.	n.a.	n.a.	n.a.	n.a.	n.a.	n.a.	n.a.	n.a.	n.a.	100.00
WI1311-26	Dol 2	29.44	17.10	6.270	0.818	46.32	0.042	0.00	n.a.	n.a.	n.a.	n.a.	n.a.	n.a.	n.a.	n.a.	n.a.	n.a.	100.00
WI1311-27	Dol 2	29.58	17.18	6.405	0.787	46.03	0.007	0.016	n.a.	n.a.	n.a.	n.a.	n.a.	n.a.	n.a.	n.a.	n.a.	n.a.	100.00
WI1311-28	Dol 2	29.65	17.91	5.301	0.592	46.54	0.00	0.00	n.a.	n.a.	n.a.	n.a.	n.a.	n.a.	n.a.	n.a.	n.a.	n.a.	100.00
WI1311-29	Dol 2	31.22	18.85	5.326	0.617	43.95	0.038	0.00	n.a.	n.a.	n.a.	n.a.	n.a.	n.a.	n.a.	n.a.	n.a.	n.a.	100.00
WI1311-30	Dol 2	29.10	16.08	7.315	0.897	46.38	0.228	0.00	n.a.	n.a.	n.a.	n.a.	n.a.	n.a.	n.a.	n.a.	n.a.	n.a.	100.00
WI1311-31	Dol 2	29.09	14.92	9.295	1.327	45.16	0.186	0.027	n.a.	n.a.	n.a.	n.a.	n.a.	n.a.	n.a.	n.a.	n.a.	n.a.	100.00
WI1311-32	Dol 2	28.96	15.99	8.343	0.964	45.46	0.282	0.002	n.a.	n.a.	n.a.	n.a.	n.a.	n.a.	n.a.	n.a.	n.a.	n.a.	100.00
WI1311-33	Dol 2	29.59	18.37	4.638	0.510	46.88	0.019	0.00	n.a.	n.a.	n.a.	n.a.	n.a.	n.a.	n.a.	n.a.	n.a.	n.a.	100.00
WI1311-34	Dol 2	29.01	15.12	8.908	1.326	45.54	0.110	0.00	n.a.	n.a.	n.a.	n.a.	n.a.	n.a.	n.a.	n.a.	n.a.	n.a.	100.00
WI1311-38	Dol 2	29.29	16.51	7.221	0.955	46.00	0.028	0.00	n.a.	n.a.	n.a.	n.a.	n.a.	n.a.	n.a.	n.a.	n.a.	n.a.	100.00
WI1311-39	Dol 2	29.48	18.60	4.651	0.507	46.75	0.018	0.00	n.a.	n.a.	n.a.	n.a.	n.a.	n.a.	n.a.	n.a.	n.a.	n.a.	100.00
WI1311-40	Dol 2	29.41	17.60	5.788	0.681	46.49	0.013	0.020	n.a.	n.a.	n.a.	n.a.	n.a.	n.a.	n.a.	n.a.	n.a.	n.a.	100.00
WI1311-41	Dol 2	29.21	15.56	8.538	1.230	45.44	0.00	0.024	n.a.	n.a.	n.a.	n.a.	n.a.	n.a.	n.a.	n.a.	n.a.	n.a.	100.00
WI1311-42	Dol 2	29.50	17.02	6.511	0.957	45.96	0.019	0.035	n.a.	n.a.	n.a.	n.a.	n.a.	n.a.	n.a.	n.a.	n.a.	n.a.	100.00
WI1311-43	Dol 2	28.72	14.00	9.550	1.525	46.17	0.014	0.019	n.a.	n.a.	n.a.	n.a.	n.a.	n.a.	n.a.	n.a.	n.a.	n.a.	100.00
WI1311-44	Dol 2	29.27	16.14	7.426	0.989	46.11	0.026	0.035	n.a.	n.a.	n.a.	n.a.	n.a.	n.a.	n.a.	n.a.	n.a.	n.a.	100.00
WI1311-45	Dol 2	30.89	16.99	7.665	1.048	43.36	0.044	0.00	n.a.	n.a.	n.a.	n.a.	n.a.	n.a.	n.a.	n.a.	n.a.	n.a.	100.00
WI1311-46	Dol 2	29.53	16.80	6.915	0.837	45.89	0.028	0.00	n.a.	n.a.	n.a.	n.a.	n.a.	n.a.	n.a.	n.a.	n.a.	n.a.	100.00
WI1311-57	Dol 2	29.14	16.44	7.402	0.993	45.92	0.112	0.00	n.a.	n.a.	n.a.	n.a.	n.a.	n.a.	n.a.	n.a.	n.a.	n.a.	100.00
WI1311-58	Dol 2	29.64	18.49	4.869	0.503	46.47	0.033	0.00	n.a.	n.a.	n.a.	n.a.	n.a.	n.a.	n.a.	n.a.	n.a.	n.a.	100.00
WI1311-60	Dol 2	29.31	16.71	6.859	0.982	46.13	0.00	0.012	n.a.	n.a.	n.a.	n.a.	n.a.	n.a.	n.a.	n.a.	n.a.	n.a.	100.00
WI1311-61	Dol 2	28.91	13.59	10.89	2.037	44.58	0.00	0.00	n.a.	n.a.	n.a.	n.a.	n.a.	n.a.	n.a.	n.a.	n.a.	n.a.	100.00
WI1311-70	Dol 2	28.31	11.32	12.46	3.193	44.62	0.101	0.00	n.a.	n.a.	n.a.	n.a.	n.a.	n.a.	n.a.	n.a.	n.a.	n.a.	100.00
WI1311-79	Dol 2	29.64	16.63	7.06	0.958	45.71	0.00	0.004	n.a.	n.a.	n.a.	n.a.	n.a.	n.a.	n.a.	n.a.	n.a.	n.a.	100.00
WI1311-80	Dol 2	29.26	16.86	7.00	0.725	46.14	0.020	0.001	n.a.	n.a.	n.a.	n.a.	n.a.	n.a.	n.a.	n.a.	n.a.	n.a.	100.00
WI1311-81	Dol 2	30.18	17.37	7.15	0.758	44.55	0.00	0.00	n.a.	n.a.	n.a.	n.a.	n.a.	n.a.	n.a.	n.a.	n.a.	n.a.	100.00
WI1311-82	Dol 2	29.40	17.68	6.32	0.369	46.21	0.017	0.00	n.a.	n.a.	n.a.	n.a.	n.a.	n.a.	n.a.	n.a.	n.a.	n.a.	100.00
WI1311-83	Dol 2	29.44	17.48	6.09	0.880	46.08	0.029	0.006	n.a.	n.a.	n.a.	n.a.	n.a.	n.a.	n.a.	n.a.	n.a.	n.a.	100.00
WI1311-89	Dol 2	29.28	16.37	7.490	0.916	45.89	0.053	0.00	n.a.	n.a.	n.a.	n.a.	n.a.	n.a.	n.a.	n.a.	n.a.	n.a.	100.00
WI1311-90	Dol 2	29.35	19.04	3.778	0.253	47.57	0.017	0.00	n.a.	n.a.	n.a.	n.a.	n.a.	n.a.	n.a.	n.a.	n.a.	n.a.	100.00
WI1311-91	Dol 2	29.44	17.32	6.050	0.755	46.43	0.002	0.00	n.a.	n.a.	n.a.	n.a.	n.a.	n.a.	n.a.	n.a.	n.a.	n.a.	100.00
WI1311-92	Dol 2	29.14	17.28	6.508	0.896	46.15	0.016	0.009	n.a.	n.a.	n.a.	n.a.	n.a.	n.a.	n.a.	n.a.	n.a.	n.a.	100.00
WI1311-93	Dol 2	29.30	16.79	7.084	1.033	45.79	0.00	0.006	n.a.	n.a.	n.a.	n.a.	n.a.	n.a.	n.a.	n.a.	n.a.	n.a.	100.00
WI1311-94	Dol 2	29.03	16.34	7.063	0.903	46.67	0.00	0.00	n.a.	n.a.	n.a.	n.a.	n.a.	n.a.	n.a.	n.a.	n.a.	n.a.	100.00
WI1311-97	Dol 2	29.42	18.63	3.914	0.277	47.74	0.010	0.00	n.a.	n.a.	n.a.	n.a.	n.a.	n.a.	n.a.	n.a.	n.a.	n.a.	100.00
WI1311-98	Dol 2	29.79	16.26	7.255	1.006	45.67	0.025	0.004	n.a.	n.a.	n.a.	n.a.	n.a.	n.a.	n.a.	n.a.	n.a.	n.a.	100.00

Notes:

The detection limits for oxides (wt.%), which are as follows: Ca, 0.03; Mg, 0.03; Fe, 0.07; Sr, 0.09; La, 0.11; K, 0.03; Mn, 0.12; P, 0.04; Ce, 0.1; Th, 0.14; Nb, 0.09; Nd, 0.19; Ti, 0.06; Y, 0.09; Ba, 0.09; Zr, 0.09.

n.a. Not analysed.

1 Calculated.

149

Appendix D: Results of electron microprobe analyses of dolomite and calcite

Name	Classification	CaO	MgO	FeO	MnO	CO₂¹	SrO	BaO	K₂O	P₂O₅	TiO₂	ThO₂	ZrO₂	Nb₂O₅	Y₂O₃	La₂O₃	Ce₂O₃	Nd₂O₃	Total
WI1311-99	Dol 2	29.84	16.78	6.993	0.960	45.39	0.011	0.021	n.a.	n.a.	n.a.	n.a.	n.a.	n.a.	n.a.	n.a.	n.a.	n.a.	100.00
WI1311-100	Dol 2	29.40	16.55	6.803	0.865	46.31	0.029	0.051	n.a.	n.a.	n.a.	n.a.	n.a.	n.a.	n.a.	n.a.	n.a.	n.a.	100.00
WI1311-101	Dol 2	30.16	20.01	2.685	0.161	46.96	0.024	0.00	n.a.	n.a.	n.a.	n.a.	n.a.	n.a.	n.a.	n.a.	n.a.	n.a.	100.00
WI1311-102	Dol 2	30.08	18.17	5.553	0.331	45.87	0.00	0.00	n.a.	n.a.	n.a.	n.a.	n.a.	n.a.	n.a.	n.a.	n.a.	n.a.	100.00
WI1311-106	Dol 2	28.74	12.85	12.32	0.786	45.07	0.235	0.00	n.a.	n.a.	n.a.	n.a.	n.a.	n.a.	n.a.	n.a.	n.a.	n.a.	100.00
WI1311-35	Dol 2	29.74	18.42	4.772	0.470	46.58	0.021	0.00	n.a.	n.a.	n.a.	n.a.	n.a.	n.a.	n.a.	n.a.	n.a.	n.a.	100.00
WI1311-36	Dol 2	29.05	16.24	7.170	0.886	46.52	0.143	0.00	n.a.	n.a.	n.a.	n.a.	n.a.	n.a.	n.a.	n.a.	n.a.	n.a.	100.00
WI1311-37	Dol 2	29.41	17.60	5.855	0.715	46.41	0.007	0.00	n.a.	n.a.	n.a.	n.a.	n.a.	n.a.	n.a.	n.a.	n.a.	n.a.	100.00
WI1311-71	Dol 2	29.41	17.59	5.80	0.693	46.45	0.032	0.019	n.a.	n.a.	n.a.	n.a.	n.a.	n.a.	n.a.	n.a.	n.a.	n.a.	100.00
WI1311-72	Dol 2	26.88	15.83	5.72	0.716	50.80	0.041	0.008	n.a.	n.a.	n.a.	n.a.	n.a.	n.a.	n.a.	n.a.	n.a.	n.a.	100.00
WI1311-73	Dol 2	29.64	18.50	5.01	0.463	46.35	0.028	0.012	n.a.	n.a.	n.a.	n.a.	n.a.	n.a.	n.a.	n.a.	n.a.	n.a.	100.00
WI1311-05	Dol 3	29.21	15.58	8.511	1.120	45.55	0.033	0.00	n.a.	n.a.	n.a.	n.a.	n.a.	n.a.	n.a.	n.a.	n.a.	n.a.	100.00
WI1311-06	Dol 3	29.72	15.09	8.731	1.221	45.14	0.081	0.020	n.a.	n.a.	n.a.	n.a.	n.a.	n.a.	n.a.	n.a.	n.a.	n.a.	100.00
WI1311-07	Dol 3	30.67	15.93	9.169	1.279	42.87	0.059	0.029	n.a.	n.a.	n.a.	n.a.	n.a.	n.a.	n.a.	n.a.	n.a.	n.a.	100.00
WI1311-08	Dol 3	28.96	14.61	9.463	1.315	45.42	0.239	0.00	n.a.	n.a.	n.a.	n.a.	n.a.	n.a.	n.a.	n.a.	n.a.	n.a.	100.00
WI1311-09	Dol 3	29.52	18.33	4.597	0.540	47.00	0.019	0.00	n.a.	n.a.	n.a.	n.a.	n.a.	n.a.	n.a.	n.a.	n.a.	n.a.	100.00
WI1311-12	Dol 3	29.28	15.50	8.502	1.059	45.55	0.104	0.00	n.a.	n.a.	n.a.	n.a.	n.a.	n.a.	n.a.	n.a.	n.a.	n.a.	100.00
WI1311-13	Dol 3	27.99	14.65	8.711	1.372	47.07	0.207	0.00	n.a.	n.a.	n.a.	n.a.	n.a.	n.a.	n.a.	n.a.	n.a.	n.a.	100.00
WI1311-15	Dol 3	28.96	14.37	9.956	1.191	45.36	0.168	0.00	n.a.	n.a.	n.a.	n.a.	n.a.	n.a.	n.a.	n.a.	n.a.	n.a.	100.00
WI1311-16	Dol 3	28.85	13.83	11.08	0.982	45.02	0.221	0.009	n.a.	n.a.	n.a.	n.a.	n.a.	n.a.	n.a.	n.a.	n.a.	n.a.	100.00
WI1311-17	Dol 3	29.43	14.20	10.23	0.928	45.12	0.076	0.018	n.a.	n.a.	n.a.	n.a.	n.a.	n.a.	n.a.	n.a.	n.a.	n.a.	100.00
WI1311-18	Dol 3	29.11	14.11	10.66	0.958	45.00	0.160	0.00	n.a.	n.a.	n.a.	n.a.	n.a.	n.a.	n.a.	n.a.	n.a.	n.a.	100.00
WI1311-19	Dol 3	28.68	14.55	9.456	1.159	45.95	0.194	0.023	n.a.	n.a.	n.a.	n.a.	n.a.	n.a.	n.a.	n.a.	n.a.	n.a.	100.00
WI1311-20	Dol 3	29.00	14.24	9.845	1.637	45.09	0.189	0.00	n.a.	n.a.	n.a.	n.a.	n.a.	n.a.	n.a.	n.a.	n.a.	n.a.	100.00
WI1311-47	Dol 3	29.56	17.94	5.555	0.692	46.21	0.011	0.031	n.a.	n.a.	n.a.	n.a.	n.a.	n.a.	n.a.	n.a.	n.a.	n.a.	100.00
WI1311-48	Dol 3	28.98	13.91	10.88	1.022	44.98	0.225	0.00	n.a.	n.a.	n.a.	n.a.	n.a.	n.a.	n.a.	n.a.	n.a.	n.a.	100.00
WI1311-49	Dol 3	29.38	14.88	9.384	1.192	44.98	0.183	0.005	n.a.	n.a.	n.a.	n.a.	n.a.	n.a.	n.a.	n.a.	n.a.	n.a.	100.00
WI1311-50	Dol 3	28.06	14.15	9.527	1.209	46.75	0.302	0.00	n.a.	n.a.	n.a.	n.a.	n.a.	n.a.	n.a.	n.a.	n.a.	n.a.	100.00
WI1311-51	Dol 3	27.44	11.54	12.73	1.254	46.76	0.235	0.053	n.a.	n.a.	n.a.	n.a.	n.a.	n.a.	n.a.	n.a.	n.a.	n.a.	100.00
WI1311-52	Dol 3	29.20	14.53	9.646	1.151	45.31	0.165	0.001	n.a.	n.a.	n.a.	n.a.	n.a.	n.a.	n.a.	n.a.	n.a.	n.a.	100.00
WI1311-53	Dol 3	28.85	14.11	10.37	1.235	45.21	0.221	0.003	n.a.	n.a.	n.a.	n.a.	n.a.	n.a.	n.a.	n.a.	n.a.	n.a.	100.00
WI1311-54	Dol 3	28.72	13.70	10.49	1.004	46.01	0.074	0.00	n.a.	n.a.	n.a.	n.a.	n.a.	n.a.	n.a.	n.a.	n.a.	n.a.	100.00
WI1311-55	Dol 3	29.38	15.33	8.527	1.159	45.52	0.072	0.015	n.a.	n.a.	n.a.	n.a.	n.a.	n.a.	n.a.	n.a.	n.a.	n.a.	100.00
WI1311-56	Dol 3	29.20	14.11	10.26	1.005	45.25	0.178	0.00	n.a.	n.a.	n.a.	n.a.	n.a.	n.a.	n.a.	n.a.	n.a.	n.a.	100.00
WI1311-59	Dol 3	28.75	15.05	9.382	1.142	45.33	0.347	0.004	n.a.	n.a.	n.a.	n.a.	n.a.	n.a.	n.a.	n.a.	n.a.	n.a.	100.00
WI1311-84	Dol 3	29.26	15.31	8.66	1.116	45.57	0.088	0.00	n.a.	n.a.	n.a.	n.a.	n.a.	n.a.	n.a.	n.a.	n.a.	n.a.	100.00
WI1311-85	Dol 3	28.27	15.30	7.04	0.894	48.41	0.056	0.021	n.a.	n.a.	n.a.	n.a.	n.a.	n.a.	n.a.	n.a.	n.a.	n.a.	100.00
WI1311-86	Dol 3	29.12	13.34	11.87	1.064	44.42	0.175	0.009	n.a.	n.a.	n.a.	n.a.	n.a.	n.a.	n.a.	n.a.	n.a.	n.a.	100.00
WI1311-87	Dol 3	28.76	14.76	9.561	0.948	45.57	0.404	0.00	n.a.	n.a.	n.a.	n.a.	n.a.	n.a.	n.a.	n.a.	n.a.	n.a.	100.00
WI1311-88	Dol 3	28.75	13.87	10.98	0.874	44.97	0.532	0.017	n.a.	n.a.	n.a.	n.a.	n.a.	n.a.	n.a.	n.a.	n.a.	n.a.	100.00
WI1311-95	Dol 3	28.44	13.30	10.20	2.135	45.81	0.089	0.024	n.a.	n.a.	n.a.	n.a.	n.a.	n.a.	n.a.	n.a.	n.a.	n.a.	100.00
WI1311-103	Dol 3	29.54	15.96	7.545	1.197	45.65	0.088	0.022	n.a.	n.a.	n.a.	n.a.	n.a.	n.a.	n.a.	n.a.	n.a.	n.a.	100.00
WI1311-104	Dol 3	29.78	16.05	7.167	1.040	45.91	0.050	0.00	n.a.	n.a.	n.a.	n.a.	n.a.	n.a.	n.a.	n.a.	n.a.	n.a.	100.00
WI1311-105	Dol 3	28.86	13.26	12.12	0.569	44.60	0.586	0.016	n.a.	n.a.	n.a.	n.a.	n.a.	n.a.	n.a.	n.a.	n.a.	n.a.	100.00
WI1311-107	Dol 3	28.92	13.42	12.09	0.537	44.46	0.577	0.00	n.a.	n.a.	n.a.	n.a.	n.a.	n.a.	n.a.	n.a.	n.a.	n.a.	100.00
WI1311-108	Dol 3	24.98	12.34	8.599	0.724	53.08	0.151	0.134	n.a.	n.a.	n.a.	n.a.	n.a.	n.a.	n.a.	n.a.	n.a.	n.a.	100.00
WI1311-109	Dol 3	25.93	12.76	8.834	0.760	51.51	0.129	0.076	n.a.	n.a.	n.a.	n.a.	n.a.	n.a.	n.a.	n.a.	n.a.	n.a.	100.00
WI1311-77	Dol 3	29.40	13.53	10.22	2.129	44.71	0.00	0.016	n.a.	n.a.	n.a.	n.a.	n.a.	n.a.	n.a.	n.a.	n.a.	n.a.	100.00
WI1311-78	Dol 3	26.57	12.34	11.57	2.098	47.36	0.00	0.062	n.a.	n.a.	n.a.	n.a.	n.a.	n.a.	n.a.	n.a.	n.a.	n.a.	100.00
WI1311-96	Dol 3	28.95	15.41	7.858	1.360	46.37	0.050	0.00	n.a.	n.a.	n.a.	n.a.	n.a.	n.a.	n.a.	n.a.	n.a.	n.a.	100.00

Notes: The detection limits for oxides (wt %), which are as follows: Ca, 0.03; Mg, 0.03; Fe, 0.07; Sr, 0.09; La, 0.11; K, 0.03; Mn, 0.12; P, 0.04; Ce, 0.1; Th, 0.14; Nb, 0.09; Nd, 0.19; Ti, 0.06; Y, 0.09; Ba, 0.09; Zr, 0.09.
n.a. Not analysed
1 Calculated.

150

Appendix D: Results of electron microprobe analyses of dolomite and calcite

Name	Classification	CaO	MgO	FeO	MnO	CO_2[1]	SrO	BaO	K_2O	P_2O_5	TiO_2	ThO_2	ZrO_2	Nb_2O_5	Y_2O_3	La_2O_3	Ce_2O_3	Nd_2O_3	Total
WI09080601	Cal	53.73	0.38	1.658	1.215	42.95	0.020	0.046	n.a.	n.a.	n.a.	n.a.	n.a.	n.a.	n.a.	n.a.	n.a.	n.a.	100.00
WI09080602	Cal	53.52	0.28	1.601	0.831	43.75	0.006	0.013	n.a.	n.a.	n.a.	n.a.	n.a.	n.a.	n.a.	n.a.	n.a.	n.a.	100.00
WI09080603	Cal	53.84	0.39	1.728	1.645	42.34	0.018	0.043	n.a.	n.a.	n.a.	n.a.	n.a.	n.a.	n.a.	n.a.	n.a.	n.a.	100.00
WI09080604	Cal	53.66	0.32	1.665	1.018	43.32	0.007	0.017	n.a.	n.a.	n.a.	n.a.	n.a.	n.a.	n.a.	n.a.	n.a.	n.a.	100.00
WI09080605	Cal	52.50	0.40	2.031	0.703	44.29	0.020	0.048	n.a.	n.a.	n.a.	n.a.	n.a.	n.a.	n.a.	n.a.	n.a.	n.a.	100.00
WI09080606	Cal	51.54	0.39	1.818	0.918	45.28	0.016	0.038	n.a.	n.a.	n.a.	n.a.	n.a.	n.a.	n.a.	n.a.	n.a.	n.a.	100.00
WI09080607	Cal	51.08	0.34	1.780	0.748	45.89	0.049	0.114	n.a.	n.a.	n.a.	n.a.	n.a.	n.a.	n.a.	n.a.	n.a.	n.a.	100.00
WI09080608	Cal	52.90	0.37	1.902	1.232	43.53	0.021	0.050	n.a.	n.a.	n.a.	n.a.	n.a.	n.a.	n.a.	n.a.	n.a.	n.a.	100.00
WI09080609	Cal	52.26	0.35	1.768	0.866	44.73	0.007	0.017	n.a.	n.a.	n.a.	n.a.	n.a.	n.a.	n.a.	n.a.	n.a.	n.a.	100.00
WI09080610	Cal	54.85	0.35	1.776	1.159	41.71	0.047	0.110	n.a.	n.a.	n.a.	n.a.	n.a.	n.a.	n.a.	n.a.	n.a.	n.a.	100.00
WI09080611	Cal	54.98	0.37	1.765	1.269	41.40	0.065	0.151	n.a.	n.a.	n.a.	n.a.	n.a.	n.a.	n.a.	n.a.	n.a.	n.a.	100.00
WI09080612	Cal	54.11	0.34	1.834	1.379	42.25	0.028	0.064	n.a.	n.a.	n.a.	n.a.	n.a.	n.a.	n.a.	n.a.	n.a.	n.a.	100.00
WI09080613	Cal	53.93	0.40	1.926	1.368	42.25	0.039	0.091	n.a.	n.a.	n.a.	n.a.	n.a.	n.a.	n.a.	n.a.	n.a.	n.a.	100.00
WI09080614	Cal	54.49	0.38	1.777	1.284	41.80	0.084	0.194	n.a.	n.a.	n.a.	n.a.	n.a.	n.a.	n.a.	n.a.	n.a.	n.a.	100.00
WI09080615	Cal	54.13	0.29	1.681	1.281	42.50	0.035	0.083	n.a.	n.a.	n.a.	n.a.	n.a.	n.a.	n.a.	n.a.	n.a.	n.a.	100.00
WI09080616	Cal	53.40	0.36	2.129	1.399	42.56	0.043	0.100	n.a.	n.a.	n.a.	n.a.	n.a.	n.a.	n.a.	n.a.	n.a.	n.a.	100.00
WI09080617	Cal	53.63	0.33	1.719	1.358	42.81	0.048	0.110	n.a.	n.a.	n.a.	n.a.	n.a.	n.a.	n.a.	n.a.	n.a.	n.a.	100.00
WI09080618	Cal	51.89	0.37	2.634	1.703	43.26	0.044	0.102	n.a.	n.a.	n.a.	n.a.	n.a.	n.a.	n.a.	n.a.	n.a.	n.a.	100.00

Notes: The detection limits for oxides (wt.%), which are as follows: Ca, 0.03; Mg, 0.03; Fe, 0.07; Sr, 0.09; La, 0.11; K, 0.03; Mn, 0.12; P, 0.04; Ce, 0.1; Th, 0.14; Nb, 0.09; Nd, 0.19; Ti, 0.06; Y, 0.09; Ba, 0.09; Zr, 0.09.

n.a. Not analysed

1 Calculated.

151

Appendix E

Results of electron microprobe analyses of biotite

Appendix E: Results of electron microprobe analyses of biotite

Name	SiO₂	TiO₂	Al₂O₃	FeO	MnO	MgO	CaO	Na₂O	K₂O	F	Cl	Total
WI-13-35-01	39.55	1.800	10.50	17.41	0.172	14.76	0.027	0.113	10.25	3.255	0.006	96.48
WI-13-35-02	39.15	1.757	10.43	19.78	0.199	13.47	0.020	0.116	10.29	2.608	0.000	96.72
WI-13-35-03	38.89	1.700	10.82	19.76	0.199	13.24	0.036	0.120	10.12	2.657	0.026	96.45
WI-13-35-04	38.73	1.716	10.59	20.06	0.221	13.42	0.006	0.139	10.07	2.746	0.007	96.54
WI-13-35-05	38.95	1.787	11.21	18.24	0.154	13.99	0.051	0.146	10.14	2.845	0.012	96.33
WI-13-35-06	35.27	2.060	15.38	21.32	0.176	9.956	0.084	0.180	10.00	1.805	0.007	95.47
WI-13-35-07	35.45	1.336	15.49	20.61	0.162	10.47	0.314	0.042	9.839	1.882	0.032	94.83
WI-13-35-08	39.86	1.671	11.27	16.45	0.111	15.31	0.019	0.126	10.47	3.210	0.003	97.15
WI-13-35-09	39.45	1.896	10.74	18.90	0.150	14.09	0.003	0.124	10.33	2.923	0.003	97.38
WI-13-37-01	38.02	1.982	12.03	20.15	0.165	12.70	0.016	0.132	10.29	2.069	0.015	96.69
WI-13-37-02	38.97	2.179	10.66	19.98	0.162	13.48	0.021	0.128	10.33	2.681	0.000	97.45
WI-13-37-03	39.45	1.929	10.83	17.97	0.156	14.67	0.013	0.125	10.53	2.864	0.000	97.32
WI-13-37-04	39.48	1.933	11.00	18.12	0.153	14.57	0.050	0.117	10.36	3.258	0.008	97.68
WI-13-37-05	39.16	1.830	10.36	19.39	0.175	13.57	0.042	0.191	10.19	3.181	0.022	96.77
WI-13-37-06	39.38	1.935	10.56	19.51	0.185	13.75	0.027	0.311	9.886	3.310	0.024	97.49
WI-13-37-07	39.54	1.718	10.54	19.34	0.153	13.90	0.047	0.155	10.14	3.243	0.008	97.42
WI-13-37-08	39.06	2.083	10.76	20.04	0.173	13.36	0.030	0.234	10.10	2.979	0.000	97.56
WI-13-37-09	39.73	1.526	11.15	17.48	0.166	14.74	0.065	0.124	10.33	3.230	0.016	97.19
WI-13-37-10	39.70	2.043	12.35	16.36	0.131	14.27	0.049	0.104	10.52	2.924	0.013	97.22
WI-13-37-11	39.91	1.617	11.75	16.22	0.137	14.86	0.060	0.139	10.59	3.364	0.002	97.24
WI-13-37-12	36.29	1.896	15.40	20.37	0.174	10.78	0.140	0.072	10.07	2.038	0.005	96.37
WI-13-37-13	35.80	1.900	15.65	20.57	0.148	10.27	0.230	0.126	10.04	1.891	0.030	95.85
WI-13-37-14	39.47	1.962	10.74	19.92	0.177	13.77	0.028	0.128	10.20	2.554	0.000	97.87
WI-13-37-15	39.35	2.000	10.69	19.37	0.170	13.92	0.017	0.113	10.32	2.649	0.017	97.50
WI-13-37-16	39.46	1.892	11.02	18.43	0.154	14.06	0.033	0.080	10.32	2.938	0.001	97.16
WI-13-37-17	39.46	2.057	10.56	18.48	0.146	14.27	0.019	0.101	10.30	2.998	0.001	97.13
WI-13-01-01	38.98	1.650	10.42	19.28	0.266	13.80	0.061	0.141	10.14	2.594	0.001	96.24
WI-13-01-02	39.22	1.763	10.42	19.63	0.270	13.97	0.038	0.131	10.15	2.707	0.001	97.16
WI-13-01-03	39.03	1.739	10.69	20.38	0.238	13.39	0.022	0.101	10.20	2.445	0.000	97.21
WI-13-01-04	38.94	1.703	10.70	18.06	0.135	14.39	0.156	0.319	9.999	3.479	0.022	96.44
WI-13-01-05	39.13	1.764	11.37	17.57	0.136	14.42	0.045	0.147	10.11	2.864	0.026	96.36
WI-13-01-06	38.19	1.994	12.78	19.10	0.142	13.20	0.069	0.069	10.22	2.360	0.000	97.12
WI-13-01-07	39.19	1.675	10.41	18.73	0.171	14.16	0.008	0.131	10.23	2.928	0.018	96.41
WI-13-01-08	38.77	1.975	10.98	20.36	0.263	13.09	0.013	0.105	10.21	2.617	0.011	97.29
WI-13-01-09	39.16	2.368	11.13	18.78	0.168	14.11	0.016	0.127	10.37	2.878	0.010	97.90
WI-13-01-10	39.18	2.285	10.48	20.52	0.302	12.90	0.040	0.187	10.11	2.683	0.004	97.55

Notes: The detection limits for oxides (wt.%), which are as follows: Si, 0.04; Ti, 0.05; Al, 0.03; Fe, 0.04; Mn, 0.04; Mg, 0.02; Ca, 0.03; Na, 0.03; K, 0.02; F, 0.17; Cl, 0.03.

153

Appendix E: Results of electron microprobe analyses of biotite

Name	SiO$_2$	TiO$_2$	Al$_2$O$_3$	FeO	MnO	MgO	CaO	Na$_2$O	K$_2$O	F	Cl	Total
WI-13-01-11	39.42	1.819	11.03	19.50	0.170	13.72	0.079	0.199	10.22	2.928	0.000	97.85
WI-13-01-12	39.21	2.010	10.43	19.72	0.203	13.52	0.067	0.193	10.22	2.904	0.021	97.27
WI-13-01-13	39.27	1.808	10.95	17.21	0.139	14.18	0.245	0.298	9.909	3.330	0.036	95.97
WI-13-01-14	38.81	2.117	11.46	18.54	0.127	13.67	0.037	0.197	10.20	2.722	b.l.	96.73
WI-13-01-15	38.74	2.492	10.74	20.41	0.171	12.99	0.042	0.180	10.11	2.694	0.005	97.45
WI-13-01-16	38.68	2.139	10.79	20.70	0.174	12.78	0.026	0.135	10.23	2.529	0.017	97.13
WI-13-01-17	38.65	2.008	11.21	20.10	0.178	12.94	0.057	0.173	10.16	2.632	0.015	97.01
WI08010I-01	38.62	1.784	11.10	19.66	0.156	13.31	0.095	0.170	9.920	2.837	0.013	96.45
WI08010I-02	39.37	1.888	11.11	17.95	0.130	14.14	0.131	0.165	10.33	3.140	0.019	97.04
WI08010I-03	38.95	2.159	10.74	20.42	0.189	13.25	0.023	0.158	10.18	2.453	0.000	97.49
WI08010I-04	39.10	1.840	10.56	20.77	0.152	13.41	0.006	0.139	10.55	2.404	0.008	97.91
WI08010I-05	39.30	1.929	10.66	20.35	0.205	13.53	0.000	0.098	10.35	2.936	0.008	98.12
WI08010I-06	39.29	1.810	11.78	17.29	0.145	14.46	0.027	0.128	10.31	2.790	0.022	96.86
WI08010I-07	39.54	1.933	10.67	18.56	0.163	14.46	0.005	0.130	10.32	2.783	0.004	97.39
WI08010I-08	39.60	1.923	10.65	18.59	0.180	14.66	0.169	0.115	10.35	2.963	0.007	97.95
WI08010I-09	39.62	1.962	11.29	17.40	0.143	14.54	0.050	0.096	10.52	3.204	0.009	97.49
WI08010I-10	39.39	1.815	11.79	17.76	0.174	14.05	0.092	0.050	10.42	2.937	0.004	97.26
WI08010I-11	39.55	1.786	10.57	17.74	0.128	14.73	0.047	0.364	9.829	3.647	0.035	96.88
WI08010I-12	36.24	1.514	14.12	20.52	0.152	11.07	0.077	0.312	9.797	2.195	0.066	95.12
WI08010I-13	38.90	1.959	10.87	18.44	0.159	14.06	0.074	0.349	9.975	3.221	0.012	96.66
WI08010I-14	39.05	1.895	10.49	18.95	0.228	14.22	0.062	0.236	10.18	3.095	0.000	97.09
08WI01-11-01	39.63	2.408	10.53	18.04	0.085	14.79	0.016	0.199	10.49	2.977	0.015	97.93
08WI01-11-02	39.48	2.672	10.33	18.40	0.231	14.10	0.071	0.224	10.35	2.537	0.013	97.34
08WI01-11-03	39.79	2.662	10.62	18.07	0.097	14.54	0.018	0.185	10.56	2.982	0.001	98.26
08WI01-11-04	42.99	1.953	11.97	16.16	0.117	12.65	0.012	1.653	9.39	2.700	0.004	98.46
08WI01-11-05	39.84	2.547	10.54	18.17	0.131	14.87	0.030	0.191	10.33	2.760	0.008	98.25
08WI01-11-06	40.07	2.065	10.66	16.72	0.071	15.48	0.021	0.133	10.56	3.079	0.001	97.57
08WI01-11-07	37.94	1.868	12.37	19.63	0.062	13.74	0.095	0.025	10.63	2.314	0.001	97.70
08WI01-11-08	39.57	2.689	10.47	18.21	0.070	14.33	0.017	0.182	10.42	2.490	0.018	97.42
08WI01-11-09	39.88	1.760	11.13	17.09	0.061	15.34	0.012	0.059	10.65	2.839	0.015	97.63
08WI01-11-10	38.88	1.637	11.62	17.93	0.046	14.82	0.061	0.025	10.63	2.567	0.000	97.13
08WI01-11-11	39.01	1.578	11.70	18.09	0.080	14.58	0.177	0.032	10.86	2.570	0.006	97.60
WI090806-01	34.84	4.049	10.37	31.14	0.539	5.952	0.038	0.122	9.780	0.163	0.007	96.93
WI090806-02	35.02	3.976	10.05	31.07	0.542	6.351	0.029	0.097	9.514	0.259	0.000	96.80
WI090806-03	34.92	3.863	9.977	30.96	0.517	6.049	0.100	0.134	9.331	0.345	0.010	96.06

Notes: The detection limits for oxides (wt.%), which are as follows: Si, 0.04; Ti, 0.05; Al, 0.03; Fe, 0.04; Mn, 0.04; Mg, 0.02; Ca, 0.03; Na, 0.03; K, 0.02; F, 0.17; Cl, 0.03.

154

Appendix E: Results of electron microprobe analyses of biotite

Name	SiO$_2$	TiO$_2$	Al$_2$O$_3$	FeO	MnO	MgO	CaO	Na$_2$O	K$_2$O	F	Cl	Total
WI090806-04	35.46	3.746	9.601	30.68	0.461	6.688	0.258	0.076	9.664	0.343	0.007	96.83
WI090806-05	35.08	2.756	9.959	31.77	0.530	6.175	0.113	0.065	9.636	0.016	0.011	96.10
WI090806-06	35.17	3.834	10.07	30.81	0.562	5.968	0.127	0.128	9.614	0.113	0.021	96.37
WI090806-07	35.06	3.884	10.16	31.40	0.507	6.030	0.029	0.122	9.938	0.137	0.000	97.21
WI090806-08	35.08	3.770	9.955	31.02	0.540	6.067	0.036	0.113	9.868	0.150	0.021	96.56

Notes: The detection limits for oxides (wt.%), which are as follows: Si, 0.04; Ti, 0.05; Al, 0.03; Fe, 0.04; Mn, 0.04; Mg, 0.02; Ca, 0.03; Na, 0.03; K, 0.02; F, 0.17; Cl, 0.03.

Appendix F

Results of electron microprobe analyses of amphibole

Appendix F: Results of electron microprobe analyses of amphibole

Name	SiO$_2$	TiO$_2$	Al$_2$O$_3$	FeO	MnO	MgO	CaO	Na$_2$O	K$_2$O	F	Cl	Total
WI-37-01-01	53.95	0.615	0.404	16.36	0.045	13.54	0.442	7.889	1.619	1.857	0.019	95.94
WI-37-01-02	54.39	0.497	3.185	16.61	0.000	10.28	0.578	7.833	1.445	1.069	0.023	95.45
WI-37-01-03	53.99	0.280	3.996	14.50	0.039	10.46	1.516	7.966	1.470	1.325	0.026	95.01
WI-37-01-04	54.77	0.368	0.472	18.29	0.077	12.39	0.432	7.381	1.503	1.609	0.030	96.63
WI-37-01-05	56.01	0.448	0.274	15.43	0.039	14.23	0.521	8.289	1.642	2.039	0.009	98.07
WI-37-01-06	54.43	0.982	0.394	16.23	0.019	13.10	0.500	7.804	1.593	2.156	0.033	96.32
WI-37-01-07	55.25	0.208	0.854	19.12	0.068	11.53	0.449	7.406	1.363	1.296	0.016	97.01
WI-37-01-08	55.49	0.805	0.346	15.21	0.029	14.09	0.416	8.179	1.600	2.173	0.007	97.43
WI-37-01-09	55.37	0.386	0.457	18.60	0.048	12.52	0.593	7.140	1.672	1.394	0.050	97.63
WI-37-01-10	56.00	0.270	0.190	15.29	0.076	14.19	0.639	8.750	1.578	2.175	0.003	98.24
WI-37-01-11	56.10	0.700	0.191	17.18	0.021	13.16	0.321	7.759	1.540	1.632	0.013	97.93
WI-37-01-12	55.60	0.224	0.225	16.62	0.035	13.52	0.535	8.015	1.597	1.822	0.000	97.43
WI-37-01-13	55.46	0.374	0.184	16.54	0.000	13.65	0.342	8.172	1.450	1.789	0.009	97.21
WI-37-01-14	55.56	1.245	0.266	15.17	0.040	14.15	0.422	8.272	1.599	1.763	0.000	97.75
WI-37-01-15	55.27	0.713	0.353	16.38	0.010	13.31	0.369	8.125	1.363	1.638	0.000	96.84
WI-37-01-16	55.57	0.248	0.166	15.51	0.060	14.13	0.592	8.386	1.717	2.109	0.008	97.60

Notes: The detection limits for oxides (wt.%), which are as follows: Si, 0.04; Ti, 0.05; Al, 0.03; Fe, 0.04; Mn, 0.04; Mg, 0.02; Ca, 0.03; Na, 0.03; K, 0.02; F, 0.17; Cl, 0.03.

Appendix G

Results of electron microprobe analyses of pyroxene

Appendix G: Results of electron microprobe analyses of pyroxene

Name	SiO$_2$	TiO$_2$	Al$_2$O$_3$	FeO	MnO	MgO	CaO	Na$_2$O	K$_2$O	F	Cl	Total
W10908-06-01	51.36	0.353	0.727	24.73	0.530	3.618	12.62	6.319	0.000	n.a.	n.a.	100.93
W10908-06-02	51.59	0.378	0.558	27.15	0.404	2.404	10.30	7.523	0.016	n.a.	n.a.	100.67
W10908-06-03	51.48	0.341	0.503	27.74	0.492	2.201	10.73	7.323	0.000	n.a.	n.a.	101.25
W10908-06-04	51.44	0.384	0.706	24.88	0.514	3.652	12.40	6.501	0.000	n.a.	n.a.	101.01
W10908-06-05	52.02	0.326	0.457	27.15	0.261	2.506	7.701	8.934	0.000	n.a.	n.a.	100.07
W10908-06-06	49.05	0.339	0.717	24.41	0.615	3.857	12.71	5.823	0.000	n.a.	n.a.	98.17
W10908-06-07	51.13	0.455	0.458	27.93	0.475	2.094	10.60	7.263	0.004	n.a.	n.a.	100.74
W10908-06-08	51.26	0.322	0.729	24.82	0.527	3.765	12.79	6.144	0.008	n.a.	n.a.	100.92
W10908-06-09	50.64	0.314	0.590	27.19	0.272	2.175	8.018	9.323	0.008	n.a.	n.a.	99.09
W10908-06-10	51.59	0.379	0.583	26.44	0.313	2.878	9.140	8.443	0.008	n.a.	n.a.	100.37
W10908-06-11	49.76	0.372	0.774	26.70	0.240	2.859	7.692	8.260	0.025	n.a.	n.a.	97.40
W10908-06-12	51.45	0.306	0.643	24.79	0.516	3.789	12.34	6.293	0.015	n.a.	n.a.	100.83
W10908-06-13	51.79	0.349	0.473	27.05	0.275	2.520	7.957	9.156	0.008	n.a.	n.a.	100.25
W10908-06-14	51.27	0.394	0.549	27.26	0.374	2.327	9.479	7.997	0.012	n.a.	n.a.	100.11
W10908-06-15	50.14	0.289	0.388	27.48	0.176	1.857	7.486	9.998	0.000	n.a.	n.a.	98.52
W10908-06-16	50.24	0.332	0.509	26.51	0.290	2.493	9.560	8.571	0.000	n.a.	n.a.	99.13
W10908-06-17	49.60	0.295	0.387	27.39	0.192	1.917	7.494	9.823	0.008	n.a.	n.a.	97.79
W10908-06-18	51.10	0.338	0.701	24.38	0.579	3.622	12.71	6.249	0.000	n.a.	n.a.	100.47
WI-13-37-01	52.57	1.740	1.032	27.09	0.032	0.408	0.356	13.96	0.004	0.045	0.005	97.21
WI-13-37-02	51.72	3.571	0.715	23.48	0.198	1.446	0.297	13.47	0.039	0.000	0.022	94.95
WI-13-37-03	52.26	1.708	0.864	27.22	0.058	0.415	0.338	14.01	0.010	0.000	0.021	96.90
WI-13-37-04	51.41	1.397	1.121	26.83	0.104	0.499	0.639	13.58	0.007	0.000	0.032	95.61
WI-13-37-05	52.45	1.115	0.858	28.18	0.011	0.399	0.228	13.93	0.000	0.000	0.000	97.17
WI-13-37-06	51.84	1.733	1.046	26.98	0.005	0.378	0.191	13.91	0.000	0.000	0.025	96.11
WI-13-37-07	52.50	1.545	0.894	27.35	0.020	0.448	0.247	14.06	0.002	0.000	0.007	97.07
WI-13-37-08	51.44	0.882	0.761	27.99	0.046	0.320	0.966	13.67	0.008	0.000	0.000	96.09
WI-13-37-09	51.95	1.730	0.896	26.76	0.026	0.460	0.388	13.52	0.013	0.024	0.000	95.76
WI-13-37-10	52.30	1.463	0.785	27.99	0.031	0.388	0.223	14.07	0.000	0.000	0.022	97.26
WI-13-37-11	52.67	2.065	0.915	26.98	0.013	0.390	0.256	14.04	0.018	0.000	0.000	97.34
WI-13-37-12	51.68	1.272	0.737	27.19	0.369	0.487	0.593	13.53	0.000	0.000	0.009	95.87
WI-13-37-13	52.08	1.680	0.951	27.47	0.000	0.442	0.227	13.96	0.015	0.000	0.080	96.89
WI-13-37-14	51.81	0.954	0.808	27.64	0.008	0.369	0.321	13.54	0.003	0.000	0.003	95.46
WI-13-37-15	52.82	5.122	0.212	23.49	0.320	1.573	0.472	13.75	0.000	0.000	0.000	97.76
08WI01-12-01	52.23	0.821	0.838	28.58	0.000	0.329	0.189	14.00	0.000	0.000	0.011	96.99
08WI01-12-02	52.73	0.797	0.978	28.59	0.000	0.361	0.126	13.86	0.004	0.000	0.007	97.45
08WI01-12-03	52.66	1.645	2.476	25.61	0.019	0.421	0.187	13.98	0.004	0.000	0.000	97.00

Notes: The detection limits for oxides (wt.%), which are as follows: Si, 0.04; Ti, 0.05; Al, 0.03; Fe, 0.04; Mn, 0.04; Mg, 0.02; Ca, 0.03; Na, 0.03; K, 0.02; F, 0.17; Cl, 0.03.

159

Appendix G: Results of electron microprobe analyses of pyroxene

Name	SiO$_2$	TiO$_2$	Al$_2$O$_3$	FeO	MnO	MgO	CaO	Na$_2$O	K$_2$O	F	Cl	Total
08WI01-12-04	52.21	0.503	1.483	27.71	0.017	0.235	0.351	13.83	0.00	0.00	0.012	96.35
08WI01-12-05	51.80	1.514	1.258	27.53	0.012	0.831	0.225	13.54	0.00	0.00	0.00	96.71
08WI01-12-06	52.55	1.670	0.996	27.50	0.045	0.600	0.118	14.09	0.016	0.030	0.005	97.61
08WI01-12-07	52.41	2.134	0.890	28.02	0.00	0.265	0.031	14.21	0.013	0.020	0.00	97.98
08WI01-12-08	52.52	1.930	0.715	26.84	0.030	0.607	0.468	14.00	0.00	0.00	0.003	97.11
08WI01-12-09	52.65	1.480	2.269	25.93	0.00	0.402	0.220	13.99	0.001	0.00	0.011	96.95
08WI01-12-10	52.38	1.823	0.938	27.19	0.004	0.443	0.317	13.84	0.022	0.00	0.025	96.98
08WI01-11-01	39.63	2.408	10.53	18.04	0.085	14.79	0.016	0.199	10.49	2.977	0.015	97.93
08WI01-11-02	39.48	2.672	10.33	18.40	0.231	14.10	0.071	0.224	10.35	2.537	0.013	97.34
08WI01-11-03	39.79	2.662	10.62	18.07	0.097	14.54	0.018	0.185	10.56	2.982	0.001	98.26
08WI01-11-04	42.99	1.953	11.97	16.16	0.117	12.65	0.012	1.653	9.39	2.700	0.004	98.46
08WI01-11-05	39.84	2.547	10.54	18.17	0.131	14.87	0.030	0.191	10.33	2.760	0.008	98.25
08WI01-11-06	40.07	2.065	10.66	16.72	0.071	15.48	0.021	0.133	10.56	3.079	0.001	97.57
08WI01-11-07	37.94	1.868	12.37	19.63	0.062	13.74	0.095	0.025	10.63	2.314	0.001	97.70
08WI01-11-08	39.57	2.689	10.47	18.21	0.070	14.33	0.017	0.182	10.42	2.490	0.018	97.42
08WI01-11-09	39.88	1.760	11.13	17.09	0.061	15.34	0.012	0.059	10.65	2.839	0.015	97.63
08WI01-11-10	38.88	1.637	11.62	17.93	0.046	14.82	0.061	0.025	10.63	2.567	0.00	97.13
08WI01-11-11	39.01	1.578	11.70	18.09	0.080	14.58	0.177	0.032	10.86	2.570	0.006	97.60

Notes: The detection limits for oxides (wt.%), which are as follows: Si, 0.04; Ti, 0.05; Al, 0.03; Fe, 0.04; Mn, 0.04; Mg, 0.02; Ca, 0.03; Na, 0.03; K, 0.02; F, 0.17; Cl, 0.03.

Appendix H

Results of electron microprobe analyses of albite and potassium feldspar

Appendix H: Results of electron microprobe analyses of albite and K-feldspar

Name	SiO$_2$	Al$_2$O$_3$	Na$_2$O	K$_2$O	SrO	BaO	Rb$_2$O	CaO	PbO	FeO	Total
55-01-01K	65.20	18.65	0.770	15.91	0.000	0.031	0.022	0.090	0.000	0.026	100.70
55-01-04K	65.29	18.64	1.698	14.01	0.004	0.070	0.049	0.149	0.000	0.138	100.04
55-01-05K	64.30	18.51	0.471	16.21	0.031	0.222	0.019	0.064	0.041	0.050	99.92
55-01-07K	66.13	18.90	3.155	12.04	0.022	0.167	0.061	0.071	0.000	0.184	100.73
55-05-01K	64.57	18.42	0.280	16.23	0.053	0.100	0.029	0.028	0.000	0.007	99.72
55-05-03K	64.87	18.48	0.172	16.35	0.000	0.089	0.054	0.309	0.000	0.018	100.34
55-05-05K	64.90	18.53	0.208	16.40	0.074	0.076	0.018	0.259	0.000	0.038	100.51
55-05-08K	63.78	18.09	0.298	16.16	0.000	0.186	0.006	0.581	0.000	0.061	99.16
55-05-10K	65.05	18.47	0.485	15.94	0.001	0.266	0.000	0.055	0.103	0.180	100.55
55-05-11K	64.12	18.11	0.212	16.37	0.000	0.109	0.032	0.381	0.000	0.213	99.55
55-08-01K	63.97	18.31	0.220	16.01	0.064	0.129	0.016	0.501	0.030	0.123	99.38
55-08-04K	64.02	18.38	0.237	16.10	0.050	0.070	0.000	0.372	0.012	0.083	99.33
55-09-01K	61.15	20.11	0.418	14.11	0.059	4.671	0.000	0.009	0.032	0.180	100.73
55-09-02K	63.36	19.32	0.310	15.10	0.022	3.118	0.001	0.013	0.000	0.034	101.28
55-09-03K	64.34	18.69	0.265	16.05	0.020	0.613	0.060	0.010	0.006	0.017	100.08
55-09-04K	63.49	18.90	0.301	15.87	0.023	1.053	0.020	0.000	0.000	0.005	99.67
55-09-05K	62.58	19.49	0.415	14.83	0.061	3.425	0.000	0.009	0.003	0.112	100.93
55-09-06K	62.48	19.67	0.377	14.80	0.043	3.474	0.000	0.000	0.000	0.181	101.02
55-09-07K	62.15	19.65	0.336	14.84	0.000	3.065	0.054	0.016	0.000	0.171	100.28
55-01-02A	68.98	19.79	11.46	0.087	0.062	0.052	0.001	0.226	0.000	0.072	100.72
55-01-03A	67.48	19.37	11.33	0.095	0.000	0.000	0.000	1.174	0.000	0.131	99.58
55-01-06A	68.31	19.60	11.33	0.114	0.023	0.042	0.000	0.175	0.007	0.111	99.71
55-01-08A	68.97	19.72	11.30	0.338	0.019	0.027	0.001	0.068	0.000	0.084	100.53
55-05-02A	68.55	19.69	11.22	0.060	0.055	0.019	0.000	0.355	0.002	0.092	100.05
55-05-04A	68.69	19.56	11.37	0.072	0.082	0.000	0.000	0.228	0.073	0.032	100.11
55-05-06A	68.57	19.72	11.45	0.075	0.047	0.014	0.000	0.150	0.007	0.009	100.04
55-05-07A	68.01	19.16	11.35	0.064	0.017	0.067	0.001	0.217	0.000	0.181	99.07
55-05-09A	67.41	18.91	11.06	0.300	0.058	0.011	0.000	0.054	0.050	0.257	98.12
55-08-02A	68.15	20.01	11.27	0.093	0.138	0.019	0.000	0.309	0.127	0.106	100.22
55-08-03A	68.29	19.66	11.46	0.176	0.044	0.017	0.000	0.141	0.012	0.163	99.97
55-09-01A	68.75	19.52	11.48	0.047	0.021	0.031	0.000	0.024	0.000	0.050	99.92
55-09-02A	67.57	19.34	11.40	0.053	0.055	0.087	0.000	0.029	0.000	0.054	98.58
55-09-03A	68.58	19.49	11.29	0.048	0.061	0.035	0.000	0.044	0.018	0.019	99.59

Notes: The detection limits for oxides (wt.%), which are as follows: Si, 0.04; Al, 0.03; Na, 0.03; K, 0.03; Sr, 0.09; Ba, 0.09; Rb, 0.07; Ca, 0.03; Pb, 0.11; Fe, 0.04.

Appendix H: Results of electron microprobe analyses of albite and K-feldspar

Name	SiO$_2$	Al$_2$O$_3$	Na$_2$O	K$_2$O	SrO	BaO	Rb$_2$O	CaO	PbO	FeO	Total
55-09-04A	68.09	19.74	11.23	0.137	0.065	0.009	0.000	0.009	0.017	0.047	99.34
55-09-05A	68.27	19.43	11.40	0.069	0.054	0.019	0.017	0.114	0.026	0.034	99.44
55-09-06A	68.15	19.67	11.13	0.162	0.000	0.021	0.000	0.052	0.155	0.006	99.35
57-01-01A	68.65	19.87	11.42	0.035	0.000	0.000	0.006	0.019	0.012	0.092	100.09
57-01-02A	68.77	19.84	11.49	0.042	0.020	0.000	0.000	0.033	0.000	0.043	100.24
57-01-03A	68.55	19.83	11.56	0.044	0.041	0.018	0.000	0.032	0.000	0.006	100.08
57-01-04A	68.63	19.85	11.45	0.065	0.072	0.000	0.000	0.047	0.010	0.019	100.14
57-01-05K	63.30	18.31	0.247	15.91	0.000	0.202	0.034	1.051	0.000	0.050	99.10
57-01-06K	64.91	18.68	0.315	16.21	0.069	0.216	0.000	0.028	0.031	0.021	100.48
57-01-07K	64.41	18.48	0.294	16.15	0.004	0.204	0.025	0.000	0.000	0.004	99.56
57-01-08K	64.74	18.67	0.314	16.21	0.002	0.326	0.024	0.000	0.006	0.021	100.31
57-01-09	49.15	31.09	0.156	9.818	0.008	0.000	0.010	0.144	0.005	1.181	91.56
57-01-10a	49.48	29.56	0.189	10.51	0.012	0.063	0.036	0.089	0.047	1.471	91.46
57-01-10b	63.87	16.93	0.298	16.35	0.043	0.151	0.040	0.004	0.000	0.009	97.70
57-02-01K	64.46	18.40	0.281	16.34	0.067	0.157	0.000	0.016	0.000	0.045	99.77
57-02-02K	64.61	18.09	0.294	16.26	0.048	0.217	0.018	0.005	0.000	0.055	99.60
57-02-03A	99.21	0.075	0.004	0.003	0.035	0.024	0.027	0.020	0.046	0.016	99.46
57-02-04A	70.81	15.74	9.227	0.140	0.033	0.010	0.000	0.004	0.000	0.230	96.19
57-02-05A	64.43	18.19	10.65	0.113	0.027	0.000	0.000	0.072	0.088	0.288	93.86
57-02-06K	64.72	18.54	0.320	16.42	0.049	0.216	0.063	0.000	0.002	0.000	100.33
57-04-01A	68.45	19.50	11.44	0.047	0.029	0.000	0.042	0.015	0.000	0.011	99.53
57-04-03A	68.82	19.53	11.52	0.046	0.041	0.000	0.000	0.016	0.000	0.006	99.98
57-04-04A	68.59	19.17	11.55	0.039	0.043	0.031	0.007	0.028	0.000	0.029	99.49
57-04-06K	64.54	18.17	0.238	16.32	0.016	0.260	0.000	0.008	0.021	0.010	99.57
57-04-07K	64.24	18.14	1.328	14.53	0.018	0.205	0.018	0.009	0.000	0.000	98.49
57-04-08K	64.77	18.25	0.266	16.48	0.054	0.178	0.012	0.015	0.030	0.007	100.06
57-04-10K	49.99	27.80	0.066	10.33	0.059	0.128	0.007	0.041	0.031	1.388	89.84
57-04-11A	68.14	19.33	11.44	0.032	0.000	0.010	0.000	0.060	0.000	0.041	99.05
38-04-01A	69.28	19.45	11.53	0.052	0.000	0.013	0.003	0.059	0.000	0.000	100.39
38-04-02	68.82	19.75	11.45	0.030	0.040	0.000	0.012	0.027	0.056	0.006	100.19
38-04-03	69.16	19.65	11.44	0.067	0.000	0.000	0.000	0.060	0.011	0.046	100.43
38-04-05	68.27	19.43	11.53	0.087	0.042	0.000	0.000	0.058	0.042	0.057	99.52
38-04-06	68.90	19.71	11.37	0.049	0.032	0.053	0.005	0.120	0.069	0.023	100.32

Notes: The detection limits for oxides (wt.%), which are as follows: Si, 0.04; Al, 0.03; Na, 0.03; K, 0.03; Sr, 0.09; Ba, 0.09; Rb, 0.07; Ca, 0.03; Pb, 0.11; Fe, 0.04.

Appendix H: Results of electron microprobe analyses of albite and K-feldspar

Name	SiO$_2$	Al$_2$O$_3$	Na$_2$O	K$_2$O	SrO	BaO	Rb$_2$O	CaO	PbO	FeO	Total
38-04-07	68.36	19.59	11.39	0.042	0.071	0.038	0.000	0.078	0.000	0.005	99.57
38-04-09	68.37	19.04	11.48	0.049	0.021	0.024	0.000	0.047	0.014	0.029	99.07
38-04-13	68.76	19.48	11.56	0.055	0.051	0.000	0.000	0.084	0.000	0.000	99.99
38-04-14	62.56	17.49	10.78	0.051	0.005	0.018	0.016	3.928	0.059	0.000	94.90
38-04-15	68.53	19.56	11.48	0.022	0.034	0.000	0.000	0.033	0.000	0.000	99.65
38-04-16	68.99	19.72	11.48	0.053	0.030	0.000	0.000	0.032	0.000	0.009	100.31
38-04-17	62.22	20.54	11.41	0.261	0.128	0.000	0.000	2.186	0.021	0.074	96.85
38-04-18	68.85	19.42	11.33	0.075	0.061	0.037	0.000	0.034	0.044	0.046	99.90
38-04-19	67.41	19.10	11.24	0.046	0.041	0.023	0.028	0.058	0.000	0.017	97.96
38-04-20	67.03	19.67	10.86	0.059	0.088	0.015	0.000	0.855	0.000	0.025	98.60
09-01-01K	63.84	18.40	0.234	16.25	0.050	0.000	0.048	0.076	0.005	0.071	98.98
09-01-02A	66.74	18.96	11.09	0.102	0.000	0.000	0.026	0.052	0.021	0.104	97.09
09-01-03A	55.20	16.07	9.481	0.353	0.019	0.093	0.000	2.546	0.000	7.575	91.34
09-01-04K	64.15	18.44	0.253	16.16	0.007	0.000	0.000	0.086	0.026	0.016	99.14
09-01-05K	64.44	18.19	0.255	16.17	0.005	0.000	0.070	0.024	0.000	0.023	99.17
09-01-06A	67.90	19.65	11.40	0.063	0.058	0.028	0.000	0.068	0.059	0.130	99.35
09-01-06A	68.19	19.65	11.21	0.062	0.000	0.000	0.000	0.058	0.026	0.080	99.28
09-01-07K	64.21	18.18	0.266	16.18	0.012	0.000	0.014	0.043	0.010	0.032	98.95
09-02-01A	68.19	19.40	11.36	0.064	0.032	0.049	0.019	0.438	0.000	0.079	99.63
09-02-02A	68.06	19.51	11.49	0.074	0.000	0.020	0.000	0.208	0.000	0.253	99.61
09-02-03A	65.98	18.60	10.84	0.059	0.027	0.035	0.000	1.459	0.000	0.068	97.07
09-02-04A	67.33	19.25	11.24	0.079	0.000	0.227	0.000	0.191	0.000	0.164	98.47
09-02-05A	67.97	19.55	11.37	0.121	0.077	0.013	0.000	0.051	0.026	0.174	99.35
09-02-06A	67.67	19.51	11.26	0.102	0.000	0.000	0.023	0.089	0.000	0.122	98.77
09-02-07A	68.27	19.61	11.61	0.058	0.098	0.036	0.000	0.042	0.000	0.049	99.77
09-02-08A	67.54	19.46	11.31	0.070	0.040	0.022	0.000	0.066	0.009	0.100	98.61
09-02-09A	68.90	19.45	11.35	0.047	0.000	0.031	0.014	0.064	0.046	0.061	99.96
09-02-10A	68.00	19.59	11.27	0.089	0.025	0.000	0.000	0.161	0.073	0.133	99.34
09-02-28K	64.36	18.36	0.253	16.24	0.062	0.000	0.022	0.181	0.004	0.033	99.52
09-02-30K	64.57	18.54	0.269	16.14	0.041	0.078	0.015	0.172	0.038	0.204	100.07
09-02-32A	67.28	18.64	11.49	0.047	0.077	0.000	0.000	0.141	0.000	1.677	99.34
09-02-33A	68.30	19.52	11.56	0.041	0.068	0.000	0.000	0.142	0.000	0.091	99.72

Notes: The detection limits for oxides (wt.%), which are as follows: Si, 0.04; Al, 0.03; Na, 0.03; K, 0.03; Sr, 0.09; Ba, 0.09; Rb, 0.07; Ca, 0.03; Pb, 0.11; Fe, 0.04.

Appendix H: Results of electron microprobe analyses of albite and K-feldspar

Name	SiO$_2$	Al$_2$O$_3$	Na$_2$O	K$_2$O	SrO	BaO	Rb$_2$O	CaO	PbO	FeO	Total
09-02-34A	67.54	19.39	11.35	0.048	0.052	0.006	0.024	0.080	0.044	0.083	98.62
09-02-35A	68.56	19.62	11.44	0.077	0.039	0.028	0.000	0.209	0.034	0.197	100.20
09-02-36A	68.96	19.80	11.44	0.042	0.082	0.020	0.000	0.165	0.065	0.048	100.61
09-02-37A	66.80	19.32	11.22	0.058	0.017	0.066	0.000	1.543	0.000	0.115	99.13
09-02-38A	66.95	19.10	11.23	0.067	0.012	0.000	0.000	0.706	0.000	0.153	98.22
09-02-39A	68.23	19.43	11.45	0.064	0.022	0.047	0.006	0.133	0.046	0.104	99.53
09-02-40A	68.20	19.61	11.42	0.075	0.009	0.000	0.000	0.042	0.000	0.095	99.45
09-02-42K	64.29	18.59	0.207	16.39	0.026	0.040	0.000	0.164	0.000	0.071	99.80
09-02-44K	65.30	18.75	2.515	13.31	0.048	0.017	0.028	0.06	0.030	0.074	100.14
09-02-46K	64.89	18.38	0.243	16.19	0.048	0.015	0.024	0.043	0.020	0.090	99.97
09-02-47A	68.66	19.44	11.62	0.086	0.042	0.000	0.049	0.127	0.000	0.063	100.04
09-02-48A	68.25	19.10	11.51	0.163	0.038	0.000	0.000	0.068	0.010	0.278	99.42
09-02-49A	68.42	19.40	11.27	0.098	0.000	0.000	0.000	0.096	0.011	0.029	99.32
09-02-50A	68.56	19.71	11.41	0.092	0.018	0.015	0.000	0.090	0.030	0.200	100.13
07-01-01A	68.75	19.85	11.36	0.041	0.047	0.000	0.000	0.043	0.000	0.000	100.09
37263.000	68.23	19.71	11.51	0.057	0.034	0.000	0.000	0.077	0.000	0.010	99.63
37628.000	68.18	19.54	11.26	0.069	0.016	0.000	0.000	0.067	0.000	0.043	99.17
37993.000	68.64	19.57	11.33	0.060	0.072	0.000	0.003	0.016	0.000	0.000	99.69
38359.000	68.68	19.72	11.25	0.139	0.066	0.014	0.000	0.032	0.000	0.035	99.92
38724.000	67.96	19.65	11.31	0.194	0.019	0.071	0.035	0.019	0.000	0.014	99.27
07-01-07A	68.59	19.75	11.45	0.061	0.032	0.000	0.000	0.035	0.016	0.000	99.93
07-01-08A	68.27	19.53	11.49	0.071	0.090	0.020	0.000	0.024	0.003	0.000	99.49
07-01-09A	68.31	19.50	11.41	0.085	0.086	0.019	0.015	0.034	0.000	0.017	99.47
WI09090201	61.15	20.11	0.418	14.11	0.059	4.671	0.000	0.009	0.032	0.180	100.73
WI09090202	63.36	19.32	0.310	15.10	0.022	3.118	0.001	0.013	0.000	0.034	101.28
WI09090203	64.34	18.69	0.265	16.05	0.020	0.613	0.060	0.010	0.006	0.017	100.08
WI09090204	63.49	18.90	0.301	15.87	0.023	1.053	0.020	0.000	0.000	0.005	99.67
WI09090205	62.58	19.49	0.415	14.83	0.061	3.425	0.000	0.009	0.003	0.112	100.93
WI09090206	62.48	19.67	0.377	14.80	0.043	3.474	0.000	0.000	0.000	0.181	101.02

Notes: The detection limits for oxides (wt.%), which are as follows: Si, 0.04; Al, 0.03; Na, 0.03; K, 0.03; Sr, 0.09; Ba, 0.09; Rb, 0.07; Ca, 0.03; Pb, 0.11; Fe, 0.04.

165

Appendix H: Results of electron microprobe analyses of albite and K-feldspar

Name	SiO$_2$	Al$_2$O$_3$	Na$_2$O	K$_2$O	SrO	BaO	Rb$_2$O	CaO	PbO	FeO	Total
W09090206	62.15	19.65	0.336	14.84	0.000	3.065	0.054	0.016	0.000	0.171	100.28

Notes: The detection limits for oxides (wt.%), which are as follows: Si, 0.04; Al, 0.03; Na, 0.03; K, 0.03; Sr, 0.09; Ba, 0.09; Rb, 0.07; Ca, 0.03; Pb, 0.11; Fe, 0.04.

166

Appendix I

Results of electron microprobe analyses of apatite

Appendix I: Results of electron microprobe analyses of apatite

Name	CaO	P₂O₅	Na₂O	SrO	SiO₂	ThO₂	Y₂O₃	La₂O₃	Ce₂O₃	Pr₂O₃	Nd₂O₃	Sm₂O₃	Eu₂O₃	Gd₂O₃	Dy₂O₃	F	Cl	Total
WI-13-01-01	54.78	40.04	0.073	0.866	0.034	0.027	0.098	0.022	0.107	0.012	0.063	0.035	0.000	0.016	0.000	4.073	0.005	98.53
WI-13-01-02	54.00	42.07	0.079	0.845	0.004	0.000	0.079	0.004	0.032	0.044	0.100	0.083	0.000	0.091	0.000	4.144	0.002	99.84
WI-13-01-03	53.60	41.66	0.053	1.192	0.053	0.001	0.007	0.001	0.067	0.000	0.067	0.000	0.056	0.072	0.025	3.846	0.003	99.09
WI-13-01-04	55.18	40.74	0.055	0.758	0.039	0.003	0.056	0.000	0.041	0.033	0.028	0.054	0.051	0.063	0.021	4.224	0.013	99.58
WI-13-01-05	55.50	41.20	0.025	0.765	0.035	0.010	0.014	0.000	0.021	0.000	0.061	0.007	0.087	0.00	0.000	3.741	0.000	99.88
WI-13-01-06	54.36	41.15	0.115	1.219	0.062	0.013	0.082	0.045	0.215	0.072	0.225	0.110	0.014	0.032	0.017	3.777	0.008	99.92
WI-13-01-07	55.23	41.17	0.084	0.890	0.000	0.000	0.083	0.000	0.074	0.000	0.000	0.070	0.009	0.098	0.037	3.948	0.000	100.05
WI-13-01-08	54.65	41.58	0.047	1.118	0.035	0.000	0.062	0.000	0.087	0.066	0.118	0.000	0.034	0.542	0.000	4.032	0.005	100.68
WI-13-01-09r	51.95	39.70	0.160	1.874	0.947	0.009	0.023	0.064	0.304	0.024	0.180	0.055	0.000	0.016	0.039	3.546	0.006	97.40
WI-13-01-10c	55.01	41.43	0.050	0.753	0.025	0.000	0.038	0.008	0.052	0.030	0.009	0.022	0.068	0.000	0.023	3.689	0.009	99.66
WI-13-01-11r	55.02	41.36	0.086	0.920	0.028	0.038	0.038	0.000	0.141	0.000	0.028	0.000	0.000	0.000	0.000	3.884	0.004	99.91
WI-13-01-12c	55.26	41.19	0.030	0.808	0.029	0.004	0.026	0.045	0.077	0.000	0.052	0.000	0.000	0.000	0.091	4.234	0.000	100.06
WI-13-01-14c	54.95	41.57	0.061	0.779	0.033	0.027	0.078	0.051	0.058	0.039	0.086	0.059	0.015	0.000	0.000	3.800	0.000	100.01
WI-13-01-15r	53.00	41.33	0.195	2.048	0.020	0.008	0.000	0.101	0.415	0.088	0.297	0.046	0.000	0.000	0.083	3.767	0.000	99.81
WI-13-37-01	54.25	41.48	0.043	0.749	0.255	0.018	0.030	0.195	0.303	0.000	0.131	0.037	0.000	0.032	0.000	3.159	0.182	99.49
WI-13-37-02	55.65	41.52	0.003	0.481	0.031	0.003	0.006	0.000	0.002	0.000	0.000	0.015	0.000	0.031	0.000	3.706	0.000	99.89
WI-13-37-03	54.28	40.94	0.058	0.887	0.370	0.031	0.025	0.207	0.434	0.030	0.173	0.000	0.082	0.000	0.000	3.373	0.145	99.58
WI-13-37-04	52.76	39.80	0.403	0.249	0.199	0.303	0.190	0.289	0.965	0.066	0.491	0.077	0.073	0.000	0.042	3.534	0.211	98.11
WI-13-37-05	55.34	40.96	0.000	0.043	0.432	0.005	0.038	0.087	0.284	0.046	0.063	0.046	0.000	0.000	0.000	3.456	0.012	99.35
WI-13-37-06	54.22	41.27	0.033	0.898	0.472	0.000	0.003	0.208	0.410	0.000	0.179	0.030	0.033	0.022	0.048	3.540	0.038	99.91
WI-13-37-07	54.67	41.19	0.048	0.280	0.286	0.016	0.068	0.083	0.285	0.045	0.145	0.000	0.041	0.035	0.000	3.377	0.208	99.31
WI-13-37-08	53.61	40.62	0.385	0.193	1.469	0.000	0.042	0.109	0.394	0.041	0.277	0.040	0.000	0.000	0.058	3.698	0.002	99.37
WI-13-37-09	54.51	40.66	0.114	0.079	0.201	0.096	0.040	0.103	0.325	0.041	0.134	0.000	0.068	0.040	0.004	3.617	0.060	98.55
WI-13-55-01	54.51	41.49	0.132	0.395	0.232	0.035	0.000	0.171	0.348	0.025	0.070	0.030	0.000	0.164	0.002	3.982	0.034	99.94
WI-13-55-02	54.51	41.53	0.173	0.914	0.061	0.005	0.006	0.165	0.453	0.035	0.207	0.057	0.010	0.049	0.019	3.766	0.000	100.38
WI-13-55-03	55.62	42.32	0.033	0.080	0.095	0.000	0.067	0.009	0.061	0.059	0.025	0.043	0.000	0.000	0.000	3.789	0.028	100.63
WI-13-55-04	54.58	42.28	0.024	0.052	0.149	0.014	0.000	0.000	0.079	0.000	0.016	0.006	0.000	0.000	0.012	4.053	0.008	99.56
WI-13-55-05	54.24	41.17	0.203	0.934	0.105	0.046	0.039	0.195	0.402	0.004	0.201	0.036	0.051	0.070	0.055	3.447	0.011	99.75
WI-13-55-06	53.32	41.48	0.322	1.031	0.092	0.000	0.047	0.462	0.823	0.132	0.145	0.034	0.000	0.000	0.007	3.410	0.000	99.86
WI-13-55-07	53.62	41.21	0.315	0.717	0.205	0.000	0.028	0.544	1.005	0.150	0.349	0.048	0.018	0.029	0.000	4.000	0.000	100.55
WI-13-55-08	53.92	42.32	0.083	0.812	0.024	0.025	0.036	0.066	0.164	0.058	0.108	0.029	0.045	0.000	0.005	3.699	0.002	99.83

Notes: The detection limits for oxides (wt.%), which are as follows: Eu, 0.13; F, 0.18; Ca, 0.03; P, 0.04; Ce, 0.08; Na, 0.02; Cl, 0.02; Y, 0.09; La, 0.08; Th, 0.03; Si, 0.03; Nd, 0.09; Sr, 0.05; Pr, 0.11; Dy, 0.14; Sm, 0.11; Gd, 0.13.

168

Appendix J

Results of electron microprobe analyses of bastnäsite-(Ce), parisite-(Ce),

synchysite-(Ce), cordylite-(Ce), and ancylite-(Ce)

Appendix J: Results of electron microprobe analyses of bastnäsite-(Ce), parisite-(Ce), synchysite-(Ce), cordylite-(Ce), and ancylite-(Ce)

Name	CaO	La₂O₃	Ce₂O₃	Pr₂O₃	Nd₂O₃	Sm₂O₃	Eu₂O₃	Gd₂O₃	Dy₂O₃	Y₂O₃	CO₂¹	SrO	BaO	MgO	ThO₂	SiO₂	Na₂O	Al₂O₃	PbO	UO₂	P₂O₅	F	Cl	Total
Bastnäsite-(Ce)																								
W08010103	0.15	31.68	33.82	2.71	6.18	0.00	0.00	0.11	b.l.	0.03	20.08	0.02	0.16	0.00	0.10	0.05	0.00	0.00	0.00	0.00	0.00	8.47	0.00	100.00
W08010104	0.06	30.36	33.56	2.85	7.24	0.18	0.00	0.23	0.01	0.09	20.36	0.02	0.05	0.00	0.28	0.05	0.00	0.00	0.01	0.00	0.03	8.00	0.00	100.00
W08010105	0.04	31.36	33.83	2.66	6.50	0.00	0.00	0.07	0.00	0.03	20.12	0.01	0.14	0.00	0.27	0.04	0.00	0.00	0.00	0.00	0.00	8.50	0.00	100.00
W08010106	0.11	28.96	34.86	2.86	7.29	0.23	0.05	0.26	0.00	0.11	20.39	0.01	0.01	0.00	0.15	0.05	0.00	0.00	0.01	0.05	0.02	7.99	0.01	100.00
W08010113	0.30	27.46	35.75	3.13	7.07	0.18	0.21	0.15	0.00	0.06	20.23	0.08	0.05	0.00	0.23	0.11	0.02	0.00	0.08	0.05	0.04	8.30	0.03	100.00
W08010114	0.48	26.92	35.76	3.00	7.01	0.22	0.00	0.15	0.00	0.04	21.00	0.09	0.13	0.00	0.23	0.08	0.00	0.00	0.00	0.01	0.00	8.38	0.00	100.00
W08010115	0.05	31.64	33.34	2.58	6.43	0.05	0.08	0.16	0.00	0.06	20.42	0.05	b.l.	0.00	0.25	0.03	0.00	0.00	0.01	0.05	0.00	8.60	0.00	100.00
W08010116	0.18	31.53	33.48	2.85	6.55	0.23	0.00	0.16	0.00	0.09	19.91	0.00	0.03	0.00	0.26	0.06	0.00	0.00	0.01	0.01	0.00	8.56	0.00	100.00
W08010117	0.34	28.38	35.08	2.85	7.43	0.23	0.07	0.18	0.00	0.07	20.02	0.00	0.05	0.00	0.14	0.05	0.00	0.00	0.07	0.01	0.02	8.81	0.01	100.00
W08010122	0.30	27.06	35.83	2.97	7.86	0.25	0.00	0.18	0.00	0.12	20.04	0.01	0.00	0.00	0.20	0.07	0.00	0.00	0.07	0.00	0.01	8.70	0.00	100.00
W08010123	0.56	30.42	34.79	2.52	7.12	0.01	0.00	0.09	0.00	0.04	20.17	0.02	0.06	0.00	0.14	0.06	0.00	0.00	0.00	0.00	0.02	8.20	0.00	100.00
W08010124	0.59	28.89	34.94	2.82	7.12	0.12	0.08	0.17	0.00	0.06	20.17	0.03	0.00	0.00	0.11	0.04	0.00	0.00	0.00	0.01	0.02	8.32	0.00	100.00
W08010125	0.14	27.79	35.76	3.03	7.88	0.34	0.00	0.22	0.00	0.09	19.81	0.03	0.01	0.01	0.10	0.04	0.00	0.00	0.00	0.03	0.00	8.14	0.01	100.00
W08010404	0.33	25.86	36.22	3.14	7.59	0.40	0.00	0.26	0.00	0.07	20.96	0.00	0.00	0.00	0.04	0.06	0.00	0.00	0.01	0.00	0.03	8.66	0.01	100.00
W08010405	0.52	25.36	36.18	3.09	7.99	0.42	0.20	0.33	0.00	0.11	20.47	0.00	0.09	0.00	0.12	0.05	0.00	0.00	0.00	0.00	0.02	8.73	0.00	100.00
W08010406	0.37	28.25	35.87	2.82	6.77	0.26	0.00	0.24	0.00	0.06	19.97	0.00	0.05	0.00	0.25	0.03	0.00	0.00	0.00	0.00	0.03	8.68	0.01	100.00
W08010407	0.17	27.55	35.03	3.10	7.76	0.36	0.05	0.43	0.00	0.06	20.38	0.00	0.00	0.00	0.17	0.07	0.00	0.00	0.02	0.01	0.01	8.34	0.01	100.00
W08010408	0.18	27.52	35.83	2.94	7.40	0.28	0.00	0.25	0.00	0.10	20.37	0.04	0.05	0.00	0.16	0.03	0.00	0.00	0.00	0.00	0.00	8.40	0.01	100.00
W08010409	0.26	26.09	34.39	2.77	6.90	0.20	0.00	0.18	0.00	0.07	24.00	0.01	0.04	0.00	0.21	0.02	0.00	0.00	0.00	0.00	0.04	8.18	0.01	100.00
W08010412	0.29	29.03	35.10	2.77	6.56	0.22	0.00	0.12	0.00	0.07	20.17	0.03	0.02	0.00	0.24	0.06	0.00	0.00	0.00	0.00	0.02	9.13	0.02	100.00
W08010413	0.39	27.77	35.55	2.92	7.23	0.17	0.02	0.23	0.00	0.03	20.49	0.01	0.00	0.00	0.09	0.04	0.00	0.00	0.00	0.01	0.00	8.74	0.01	100.00
W08010414	0.38	26.30	36.25	3.07	7.53	0.35	0.00	0.16	0.00	0.05	20.78	0.00	0.24	0.00	0.14	0.02	0.00	0.00	0.00	0.02	0.02	8.06	0.01	100.00
W08010415	0.32	27.49	35.89	3.05	7.65	0.31	0.10	0.32	0.00	0.07	20.11	0.01	0.00	0.00	0.00	0.05	0.00	0.00	0.05	0.00	0.00	7.91	0.01	100.00
W08010416	0.28	25.95	35.89	3.24	8.23	0.37	0.23	0.36	0.00	0.09	20.13	0.01	0.00	0.05	0.21	0.20	0.00	0.00	0.04	0.00	0.02	8.08	0.00	100.00
W08010417	0.47	26.45	36.04	3.01	8.03	0.22	0.00	0.32	0.00	0.08	19.98	0.09	0.05	0.00	0.40	0.07	0.00	0.00	0.00	0.00	0.01	8.25	0.02	100.00
W08010418	0.20	26.31	36.40	3.15	7.80	0.34	0.00	0.28	0.00	0.13	20.63	0.00	0.00	0.18	0.08	0.02	0.00	0.13	0.03	0.00	0.00	8.07	0.05	100.00
W08010422	0.31	26.33	34.18	2.99	7.22	0.26	0.21	0.26	0.00	0.05	21.85	0.04	0.12	0.00	0.30	0.07	0.00	0.00	0.03	0.00	0.00	8.52	0.01	100.00
W08010423	0.61	25.84	35.32	3.22	8.20	0.44	0.00	0.33	0.00	0.09	20.54	0.09	0.05	0.00	0.35	0.11	0.00	0.13	0.00	0.00	0.02	8.26	0.05	100.00
W08010426	0.40	27.87	34.88	2.76	7.50	0.23	0.10	0.32	0.01	0.06	20.76	0.02	0.00	0.03	0.10	0.25	0.00	0.04	0.01	0.00	0.01	7.95	0.01	100.00
W08010427	0.20	27.36	35.82	3.25	7.40	0.25	0.07	0.21	0.00	0.04	20.26	0.02	0.19	0.03	0.17	0.13	0.00	0.01	0.00	0.00	0.00	8.01	0.01	100.00
W08010428	0.64	27.72	35.04	2.96	7.18	0.17	0.07	0.22	0.00	0.02	20.72	0.02	0.17	0.04	0.12	0.17	0.00	0.01	0.00	0.01	0.00	8.16	0.01	100.00
W08010429	0.43	27.44	35.39	2.78	7.64	0.32	0.09	0.37	0.00	0.09	20.73	0.04	0.02	0.00	0.02	0.04	0.00	0.00	0.02	0.01	0.01	7.94	0.00	100.00
W08010430	0.53	28.03	35.42	2.88	6.98	0.10	0.10	0.29	0.00	0.09	20.57	0.04	0.14	0.00	0.18	0.08	0.00	0.00	0.01	0.00	0.01	7.99	0.02	100.00
W08010823	0.13	27.45	35.47	3.23	8.41	0.35	0.10	0.14	0.00	0.04	19.72	0.02	0.08	0.00	0.16	0.03	0.00	0.00	0.00	0.00	0.00	8.07	0.02	100.00
W08010824	0.21	26.94	36.00	2.99	8.03	0.31	0.00	0.12	0.00	0.03	20.38	0.05	0.00	0.00	0.31	0.03	0.00	0.00	0.01	0.00	0.00	7.93	0.01	100.00
W08010826	0.18	26.86	35.97	3.17	8.18	0.34	0.00	0.07	0.00	0.03	20.16	0.01	0.16	0.00	0.00	0.07	0.00	0.00	0.03	0.00	0.00	8.22	0.01	100.00
W08010830	0.08	26.93	36.42	3.11	8.01	0.34	0.00	0.13	0.00	0.04	19.62	0.02	0.03	0.00	0.19	0.05	0.00	0.18	0.03	0.02	0.00	8.24	0.01	100.00
W09100627	0.05	28.95	36.11	2.57	6.66	0.16	0.05	0.24	0.00	0.05	20.55	0.00	0.06	0.00	0.14	0.03	0.00	0.00	0.03	0.00	0.00	7.64	0.00	100.00
W09100628	0.43	31.07	35.15	2.36	5.62	0.00	0.00	0.02	0.00	0.01	20.46	0.00	0.10	0.00	0.10	0.03	0.00	0.00	0.01	0.00	0.00	8.10	0.00	100.00
W09100629	0.02	32.35	34.92	2.47	5.39	0.00	0.00	0.06	0.00	0.00	20.02	0.00	0.00	0.00	0.05	0.04	0.00	0.00	0.03	0.00	0.00	7.90	0.00	100.00
W09100630	0.16	29.59	35.69	2.55	6.60	0.00	0.00	0.10	0.00	0.05	20.15	0.01	0.00	0.00	0.04	0.05	0.00	0.00	0.03	0.00	0.03	7.90	0.01	100.00
W09100631	0.04	29.98	35.45	2.73	6.20	0.12	0.00	0.10	0.00	0.03	20.85	0.01	0.02	0.00	0.02	0.01	0.00	0.00	0.04	0.00	0.00	7.61	0.00	100.00
W09100632	0.31	31.55	34.33	2.44	5.31	0.00	0.00	0.06	0.00	0.00	20.91	0.00	0.03	0.00	0.05	0.02	0.00	0.29	0.02	0.00	0.02	8.04	0.01	100.00
Parisite-(Ce)																								
W08010101	10.59	21.43	28.97	2.66	7.22	0.33	0.00	0.26	0.00	0.10	23.45	0.03	0.12	b.l.	0.21	0.09	0.00	0.54	0.00	0.04	0.01	6.83	0.01	100.00
W08010102	10.58	22.16	28.64	2.79	7.18	0.32	0.01	0.29	0.00	0.10	23.49	0.06	0.03	b.l.	0.24	0.06	0.03	0.00	0.03	0.02	0.00	6.92	0.00	100.00
W08010111	9.92	19.89	30.53	2.70	6.96	0.29	0.00	0.16	0.00	0.07	24.03	0.76	0.06	b.l.	0.35	0.06	0.02	0.00	0.01	0.01	0.01	7.22	0.02	100.00
W08010112	9.51	19.88	31.00	2.55	6.72	0.28	0.03	0.21	0.00	0.07	24.30	0.75	0.06	b.l.	0.45	0.05	0.00	0.00	0.00	0.01	0.02	7.04	0.02	100.00
W08010118	10.59	21.24	28.84	2.68	7.44	0.39	0.00	0.33	0.00	0.16	23.51	0.05	0.07	b.l.	0.32	0.07	0.00	0.00	0.03	0.00	0.02	7.37	0.00	100.00
W08010119	10.38	22.43	28.23	2.64	7.11	0.25	0.00	0.26	0.00	0.13	23.82	0.38	0.06	b.l.	0.24	0.04	0.00	0.00	0.01	0.00	0.00	6.94	0.01	100.00
W08010120	10.77	21.25	28.97	2.86	7.45	0.33	0.00	0.37	0.00	0.17	23.36	0.00	0.16	b.l.	0.37	0.06	0.00	0.00	0.04	0.00	0.00	6.60	0.00	100.00
W08010121	10.64	21.89	29.24	2.73	7.05	0.36	0.15	0.24	0.00	0.07	23.41	0.02	b.l.	b.l.	0.31	0.06	0.00	0.00	0.04	0.00	0.00	6.64	0.00	100.00
W08010126	10.72	21.51	29.10	2.53	7.35	0.30	0.00	0.25	0.00	0.09	23.82	0.04	b.l.	b.l.	0.25	0.05	0.00	0.00	0.01	0.00	0.00	6.91	0.01	100.00
W08010127	10.62	21.76	27.89	2.54	7.01	0.31	0.00	0.32	0.00	0.13	24.61	0.13	0.01	b.l.	0.68	0.05	0.00	0.00	0.00	0.00	0.01	6.81	0.01	100.00
W08010128	10.11	21.05	30.43	3.10	6.63	0.21	0.00	0.20	0.00	0.09	23.45	0.71	b.l.	b.l.	0.18	0.05	0.01	0.00	0.03	0.02	0.01	7.47	0.01	100.00
W08010129	10.19	20.56	30.37	2.65	6.51	0.27	0.00	0.31	0.00	0.15	23.55	0.76	0.12	b.l.	0.20	0.02	0.00	0.00	0.01	0.00	0.02	7.47	0.00	100.00
W08010130	10.25	20.50	30.86	2.60	6.43	0.26	0.04	0.17	0.00	0.07	23.12	0.83	b.l.	b.l.	0.66	0.03	0.00	0.00	0.05	0.00	0.02	7.22	0.00	100.00
W08010401	10.07	17.70	29.17	3.45	9.64	0.83	0.00	0.53	0.00	0.11	23.61	0.39	0.04	b.l.	0.44	0.07	0.00	0.00	0.00	0.00	0.00	6.84	0.01	100.00
W08010402	10.04	17.48	29.20	3.21	9.34	0.80	0.00	0.64	0.00	0.10	24.33	0.41	0.06	b.l.	0.46	0.05	0.00	0.00	0.00	0.00	0.00	6.68	0.00	100.00
W08010403	10.24	17.24	29.37	3.43	9.29	0.89	0.00	0.61	0.00	0.14	23.95	0.36	0.11	b.l.	0.12	0.03	0.00	0.00	0.00	0.00	0.00	7.27	0.01	100.00
W08010411	9.97	17.25	29.32	3.10	8.94	0.77	0.11	0.64	0.00	0.15	25.01	0.38	b.l.	b.l.	0.47	0.04	0.00	0.00	0.03	0.00	0.01	6.63	0.00	100.00
W08010419	10.34	21.05	28.77	2.75	7.31	0.51	0.29	0.60	0.00	0.21	23.73	0.09	0.06	b.l.	0.22	0.06	0.00	0.00	0.00	0.00	0.00	6.93	0.01	100.00
W08010420	10.25	17.92	29.85	3.25	8.83	0.79	0.00	0.59	0.03	0.16	23.27	0.37	0.18	b.l.	0.44	0.02	0.00	0.00	0.00	0.00	0.00	7.00	0.00	100.00
W08010421	10.26	16.64	28.96	3.45	10.00	0.89	0.00	0.71	0.00	0.16	24.01	0.37	0.05	b.l.	0.25	0.06	0.00	0.00	0.05	0.00	0.00	7.20	0.00	100.00
W08010424	10.25	20.94	29.06	2.56	7.14	0.46	0.04	0.37	0.00	0.12	24.57	0.15	b.l.	b.l.	0.30	0.04	0.00	0.00	0.02	0.00	0.00	7.00	0.01	100.00
W08010425	10.24	19.00	29.19	3.07	8.36	0.62	0.00	0.52	0.00	0.08	23.95	0.40	0.01	b.l.	0.38	0.02	0.00	0.00	0.03	0.00	0.01	7.10	0.01	100.00
W08010822	10.54	19.30	29.54	2.77	8.23	0.63	0.00	0.35	0.00	0.08	24.06	0.19	0.21	b.l.	0.30	0.02	0.00	0.00	0.00	0.01	0.00	6.52	0.00	100.00
W08010825	10.17	21.30	29.54	2.64	6.66	0.21	0.00	0.02	0.00	0.03	24.08	0.49	0.02	b.l.	0.23	0.03	0.00	0.00	0.00	0.00	0.02	6.84	0.01	100.00
W08010827	10.29	21.84	29.33	2.37	6.41	0.13	0.00	0.10	0.00	0.01	24.42	0.54	0.10	b.l.	0.27	0.03	0.00	0.06	0.00	0.02	0.00	7.06	0.00	100.00

Notes: The detection limits for oxides (wt.%), which are as follows: F, 0.11; Na, 0.03; Ca, 0.03; P, 0.04; La, 0.13; Al, 0.02; Cl, 0.01; Ba, 0.25; Ce, 0.12; Mg, 0.02; Th, 0.09; Pb, 0.05; Dy, 0.11; U, 0.06; Sr 0.02; Pr, 0.23; Y, 0.04; Sm, 0.14; Sr, 0.04; Gd, 0.13; Eu, 0.46; Nd, 0.21.

Appendix J: Results of electron microprobe analyses of bastnäsite-(Ce), parisite-(Ce), synchysite-(Ce), cordylite-(Ce), and ancylite-(Ce)

Name	CaO	La₂O₃	Ce₂O₃	Pr₂O₃	Nd₂O₃	Sm₂O₃	Eu₂O₃	Gd₂O₃	Dy₂O₃	Y₂O₃	CO₂ᶦ	SrO	BaO	MgO	ThO₂	SiO₂	Na₂O	Al₂O₃	PbO	UO₂	P₂O₅	F	Cl	Total
W08010828	10.32	20.75	29.91	2.77	7.33	0.36	b.l.	0.04	b.l.	0.02	23.54	0.46	b.l.	b.l.	0.09	0.04	b.l.	b.l.	b.l.	b.l.	b.l.	7.60	b.l.	100.00
W08010829	10.19	20.45	29.48	2.79	7.71	0.30	b.l.	0.10	b.l.	0.05	23.79	0.44	b.l.	b.l.	b.l.	0.03	b.l.	0.33	0.03	b.l.	0.05	7.37	b.l.	100.00
W09100201	10.61	22.62	28.12	2.67	7.01	0.33	b.l.	0.46	b.l.	0.20	23.82	0.00	0.01	b.l.	0.09	0.04	b.l.	b.l.	b.l.	b.l.	b.l.	6.96	b.l.	100.00
W09100202	10.30	21.81	28.13	2.48	7.43	0.56	0.10	0.45	b.l.	0.16	23.75	0.54	0.19	b.l.	0.20	0.01	b.l.	b.l.	b.l.	0.03	0.00	6.67	b.l.	100.00
W09100203	10.60	22.10	27.96	2.66	7.12	0.53	0.14	0.36	b.l.	0.14	24.06	b.l.	b.l.	b.l.	0.06	0.04	b.l.	b.l.	b.l.	b.l.	b.l.	7.28	0.00	100.00
W09100208	10.61	22.74	27.47	2.46	6.99	0.55	b.l.	0.56	b.l.	0.21	24.30	0.01	0.06	b.l.	0.09	0.02	b.l.	b.l.	0.02	b.l.	0.04	6.71	b.l.	100.00
W09100209	10.58	22.48	28.28	2.48	7.24	0.33	0.05	0.37	b.l.	0.09	23.98	0.02	0.08	b.l.	0.13	0.01	b.l.	b.l.	b.l.	0.00	b.l.	6.72	b.l.	100.00
W09100210	10.74	22.41	27.92	2.48	7.31	0.55	b.l.	0.46	b.l.	0.14	23.79	0.01	0.07	b.l.	0.19	b.l.	b.l.	b.l.	b.l.	b.l.	0.01	6.88	0.00	100.00
W09100213	10.65	21.91	28.33	2.56	7.13	0.51	0.02	0.43	b.l.	0.17	23.85	b.l.	b.l.	b.l.	0.14	0.01	b.l.	b.l.	0.05	b.l.	0.01	7.34	b.l.	100.00
W09100214	10.65	22.94	26.92	2.30	6.62	0.37	0.21	0.36	b.l.	0.15	23.93	0.10	b.l.	b.l.	1.28	0.03	b.l.	b.l.	b.l.	b.l.	0.01	7.10	0.03	100.00
W09100215	10.65	22.30	27.77	2.83	7.40	0.47	b.l.	0.46	0.08	0.18	23.64	0.03	b.l.	b.l.	0.10	0.02	b.l.	b.l.	0.04	b.l.	b.l.	6.97	b.l.	100.00
W09100216	10.66	21.81	28.36	2.50	7.01	0.45	b.l.	0.38	b.l.	0.16	23.86	0.01	b.l.	b.l.	0.56	0.02	b.l.	b.l.	b.l.	0.02	b.l.	7.25	b.l.	100.00
W09100625	10.68	21.68	28.94	2.43	6.94	0.33	b.l.	0.31	b.l.	0.08	24.34	0.07	b.l.	b.l.	0.23	0.03	b.l.	0.07	0.02	b.l.	0.01	6.66	b.l.	100.00
W09100626	10.69	20.39	29.49	2.60	7.73	0.62	0.05	0.38	b.l.	0.10	23.78	0.03	0.01	b.l.	0.17	0.03	b.l.	b.l.	0.02	b.l.	0.03	6.76	b.l.	100.00
Synchysite-(Ce)																								
W09100611	19.35	17.62	23.18	1.99	5.12	0.36	0.17	0.17	b.l.	0.09	28.53	0.40	0.04	0.04	0.13	0.16	b.l.	b.l.	b.l.	b.l.	b.l.	5.23	b.l.	100.00
W09100612	19.07	18.09	23.08	1.89	4.96	0.42	b.l.	0.05	b.l.	0.07	28.41	0.53	0.13	b.l.	0.37	0.04	b.l.	b.l.	b.l.	b.l.	0.02	5.68	b.l.	100.00
W09100616	19.02	17.92	23.44	1.97	5.37	0.41	b.l.	0.16	b.l.	0.10	28.09	0.57	0.04	b.l.	0.10	0.03	b.l.	b.l.	b.l.	b.l.	0.02	5.49	b.l.	100.00
W09100617	18.49	18.90	23.12	1.97	4.94	0.31	b.l.	0.26	b.l.	0.06	27.87	0.61	b.l.	b.l.	0.34	0.02	b.l.	b.l.	0.06	0.04	0.02	5.72	b.l.	100.00
Cordylite-(Ce)																								
W09100615	2.21	15.76	22.50	0.58	3.47	0.09	0.00	0.06	b.l.	0.02	24.00	2.03	24.54	b.l.	b.l.	0.02	3.05	0.18	0.01	b.l.	b.l.	2.54	0.00	100.00
W09100617	2.19	16.00	22.46	0.67	3.36	0.14	0.00	0.15	b.l.	0.03	22.58	1.95	25.86	b.l.	b.l.	0.01	2.95	0.20	0.00	b.l.	b.l.	2.48	b.l.	100.00
W09100618	2.17	15.66	22.52	0.59	3.54	0.05	0.00	0.14	b.l.	0.04	23.36	1.96	25.34	b.l.	b.l.	0.02	2.82	0.22	b.l.	b.l.	0.01	2.73	0.00	100.00
W09100619	1.89	16.67	22.38	0.40	3.11	0.04	0.00	0.10	b.l.	0.02	23.13	1.83	25.79	b.l.	0.05	0.03	2.89	0.20	b.l.	b.l.	0.00	2.55	b.l.	100.00
W09100620	2.53	15.93	21.76	0.42	3.24	0.05	0.00	0.19	b.l.	0.04	22.99	2.43	25.88	b.l.	0.11	0.03	2.62	0.22	0.04	b.l.	b.l.	2.64	b.l.	100.00
W09100622	2.75	15.64	22.01	0.29	3.14	0.10	0.00	0.14	b.l.	0.04	23.08	2.35	25.96	b.l.	0.06	0.04	2.75	0.19	b.l.	b.l.	0.02	2.49	b.l.	100.00
W09100623	2.19	15.44	20.55	0.54	2.64	0.07	0.00	0.10	b.l.	0.03	28.91	2.06	23.01	b.l.	0.09	0.02	2.45	0.19	b.l.	0.03	0.02	2.88	0.00	100.00
W09100624	2.36	15.97	22.12	0.56	3.32	0.13	0.00	0.08	b.l.	0.03	22.94	2.20	25.69	b.l.	0.10	0.02	2.79	0.20	b.l.	b.l.	b.l.	2.61	0.00	100.00
Ancylite-(Ce)																								
W09100602	2.47	18.36	25.12	2.06	5.45	0.14	0.04	0.09	b.l.	b.l.	28.31	14.13	1.63	0.04	1.15	0.27	b.l.	0.13	b.l.	b.l.	b.l.	0.98	0.05	100.00
W09100603	1.91	19.32	23.42	2.07	5.64	0.02	b.l.	b.l.	b.l.	b.l.	27.39	15.70	2.69	0.01	1.04	0.17	b.l.	0.01	b.l.	b.l.	b.l.	1.02	0.02	100.00
W09100604	2.01	19.84	24.10	2.27	5.43	0.07	b.l.	0.09	b.l.	0.01	26.97	15.78	1.10	b.l.	1.18	0.54	b.l.	b.l.	0.03	b.l.	0.02	0.96	0.01	100.00
W09100612	2.22	18.37	25.50	2.07	5.11	0.09	b.l.	b.l.	b.l.	b.l.	27.02	15.83	1.22	b.l.	1.92	0.04	b.l.	b.l.	0.04	0.02	0.01	0.93	0.00	100.00
W09100613	2.40	19.22	25.10	2.24	5.48	0.22	b.l.	0.05	b.l.	b.l.	27.46	15.40	0.87	b.l.	0.89	0.11	b.l.	b.l.	b.l.	b.l.	0.01	0.94	0.00	100.00
W09100614	2.28	19.49	23.96	2.15	5.58	0.25	b.l.	0.22	b.l.	0.04	27.47	13.98	0.44	0.01	1.89	1.68	b.l.	0.03	0.02	b.l.	0.06	0.75	0.03	100.00
W09100616	2.34	18.51	25.99	2.19	5.07	0.17	b.l.	0.03	b.l.	0.00	27.58	14.85	0.47	b.l.	1.98	0.25	b.l.	b.l.	0.03	0.01	0.02	0.91	0.02	100.00
W09100621	2.40	20.40	23.14	2.32	5.55	0.19	b.l.	0.09	b.l.	0.02	28.01	14.64	0.32	b.l.	1.78	0.49	b.l.	0.01	0.02	b.l.	0.03	0.98	0.03	100.00

Notes: The detection limits for oxides (wt %), which are as follows: F, 0.11; Na, 0.03; Ca, 0.03; P, 0.04; La, 0.13; Al, 0.02; Cl, 0.02; Ce, 0.12; Mg, 0.02; Th, 0.09; Pb, 0.05; Dy, 0.11; U, 0.06; Si 0.02; Pr, 0.23; Y, 0.04; Sm, 0.14; Sr, 0.04; Gd, 0.13; Eu, 0.46; Nd, 0.21.

Appendix K

Results of electron microprobe analyses of monazite-(Ce)

Appendix K: Electron microprobe analyses of monazite-(Ce)

Name	La₂O₃	Ce₂O₃	Pr₂O₃	Nd₂O₃	Sm₂O₃	Eu₂O₃	Gd₂O₃	Dy₂O₃	Y₂O₃	P₂O₅	CaO	SrO	BaO	MgO	ThO₂	Na₂O	SiO₂	Al₂O₃	PbO	UO₂	F	Cl	Total
WI08010107	25.35	33.04	2.90	7.11	0.27	0.00	0.22	0.00	0.08	30.87	0.18	0.08	0.06	0.00	1.22	0.00	0.26	b.l.	0.02	0.01	0.24	0.00	101.82
WI08010108	23.53	35.35	2.93	6.75	0.34	0.00	0.13	0.00	0.04	30.63	0.13	0.05	0.17	0.00	0.92	0.00	0.22	0.03	0.03	0.06	0.29	0.00	101.47
WI08010109	25.54	33.25	2.81	6.83	0.24	0.05	0.22	0.00	0.06	29.95	0.09	0.08	0.10	0.00	1.05	0.00	0.27	0.00	0.00	0.03	0.22	0.01	100.69
WI08010110	24.81	33.32	2.82	6.97	0.29	0.21	0.24	0.00	0.04	29.60	0.43	0.14	0.04	0.00	1.14	0.00	0.22	0.00	0.02	0.00	0.39	0.02	100.52
WI08010801	23.17	30.91	2.89	8.80	1.13	0.35	0.80	0.12	0.33	28.77	0.24	0.35	0.12	0.00	0.86	0.00	0.10	0.00	0.01	0.11	0.24	0.02	99.22
WI08010802	23.01	31.10	2.98	8.73	0.97	0.49	0.75	0.03	0.38	28.52	0.32	0.57	0.12	0.00	0.55	0.00	0.07	0.00	0.02	0.07	0.26	0.02	98.84
WI08010803	22.81	31.66	2.84	9.24	1.00	0.45	0.78	0.05	0.37	28.68	0.31	0.58	0.06	0.00	0.42	0.00	0.09	0.00	0.00	0.02	0.12	0.01	99.42
WI08010804	22.62	31.57	2.92	9.24	1.02	0.73	0.71	0.04	0.34	28.09	0.34	0.48	0.02	0.00	0.59	0.00	0.10	0.00	0.02	0.02	0.26	0.01	98.99
WI08010805	23.67	31.38	2.79	8.72	0.82	0.62	0.72	0.05	0.35	28.67	0.28	0.46	0.00	0.00	0.59	0.00	0.08	0.00	0.00	0.03	0.23	0.01	99.30
WI08010806	23.36	31.10	2.86	8.28	0.78	0.29	0.71	0.03	0.33	29.25	0.31	0.44	0.18	0.00	0.87	0.00	0.06	0.00	0.02	0.02	0.23	0.00	99.00
WI08010807	23.56	30.92	2.97	8.53	0.89	0.40	0.69	0.06	0.37	28.78	0.37	0.56	0.16	0.00	0.69	0.00	0.08	0.00	0.05	0.06	0.23	0.01	99.26
WI08010808	22.32	32.57	3.08	9.40	0.83	0.43	0.40	0.00	0.18	28.07	0.19	0.42	0.17	0.00	0.46	0.00	0.33	0.02	0.02	0.00	0.21	0.03	99.10
WI08010809	21.43	32.51	3.02	9.58	0.83	0.00	0.48	0.00	0.20	27.99	0.23	0.51	0.10	0.00	0.64	0.00	0.13	0.00	0.05	0.00	0.30	0.03	97.90
WI08010811	21.47	32.51	3.25	9.49	0.98	0.19	0.56	0.04	0.20	28.84	0.20	0.42	0.08	0.00	0.28	0.00	0.14	0.00	0.02	0.00	0.23	0.03	98.89
WI08010812	21.77	32.11	3.09	9.41	0.80	0.19	0.36	0.00	0.20	28.61	0.39	0.45	0.13	0.00	0.62	0.00	0.09	0.00	0.03	0.02	0.19	0.05	98.58
WI08010813	22.45	32.24	3.13	8.92	0.86	0.42	0.61	0.02	0.26	28.66	0.28	0.42	0.02	0.00	0.47	0.00	0.12	0.00	0.05	0.00	0.12	0.02	99.00
WI08010814	23.09	31.72	3.08	8.83	0.86	0.12	0.60	0.02	0.30	29.10	0.30	0.38	0.00	0.00	0.45	0.00	0.08	0.05	0.02	0.02	0.16	0.01	99.12
WI08010815	23.80	31.51	2.88	8.75	0.88	0.35	0.59	0.11	0.40	29.01	0.32	0.51	0.15	0.00	0.30	0.00	0.04	0.00	0.01	0.01	0.11	0.01	99.69
WI08010816	23.43	30.96	2.96	8.53	0.91	0.33	0.75	0.02	0.34	28.85	0.29	0.50	0.04	0.00	0.49	0.00	0.06	0.00	0.04	0.03	0.21	0.01	98.65
WI08010817	23.34	31.02	2.76	8.78	0.96	0.44	0.75	0.04	0.42	28.58	0.32	0.52	0.09	0.00	0.34	0.00	0.04	0.00	0.01	0.10	0.20	0.00	98.62
WI08010818	23.64	31.46	3.06	8.86	1.03	0.47	0.81	0.02	0.32	28.49	0.20	0.29	0.05	0.00	0.31	0.00	0.06	0.00	0.03	0.06	0.21	0.00	100.26
WI08010819	22.68	32.49	2.88	8.57	0.78	0.37	0.54	0.00	0.27	29.03	0.27	0.43	0.16	0.00	0.33	0.00	0.06	0.00	0.02	0.00	0.28	0.00	99.06
WI08010820	23.29	32.51	2.88	8.49	0.77	0.48	0.66	0.06	0.27	28.86	0.28	0.37	0.06	0.00	0.40	0.00	0.07	0.00	0.00	0.00	0.28	0.00	99.61
WI08010821	23.42	32.33	2.91	8.75	0.80	0.49	0.55	0.07	0.18	28.98	0.24	0.21	0.00	0.00	0.48	0.00	0.08	0.00	0.01	0.00	0.12	0.02	99.57
WI09100204	23.68	35.70	2.74	6.71	0.34	0.00	0.23	0.00	0.06	28.99	0.28	0.00	0.16	0.00	0.36	0.00	0.10	0.00	0.01	0.00	0.15	0.02	99.44
WI09100205	23.96	35.44	2.93	6.73	0.21	0.00	0.17	0.00	0.02	28.92	0.19	0.03	0.16	0.00	0.33	0.00	0.13	0.00	0.02	0.00	0.17	0.01	99.33
WI09100206	23.89	35.94	2.89	6.55	0.28	0.08	0.16	0.00	0.03	28.78	0.32	0.02	0.20	0.00	0.32	0.00	0.08	0.00	0.00	0.00	0.17	0.00	99.64
WI09100207	24.02	35.52	2.72	6.42	0.21	0.11	0.17	0.00	0.03	28.98	0.03	0.06	0.00	0.00	0.38	0.00	0.12	0.00	0.04	0.02	0.24	0.00	98.94
WI09100211	25.14	32.85	2.74	6.88	0.41	0.06	0.26	0.00	0.07	28.83	0.11	0.12	0.00	0.00	1.32	0.00	0.23	0.00	0.01	0.00	0.18	0.00	99.12
WI09100212	25.67	32.82	2.63	6.48	0.28	0.04	0.34	0.00	0.10	28.82	0.16	0.28	0.19	0.00	1.16	0.00	0.17	0.00	0.01	0.00	0.29	0.00	99.23
WI09100217	24.51	35.64	2.79	6.48	0.19	0.00	0.24	0.02	0.03	29.47	0.06	0.03	0.08	0.00	0.42	0.00	0.15	0.00	0.04	0.00	0.19	0.00	100.28
WI09100218	23.96	35.38	2.89	6.69	0.28	0.00	0.21	0.00	0.06	28.82	0.06	0.05	0.09	0.01	0.48	0.00	0.14	0.00	0.00	0.00	0.20	0.00	99.20
WI09100219	24.15	35.13	3.00	7.09	0.28	0.00	0.34	0.00	0.02	29.13	0.08	0.08	0.00	0.00	0.66	0.00	0.15	0.00	0.06	0.00	0.14	0.01	100.23
WI09100220	24.15	35.04	2.95	6.92	0.33	0.32	0.21	0.00	0.02	29.97	0.05	0.06	0.00	0.00	0.59	0.00	0.16	0.00	0.00	0.02	0.23	0.01	100.92
WI09100221	23.87	34.53	2.87	6.87	0.32	0.00	0.20	0.00	0.05	29.49	0.12	0.07	0.07	0.00	0.52	0.00	0.15	0.00	0.00	0.02	0.16	0.01	99.29
WI09100222	21.81	32.20	2.60	6.56	0.25	0.14	0.19	0.00	0.03	27.33	0.04	0.06	0.09	0.00	1.43	0.00	0.12	0.00	0.00	0.00	0.12	0.05	92.05
WI09100223	24.54	35.43	2.82	6.56	0.21	0.00	0.18	0.00	0.04	29.86	0.06	0.02	0.15	0.00	0.44	0.00	0.26	0.00	0.04	0.04	0.27	0.01	100.81
WI09100223a	24.31	35.56	2.83	6.56	0.12	0.00	0.25	0.00	0.02	29.95	0.05	0.06	0.08	0.00	0.48	0.00	0.26	0.00	0.00	0.00	0.25	0.01	100.66
WI135701	23.85	32.89	2.95	8.61	0.77	0.23	0.55	0.00	0.11	29.61	0.21	0.04	0.06	0.00	0.12	0.00	0.13	0.00	0.03	0.00	0.20	0.02	100.26
WI135702	22.79	33.65	2.98	8.67	0.78	0.33	0.56	0.00	0.16	30.11	0.18	0.11	0.14	0.00	0.26	0.00	0.15	0.00	0.07	0.01	0.25	0.02	101.02
WI135703	24.51	32.77	2.98	7.98	0.58	0.25	0.48	0.01	0.09	29.91	0.25	0.08	0.11	0.00	0.50	0.00	0.13	0.00	0.07	0.01	0.32	0.00	100.67
WI135704	24.49	32.42	2.79	8.26	0.61	0.15	0.50	0.00	0.12	29.95	0.35	0.04	0.02	0.00	0.29	0.00	0.14	0.00	0.00	0.00	0.16	0.00	100.20
WI135705	22.33	32.76	2.84	8.31	0.64	0.14	0.47	0.00	0.14	28.88	0.19	0.51	0.00	0.00	0.11	0.00	0.29	0.03	0.02	0.06	0.32	0.01	97.91
WI135706	22.90	32.40	2.81	8.40	0.63	0.00	0.52	0.00	0.19	29.42	0.33	0.34	0.17	0.00	0.51	0.00	0.16	0.00	0.03	0.03	0.21	0.01	98.95
WI135707	19.96	33.05	3.49	9.53	0.84	0.27	0.48	0.00	0.09	30.12	0.17	0.35	0.01	0.00	1.99	0.00	0.27	0.00	0.06	0.00	0.21	0.01	100.79
WI135708	19.50	33.35	3.26	9.20	0.92	0.18	0.53	0.00	0.11	29.13	0.23	0.29	0.11	0.00	2.00	0.00	0.37	0.00	0.04	0.03	0.27	0.04	99.44
WI135709	20.07	34.04	3.20	8.92	0.79	0.00	0.41	0.02	0.09	29.77	0.29	0.26	0.11	0.00	1.64	0.00	0.28	0.01	0.00	0.03	0.29	0.01	100.06
WI135710	19.61	33.76	3.34	9.67	0.90	0.38	0.48	0.00	0.14	29.03	0.23	0.30	0.11	0.00	1.43	0.00	0.18	0.00	0.06	0.00	0.26	0.01	99.74
WI135711	19.74	33.79	3.39	9.37	0.91	0.19	0.51	0.00	0.13	29.58	0.17	0.32	0.11	0.01	1.71	0.00	0.34	0.01	0.05	0.05	0.33	0.02	100.47
WI135712	21.46	33.45	3.31	9.25	0.78	0.00	0.48	0.05	0.15	29.78	0.30	0.34	0.00	0.00	0.83	0.00	0.13	0.01	0.02	0.00	0.12	0.02	100.41
WI135713	21.33	32.70	3.10	9.22	0.93	0.13	0.84	0.00	0.31	29.40	0.37	0.41	0.11	0.00	0.35	0.00	0.10	0.00	0.03	0.00	0.25	0.01	99.47
WI135714	21.73	32.71	3.02	9.03	0.87	0.37	0.70	0.00	0.28	29.64	0.37	0.36	0.09	0.00	0.30	0.00	0.09	0.01	0.01	0.00	0.25	0.02	99.72
WI135715	22.17	30.88	2.84	8.13	0.79	0.25	0.77	0.07	0.26	29.54	0.39	0.27	0.16	0.00	2.12	0.00	0.39	0.00	0.06	0.03	0.17	0.02	99.21
WI135716	25.22	30.82	2.60	7.24	0.70	0.51	0.83	0.12	0.47	29.87	0.26	0.46	0.04	0.00	0.59	0.00	0.09	0.01	0.03	0.01	0.22	0.00	99.98
WI135717	24.69	31.70	2.65	7.44	0.53	0.11	0.78	0.15	0.58	29.44	0.33	0.51	0.06	0.00	0.12	0.00	0.10	0.00	0.06	0.06	0.28	0.02	99.42
WI135718	22.35	31.10	2.85	8.98	1.05	0.36	1.04	0.10	0.55	28.87	0.31	0.49	0.02	0.00	0.93	0.00	0.12	0.00	0.03	0.02	0.25	0.01	99.27
WI135719	23.74	31.46	2.91	7.78	0.78	0.54	0.88	0.14	0.63	29.31	0.32	0.47	0.09	0.00	0.69	0.00	0.12	0.00	0.02	0.02	0.31	0.02	100.08

Notes: The detection limits for oxides (wt.%), which are as follows: Ca, 0.03; Mg, 0.03; Fe, 0.07; Sr, 0.09; La, 0.11; K, 0.03; Mn, 0.12; P, 0.04; Ce, 0.1; Th, 0.14; Nb, 0.09; Nd, 0.19; Ti, 0.06; Y, 0.09; Ba, 0.09; Zr, 0.09.